MODELING AND OPTIMIZATION OF A HYBRID SOLAR COMBINED CYCLE (HYCS)

BY

AHMAD ADEL ETER

A Thesis Presented to the
DEANSHIP OF GRADUATE STUDIES

KING FAHD UNIVERSITY OF PETROLEUM & MINERALS

DHAHRAN, SAUDI ARABIA

In Partial Fulfillment of the
Requirements for the Degree of

MASTER OF SCIENCE

In

MECHANICAL ENGINEERING

October, 2011

In the name of Allah, the Most Gracious and the Most Merciful

KING FAHD UNIVERSITY OF PETROLEUM AND MINERALS

DHAHRAN 31261, SAUDI ARABIA

DEANSHIP OF GRADUATE STUDIES

This thesis, written by AHMAD ETER under the direction of his thesis advisor and approved by his thesis committee, has been presented to and accepted by the Dean of Graduate Studies, in partial fulfillment of the requirements for the degree of MASTER OF SCIENCE in MECHANICAL ENGINEERING.

Thesis Committee

Dr. Esmail M. A. Mokheimer (Advisor)

Dr. Mohamed A. Habib (Co-Advisor)

Dr.Faleh Al-Sulaiman (Member)

Dr. Amro Al-Qutub (Member)

Dr. Sayed A. M. Said (Member)

Dr. Amro M. Al-Qutub
(Department Chairman)

Dr. Salam A. Zummo
(Dean of Graduate Studies)

Date 4/1/12

Dedicated

to

My Beloved Parents and Brothers

ACKNOWLEDGMENTS

All praise and thanks are due to Almighty Allah, Most Gracious and Most Merciful, for his immense beneficence and blessings. He bestowed upon me health, knowledge and patience to complete this work. May peace and blessings be upon prophet Muhammad (PBUH), his family and his companions.

Thereafter, acknowledgement is due to KFUPM for the support extended towards my research through its remarkable facilities and for granting me the opportunity to pursue graduate studies.

I acknowledge, with deep gratitude and appreciation, the inspiration, encouragement, valuable time and continuous guidance given to me by my thesis advisor, Dr. Esmail M. A. Mokheimer. I am highly grateful to my thesis co-advisor Dr. Mohamed A. Habib for his valuable guidance, suggestions and motivations. I am also grateful to my Committee members, Dr. Faleh Al-Sulaiman, Dr. Amro Al-Qutub, Dr. Syed A. M. Said for their constructive guidance and support.

I would like to acknowledge the support of the Center of Excellence for Scientific Research Collaboration with MIT, and valuable support of the Center Director and ME Department Chairman, Dr. Amro Al-Qutub, in my research endeavors.

My heartfelt thanks are due to my parents and brothers for their prayers, guidance, and moral support throughout my academic life. My parents' advice, to strive for excellence has made all this work possible.

Finally, special thanks are due to all professors and friends who made my study's life beautiful and easy.

TABLE OF CONTENTS

LIST OF TABLES

LIST OF FIGURES

THESIS ABSTRACT (ENGLISH)

NAME: **AHMAD ADEL ETER**

TITLE: **MODELING AND OPTIMIZATION OF A HYBRID SOLAR COMBINED CYCLE (HYCS)**

MAJOR FIELD: **MECHANICAL ENGINEERING**

DATE OF DEGREE: **OCTOBER / 2011**

The main objective of this thesis is to investigate the feasibility of integrating concentrated solar power (CSP) technology with the conventional combined cycle technology for electric generation in Saudi Arabia. The generated electricity can be used locally to meet the annual increasing demand. Specifically, it can be utilized to meet the demand during the hours 10 am – 3 pm and prevent blackout hours, of some industrial sectors. The proposed CSP design gives flexibility in the operation system. Since, it works as a conventional combined cycle during night time and it switches to work as a hybrid solar combined cycle during day time.

The first objective of the thesis is to develop a thermo-economical mathematical model that can simulate the performance of a hybrid solar-fossil fuel combined cycle. The second objective is to develop a computer simulation code that can solve the thermo-economical mathematical model using available software such as E.E.S. The developed simulation code is used to analyze the thermo-economic performance of different configurations of integrating the CSP with the conventional fossil fuel combined cycle to achieve the optimal integration configuration. This optimal integration configuration has been investigated further to achieve the optimal design of the solar field that gives the optimal solar share. Thermo-economical performance metrics which are available in the literature have been used in the present work to assess the thermo-economic performance of the investigated configurations. The economical and environmental impact of integration CSP with the conventional fossil fuel combined cycle are estimated and discussed. Finally, the optimal integration configuration is found to be solarization steam side in conventional combined cycle with solar multiple 0.38 which needs 29 hectare and LEC of HYCS is 63.17 $/MWh under Dhahran weather conditions.

MASTER OF SCIENCE DEGREE

KING FAHD UNIVERSITY OF PETROLEUM AND MINERALS

Dhahran, Saudi Arabia

THESIS ABSTRACT (ARABIC)

ملخص الرسالة

الاسم: أحمد عادل عتر

عنوان الرسالة: تصميم وايجاد الحل الأمثل لمحطات الطاقه الكهربائيه الشمسيه الهجينه

التخصص: الهندسة الميكانيكية

تاريخ التخرج: ذوالحجه/1433

الهدف الرئيسي من هذه الأطروحة هو دراسة جدوى دمج تكنولوجيا الطاقة الشمسية المركزة (ط ش م) مع تكنولوجيا الدورة المركبة التقليدية لتوليد الكهرباء في المملكة العربية السعودية. ويمكن استخدام الطاقة المولدة محليا لتلبية الطلب السنوي المتزايد. تحديدا، فإنه سيتم تلبية الطلب خلال ساعات الذروة من 10:00 صباحا حتي 3:00 مساء ، ومنع الاغلاق لبعض القطاعات الصناعيه. تصميم (ط ش م) المقترح يعطي المرونة في نظام التشغيل. حيث أن هذا التصميم يعمل كدوره مركبه تقليديه خلال ساعات الليل وتتحول للعمل كدورة مركبه حرارية- شمسية هجينه أثناء ساعات النهار.الهدف الأول من الأطروحة هو تطوير نموذج رياضي اقتصادي حراري يستطيع محاكاة أداء الدوره الهجينه ما بين الوقود الأحفوري و الطاقة الشمسية. الهدف الثاني هو تطوير برنامج المحاكاة الحاسوبية الذي يمكن أن يحل النموذج الرياضي حراريا واقتصاديا باستخدام البرمجيات المتاحة مثل EES ويستخدم برنامج المحاكاة المصمم لتحليل الأداء الاقتصادي الحراري لعده تكوينات مختلفة من دمج (ط ش م) مع دورة الوقود الأحفوري التقليدية للحصول على التكوين الأمثل للدورة الهجينة. هذا التكوين الامثل قد اختبر للحصول على التصميم الأمثل لحقل الطاقة الشمسية الذي يعطي نسبه المشاركه الأمثل للطاقة الشمسية. ولقد استخدمت مقاييس الأداء الحرارية الاقتصادية التي تتوفر في هذ المجال في العمل الحالي لتقييم الأداء الحراري الاقتصادي للتكوينات المقترحة. ولقد تم تقييم و مناقشه الأثر الحراري الاقتصادي لدمج الطاقه الشمسيه مع طاقه الوقود الاحفوري. و لقد كشفت نتائج البحث أن التكوين الامثل للدورة المركبة الهجينة هو ذلك المكون من تكامل الطاقه الشمسيه مع الجانب البخاري في الدوره المركبه بنسبة 0.38 من الطاقة الحرارية المطلوبة للدورة البخارية في الدورة المركبة والذي يحتاج إلى حقل شمسي مساحته 29 هيكتار و ينتج طاقة كهربية من الدورة الهجينة بتكلفة مقدارها 63.17 دولار أمريكي لكل ميجاوات ساعة ($/MWh) تحت تاثير اجواء الظهران.

شهادة ماجستير علوم
جامعة الملك فهد للبترول والمعادن
الظهران ، المملكة العربية السعوديه

CHAPTER 1

INTRODUCTION

1.1 WORLDWIDE GROWTH OF ENERGY CONSUMPTION

World marketed energy consumption is expected to increase by 44 percent from 2006 to 2030. The total demand of energy in the non-OECD countries increases by 73 percent with comparison of 15 percent as an increment in the OECD countries (Current OECD member countries are the United States, Canada, Mexico, Austria, Belgium, Czech Republic, Denmark, Finland, France, Germany, Greece, Hungary, Iceland, Ireland, Italy, Luxembourg, the Netherlands, Norway, Poland, Portugal, Slovakia, Spain, Sweden, Switzerland, Turkey, the United Kingdom, Japan, South Korea, Australia, and New-Zealand). This OECD is an organization for economic cooperation development. World net electricity generation increases by 77 percent from 18.0 trillion kilowatt hours in 2006 to 23.2 trillion kilowatt hours in 2015 and 38 trillion kilowatt hours in 2030. Although the current economic downturn is expected to dampen electricity demand in the near term, the *IEO2009* reference case assumes that growth in electricity demand will return to trend after 2010 [1]. In general, the growth in OECD countries, where electricity markets are well established and consuming patterns are mature, is slower than in the non-OECD countries, where a large amount of potential demand remains unsatisfied. In summary, 3.5 percent per year is the average increment of the total net generation in the non-OECD

countries, with comparison of 2 percent per year as the average increment of the OECD nations. The industrial sector uses more energy than any other end-use sector. Currently, it consumes about one-half of the world's total delivered energy. Energy is consumed in the industrial sector by a diverse group of industries including manufacturing, agriculture, mining, and construction, and for a wide range of activities, such as processing and assembly, space conditioning, and lighting. Worldwide, industrial energy consumption is expected to grow from 0.051 quadrillion KWh in 2006 to 0.072 quadrillion KWh in 2030 [1].

1.2 GROWTH OF ENERGY IN SAUDI ARABIA

Growth of energy in Saudi Arabia has recorded over the last 25 years a rapid increase in electricity demand in Saudi Arabia due to rapid population growth and economic development. Statistical data of the growth of electricity generation and energy demand in Saudi Arabia shows a sharp increase in electrical energy consumption with an average annual growth of 14.8%, Table 1.1 shows growth of electricity supply and demand in Saudi Arabia since 1978.

Table 1.1 Growth of electricity supply and demand in Saudi Arabia since 1978

Year (G)	Nominal generated capacity (MW)	Actual Gen. Capacity MW	Peak Load MW	Number of Customers (Thousands)	Generated Energy GWH	Sold Energy GWH	Industrial Consumption GWH	Average energy per consumer (kWh)
1978	2940	2368	2161	465	7148	6353	3140	13667
1979	4073	3213	2955	583	9723	8465	4064	14528
1980	5497	4129	3986	725	15183	13456	6643	18565
1985	14599	11857	9424	1586	30996	36111	9280	22773
1986	16762	13939	10252	1762	32782	40320	11586	22885
1987	17777	14763	10690	1902	37101	45796	12037	24072
1988	18215	14910	11202	2043	39607	48906	12443	23934
1989	18527	15212	11573	2154	41081	51531	12576	23928
1990	20194	16471	13069	2259	46164	55201	15450	24433
1991	20214	16459	12889	2367	45267	58972	16666	24916
1992	20733	16849	14389	2461	49863	63632	16993	25857
1993	20888	17051	16136	2588	54100	67437	18316	26060
1994	21415	17627	17387	2687	61738	74113	19083	27582
1995	21917	17544	17706	2815	69962	82198	20908	29195
1996	21910	17494	17995	2926	71946	85908	21388	29357
1997	23130	18805	19326	3036	75946	89641	22509	29522
1998	23204	19351	20236	3151	81079	92228	23422	29267
1999	24569	20266	21101	3257	86595	97050	25569	31324
2000	25995	22060	21673	3622	103547	114161	27657	31519
2001	27238	23230	23582	3792	111161	122944	28232	32422
2002	29610	25457	23938	4029	117864	128629	29319	31926

2003	31272	27018	26272	4247	128371	142194	33383	33481
2004	31889	27423	27847	4491	135812	145466	33058	32391
2005	33386	29051	29913	4727	150214	153283	33801	32427
2006	34439	30668	31240	4956	156119	163151	32549	32919
2007	36733	32957	34953	5182	165342	169780	30635	32763

Actual generation capacity has reached 33 GW in 2007, equal to 14 times that of 1978 level and generated electric energy has reached 165342 GWh in the year 2007, which is more than 23 times of power generated in 1978. The kingdom's peak load in 2007 was 34953 MW; which is equivalent to sixteenth times greater than that in 1978. The number of consumers increased eleven-fold during the same period, to about 5.2 million. Fig. 1.1 shows the annual growth of generating capacity and peak load in Saudi Arabia for the period from 1975 to 2002 and its forecast till 2023 [2].

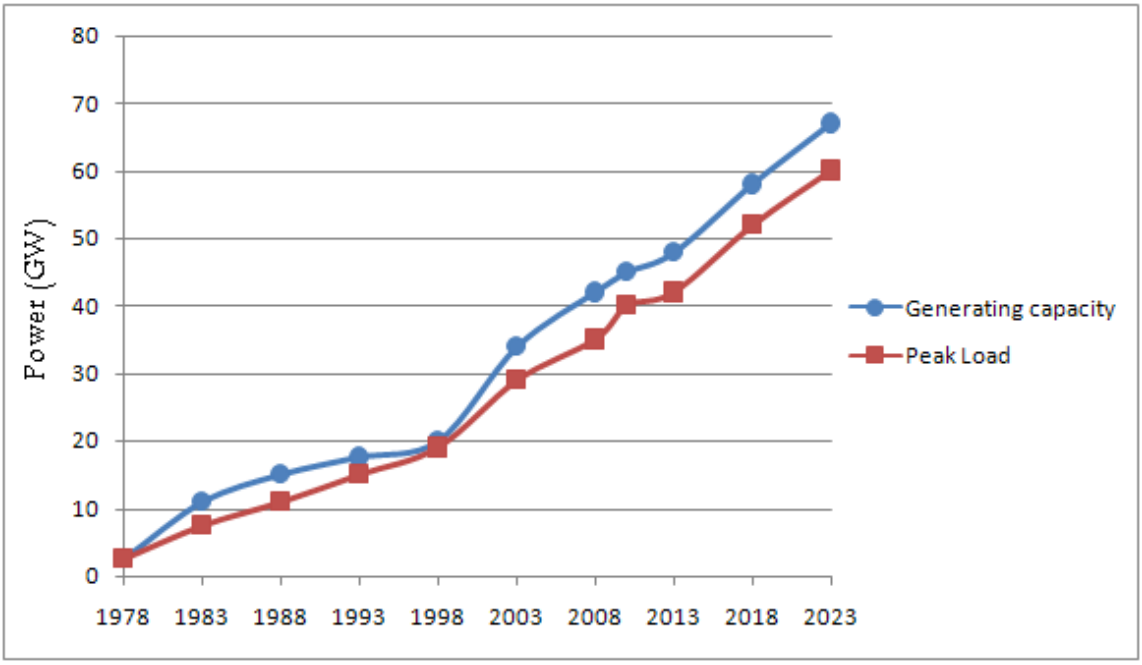

Figure 1.1 Annual growth of generating capacity and peak load in Saudi Arabia for the period from 1975 to 2023 [2]

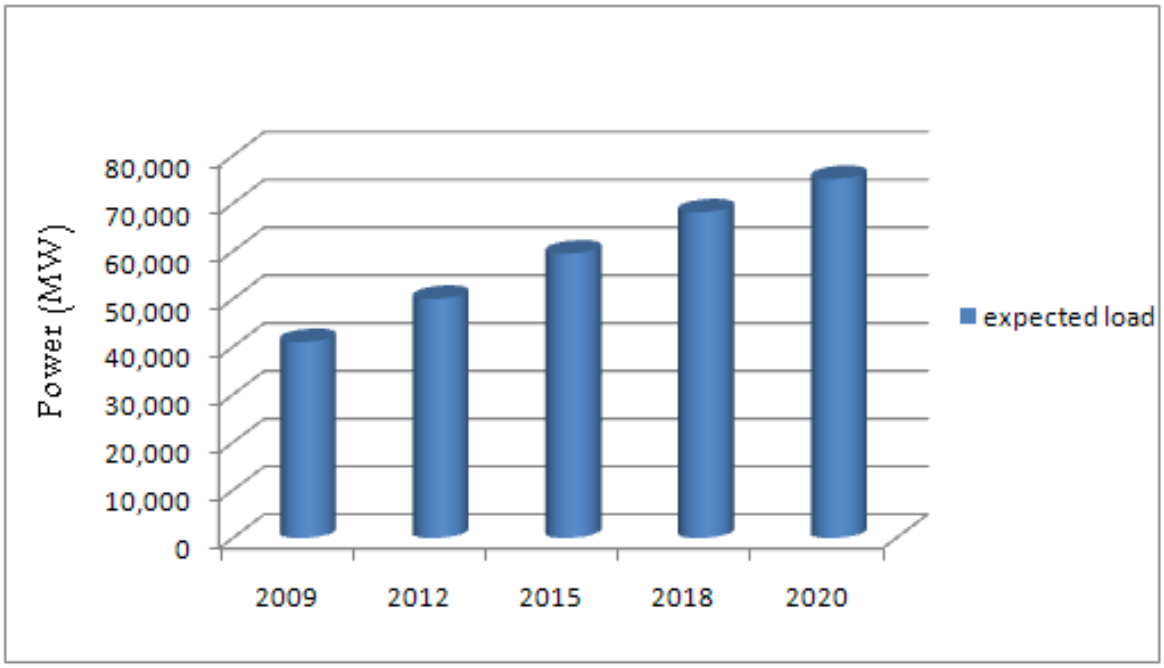

Figure 1.2 Expected load in Saudi Arabia [2]

1.3 ENVIRONMENTAL IMPACTS DUE TO FOSSIL FUEL COMBUSTION

The energy sector worldwide and in Saudi Arabia is largely dominated by the direct combustion of fuels, a process leading to large emissions of CO_2. The by-product of fossil fuel combustion (CO_2) results from the oxidation of carbon in fuels (in perfect combustion conditions, the total carbon content of fuels would be converted to CO_2). CO_2 emissions are consequently expected to continue their growth unabated, reaching 40.4 Gt (Giga tone) CO_2 by 2030. There is real evidence shows that most of the global warming observed over the last 50 years is related to human activities. This conclusion was adopted by the Intergovernmental Panel on Climate Change (IPCC) in its published assessment report [3]. Energy production and its usage have various environmental implications. In particular, fuel combustion is responsible for the largest share of global anthropogenic greenhouse gas (GHG) emissions. It has been significantly increasing compared to the rather steady level of the pre-industrial era (about 280 parts per million in volume (ppmv)). The 2004 concentration of CO_2 is (377 ppmv) with the fastest growth occurring in the most recent years (8 ppmv/year in the period 1999–2004). Comparable growth has occurred in levels of methane (CH_4) and nitrous oxide (N_2O). Even after stabilization of the atmospheric concentration of CO_2, surface air temperature is projected to increase for a century or more. The Intergovernmental Panel on Climate Change (IPCC) offers a broader picture for the climate impacts of the development of our society. Various scenarios based on different socioeconomic assumptions result in concentrations of CO_2 for the year 2100 ranging from 540 to 970 ppmv, as compared to the 280 ppmv of the pre-industrial era. For instance, in 2004, two sectors, electricity and heat generation

produced nearly two-thirds of the global CO_2 emissions. The emissions of these same sectors also increased at faster rates than global emissions (53% and 37%, respectively, versus the average 28%, between 1990 and 2004). Generation of electricity and heat was responsible in 2004, for 40% of the world total emissions, as compared to 26% in 1970. By 2030, the demand for electricity is projected to be almost twice as high as in 2004 [4].

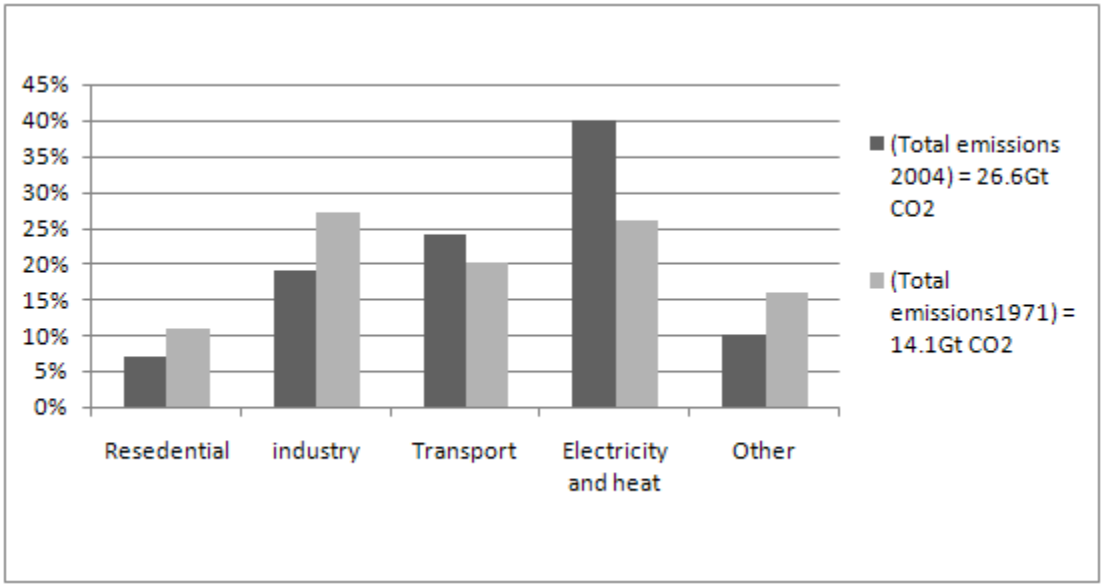

Figure 1.3 World CO_2 emissions by sector[4]

1.4 GREEN SOLUTIONS

Green solutions are energy which comes from natural resources such as solar energy, wind, tides, and geothermal energy which are renewable (naturally replenished). Recently, about 18.4% of global total energy consumption came from green solutions. New renewable (small hydro, modern biomass, wind, solar, geothermal, and bio fuels) are growing very rapidly. The share of new renewable in electricity generation is around 18.4%, with 15% of global electricity coming from hydroelectricity and 3.4% from others.

1.4.1 Wind Energy

Airflows can be used to run wind turbines. Modern wind turbines range from around 600 kW to 5 MW of rated power, although turbines with rated output of 3–5 MW have become the most common for commercial use. The power output of a turbine is a function of the cube of the wind speed. So, as wind speed increases, power output increases dramatically. Locations where winds are stronger and more constant such as offshore and high altitude sites are preferred locations for wind farms[5]. As clarified by Rehman and Ahmad[6], wind energy is applicable for specific regions, Yanbo and Dhahran, in Saudi Arabia. In general, availability of solar energy is higher than availability of wind energy in Saudi Arabia.

1.4.2 Solar Energy

Solar energy is by far the Earth's most available energy source, easily capable of providing many times the total current energy demand. As shown in Fig. 1.4, the average insolation showing land area (small black dots) required to replace the world primary energy supply with solar electricity. In general, insolation for most locations ranges from 150 to 300 W/m² or 3.5 to 7.0 kWh/m²/day. Based on these numbers, solar energy is one of the most promising green solutions, especially in Saudi Arabia [7].

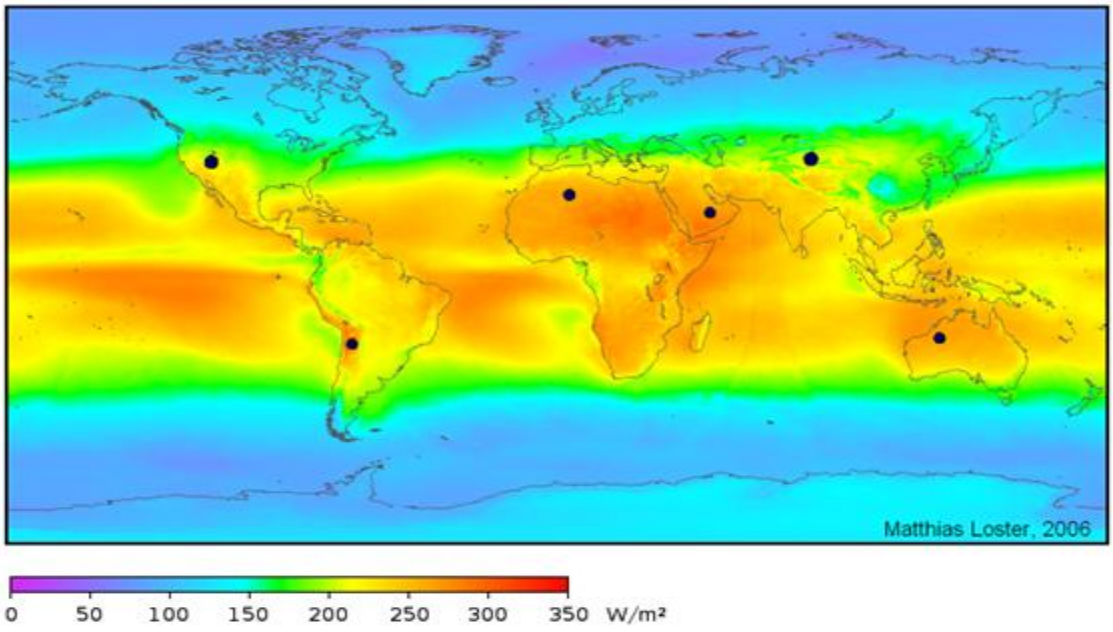

Figure 1.4 Solar radiation of world land [7]

There are two ways to make use of solar energy. The first way is Photovoltaic and the second way is solar thermal energy applications. Photovoltaic (PVs) are arrays of cells containing a solar photovoltaic material that converts solar radiation into direct current electricity. Materials presently used for photovoltaic include mono crystalline silicon, polycrystalline silicon, microcrystalline silicon, cadmium telluride, and copper indium selenide / sulfide.

Figure 1.5 Nellis Solar Power Plant at Nellis Air Force Base in the USA [7]

1.5 AVAILABILITY OF SOLAR ENERGY IN GULF COUNTRIES (GCC) & SAUDI ARABI

The area is wealthy in solar radiation. Table 1.2 shows that. On average, the total solar radiation for use PV is nearly 6 KWh/m^2/day and the direct solar radiation for use of solar trough concentrator is 4.5 KWh/m^2/day. Since, parabolic trough concentrates direct radiation only without diffused radiation. The GCC consumed nearly 400 TWh of electrical energy in 2006. This means that for an area of 10 km^2 (10 million m^2), with solar systems having efficiency of only 20%. We will be able to produce 4380 GWh, For 1000 km^2 area we will produce 438,000 GWh, which is small percent of the total GCC land area (GCC land area is 2,423,065 km^2) [8].

Table 1.2 Availability of solar energy in GCC [8]

Countries	Global solar radiation (KWh/m^2/day)	Direct normal solar radiation (KWh/m^2/day)
Bahrain	6.5	6.4
Kuwait	6.5	6.2
Oman	6.2	5.1
Saudi Arabia	7.0	6.5
United Arab Emirates	6.5	6
Qatar	5.6	5.5

CHAPTER 2

LITERATURE REVIEW

Due to availability of abundant amount of solar radiation in specific regions, there are many studies carried out by researchers to investigate the feasibility of conversion solar energy into electrical energy. Woditsch [9] carried out an economical study of PV cells. The study is based on the assumption of doubling the market volume every 4 years; accompanied with a reduction of cost 20% for every doubling. This study leads to cost reduction by 50% for the next decade, when growth rate is increasing in the same rate. On the other hand, Enermodal [10] made an economical study for parabolic trough collector similar to the study of Woditsch [9]. The result shows a cost reduction of 12% when doubling the market volume. This will lead to cost reduction of 40% in the next decade. Moreover, Quaschning[11] made an economical study for 61 sites around the world considering both PV and parabolic trough technology in solar thermal systems for electric generation. The study is based on economical basics, where cost assumptions were made for its current day's cost and expected cost in 10 years. The results revealed that parabolic trough type solar thermal power plants are more economical at sites with annual global irradiations of more than 1300 kWh/$m^2/year$ and 1600 kWh/$m^2/year$ for the next 10 years due to higher chance of cost reduction of PV cells. This conclusion was based on two considerations; the first one is cost reduction of PV cells and solar thermal systems. The second consideration is the variation of system efficiencies.

The solar thermal conversion into electric energy depends mainly on solar power concentration technology. The available concentrated solar power (CSP) technologies can be divided into four types which are solar tower, parabolic trough, Fresnel reflector, and dish solar collector. Table 2.1 shows a comparison among these different types of CSP technologies. Tables (2.2 - 2.5) show operational solar thermal power stations and Tables (2.6 - 2.8) show solar thermal power stations under construction. According to these CSP technologies, the actual output around the world till 2010 is 884 MW produced by parabolic trough, 37.5 MW produced by solar tower, 8.4 MW produced by Fresnel collector, and 5 MW produced by dish solar collector. On the other hand, the output distribution for the under construction plants is 1782 MW from parabolic trough, 388.4 MW from solar tower and 1 MW from Fresnel reflector.

Table 2.1 Comparison between different types of solar collector that might be integrated with power plant as concentrated solar power technologies (CSP)

Name of collector	**Picture**	**Annual solar Efficiency**	**Possible configurations**	**Temperature range**	**comments**	**Installed capacity** till 2009
Solar tower		15-25%.	-Heat pressurized air. -Direct steam generation. -indirect steam generation	Can reach T> 600 °C	-Uses huge land spaces -Difficult of reflector cleaning & absorber.	37.5 MW
Parabolic trough	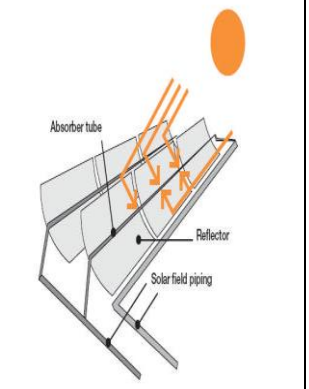	14-16%	-Heat pressurized air. -Direct steam generation. -indirect steam generation.	Can reach maximum T< 600 °C	-Can contribute with steam cycles of capacity from 5-200MW with efficiency 30-40%. -Difficult of reflector cleaning& absorber.	884MW
Linear Fresnel collector		10-12%	-Heat pressurized air. -Direct steam generation. -indirect steam generation.	60°C<T<250 °C	-Can contribute with steam cycles of capacity from 5-200MW with efficiency 30-40%. -Ease of reflector cleaning & absorber.	8.4 MW

Dish collector		29%	- Connected to sterling engine.	Can reach maximum T< 600 °C	-Uses sterling engine.	5MW

Table 2.2 Operational solar thermal power stations using solar power tower

Name	**Country**	**Location**	**Capacity (MW)**	**CSP technology**	**Information about plant**
PS20 solar power tower	Spain	Seville	20	solar power tower	Completed April 2009
PS10 solar power tower	Spain	Seville	11	solar power tower	World's first commercial solar tower
Sierra Sun Tower	USA	Lancaster	5	solar power tower	completed August 2009
Jülich Solar Tower	Germany	Jülich	5	solar power tower	Completed December 2008

Over all = 37.5 MW

Table 2.3 Operational solar thermal power stations using solar dish

Name	**Country**	**Location**	**Capacity (MW)**	**CSP technology**	**Information about plant**
Maricopa Solar	USA	Peoria, Arizona	5	Dish stirling	Completed January 2010

Over all = 5 MW

Table 2.4 Operational solar thermal power stations using solar Fresnel reflector

Name	Country	Location	Capacity (MW)	CSP technology	Information about plant
Kimberlina Solar Thermal Energy Plant	USA	Bakersfield, California	5	Fresnel reflector	AREVA Solar, formerly Ausra demonstration plant
Liddell Power Station Solar Steam Generator	Australia	New South Wales	2	Fresnel reflector	electrical equivalent steam boost for coal station
Puerto Errado 1	Spain	Murcia	4	Fresnel reflector	Completed April 2009

Over all = 8.4 MW

Table 2.5 Operational solar thermal power stations using solar parabolic trough

Name	Country	Location	Capacity (MW)	CSP technology	Information about plant
Solar Energy Generating Systems	USA	Mojave Desert California	345	Parabolic trough	Collection of 9 units
Solnova	Spain	Seville	150	Parabolic trough	Solnova 1 Solnova 3 completed May 2010 Solnova 4 completed August 2010
Andasol solar power station	Spain	Granada	100	Parabolic trough	Andasol 1 completed, 2008 Andasol 2 completed, 2009
Nevada Solar One	USA	Boulder City, Nevada	64	Parabolic trough	

Ibersol Ciudad Real	Spain	Puertollano, Ciudad Real	50	Parabolic trough	Completed May 2009
Alvarado I	Spain	Badajoz	50	Parabolic trough	Completed July 2009
Extresol 1	Spain	Torre de Miguel Sesmero (Badajoz)	50	Parabolic trough	Completed February 2010
La Florida	Spain	Alvarado (Badajoz)	50	Parabolic trough	completed July 2010
Yazd integrated solar combined cycle power station	Yazd	Iran	17	Parabolic trough	World's first solar combined cycle power plant
Archimede solar power plant	Italy	near Siracusa, Sicily	5	Parabolic trough	ISCC with heat storage Completed July 2010
Saguaro Solar Power Station	USA	Red Rock	1	Parabolic trough	
Keahole Solar Power	USA	Hawaii	2	Parabolic trough	

Over all = 884 MW

Table 2.6 Solar thermal power stations under construction using solar power tower

Name	Country	Location	Capacity (MW)	CSP technology	Information about plant
Ivanpah Solar Power Facility	USA	San Bernardino County, California	370	solar power tower	
Gemasolar, former Solar Tres Power Tower	Spain	Fuentes de Andalucia (Seville)	17	solar power tower	with 15h heat storage
THEMIS Solar Power Tower	France	Pyrénées-Orientales	4	solar power tower	Hybrid solar/gas electric power, using solar energy to heat the air entering a gas turbine

Over all = 388.4 MW

Table 2.7 Solar thermal power stations under construction using solar dish

Name	Country	Location	Capacity (MW)	CSP technology	Information about plant
Renovalia	Spain	Albacete	1	Dish stirling	

Over all = 1MW

Table 2.8 Solar thermal power stations under construction using parabolic trough

Name	Country	Location	Capacity (MW)	CSP technology	Information about plant
Extresol 2-3	Spain	Torre de Miguel Sesmero (Badajoz)	100	Parabolic trough	with 7.5h heat storage
Andasol 3–4	Spain	Granada	100	Parabolic trough	with 7.5h heat storage
Palma del Rio 1, 2	Spain	Cordoba	100	Parabolic trough	with heat storage
Helioenergy 1, 2	Spain	Ecija	100	Parabolic trough	
Solaben 1, 2	Spain	Logrosan	100	Parabolic trough	
Valle Solar Power Station	Spain	Cadiz	100	Parabolic trough	with 7.5h heat storage
Termosol 1+2	Spain	Navalvillar de Pela (Badajoz)	100	Parabolic trough	
Helios 1+2	Spain	Ciudad Real	100	Parabolic trough	
Martin Next Generation Solar Energy Center	USA	Florida	75	ISCC, Parabolic trough	steam input into a combined cycle
Majadas de Tiétar	Spain	Caceres	50	Parabolic trough	
Lebrija-1	Spain	Lebrija	50	Parabolic trough	
Manchasol-1	Spain	Ciudad Real	50	Parabolic trough	
La Dehesa	Spain	La Garrovilla	50	Parabolic	

		(Badajoz)		trough	
Axtesol 2	Spain	Badajoz	50	Parabolic trough	
Arenales PS	Spain	Moron de la Frontera (Seville)	50	Parabolic trough	
Serrezuella Solar 2	Spain	Talarrubias (Badajoz)	50	Parabolic trough	
El Reboso 2	Spain	El Puebla del Rio (Seville)	50	Parabolic trough	
Moron	Spain	Frontera (Sevilla)	50	Parabolic trough	
Olivenza 1	Spain	Olivenza (Badajoz)	50	Parabolic trough	
Medellin	Spain	Medellin (Badajoz)	50	Parabolic trough	
Valdetorres	Spain	Valdetorres (Badajoz)	50	Parabolic trough	
Badajoz 2	Spain	Talavera la Real (Badajoz)	50	Parabolic trough	
Santa Amalia	Spain	Santa Amalia (Badajoz)	50	Parabolic trough	
Torrefresneda	Spain	Torrefresneda (Badajoz)	50	Parabolic trough	
La Puebla 2	Spain	La Puebla del Rio (Sevilla)	50	Parabolic trough	
Termosolar Borges	Spain	Borges Blanques (Lerida)	25	Parabolic trough	
Gemasolar,	Spain	Fuentes de	17	Parabolic	with 15h heat

former Solar Tres Power Tower		Andalucia (Seville)		trough	storage
Kuraymat Plant	Egypt	Kuraymat	20	ISCC, Parabolic trough	
Hassi R'mel integrated solar combined cycle power station	Algeria	Hassi R'mel	25	ISCC, Parabolic trough	
Beni Mathar Plant	Morocco	Ain Bni Mathar	20	ISCC, Parabolic trough	

Over all = 1782 MW

2.1 CONFIGURATIONS OF INTEGRATED SOLAR POWER PLANTS

There are different types of conventional thermal electric power plants. These power plants can be divided into three types. First type is gas turbine power plants (GT) that are based on Brayton cycle. The second type is steam turbine power plants (ST) that are based on Rankine cycle. The third type is combined cycle power plant (CC).

Electricity generation currently relies on fossil fuel, leading to waste of precious national resources and significant carbon emissions. In many countries where the solar energy is abundant resource, e.g., the sunbelt countries, Hybrid Concentrated Solar-Fossil fuel (HYCS-FF) thermal power plants is a promising solution for electricity generation. The same applies to many countries in the sunbelt where recent expansion in the utilization of natural gas for electricity generation has created a significant base for

introducing concentrated solar energy as a supplement. Expanding the rating of the existing natural gas powered fleet by adding a solar field to each plant wherever possible can increase the available base power with a relatively small investment. HYCS-FF thermal power plants reduce the need for thermal energy storage in traditional concentrated solar thermal plants, and result in dispatchable power on demand at lower cost than stand-alone concentrated thermal power and much cheaper than photovoltaic plants. This is because gas can be used when solar energy is not available to respond to demand. It is also noticed that in the sunbelt countries, e.g. Saudi Arabia, the peak of the electric demand is matching of the solar irradiation almost at the mid of the day due to the demand for the air conditioning. The fact that solar power is at its maximum at the same time of the day (and year) when peak demands are reached makes this solution ideal for “peak-shaving” instead of building a standby fleet for this purpose. Moreover, at the solar irradiation peak, the extra solar energy can be used to reform natural gas into syngas, which can be compressed and stored on location, to be used later as a supplement to natural gas. Storing energy in the chemical form is likely to be more compact than traditional molten based thermal energy storage, and is much cheaper than storing electricity, which is required if PVs are used. Integrating concentrated solar power technologies with the conventional thermal power plant technologies can be achieved in different configurations as outlined hereunder.

2.1.1 Configuration of Integrated Solar Gas Turbine

Integration of solar with gas turbine could be done by two ways. The first way is preheating compressed air before entering combustion chamber and the second way is solar reforming. Schwarzbözl, *et al.* [12] studied the integration of solar energy with three industrial gas turbine systems of power levels 1 MW, 5MW, and 15MW in two different locations (Seville in (Spain) and Daggett in (California, USA)) as shown in Figs. (2.1-2.4), temperature of air reached 800 ºC in all cases and 1000 ºC just in one case using solar tower receiver. Also, he used different solar fields' combination to optimize the cycle with solar energy technology. As support to study [12], Heller,*et al.* [13] designed, installed, and tested a solar powered gas turbine system capable of delivering pressurized air at 1000 ºC using solar tower system. The results showed that system would be a promising system in near future. Moreover, Alrobaei [14] conducted a simulation of concentrating solar cogeneration power plants (CSCPP), where parabolic trough is used as solar collector. The result shows the effectiveness of proposed CSCPP schemes especially, the integrated gas turbine solar cogeneration power plant (IGSCP) scheme seems to be an alternative of the most effective technologies in terms of technical, economical and environmental sustainability.

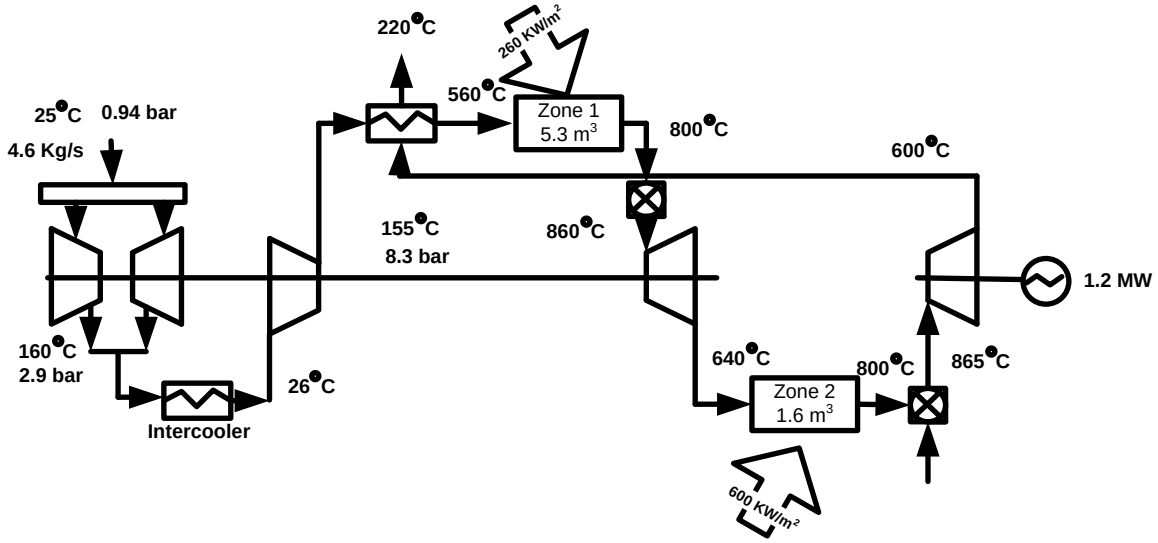

Figure 2.1 Solarized gas turbine prototype plant: Heron unit, 800°C location Daggett (reproduced from Ref. [12])

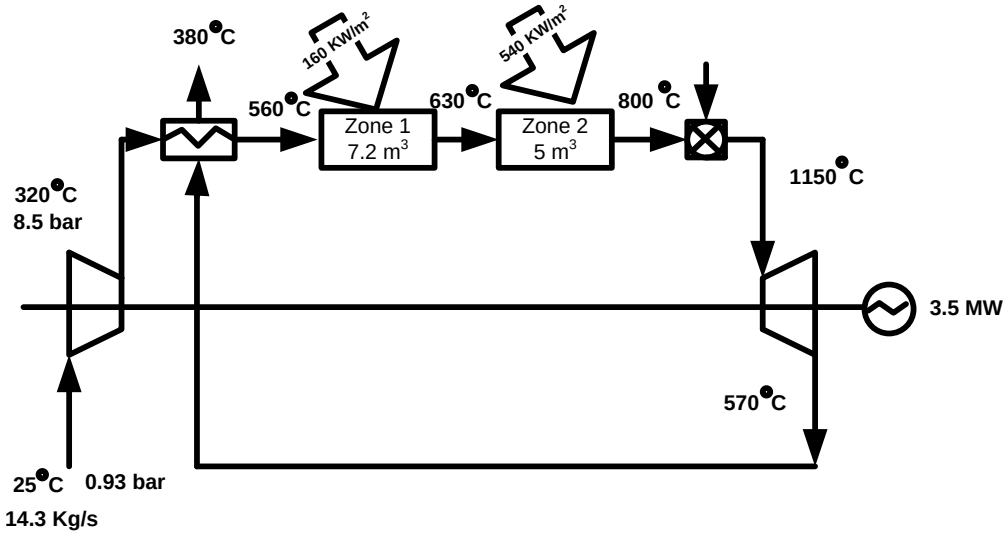

Figure 2.2 Solarized gas turbine prototype plant: Mercury unit, 800°C location Daggett (reproduced from Ref. [12])

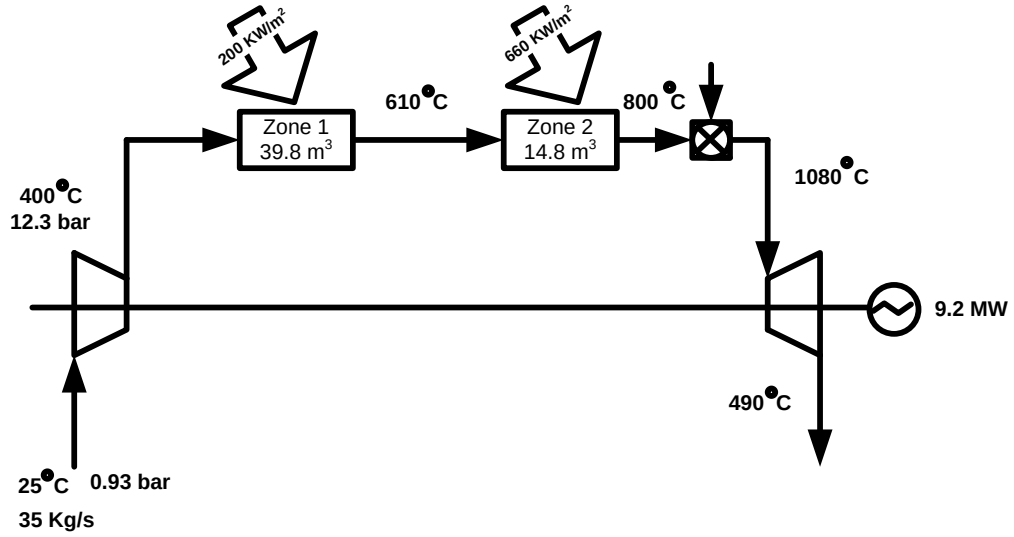

Figure 2.3 Solarized gas turbine prototype plant: PGT10 unit, 800°C location Daggett (reproduced from Ref. [12])

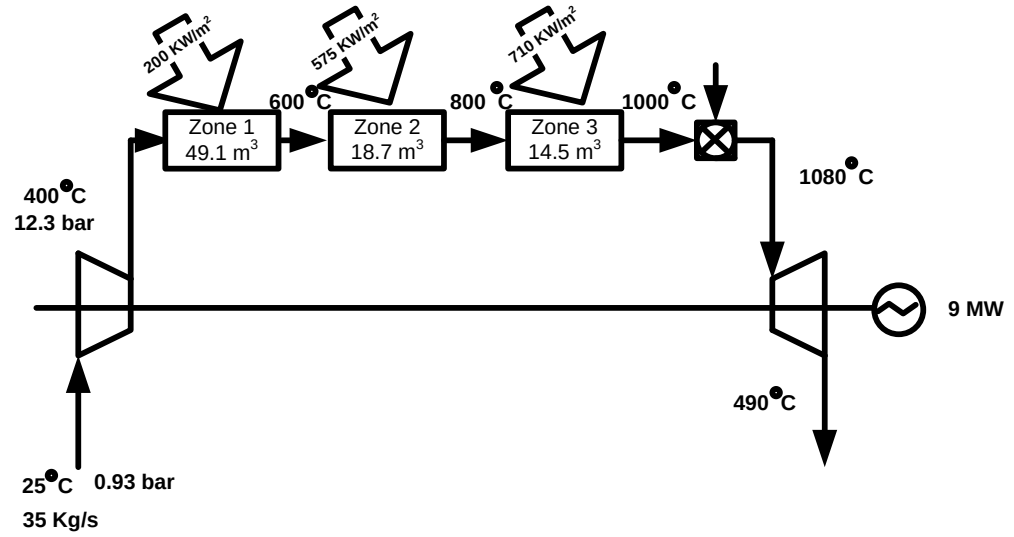

Figure 2.4 Solarized gas turbine prototype plant: PGT10 unit, 1000 °C location Daggett (reproduced from Ref. [12])

Schwarzbo¨zl et al [12] introduced the solar incremental electricity is defined as the annual amount of net electricity produced by the solar-hybrid plant compared to the pure fossil reference plant (i.e. same gas turbine system without solarization) using the same amount of fuel. The solar incremental electricity and all other figures of merit which are derived from the solar incremental electricity are given in Table 2.9.

The cost analysis showed total plant investment costs from 7000 €/kW down to below 1800 €/kW, depending on power level and solar share. Solar LEC represents how much does the cost of produced energy due to the solar technology existence which is about 13 €cent/kWh up to 90 €cent/kWh. Using the cost reduction potential that lies in combined design, construction and operation of multiple distributed plants leads to solar LEC of below 10 €cent/kWh for an electric power level of 16.1 MW, as shown in Fig. 2.5. So, the solar-hybrid gas turbine power technology shows interestingly low cost for solar produced bulk electricity at a moderate power level. The values predicted for ISCC plants can be reached, but with a smaller system (e.g. 16 MW instead of 310 MW) and with a significantly higher solar share (28% instead of 9%).

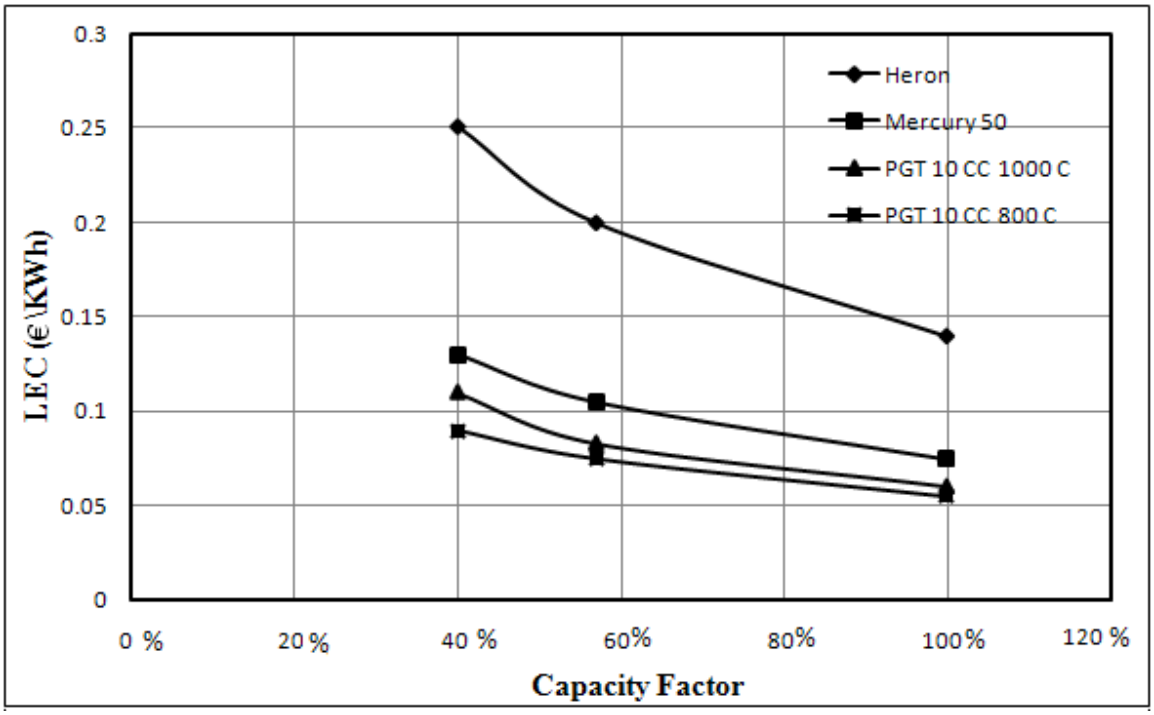

Figure 2.5 Total LEC as a function of capacity factor for 2nd generation plant in Daggett (reproduced from Ref. [12])

Where: capacity factor is operation load during day time which ranges from partial load 40% up to full load 100%.

2.1.2 Configuration of Integrated Solar Steam Turbine

There are two ways to integrate solar energy with steam power plants. The first way is direct steam generation (DSG), where water is used as a working fluid in solar field. The second way is indirect steam generation, where heat transfer fluid instead of water is used to transport heat from solar field to the power plant. Odeh, *et al.* [15] presented a model of a solar electric generation system (SEGS). This model is developed in order to study different configurations of a DSG under Australian weather conditions. Three configurations were studied. The first configuration utilized the solar energy for the boiling process, where water is provided from the feed water heater to the solar collector

as shown in Fig. 2.6. In the second configuration, the solar energy is used for the preheating process, where solar collectors just preheat water before entering steam boiler as shown in Fig. 2.7. In the third configuration, the solar energy is utilized for both preheating and boiling process as shown in Fig. 2.8. In conclusion, all arrangements are below the specific fuel value of the conventional cycle which is 0.21 Kg/KWh, as shown in Fig. 2.9. Moreover, Yang, *et al.* [16] made a study based on integration of parabolic trough collectors with a conventional coal-fired power unit. There are two basic different configurations have been used. The first configuration is introducing water form condensate pump outlet into solar collector; as shown in Fig. 2.7. The second configuration is introducing water from feed water pump outlet into solar collector; as shown in Fig. 2.6. In conclusion, there is an opportunity to reduce levelized electricity cost while the cost of solar collector is reducing, as shown in Fig. 2.10. The cost of solar collector can be reduced from time to time due to improving studies which take care of solar collector performance and its cost.

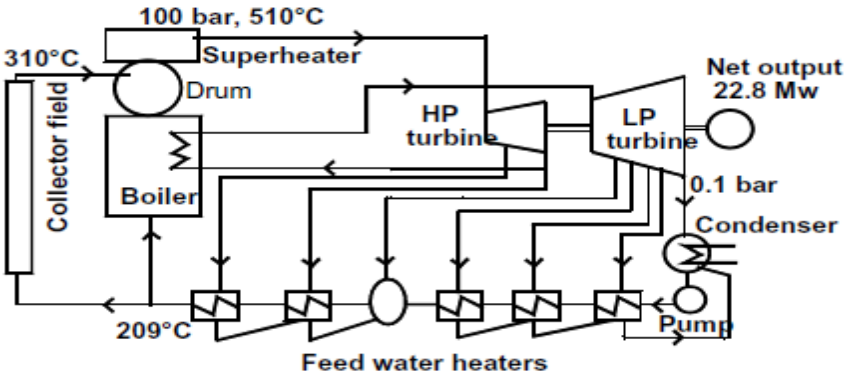

Figure 2.6 Using solar for boiling process [15]

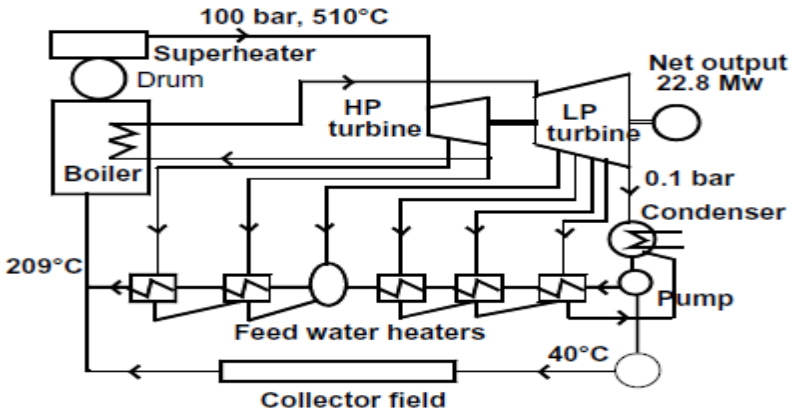

Figure 2.7 Using solar for preheating process [15]

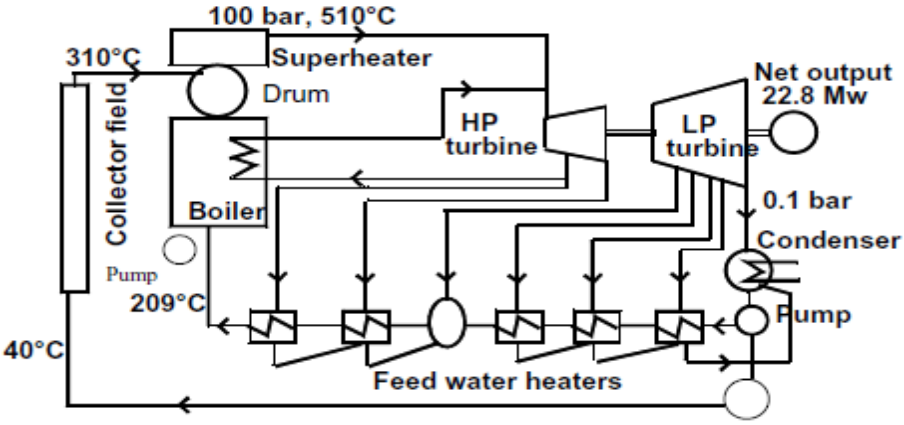

Figure 2.8 Using solar for preheating-boiling process [15]

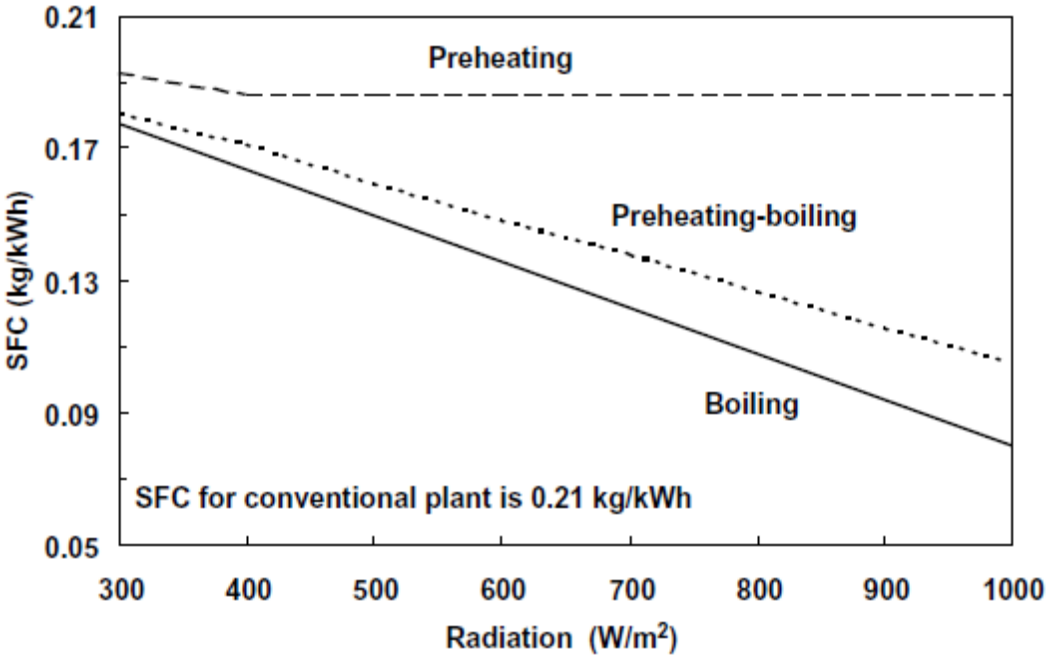

Figure 2.9 Specific fuel consumption of three collector field–power house arrangements [15]

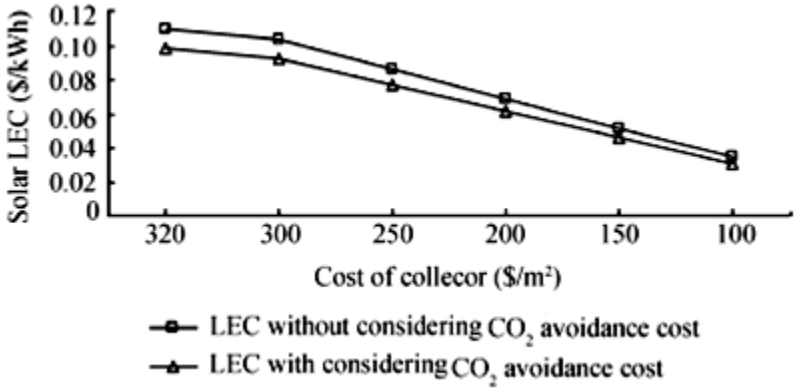

Figure 2.10 LEC variation with reducing the cost of solar collectors [16]

Table 2.9 Figures of merit

Figure of merits	Variant (1)	Variant (2)	Ref. used
Over all plant efficiency	$\eta_{ref} = \frac{P_{el,ref}}{\dot{m_{fuel}} * lHV}$ [17]		[17]
net incremental solar efficiency	$\eta_{net\_incr\_solar} = \frac{P_{el,hybrid} - \eta_{ref} * \dot{m_{fuel}} * lHV}{P_{th,solar}}$ [17],[46],[16]	$\Delta_{\eta_{solel}} = \frac{E_{el,hybrid} - \eta_{ref} * E_{fuel,hybrid}}{A_{Hel.field} * \int DNI(t).dt}$ [12]	[12], [16], [17], [46]
instantaneous net electrical solar fraction (Share)	$X_{net,elec,solar} = \frac{\eta_{net\_incr\_solar} * P_{th,solar}}{P_{el,net}}$ [17],[46]	$\Delta_{E,el} = E_{el,hybrid} - \eta_{ref} * E_{fuel,hybrid}$ $\Delta_{solarshare} = \frac{\Delta_{E,el}}{E_{el,hybrid}} = \frac{E_{el,hybrid} - \eta_{ref} * E_{fuel,hybrid}}{E_{el,hybrid}}$ [12]	[12], [17], [46]
Annual solar share	$SS = 1 - \frac{(annual\ fuel\ consumption/KWh)_{ISCCS,SEGS}}{(annual\ fuel\ consumption/KWh)_{CC\ reference}}$ [17]		[17]

Incremental co_2 avoidance	$\Delta_{co_2} = \left(\frac{E_{el,hybrid}}{\eta_{ref}} - E_{fuel,hybrid}\right) * f_{co_2}$ [12]		[12]
Levelized cost (LEC,ref)	$LEC = \frac{I_{PV}^{tot} * fcr + OM_{PV}^{ann} + F_{PV}^{ann}}{E_{gen}^{ann}}$ [17]		[17]
Solar levelized electricity cost (LEC,solar)	$Solar, LEC = \frac{Cost_{solar\ field}}{W_s}$ [17]	$\frac{levelizedTRR - \left(E_{el,hybrid} - \Delta_{E,el}\right) * LEC_{ref}}{\Delta_{E,el}}$ [12]	[12], [17]

Note :

There is no difference between variant (1) and variant (2) as proved in Appendix C

2.1.3 Configuration of Integrated Solar Combined Cycle

Integration of solar with combined cycle could be carried out by two ways. The first way is direct steam generation (DSG) as shown in Fig. 2.11. The second way is indirect steam generation as shown in Fig. 2.12. Dersch, *et al.* [17] studied three types of electrical generation systems which are integrated solar combined cycle (ISCCS) system, solar electric generation system (SEGS), and combined cycles (CC). This study has been done by proceeding two ways. The first way is two meet a scheduled load where supplementary firing is needed, because the power plants should be able to follow a load curve even in times of low or without insolation. The second way is solar dispatching (Free load). This study is accomplished in two different sites Barstow in California and Tabernas in Spain where they have different solar radiation. In conclusion, solar LEC for two ways are shown in Fig. 2.13 and Fig. 2.14 using figures of merit which are given in Table 2.9.

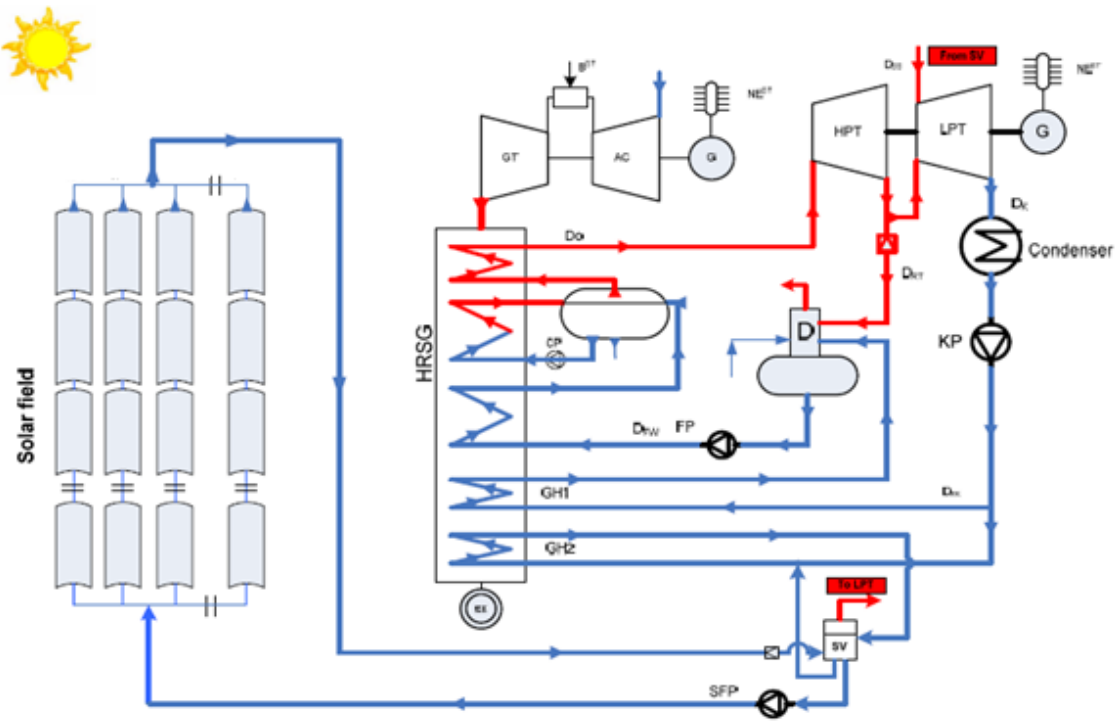

Figure 2.11 Proposed plant in Libya, Gamal Elsaket [18]

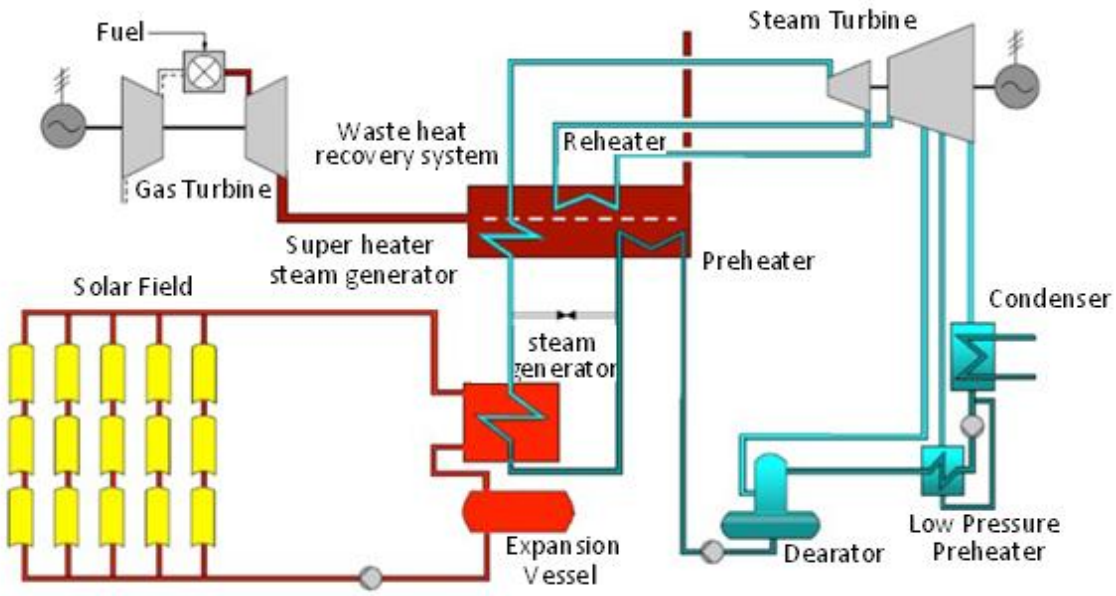

Figure 2.12 Indirect steam generation for combined cycle

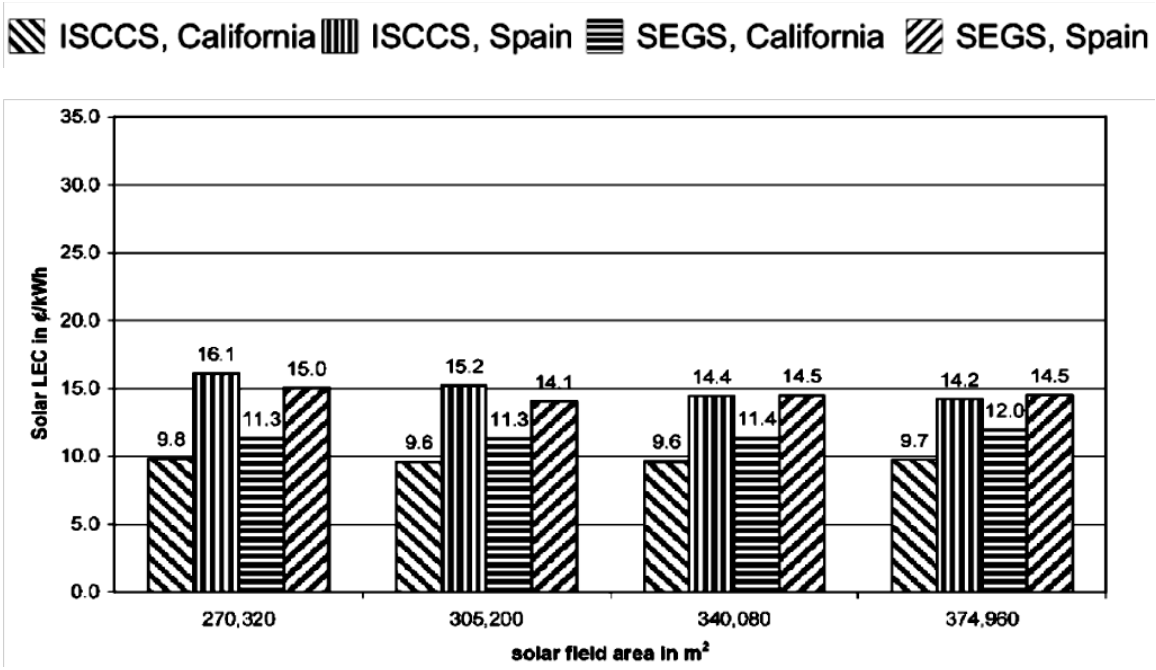

Figure 2.13 Solar LEC for different sites, plant configurations, operation modes and solar field areas for solar dispatching [17]

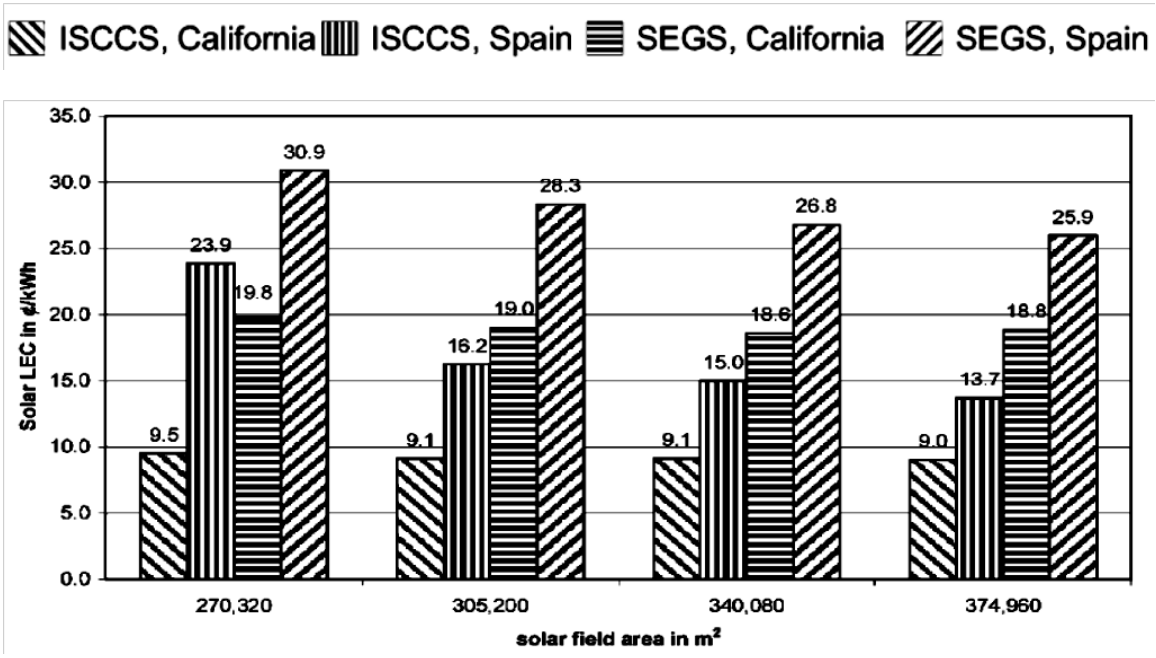

Figure 2.14 Solar LEC for different sites, plant configurations, operation modes and solar field areas for scheduled load [17]

As shown in Fig. 2.13 and Fig. 2.14, solar LEC is lower for ISCCS in scheduled load operation than in solar dispatching operation mode in most of the cases. Elsaket [18] made a list of projects and studies related to this topic, which are organized in Table 2.10. Also, Charles and Davis, et al. [19] presented Nine large commercial scale existing solar power plants; the oldest of which has been operating in California's Mojave desert since 1984. These plants continue in operation, range in size from 14 - 80 (MWe) and represent a total of 345 MWe of installed electric generating capacity. Mills [20] mentioned the linear Fresnel reflector (LFR) delivers beam to electricity annual efficiency between 10% to 12% and 14% to16% for a trough collector. Mills, ***et al.*** [21] presented a proposal to serve Liddell coal fired power station. The solar array contains CLFR technology. This configuration type will be a direct steam generation system, where 5MWe will be provided as a trial, and then 20MWe will be provided later on. The target of this proposal is to reduce the levelized cost by using existing generation infrastructure and to maximize greenhouse gas savings by directly offsetting coal usage. In conclusion, electricity cost is estimated to be about $A0.07 per kWh. Furthermore, Mills, ***et al.*** [22] made design of a large 240 MWe pure solar storage plant which based on compact linear Fresnel reflector (CLFR).

Table 2.10 Early solar thermal power plants [18]

Name	Location	Size (MW)	Type	Start – up date	Funding
Aurelios	Adrano, Sicily	1	Tower, Water-Steam	1981	European Community
SSP/CRS	Almeria, Spain	0.5	Tower, Sodium	1981	8 European countries & USA
		0.5	Trough, Oil		
Sunshine	Nio, Japan	1	Tower, Water-Steam	1981	Japan
Solar one	California, USA	10	Tower, Water-Steam	1982	US Dept. of Energy& utilities
Themis	Targasonne, France	5	Tower, Molten Salt	1982	France
CESA-1	Almeria, Spain	1	Tower, Water-Steam	1983	Spain
MEGS-1	Albuquerque, USA	0.75	Tower, Molten Salt	1984	US Dept. of Energy & utilities
SEGS-1	California, USA	14	Trough, Oil, Oil Storage	1984	Luz (private company)
Vanguard-1	USA	0.025	Dish	1984	Advanco Corp
MDA	USA	0.025	Dish	1984	McDonnell-Douglas
C3C-5	Crimea, Russia	5	Tower, Water-Steam	1985	Russia

2.2 OPTIMIZATION

There are many studies available in the public literature pertinent to the optimization of conventional thermal power plants. Some of these optimization studies were devoted to the optimization gas turbine power plants [23-27]. Examples of optimization of steam cycles can be found in [28-30]. Optimization of combined cycle was handled by [31-36]. The present thesis is focusing on the optimization studies for integrated solar-fossil fuel power plants. This topic can be subdivided into three main divisions. The first one is optimization studies related to system (configuration). The second divesion is optimization studies related to size of plant. Finally, optimization studies related to components of the system.

2.2.1 Optimization Studies Related to System or Configuration

Lovegrove, *et al.* [37] conducted experiments on solar driven ammonia based on closed loop thermo chemical energy storage system where solar energy is collected from dish concentrator. Results show that electrical power potential from ammonia synthesis reactors can be maximized through appropriate choice of operating temperatures and the system efficiency will be 53%. Kane, *et al.* [38] presented modeling and thermodynamic optimization based on a pinch technology approach that is developed for the synthesis design and operation of advanced solar-fossil combined power plants. This study is realized in two phases. In the first phase, a mixed approach, based on pinch technology principles coupled with a mathematical optimization algorithm, is used to minimize the heat transfer exergy losses in the steam generators. In the second phase, an economic analysis based on the Levelized Electricity Cost (LEC) approach was carried out for the configurations, which provided the best concepts during the first phase. Results reflected

future of these hybrid solar thermal power plants which could be competitive against conventional power plants. Dersch, *et al.* [17] made a comparison based on the economic and performance between three types of electrical generation systems which are integrated solar combined cycle (ISCCS) system, solar electric generation system (SEGS), and combined cycles (CC). This is done by varying percentage of solar share. Results revealed that ISCCS has the highest efficiency as shown in Fig. 2.15 where the fuel based net electric efficiency is defined as net electric output of the plant divided by fuel mass flow times LHV. In addition, it has lower cost per KWe than SEGS (operated system only by solar without any fossil fuel back up).

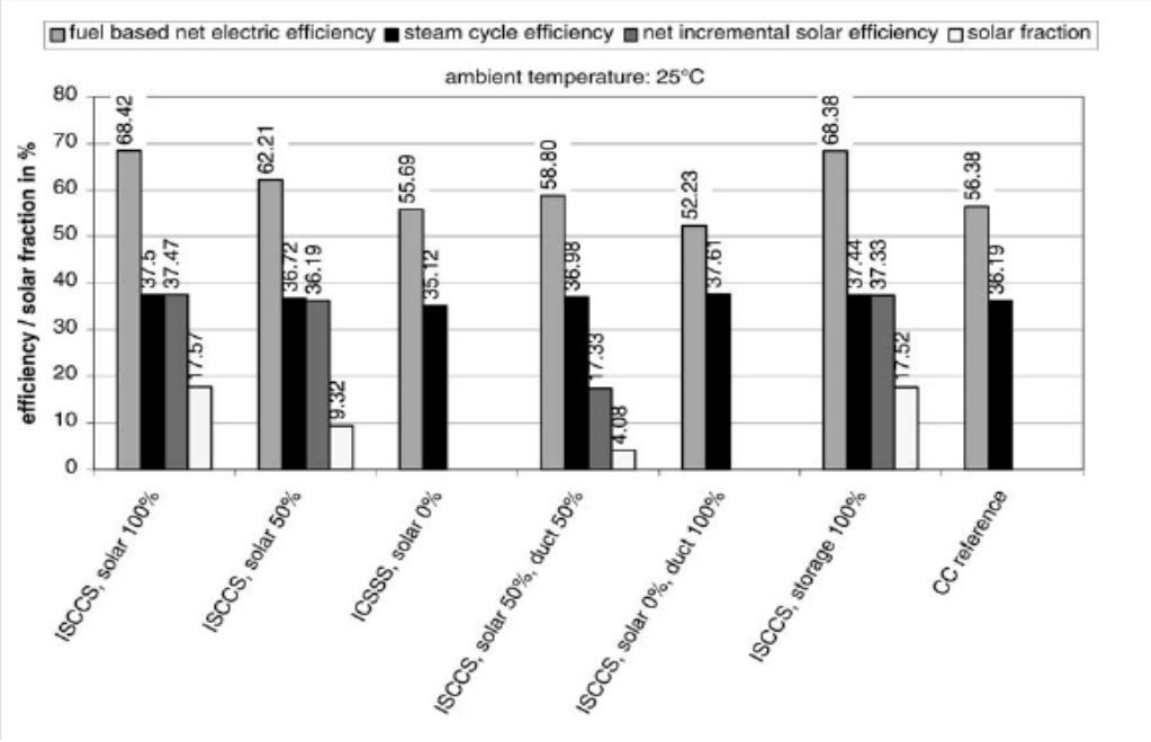

Figure 2.15 Instantaneous efficiencies and solar fraction for different systems of power plant [17]

Blanco, *et al.* [39] mentioned that parabolic troughs and linear Fresnel systems can be coupled to steam cycles of 5 to 200 MW of electric capacity with thermal cycle efficiencies of 30 – 40 %. Power produced by CSP technology is already a reality in countries such as Spain and it could cover the 14% of the electricity demand of MENA (Middle East and North African) countries by 2025; by 2050 it could become the dominating power source in the region with a share of 57% and an estimated energy cost in the range of 8 c€/kWh to 15 c€/kWh. Lewandowski and Simms [40] made a comparison between linear Fresnel lens and parabolic trough. This comparison based on the performance of collectors and on the documented costs of those collectors at that era. Results indicate that the Fresnel lens systems have a levelized energy cost about one-third less than the parabolic trough systems. This is primarily due to less expensive concentrators. Odeh, *et al.* [15] evaluated solar energy contribution and specific fuel consumption of the auxiliary gas fired boiler. In conclusion, the best process of SEGS is boiling process because the boiling process has the lowest specific fuel consumption among the three solar powered configurations. In summary of Yang, *et al.* [16] study, the second configuration is the best. Since, it has high efficiency and low levelized cost (LEC). Eck and Zarza [41] presented a comparative study between cycles operated by saturated steam turbine and superheated turbine using parabolic trough solar collector as direct steam generator. This study has been done based on economical and performance principles. Results revealed that the saturated turbine gives annual net electricity production 4% higher than production of the super-heated turbine. On the other hand, the initial investment cost of the saturated turbine is higher by 5% than the superheated turbine. In addition, it has higher operation and maintenance (O&M) cost than the

superheated turbine. A succession of three commission funded projects, DISS, DISS-2, and the INDITEP projects have been concentrated efforts on research related to direct steam generation in the absorber pipes of parabolic trough collectors. In summary, results show this research could lead to 26% reduction in the cost of the electricity produced [42]. Zarza, *et al.* [43] presented a conceptual design of the first solar power plant using direct steam generation (DSG) in a parabolic-trough solar field. Solar field produces 410°C and 70 bar superheated steam delivering a power output of 5 MW. Morrison, *et al.*[44] made a study using the compact linear Fresnel reflector (CLFR) in a solar array connected with Stanwell coal fired power station. The result of this configuration is considered very effective based on the cost of production and performance as compared to solar collector (LUZ LS3) array, which used as parabolic trough in majority of solar thermal power plants.

2.2.2 Optimization Studies Related to Size of Plant

There are many studies in the literature that reported the optimization of solar hybrid-fossil fuel power plants. Schwarzbözl, *et al.* [12] made an optimization based on performance and an economy of three power levels 1 MW, 5MW, and 15MW. Results reveal that hybrid system is economically feasible if power levels below 10 MWe and gas turbine systems are mainly used for decentralized power generation with cogeneration of heat or cooling power. Montes, *et al.* [45] studied the influence of the solar multiple on daily operation, annual performance, and economy of a direct steam generation (DSG) parabolic trough power plants. Results revealed that levelized cost of electricity was growing up while solar multiple of the power plant was increasing. On the other hand, the annual fuel consumption was reducing while solar multiple was increasing due to the

thermal power fractions from the solar field and the storage became greater. Hong, *et al.* [46] proposed a new solar thermal power cycle with the integration of middle-temperature solar thermal energy and methanol decomposition which is based on parabolic trough concentrator. Results revealed that configuration is effective if and only if turbine inlet temperature is 1300°C, and then the net solar-to electric conversion efficiency could be 35% with a 220 °C as collector temperature and the exergy loss of combustion could be reduced by about 7%. Moreover, the exergy efficiency of the specified cycle could be higher by about 6% than gas turbine combined cycle.

2.2.3 Optimization Studies Related to Component of The System

Segal and M. Epstein [47] made an optimization of a solar central receiver power plant parameters using thermodynamic principles, where solar system based on solar tower receiver. So, there are three parameters control the optimization which are the heliostat field and tower, the receiver and its secondary concentrator, and the power block. It is obvious in this study; the maximum overall efficiency of the system is reached at about 1600 K with an average field density of 35%. Imenes, *et al*. [48] proposed a new strategy by the collected beam is split into optimized components for two or more spectral receivers. This could be achieved based on flux mappings which are produced by ray tracing methods for a multi-tower solar array central receiver system in Australia. Moreover, there are many of studies such as Martínez and Almanza[49] who studied the temperature profile around the absorber tube of a parabolic trough concentrator with low fluid flow of water under saturated and low pressure conditions by keeping feed flow as the control variable and solar irradiance as the restriction variable. In summary, theoretical analysis is agreed very well with experimental analysis.

2.3 EXAMPLES OF E XISTING PLANTS AROUND THE WORLD

As shown in Table 2.11, there are different available plants around the world such as Crosbyton solar project in TX using hemispherical bowl collectors which installed over 308 m^2 to produce 225 KWe, where maximum exit temperature is 649°C. It operates with these conditions at steam turbine inlet (538 °C and 6.2 MPa). Moreover, international energy project in Almeria, Spain, has 3 projects. The first one is using 1-Axis parabolic trough collectors which installed over 2674 m^2 to produce 500 KWe, where maximum exit temperature is 295°C. It operates with these conditions at steam turbine inlet (285 °C and 5 MPa) with 114 m^3oil storage. The second project is using 2-Axis parabolic trough collectors which installed over 2698 m^2 to produce 500 KWe, where maximum exit temperature is 295°C. It operates with these conditions at steam turbine inlet (285 °C and 5 MPa) with 114 m^3oil storage. The last one is using central receiver collectors which installed over 3700 m^2 to produce 517 KWe, where maximum exit temperature is 530°C. It operates with these conditions at steam turbine inlet (510 °C and 10 MPa) with Liquid sodium thermal storage. In addition, 10 MWe Pilot plant in Barstow using central receiver collectors which installed over 72611 m^2 to produce 10 MWe, where maximum exit temperature is 516°C. It operates with these conditions at steam turbine inlet (510 °C and 16.4 MPa) with 3340 m^3 of rock-oil-sand thermal storage. Now, I will touch modern projects such as Kuraymat Plant in Egypt. This plant is designed as integrated solar combined cycle (ISCC) using trough solar technology to produce 14.3% from the total output which equals 140 MWe. Solar contribution is providing energy into evaporator in HRSG to increase steam quantity. The same idea has been used in Morocco and Algeria using trough solar technology in Ain Beni Mathar

plant to produce 4.25% from total output which equals 472 MWe in Morocco, and 19.25% as solar contribution from total output which equals 130 MWe in Hassi R'Mel plant in Algeria. In addition, Iran started installation process of Yazd plant using trough solar technology to produce 15.6% from the total output which equals 430 MWe, where solar field produce hot streams to preheat steam before going into super heater section. Also, Agua Prieta plant in Mexico using trough solar technology to produce 6.5% from the total output which equals 480 MWe, where the HTF is used to generate high-pressure superheated steam. Moreover, USA has many projects distributed in different states such as Victorville and Palmdale in California using trough solar technology to produce 9% from the total output which equals 563 MWe in Victorville and 12% from the total output which equals 555 MWe in Palmdale (all these informations are organized nicely in Table 2.12. As mentioned before HTF can be water or different type of working fluids. This point depends on steam generation method either direct or indirect. Table 2.13 shows different types of HTF with their properties. In addition, Table 2.14 presents cost for different storage media.

Table 2.11 Comparison between existing real solar power plants [50]

Project	Process	Collector type	Collector fluid	Maximum collector temperature	Collector area (m^2)	Cycle type	Cycle fluid	Turbine inlet conditions (^{0}C/Mpa)	Thermal storage (m^3)
Crosbyton solar project Crosbyton,TX	Electricity	Hemispherical bowl	Water steam	649	308	Rankine	Steam	538/6.2	None
International energy project Almeria, Spain	Electricity	1-Axis parabolic trough	Oil	295	2674	Rankine	Steam	285/5	114oil
	Electricity	2-Axis parabolic trough	Oil	295	2698	Rankine	Steam	285/5	114oil
	Electricity	Central receiver (solar tower)	Sodium	530	3700	Rankine	Steam	510/10	Liquid sodium
10MWe Pilot plant Barstow , CA	Electricity	Central receiver (solar tower)	Water steam	516	72611	Rankine	Steam	510/16.4	3340 rock-oil-sand

Table 2.12 Available integrated solar combined cycles (no thermal storage) [51]

ISCC Project	Location	Solar Technology Plant	Output, MWe	Solar Contribution , MWe	Solar MWe / Output Mwe (%)
Kuraymat	Egypt	Trough	140	20	14.3
Victorville	California	Trough	563	50	8.88
Palmdale	California	Trough	555	62	12
Hassi R'Mel	Algeria	Trough	130	25	19.23
Yazd	Iran	Trough	430	67	15.6
Martin	Florida	Trough	3,705	75	02
Agua Prieta	Mexico	Trough	480	31	6.46
Ain Beni Mathar	Morocco	Trough	472	20	4.24

Where, the solar contribution is at the design conditions.

Table 2.13 Properties of different Heat transfer fluid (HTF) [52]

Fluid	Application temperature (°C)	Properties
Synthetic oil, e.g., VP-1 Biphenyl diphenyloxide	13–395	Relatively high application temperature, Flammable
Mineral oil, e.g., Caloria	-10–300	Relatively inexpensive, flammable
Water, pressurized, 1glycol	-25–100	Only low-temperature IPH applications
Water/steam	0–>500	High receiver pressure required, thick wall Tubing
Silicon oil	-40–400	Odorless, nontoxic, expensive, flammable
Nitrate salt, e.g., HITEC XL	220–500	High freezing temperature, high thermal stability, corrosive
Ionic liquids, e.g., C8mimPF6	-75–416	Organic methyl-imidazole salts, good thermal properties, very costly, no mass Product
Air	-183–500	Low energy density, only special IPH Applications

Table 2.14 Cost of different thermal storages [53]

Storage medium	Heat capacity (kWht/m^3)	Media cost ($/kWht)
Synthetic oil	57	43
Silicone oil	52	80
Nitrite salts	76	24
Nitrate salts	83	16
Carbonate salts	108	44
Liquid sodium	31	55

CHAPTER 3

OBJECTIVES

The main objective of this thesis is to develop a thermo-economic mathematical model for the hybrid solar fossil fuel combined cycle. This model will be used to analyze the thermodynamic performance of the plant under Saudi Arabia weather conditions. In this regard, a computer simulation code will be developed using the available software (e.g. EES). This simulation code will be validated using the results available in the literature. The validated code will be used for thermo-economical evaluation of different conceptual designs of the integrated (hybrid) solar fossil fuel combined cycle. Design modifications will be suggested for optimal operation based on thermo-economic analysis.

The specific objectives are:

1- To develop a mathematical model for the cycle on component level and cycle level integration.

2- To develop a simulation code for the hybrid cycle utilizing available soft wares such as EES, Thermo-flex.

3- To utilize the developed code to size, analyze and optimize the hybrid cycle for different integration configurations with different percentage of solar share under Saudi Arabia weather conditions.

CHAPTER 4

APPROACH

The main objective of this thesis is to develop a thermo-economical model to assess the performance of a hybrid solar/ fossil fuel combined cycle under the Saudi Arabia weather conditions. The approach to tackle this problem is as follows:

1- Conduct a literature survey to identify the different system or configurations.

2- Develop mathematical model based on thermodynamic analysis of each component of the cycle.

3- Integrate the component mathematical models to describe the performance of the complete plant.

4- Identify and apply the performance metrics including thermodynamics and economic metrics.

5- Assess the thermo-economic performance of each of the proposed configurations.

6- Identify the optimal configuration, its optimal design and optimal operating conditions and parameters.

4.1 SYSTEMS TO BE ANALYZED

This study focuses on the thermo-economic analysis of four different configurations. The main system is shown in Fig. 4.1. However, the 4 specific systems to be analyzed in this study are namely:

1- Reference combined cycle which is basically simple GT cycle with HRSG and Rankine cycle as shown in Fig. 4.1.

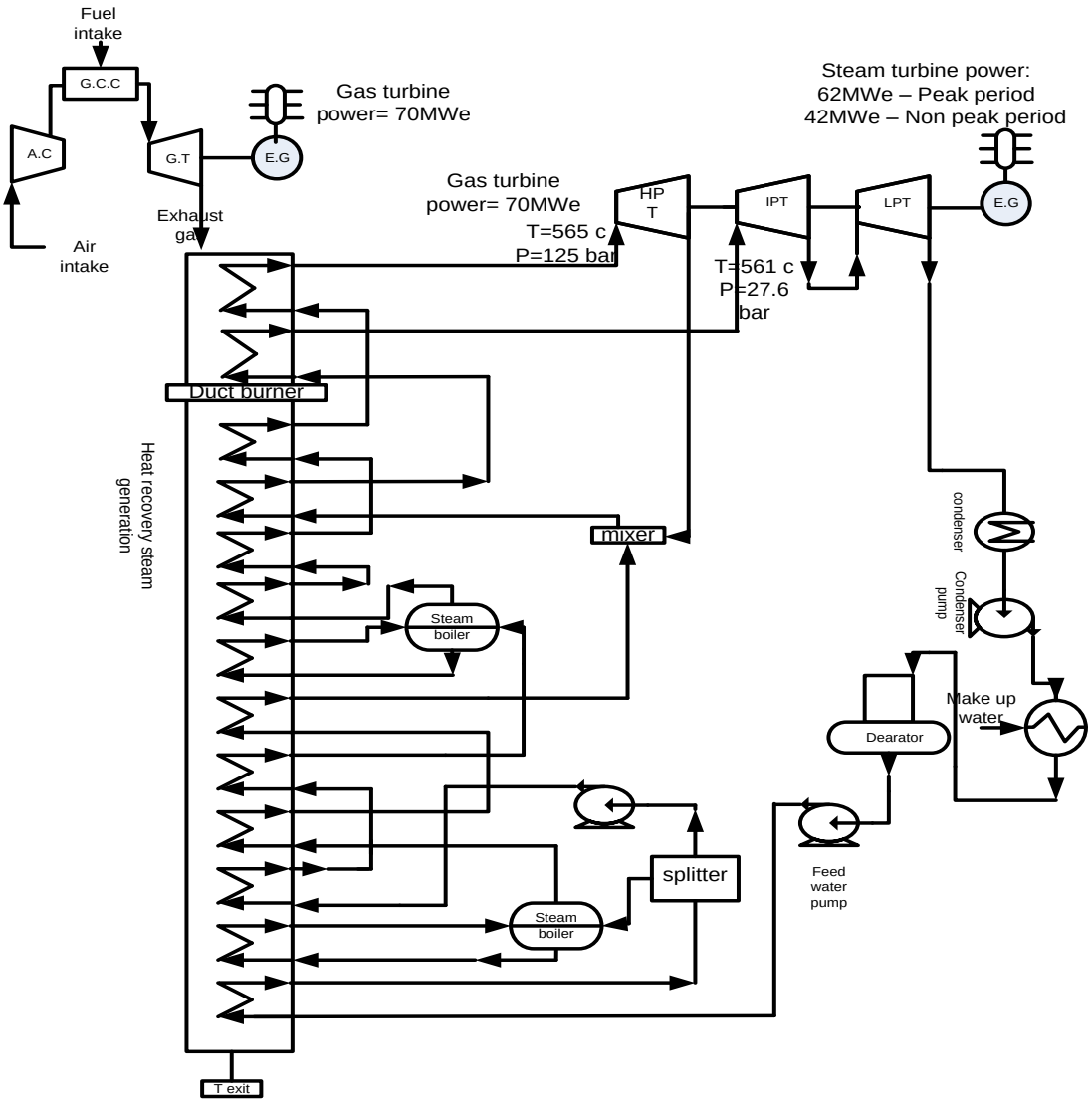

Figure 4.1 Schematic diagram of reference combined cycle

2- Integration of solar with gas turbine only, where solar energy is used to pre-heat compressed air before entering combustion chamber as shown in Fig. 4.2.

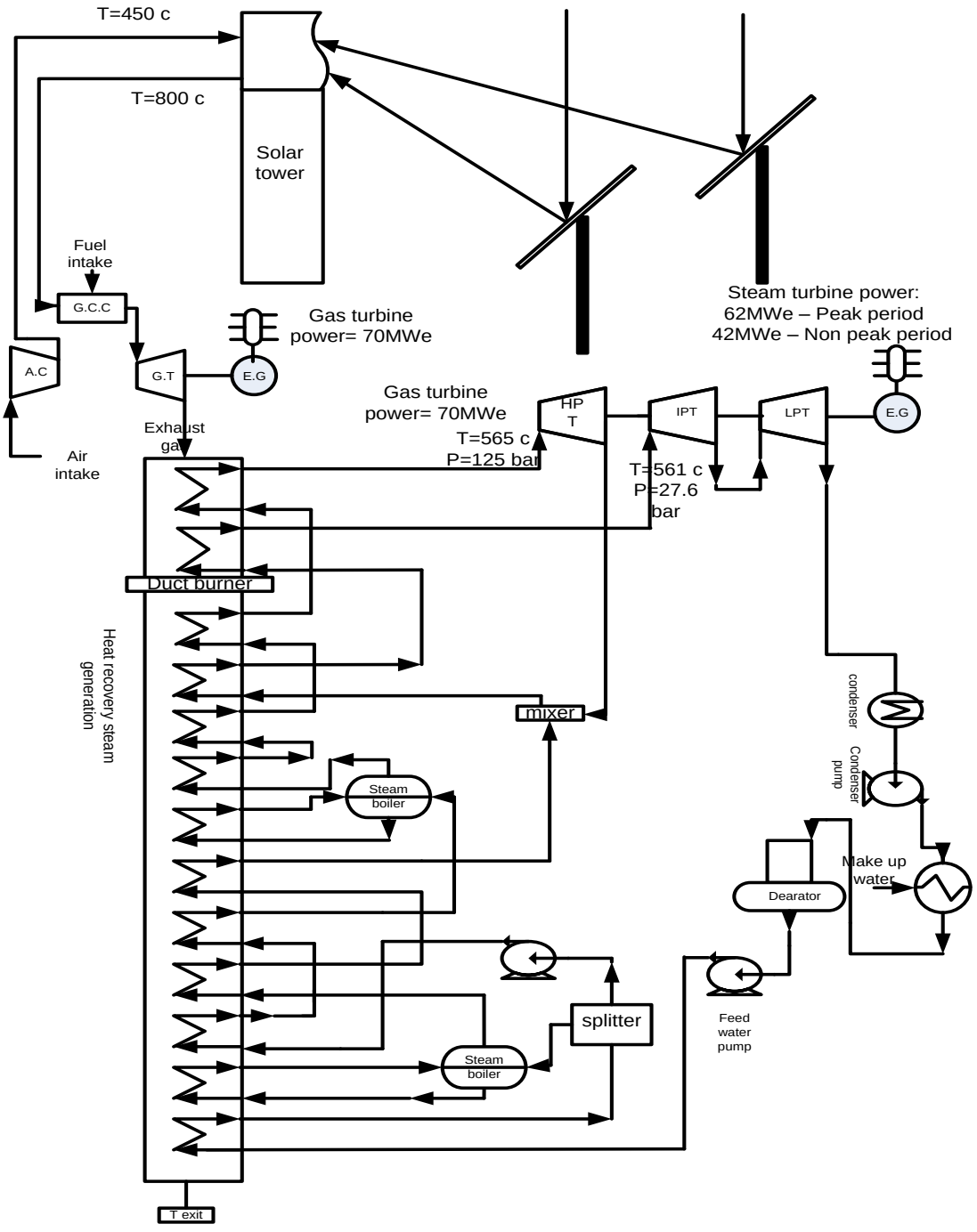

Figure 4.2 Schematic diagram of integration solar with gas turbine in combined cycle

3- Integration of solar with steam turbine in combined cycle as shown in Fig. 4.3.

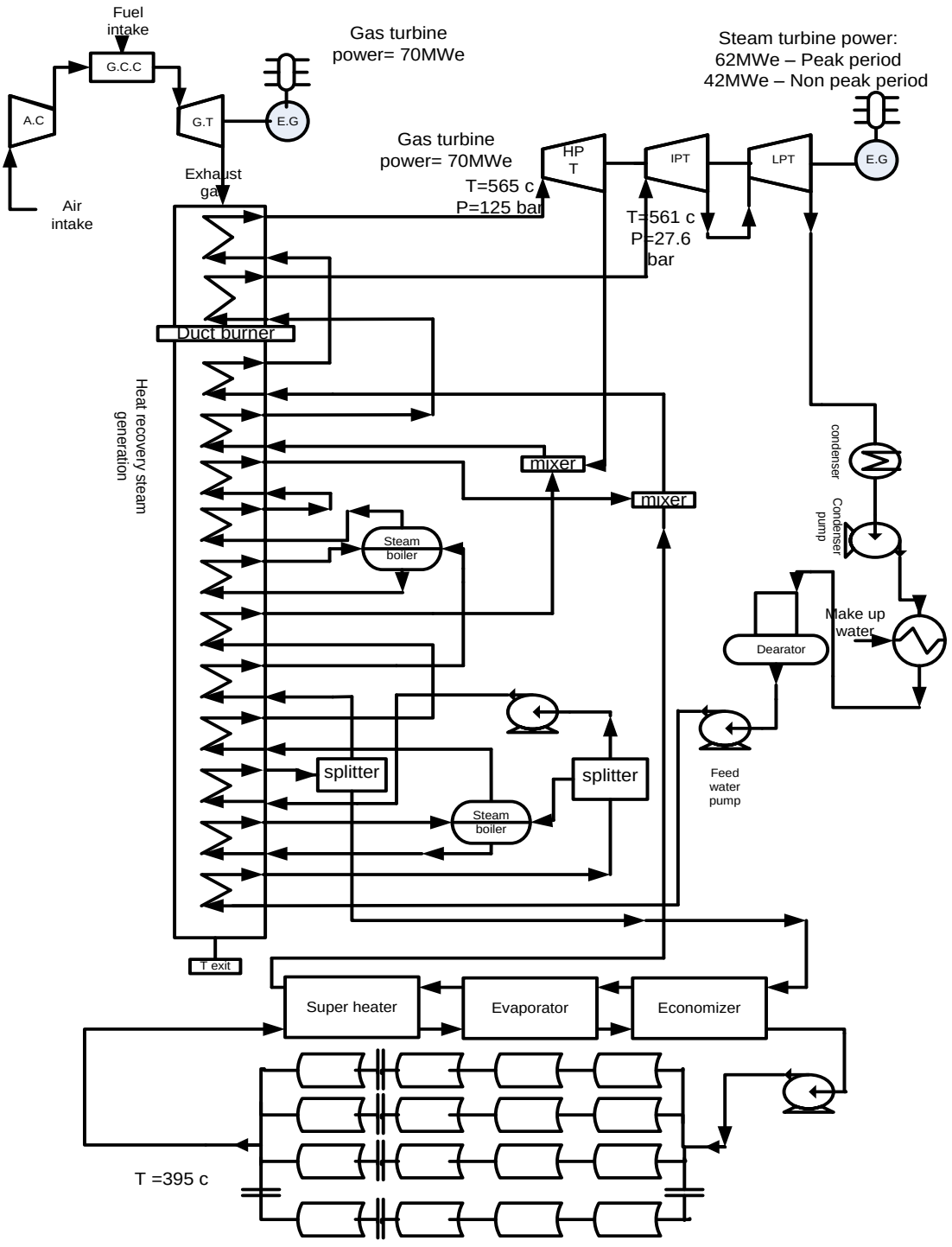

Figure 4.3 Schematic diagram of integration solar with steam turbine in combined cycle

4- Integration of solar with both gas turbine and steam turbine as clarified in the previous two steps as shown in Fig. 4.4.

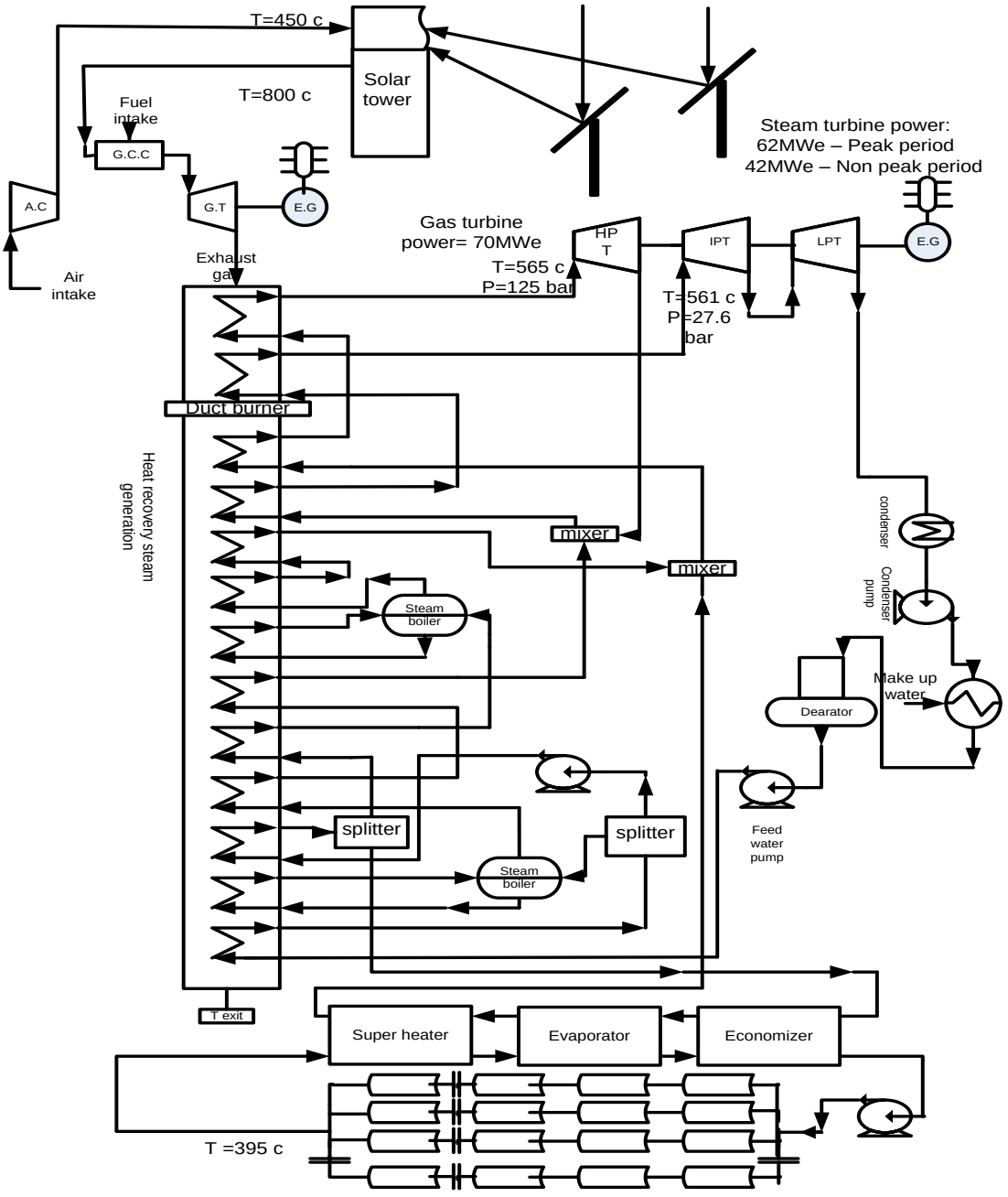

Figure 4.4 Schematic diagram of integration solar with both gas turbine and steam turbine

4.2 MATHEMATICAL MODEL

The intended thermo-economical study includes the following main steps:

4.2.1 Thermodynamic Modelling

The first law of thermodynamics is applied to each system of the 4 configurations. In this regard, the energy conservation and mass conservation is applied to the whole plant and to each component.

4.2.1.1 Mass Conservation

Total mass flow rate entering the control volume — *Total mass flow rate leaving the control volume* = *Net change in mass flow rate*

$$\sum_{k} \dot{m}_i - \sum_{k} \dot{m}_e = \frac{dm_{cv}}{dt} \tag{4.1}$$

Where m and $\dot{m}$ are the mass and mass flow rate, respectively, and the subscripts i and e refer to the inlet of the control volume and exit of the control volume, respectively. The subscript cv indicates the control volume.

4.2.1.2 Energy Conservation

Net rate at which energy is being transferred in by heat transfer − *Net rate at which energy is being transferred out by work* + *Net rate of energy transfer into the control volume accompanying mass flow* = *Time rate of change of the energy contained within the control volume*

$$\dot{Q} - \dot{W} + \sum_i \dot{m}_i (h_i + \frac{V_i^2}{2} + g z_i) - \sum_i \dot{m}_e (h_e + \frac{V_e^2}{2} + g z_e) = \frac{dE_{cv}}{dt} \quad (4.2)$$

Where E, $\dot{Q}$, $\dot{W}$ and t are the energy, heat transfer rate, power and time, respectively. The other symbols, h, V, g, and z, stand for specific enthalpy, velocity, gravity, and elevation.

4.2.2 Energy Efficiency

The energy efficiency is a measure of the useful energy from a system to the input energy for this system. The energy efficiencies of different systems are defined in the following text.

The thermal efficiency of the reference combined cycle:

$$\eta_{Ref,cycle} = \frac{\dot{W}_{cycle}}{\dot{Q}_i} = 1 - \frac{\dot{Q}_e}{\dot{Q}_i} \quad (4.3)$$

The net incremental solar efficiency of the integrated solar combined cycle means the efficiency of converting solar energy to electric energy.

$$\eta_{net\_incr\_solar} = \frac{P_{el,net} - \eta_{Ref,cycle} * \dot{m_{fuel}} * lHV}{P_{th,solar}} \quad (4.4)$$

Where $P_{el,net}$, $\dot{m_{fuel}}$, lHV, $P_{th,solar}$ are the net power of the integrated solar combined cycle, mass flow rate of fuel, lower heating value of fuel, and thermal power collected by solar field, respectively.

4.2.3 Thermo-Economics

In order to assess reliability of power plants, there is one important parameter should be taken into consideration which is cost. As known, there are two types of cost which are investment and running cost. These two costs are combined together then they are weighted with respect to the net annual energy to give one common parameter which is levelized energy cost (LEC). This LEC represents how much does energy cost? The levelized energy cost for these configurations can be defined as follows:

The levelized energy cost of reference combined cycle:

$$LEC_{ref.CC} = \frac{I_{PV}^{tot} * fcr + OM_{PV}^{ann} + F_{PV}^{ann}}{E_{gen}^{ann}} \quad (4.5)$$

Where $LEC_{ref.CC}$, I_{PV}^{tot}, fcr, OM_{PV}^{ann}, F_{PV}^{ann}, and E_{gen}^{ann} are the levelized energy cost for reference combined cycle, present value of total investment cost ($), weighted number measures the depreciation of the plant per year (%), present value of operating and maintenance cost ($/annual), present value of annual fixed maintenance cost ($), and annual electricity output (kW h/annual), respectively.

The solar levelized energy cost of hybrid solar combined cycle (HYCS) which represents by the following Equation (4.6)

$$Solar, LEC = \frac{Cost_{solar\ field}}{W_s} \tag{4.6}$$

Where $Solar, LEC$, $Cost_{solar\ field}$, and W_s are the solar levelized energy cost of HYCS, capital cost of solar field, and annual electrical energy produced due to existence of solar field, respectively. Moreover, other forms of solar levelized electricity cost which have the same physical meaning of Equation (6.4) are included in appendix C. Mathematical model is developed to describe the performance of each configuration. The general algorithms to develop the computer code are shown in Figs. (4.7, 4.9, and 4.10).

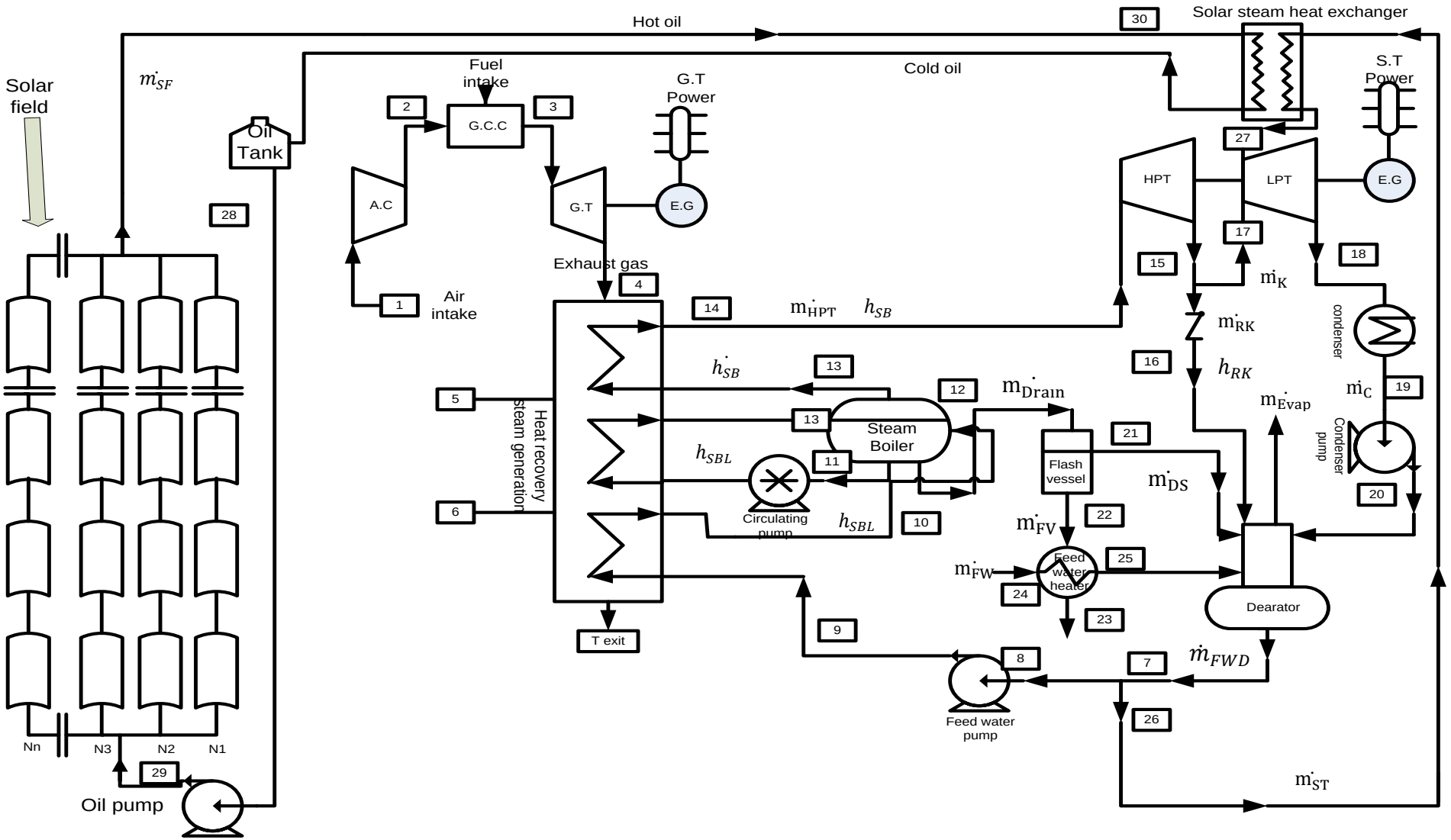

Figure 4.5 Schematic diagram of hybrid solar combined cycle

- **Developed algorithms and flow charts for components and hybrid cycle:**

❖ Gas Turbine:

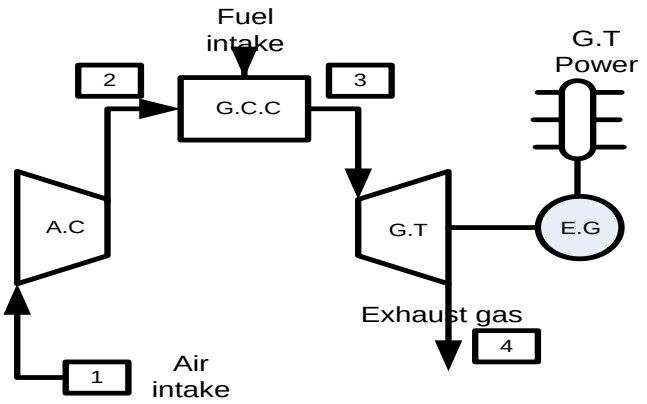

Figure 4.6 Schematic diagram of gas turbine

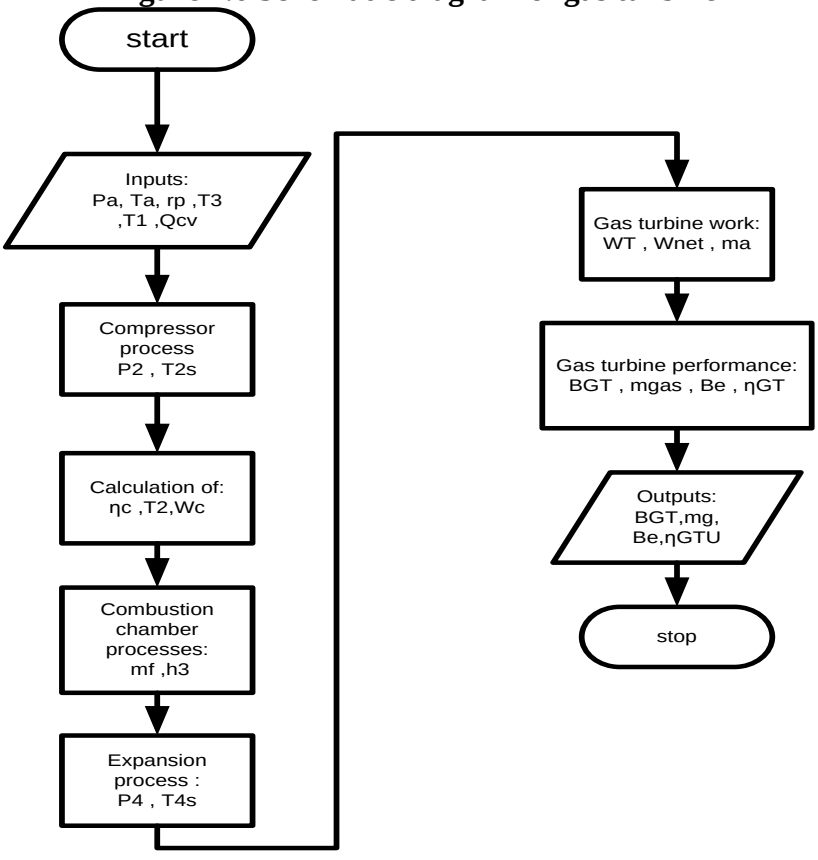

Figure 4.7 Flow chart of gas turbine simulation

❖ Solar collector field:

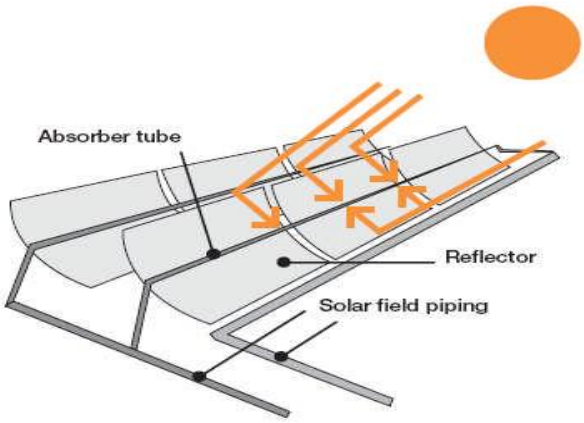

Figure 4.8 Parabolic trough concentrator.

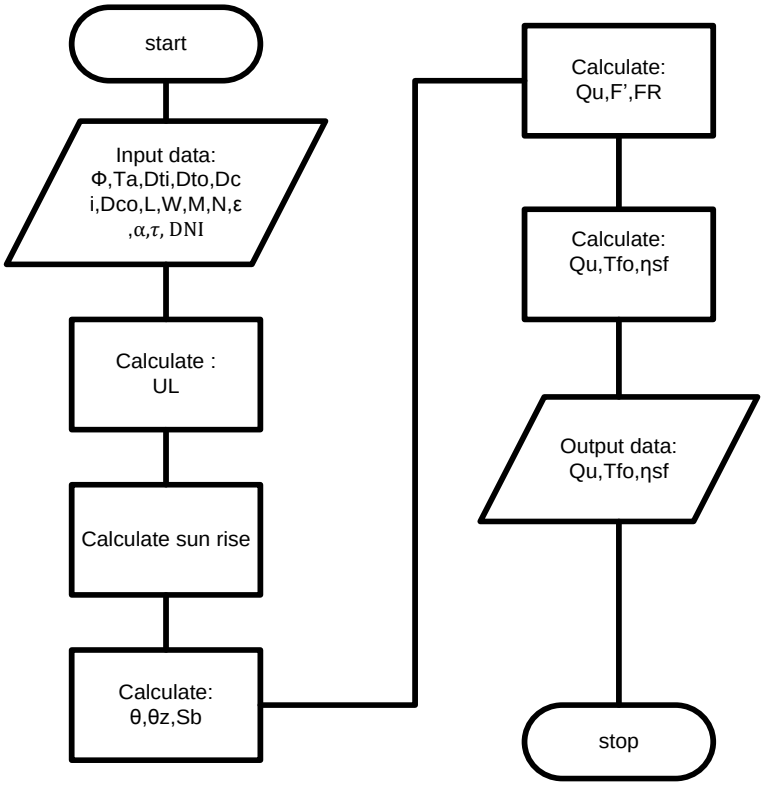

Figure 4.9 Flow chart of solar collector field simulation.

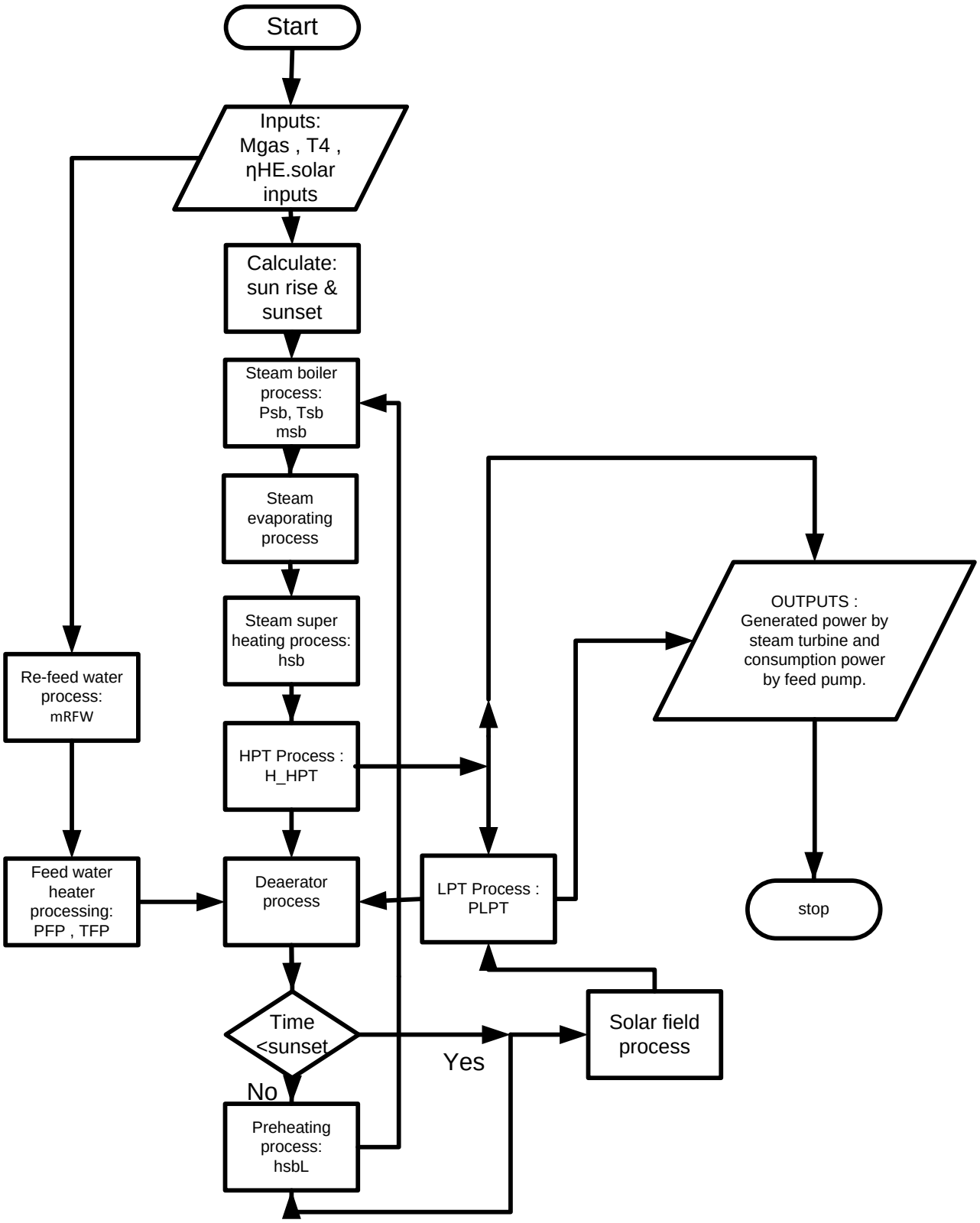

Figure 4.10 Flow chart of hybrid solar combined cycle simulation

CHAPTER 5

MATHEMATICAL MODELLING

5.1 GAS TURBINE

The most common applications of gas turbines are in electricity power plants and aircraft propulsion. In the electricity generation field, the gas turbine can be employed as stand-alone units or with combined cycle power plants. Electricity generating gas turbines are usually open cycle operated. The thermodynamic cycle of the gas turbine is known as the Brayton cycle.

Four processes are employed by the ideal Brayton cycle:

1- Isentropic compression.

2- Constant pressure heat addition in the combustion chamber.

3- Isentropic expansion.

4- Constant pressure heat rejection.

But, there is no ideal Brayton cycle due to losses of pressure drop in compression and expansion process. In addition, pressure drop during heat adding.

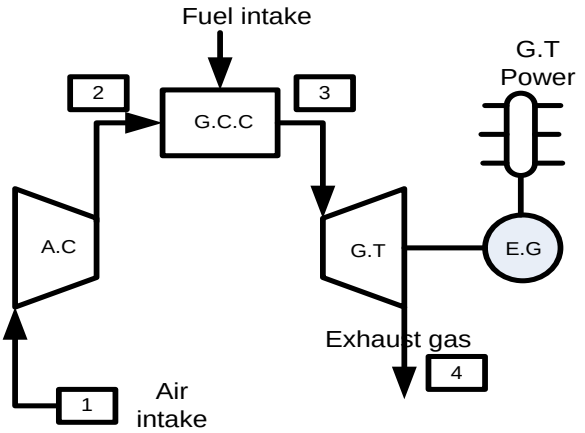

Figure 5.1 Schematic diagram of Gas turbine

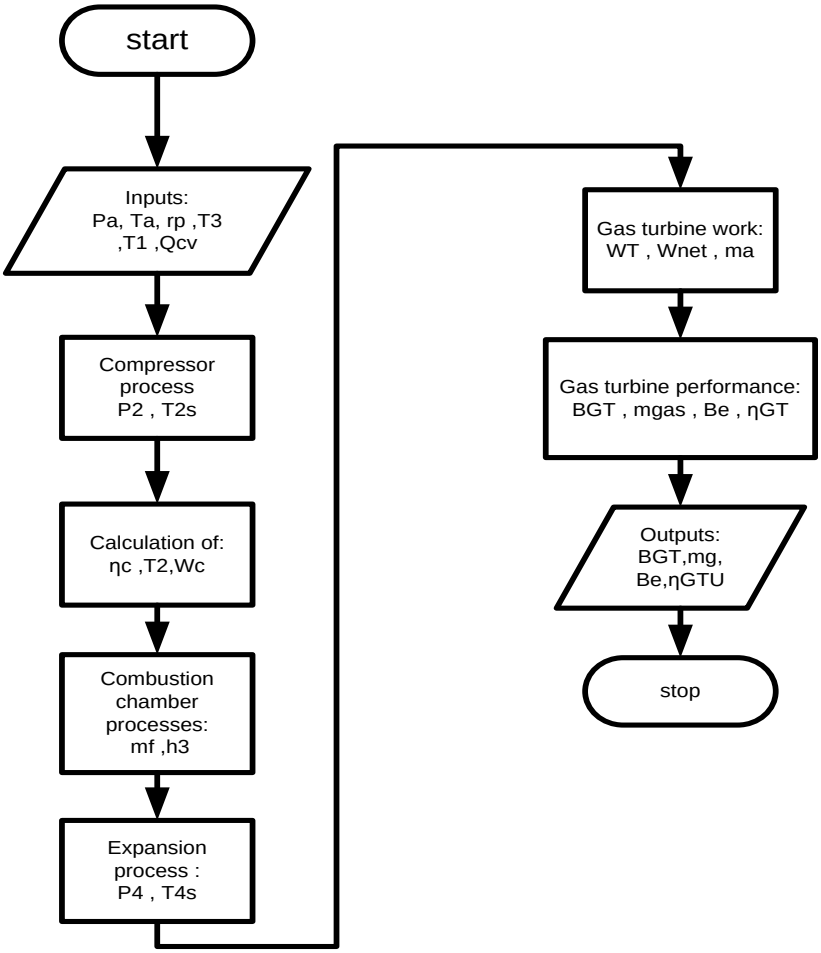

Figure 5.2 Flow chart of gas turbine simulation

➢ ***Mathematical modeling of Gas turbine:***

a- Compressor :

1- Pressure losses at the inlet of compressor ΔP_1= (0.01:0.015) [bar].

ΔP_1: The hydraulic losses due to air flow through the compressor intake.

At state (1):

$$P_1 = P_a - \Delta P_1 \quad (5.1)$$

Where:

P_a: Atmospheric pressure =1.01325 [bar].

$$T_1 = T_a \quad (5.2)$$

Where:

T_a: Ambient temperature [°K].

At state (2):

2- Compression ratio:

$$r_p = \frac{P_2}{P_1} \quad (5.3)$$

3- Isentropic temperature at the compressor exit :

$$\frac{T_2{}^S}{T_1} = (\frac{P_2}{P_1})^{\frac{\gamma a-1}{\gamma a}} \quad (5.4)$$

Where:

ɣa : specific heat ratio or isentropic expansion factor.

$T_2{}^S$: Isentropic temperature at the compressor exit [°K].

4- The compressor isentropic efficiency is :

$$\eta_c = \frac{\left(\frac{P_2}{P_1}\right)^{\frac{\gamma a-1}{\gamma a}} - 1}{\left(\frac{P_2}{P_1}\right)^{\frac{\gamma a-1}{\gamma a * \eta n^k}} - 1} = \frac{h_2{}^S - h_1}{h_2 - h_1} \quad (5.5)$$

Where:

η_c: Compressor's isentropic efficiency.

ηn^k: Compressor's polytropic efficiency.

$h_2{}^S$: Isentropic specific enthalpy at the exit of compressor [KJ/Kg].

h_1: Specific enthalpy at the inlet of compressor [KJ/Kg].

h_2: Actual specific enthalpy at the outlet of compressor [KJ/Kg].

For gas turbine applications ηn^k=0.9 to 0.91 as mentioned in [54]. So, the actual air condition after the compression process is evaluated by Equation (5.6).

$$h_2 = h_1 + \frac{h_2{}^S - h_1}{\eta_c} \quad (5.6)$$

5- The compressor specific work :

$$W_C = h_2 - h_1 \quad (5.7)$$

b- combustion chamber:

$$\left(1 + m_f - m_{loss}\right) * h_2 + \left(m_f * Q_{cv} * \eta_{c.c}\right) = \left(1 + m_f - m_{loss}\right) * h_3 \quad (5.8a)$$

Or:

$$m_f = \frac{(1\ - m_{loss}) * (h_3 - h_2)}{(Q_{cv} * \eta_{c.c})\ +\ h_2\ - h_3} \quad (5.8b)$$

Where:

m_f: Fuel mass flow rate [kg fuel/kg air].

m_{loss}: Relative air losses mass flow, its typical value 0.005 [kg air/kg air].

$\eta_{c.c}$: Combustion chamber efficiency, its typical value 0.9 to 0.98. [54]

Q_{cv}: Fuel calorific value (lower heating value), for natural gas 44.3 [MJ/Kg].

At state (3):

$$h_3 = f(T_3) \quad (5.9)$$

$$P_3 = P_2 * (1 - \xi_{c.c}) \quad (5.10)$$

$\xi_{c.c}$ is the hydraulic losses coefficient within the gas turbine combustion chamber, its typical value 0.015 to 0.025 [54].

c- Turbine:

At state (4):

$$P_4 = P_a + \Delta P_4 \tag{5.11}$$

ΔP_4: Hydraulic resistance after the turbine, its typical value depends on the conditions after the turbine exit [54].

ΔP_4 =0.02-0.03 [bar] when the turbine is connected to heat exchanger or HRSG.

ΔP_4 =0.005-0.001 [bar] when exhaust gases are sent to stack.

The gases expansion ratio:

$$\acute{o}_T = \frac{P_3}{P_4} \tag{5.12}$$

Estimating the gases conditions at the exit of turbine [55]:

$$\eta_T = \frac{1 - \left(\frac{P_3}{P_4}\right)^{-\left(\frac{\gamma_G - 1}{\gamma_G}\right) * {\eta_n}^T}}{1 - \left(\frac{P_3}{P_4}\right)^{-\left(\frac{\gamma_G - 1}{\gamma_G}\right)}} = \frac{h_3 - h_4}{h_3 - {h_4}^s} \tag{5.13}$$

Where:

γ_G: The heat capacity ratio for products' gases.

η_T: Turbine isentropic efficiency.

${\eta_n}^T$: The turbine polytropic efficiency, its typical value 0.84 to 0.87 [54].

Now, the actual air condition after the expansion process is evaluated by Equation (5.14).

$$h_4 = h_3 - \eta_T * (h_3 - {h_4}^s) \tag{5.14}$$

Where:

h_3: Specific enthalpy of gasses before entering gas turbine [KJ/Kg].

$h_4{}^s$: Isentropic specific enthalpy of gasses at the outlet of gas turbine [KJ/Kg].

h_4: Actual specific enthalpy of gasses at the outlet of gas turbine [KJ/Kg].

The relative turbine work for product gases can be calculated by Equation (5.15): [54]

$$W_T = \left(1 + m_f - m_{loss}\right) * (h_3 - h_4) \tag{5.15}$$

Where:

W_T: Relative turbine work for product gases [KJ/Kg].

T_4: Gas temperature at the end of the expansion process [°K].

The net gas turbine relative output is:

$$W_{Net} = W_T - W_C \tag{5.16}$$

For a given capacity of the gas turbine the required air mass flow (kg air/sec) can be calculated by Equation (5.17).

$$m_a = \frac{1000 \ * \ NE_{GT}}{W_{Net} * \ \eta_m \ * \ \eta_G} \tag{5.17}$$

NE_{GT} : The net power of gas turbine (MWe).

W_{Net}: Net specific output per kilogram unit mass of inlet air [KJ/Kg].

η_m: Mechanical efficiency of gas turbine [%].

η_G: Electrical efficiency of gas turbine [%].

m_a: Air mass flow rate [Kg/sec].

The gas turbine fuel consumption (tone /hour) can be evaluated by:

$$B_{GT} = m_f * m_a * \frac{3600}{1000} \tag{5.18}$$

Where:

B_{GT}: Gas turbine fuel consumption [tonne/hour].

The mass flow rate of exhaust gases from the gas turbine unit (kg gas/sec):

$$m_{gas} = m_a * \left(1 + m_f - m_{loss}\right) \tag{5.19}$$

The specific fuel consumption of the gas turbine unit (tonne/MWh):

$$be = \frac{B_{GT}}{NE_{GT}} \tag{5.20}$$

The gas turbine unit efficiency is:

$$\eta_{GTU} = \frac{3600 * NE_{GT}}{B_{GT} * Q_{c.v}} \tag{5.21}$$

5.2 SOLAR COLLECTOR FIELD

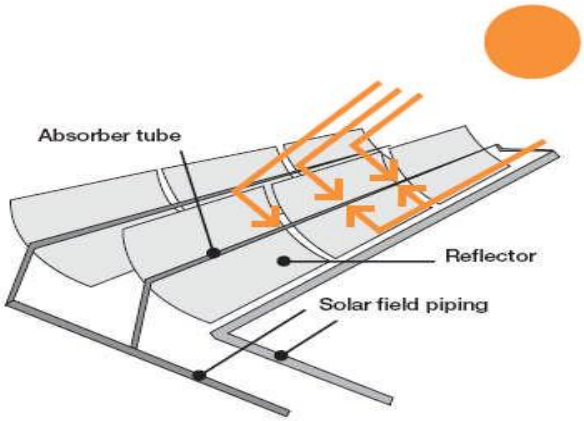

Figure 5.3 Parabolic trough concentrator

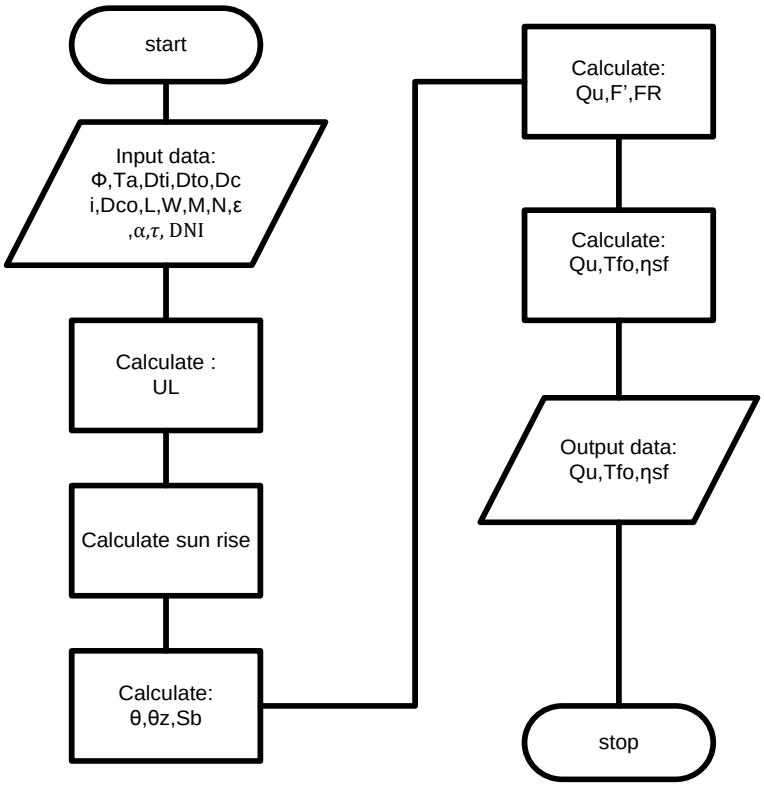

Figure 5.4 Flow chart of solar collector field

➢ ***Mathematical modeling of parabolic trough:***

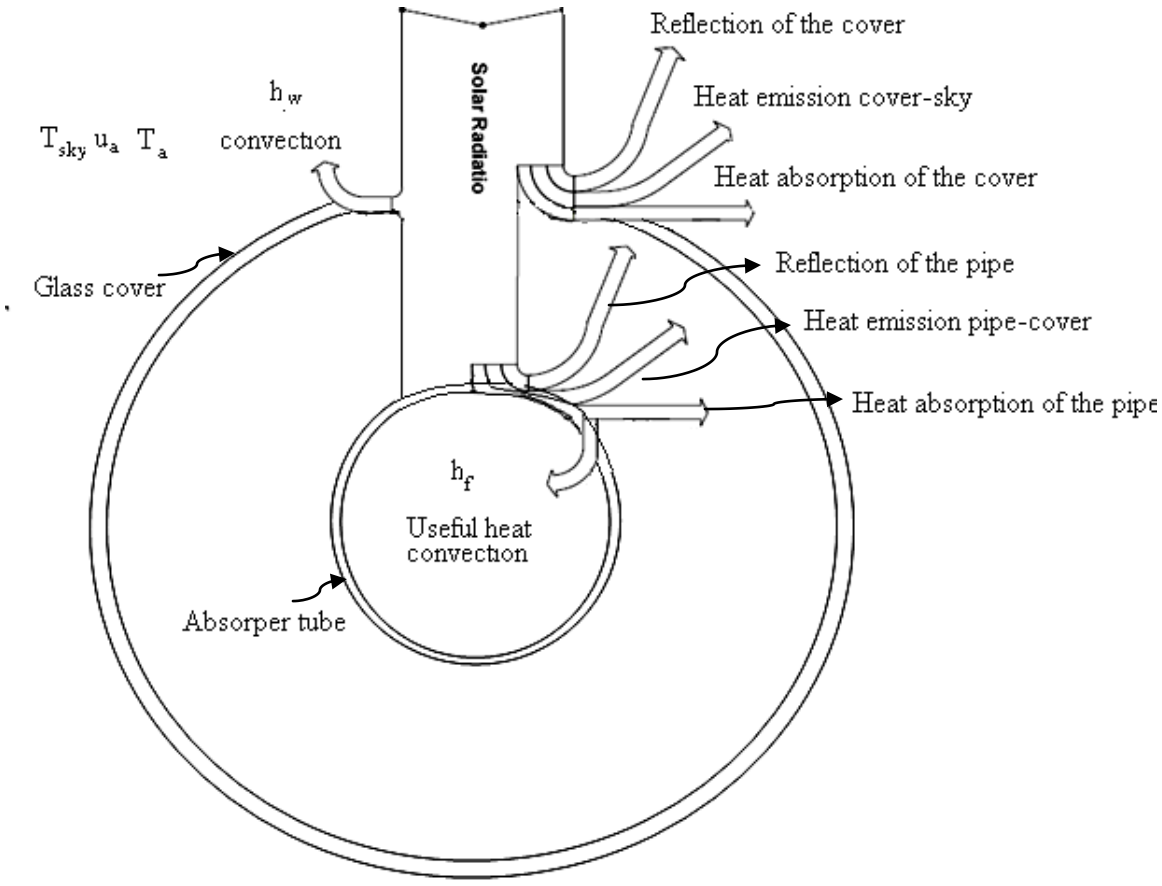

Figure 5.5 Energy flow diagram of solar collector field

Programmed code of solar collector field needs some inputs such as direct normal irradiation (DNI), mass flow rate in solar collector ($\dot{m}_S$), inlet temperature of HTF (T_{fi}), and weather data (ambient temperature and wind velocity). As a result of this analysis, performance of solar collector could be evaluated in term of efficiency ($\eta_{collector}$). Moreover, outlet temperature of solar field (T_{fo}) and useful energy can be determined.

- **Thermal analysis of solar collector**

5.2.1 Absorbed Energy by Heat Collector Element (HCE)

The absorbed energy of heat collector element can be calculated by Equation (5.22).

$$Q_{absorbed} = DNI * \cos(\theta) * IAM * \text{Row shadow} * \text{End loss} * \eta_{field} * \eta_{HCE} \quad (5.22)$$

Where:

$Q_{absorbed}$: Solar radiation absorbed by the receiver tubes [W/m2].

DNI: Direct normal insolation [W/m^2].

θ: Angle of incidence [deg].

IAM: Incidence angle modifier.

Row shadow: performance factor that accounts for mutual shading of parallel collector rows during early morning and late evening.

End loss = performance factor that accounts for losses from ends of heat collector element (HCE).

η_{field}: Solar field efficiency.

η_{HCE}: HCE efficiency that accounts for losses due to HCE optics.

The explanation of parameters in previous Equation (5.22) is briefed as hereunder:

A. Direct Normal Insolation (DNI)

DNI or what is called beam radiation is a portion of extraterrestrial solar radiation which has not been scattered or absorbed by the atmosphere. So, it reaches the surface of the earth and then can be measured by specialized measurement instruments, where the surface of instrument is normal to incident radiation. In tracking systems, only the beam

radiation (DNI) can be focused into absorber tube and thus be available to warm the absorber tubes.

B. Angle of incidence (θ)

The angle of incidence (θ) represents the angle between the beam radiation (DNI) on a surface and the plane normal to that surface. The angle of incidence changes over the whole day as well as throughout the year. In conclusion, heavily influence of the solar collector performance will appear. Angle of incidence (θ) for a collector rotates about a horizontal north-south axis with continuous east-west tracking could be calculated by the following Equation (5.23) [56].

$$\cos(\theta) = \sqrt{cos_{\theta z}{}^2 + (cos_{\delta}{}^2 * sin_{\omega}{}^2)} \tag{5.23}$$

To calculate angle of incidence (θ), there are three angles required, which are zenith angle (θz), declination angle (δ), and angular hour (ω). Calculations of these angles as follows:

Declination angle (δ)

Declination angle varies as -23.45°$\leq \delta \leq$ 23.45° according to the following Equation (5.24).

$$\delta = 23.45 * \sin\left(360 * \frac{280 + n}{365}\right) \tag{5.24}$$

Where:

n: The day number of the year which has a range starts from 1, which is 1_{St} of January, up to 365, which is thirty first of December.

Angular hour (ω)

Angular hour comes as a result of the rotation on the earth, which spins on its axis at a rate of 15° per hour. Calculation of angular hour could be done by the following Equation (5.25):

$$\omega = (solar\ time - 12) * 15\ ^{0}/\ hour \tag{5.25}$$

$$solar\ \ time\ = standard\ \ time - \frac{4 * (L_{standard}\ -\ L_{Local})\ +\ E}{60} \tag{5.26}$$

Where:

$standardtime$: Based on a standard meridian for the local time zone [h].

$L_{standard}$: Standard meridian for the local time zone [deg].

L_{Local}: The local meridian of the collector site [deg].

E: Time [min].

The Equation of (*E*), time, accounts for the small irregularities in day length that occur due to the Earth's elliptical path around the sun and can be determined either by calculation from the following Equation (5.27) or determined from Fig. 5.6.

$$E = 229.2 * [0.000075 + (0.001868 * \cos(B))\ - (0.032077 * \sin(B)) - (0.014615 * \cos(2 * B)) - (0.04089 * \sin(2 * B))] \tag{5.27}$$

$$B = \frac{360}{365} * (n - 1) \tag{5.28}$$

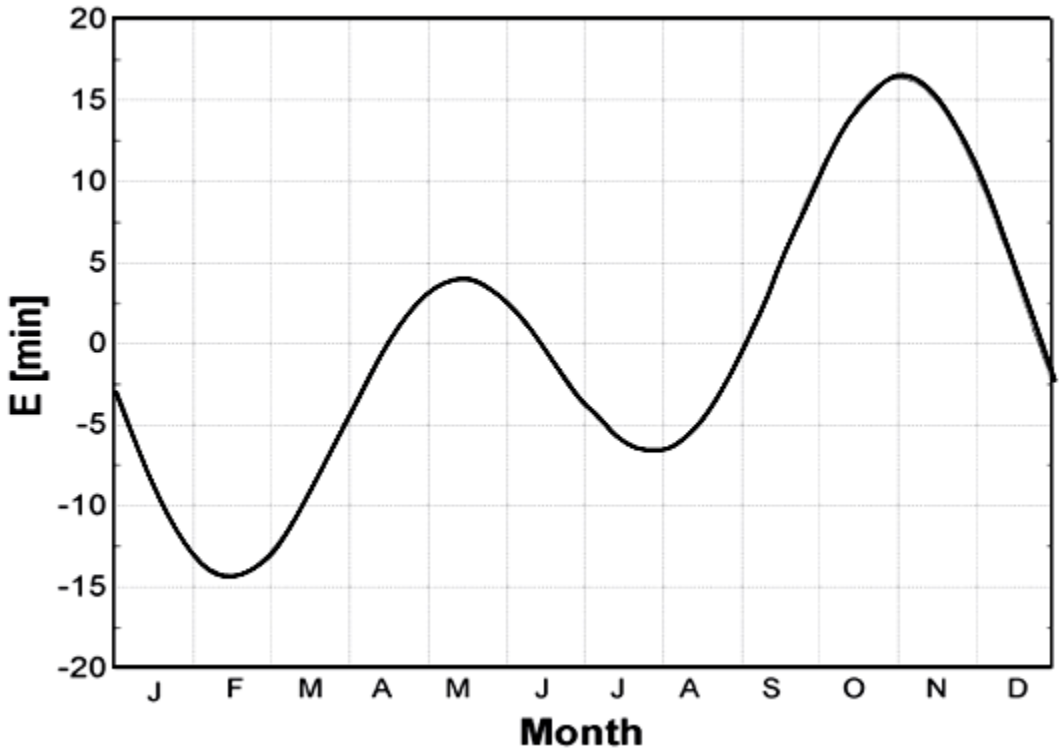

Figure 5.6 The equation of time (E) in minutes as a function of time of year [56]

Zenith angle (θz)

This is the angle between the line of sight to the sun and the vertical. Zenith angle could be calculated by the following Equation (5.29).

$$\cos(\theta z) = (\cos(\delta) * \cos(\emptyset) * \cos(\omega)) + (\sin(\delta) * \sin(\emptyset)) \quad (5.29)$$

Where:

$\emptyset$: Latitude location of the solar field.

C. Incidence Angle Modifier (IAM)

Incidence angle modifier is given as an empirical formula in term of incidence angle (θ). Each specific solar collector has its formula. For instance, incidence angle modifier for second generation of Luz solar collectors (LS-2) is given by the following Equation (5.30). [57]

$$IAM = 1 + 0.000884 * \frac{\theta}{\cos(\theta)} - 0.00005369 * \frac{\theta^2}{\cos(\theta)} \quad (5.30)$$

D. Row Shadowing and End Losses

Due to arranging of collectors in parallel rows, effect of shading appears twice in daily time (early morning and before sun set), where the most eastern row receives solar radiation on the whole area in early morning but next rows receive partially solar radiation due to shaded area as shown in Fig. 5.7. Also, the most western do the same behavior before sunset. So, the focused radiations will be reduced. This results in reduction of absorbed energy percentage and a consequent reduction of the useful energy.

Figure 5.7 Decreasing of collector shading during day operation[58]

Shading factor could be calculated by the following Equation (5.31) [58].

$$row\ \ shadow = \frac{L_{space}}{W_a} * \frac{\cos(\theta z)}{\cos(\theta)} \quad (5.31)$$

Where:

L_{space}: Distance between two parallel collectors [m].

W_a: Aperture width [m].

Regarding end losses, it happens at the end portion of HCE, where there is no focused radiation on that portion as shown in Fig. 5.8.

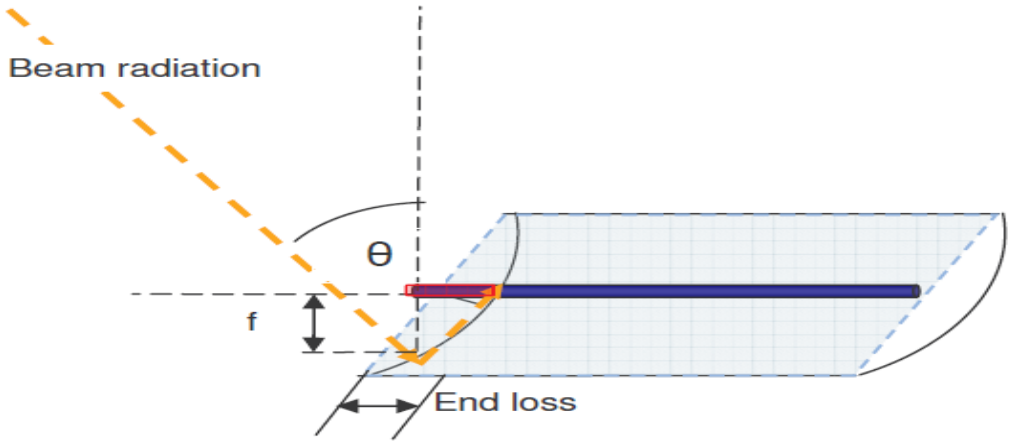

Figure 5.8 End losses from heat collector element (HCE) [59]

End losses depend on the focal length of the collector and the incident angle. End losses could be given by Equation (5.32) [60].

$$End\ \ loss = 1 - \frac{f\ *\ \tan(\theta)}{L_{SCA}} \tag{5.32}$$

Where:

f: Focal length of the collectors [m].

LSCA: Length of a single solar collector [m].

5.2.2 Field Efficiency and HCE Efficiency

These efficiencies are measures of the useful energy from solar system to the input energy for this system which is solar radiation. Many factors affect these efficiencies such as mirror cleanliness, mirror reflectivity, absorbed energy by glass envelope …etc.

$$\eta_{field} = TT_{error} * G_{accuracy} * Mir_{ref} * Mir_{clean} \quad (5.33)$$

Where:

TT_{error}: Tracking and twisting error associated with the collector type.

$G_{accuracy}$: Geometric accuracy of the collector mirrors.

Mir_{ref}: Mirror reflectivity.

Mir_{clean}: Mirror cleanliness.

$$\eta_{HCE} = HCE_{dust} * SH_{Loss} * Tr_{glass} * Ab_{HCE} * HCE_{misc} \quad (5.34)$$

Where:

HCE_{dust}: Losses due to covering of HCE by dust on the glass envelope.

SH_{Loss}: Losses from covering ends of HCE due to bellows.

Tr_{glass}: Transmissivity of the glass envelope.

Ab_{HCE}: Absorbability of the HCE selective coating.

HCE_{misc}: Miscellaneous factor to adjust for other HCE losses.

Table 5.1 Typical optical parameters and correction values for solar field [61]

Name	Value	Name	Value
$Trk\ Twst\ Err$ = (TT_{error})	0.99	$HCE\ dust$= (HCE_{dust})	0.98
$Geo\ Acc$ = ($G_{accuracy}$)	0.98	$BelS\ hade$ = (SH_{Loss})	0.97
Mir Ref = (Mir_{ref})	0.93	$Env\ Trans$ = (Tr_{glass})	0.96
Mir Cle = (Mir_{clean})	0.95	$HCE\ abs$ = (Ab_{HCE})	0.95
		$HCE\ misc$ = (HCE_{misc})	0.96

A. Heat losses from HCE and useful energy

Heat loss from HCE is based on a combination of the collector thermal loss due to radiation, convection, and conduction. The main thermal loss from the absorber tube outer wall to the evacuated glass tube occurs by radiation. The heat loss from the glass cover tube occurs by radiation to the sky and by convection to the surrounding air via wind or natural convection, as shown in Fig. 5.9.

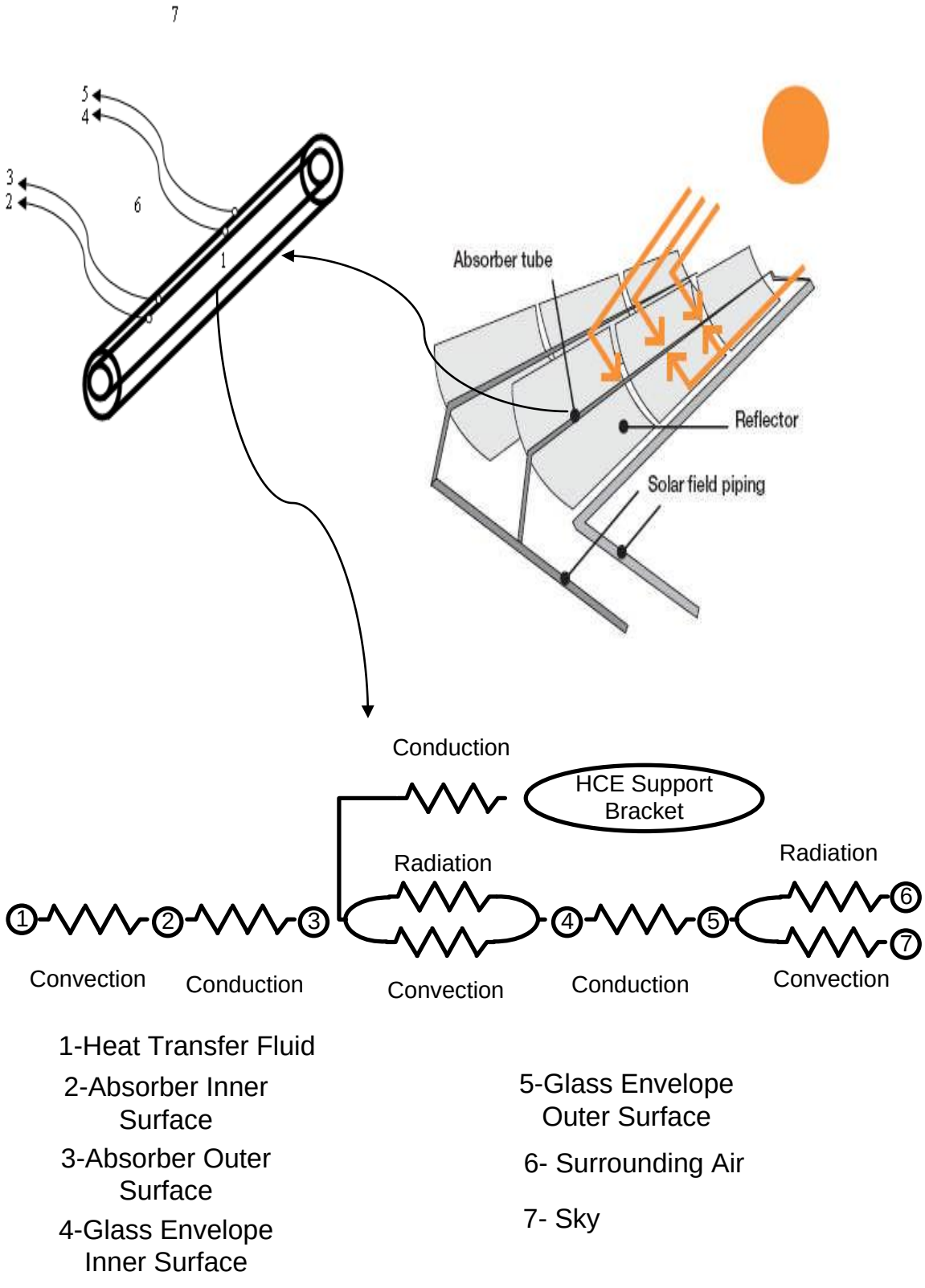

Figure 5.9 Thermal resistance of HCE

To calculate heat loss from HCE, an iterative method is used. As a result, temperatures at different locations in HCE can be determined such as outer surface of absorber tube, inner and outer surface of glass envelop, and then heat transfer can be evaluated because it is governed mainly by temperature gradient.

First of all, the mass flow rate is assumed to be constant and it is given based on the nominal solar field output as given in Equation (5.35).

$$Q_{SF} = \dot{m_{SF}} * CP_f * \left(T_{fo} - T_{fi}\right) \quad (5.35)$$

Where:

T_{fi}: Inlet temperature of solar field. [°K]

T_{fo}: Outlet temperature of solar field. [°K]

CP_f: Heat capacity of HTF [KJ/Kg.°K]

Q_{SF}: Nominal solar field of absorbed energy. [KJ/Kg]

$\dot{m_{SF}}$: Total mass flow rate of solar field. [Kg/sec]

Now, thermal analysis of solar collector will be done for one row of solar collectors. So, mass flow rate for each row is required and it is given by the following Equation (5.36).

$$\dot{m_S} = \frac{\dot{m_{SF}}}{N} \quad (5.36)$$

Where:

N: Number of parallel rows.

With assumed value of the temperature at the outlet of solar field (T_{fo}), the mean fluid temperature can be calculated by Equation (5.37).

$$T_{fm} = \frac{T_{fo} + T_{fi}}{2} \tag{5.37}$$

In order to calculate Nusselt number inside the tube, properties of HTF should be known such as kinematics viscosity (v_f), Prandtl number (Pr_f), thermal conductivity (K_f), heat capacity (CP_f), and density (ρ_f). So, these properties are given at the mean fluid temperature (T_{fm}). Also, value of Nusselt number depends on status of fluid flow, laminar or turbulent. In this regard, Reynolds number is given by the following Equation (5.38).

$$Re_f = \frac{U_f * D_{ti}}{v_f} \tag{5.38}$$

Where:

U_f: Velocity of HTF inside the tube. [m/sec]

D_{ti}: Inner diameter of absorber tube. [m]

$$U_f = \frac{4 * \dot{m}_S}{\rho_f * A_i} \tag{5.39}$$

Where:

A_i: Inside cross sectional area of the absorber tube [m^2].

$$A_i = \pi * \frac{{D_{ti}}^2}{4} \tag{5.40}$$

Laminar Flow Case:

When the laminar option is chosen and the Reynolds number (Re_f) is lower than 2300, the Nusselt number will be constant. For pipe flow, the value will be 4.36 [62].

Turbulent and Transitional Flow Cases:

Convective heat transfer from the absorber to the HTF for turbulent and transitional case (Reynolds number > 2300) the Nusselt number is given by Equation (5.41). [63]

$$Nu_f = \frac{\frac{f_2}{8} * (Re_{Di} - 1000) * Pr_1}{1 + 12.7 * \sqrt{\frac{f_2}{8}} * (Pr_1^{\frac{2}{3}} - 1)} \left(\frac{Pr_1}{Pr_2}\right)^{0.11} \quad (5.41)$$

Where:

f_2: Friction factor for the inner surface of the absorber pipe

Pr_1: Prandtl number evaluated at the HTF temperature, (T_{fi}).

Pr_2: Prandtl number evaluated at the absorber inner surface temperature (T_t), where (T_t) as a first guess =$T_{fm} + 2$.

After evaluation value of the Nusselt number, heat transfer coefficient (h_f) can be calculated by the following Equation (5.42).

$$h_f = \frac{Nu_f * K_f}{D_{ti}} \quad (5.42)$$

Now, to get a new guessed value of absorber tube temperature (T_t) the following formula could be used. For first iteration, assumed values of outlet temperature from solar field (T_{fo}) and nominal output (Q_u) from solar field are given.

$$Q_u = A_{ti} * M * h_f * (T_t - T_{fm}) \quad (5.43)$$

Where:

A_{ti}: Inner surface area of absorber tube for one collector [m^2].

M: Number of collectors connected in series.

$$A_{ti} = \pi * D_{ti} * L \tag{5.44}$$

$$T_t = T_{fm} + \frac{Q_u}{A_{Si} * M} \tag{5.45}$$

Where:

T_t: New guessed value of absorber tube temperature.

L: Collector length.

B. Useful and loss energy

An assumption is made for U_L in order to calculate the collector effectiveness (F'). [56]

$$U_o = \frac{1}{\left(\frac{1}{UL}\right) + \left(\frac{D_{to}}{h_f * D_{ti}}\right) + D_{to} * \left(\frac{ln\left[\frac{D_{to}}{D_{ti}}\right]}{2 * K_t}\right)} \tag{5.46}$$

$$F' = \frac{U_o}{U_L} \tag{5.47}$$

Where:

K_t : Thermal conductivity of absorber tube [W/m.°K].

D_{to}: Outer diameter of absorber tube [m].

Collector heat removal (F_R) is given by the following equation (5.49)[56].

$$F'' = \frac{\dot{m}_S * CP_f}{A_{to} * U_L * F'} * \left(1 - \exp\left(-\frac{1}{\frac{\dot{m}_S * CP_f}{A_{to} * U_L * F'}}\right)\right) \tag{5.48}$$

$$F_R = F' * F'' \tag{5.49}$$

Where:

A_{to}: Outer surface area of absorber tube [m^2].

Now, code will calculate new value of Q_u and Q_L using the following formulas.

$$Q_u = F_R * A_a * \left(Q_{absorbed} - \frac{A_{to}}{A_a} * U_L(T_{fi} - T_a) \right) \quad (5.50)$$

$$A_a = (W_a - D_{to}) * L \quad (5.51)$$

$$Q_L = (Q_{absorbed} * A_a * M) - Q_u \quad (5.52)$$

Where:

Q_u: Useful energy [W].

Q_L: Loss energy [W].

A_a: Aperture area [m^2].

T_a: Ambient temperature [°K].

W_a: Aperture width [m].

To calculate new value of absorber temperature, the following Equation (5.53) could be used [18]:

$$T_t^* = \frac{Q_L}{U_L * A_{to}} + T_a \quad (5.53)$$

C. Convection heat transfer from HCE to ambient:

There is convection loss from glass to ambient, but convection loss between absorber tube and glass cover assumed zero due to using evacuated tube. Thus, to calculate convection loss from glass to ambient, glass temperature should be given. So, guessed value is given for first iteration [18].

$$T_{Cm} = \frac{T_a + T_t^*}{2} \tag{5.54}$$

$$T_{C1} = T_{Cm} + 3 \tag{5.55}$$

$$T_{C2} = T_{Cm} - 3 \tag{5.56}$$

Where:

T_{Cm}: Mean cover temperature.

T_{C2}: Outer temperature of glass surface.

T_{C1}: Inner temperature of glass surface.

Due to dependency of convection loss on wind speed, heat transfer coefficient from glass cover to ambient should be calculated. In this regard, Reynolds number should be given to calculate Nusselt number.

Reynolds number is given by:

$$Re_a = \frac{U_a * D_{co}}{v_a} \tag{5.57}$$

Where:

Re_a: Reynolds number of ambient air.

v_a: Kinematic viscosity at ambient temperature [m^2/sec].

D_{co}: Outer diameter of glass cover [m].

U_a: Ambient air velocity [m/sec].

To calculate Nusselt number, the following Equations could be used based on the value of Reynolds number (Re_a) [18].

If $5 < Re_a < 1000$ then:

$$Nu_a = 0.5 * {Re_a}^{0.5} * {Pr_a}^{0.38} * \left(\frac{Pr_a}{Pr_c}\right)^{0.25} \quad (5.58)$$

If $1000 < Re_a < 200{,}000$ then:

$$Nu_a = 0.26 * {Re_a}^{0.6} * {Pr_a}^{0.38} * \left(\frac{Pr_a}{Pr_c}\right)^{0.25} \quad (5.59)$$

If $200{,}000 < Re_a < 10{,}000{,}000$ then:

$$Nu_a = 0.23 * {Re_a}^{0.8} * {Pr_a}^{0.4} * \left(\frac{Pr_a}{Pr_c}\right)^{0.25} \quad (5.60)$$

Now, heat transfer coefficient is given by:

$$hc_{c-a} = \frac{Nu_a * K_a}{D_{co}} \quad (5.61)$$

Where:

Nu_a: Nusselt number of ambient air.

Pr_a: Evaluated value of Prandtl number at temperature of ambient air.

Pr_c: Evaluated value of Prandtl number at temperature of outer surface of glass cover (T_{C2}).

hc_{c-a}: Convection heat transfer coefficient from glass cover to ambient air [W/m^2.ºK].

K_a: Evaluated value of thermal conductivity at temperature of ambient air [W/m.ºK].

D. Radiation heat transfer from HCE to ambient:

There are 2 stages of heat transfer by radiation. The first stage is from absorber tube to glass cover and the second stage is from glass cover to the sky. In this regard, radiation heat transfer coefficients in both stages will be calculated to calculate heat losses due to radiation. The following Equations could be used to calculate radiation heat transfer coefficients [56].

$$h_{rad\ t-c} = \frac{б * \left({T_t}^{*2} + {T_{c1}}^2\right) * \left(T_t^* - T_{c1}\right)}{\frac{1-\varepsilon_t}{\varepsilon_t} + \frac{1}{F_{tc}} + \frac{(1-\varepsilon_c)*D_{to}}{\varepsilon_c * D_{ci}}} \quad (5.62)$$

Where:

$h_{rad\ t-c}$: Radiation heat transfer coefficient between tube and cover [W/m^2.ºK].

σ: Stefan Boltzmann constant = 5.67×10^{-8}[W/m^2.ºK^{-4}]

ε_c: Cover emissivity.

ε_t: Receiver tube emissivity.

F_{tc}: View factor between tube and cover, for two long concentric cylinders, view factor equals one.

D_{ci}: Inner diameter of glass cover [m].

D_{to}: Outer diameter of absorber tube [m].

$$h_{rad\ c-s} = \varepsilon_c * б * \left({T_{c2}}^3 - {T_S}^3\right) \quad (5.63)$$

Where:

$h_{rad\ c-s}$: Radiation heat transfer coefficient between glass cover and sky [W/m^2.ºK].

T_S: Sky temperature= T_a- 6

After calculations of convection and radiation heat transfer coefficients, new iteration loop will run to solve Q_{loss} equations until convergence criteria met. Convergence criteria in this loop will be the difference between new values and old guessed values less than 0.001 of cover temperatures and absorber tube. The following equations describe heat loss from HCE.

Heat loss by radiation from absorber tube to cover:

$$Q_{loss} = h_{rad\ t-c} * A_{to} * M * (T_t^{**} - T_{c1}^{*}) \quad (5.64)$$

Heat loss due to absorption energy by glass cover:

$$Q_{loss} = 2 * \pi * K_c * L * M * \frac{T_{c1}^{*} - T_{c2}^{*}}{\ln\left(\frac{D_{co}}{D_{ci}}\right)} \quad (5.65)$$

Heat loss from glass cover to ambient air by radiation and convection:

$$Q_{loss} = (h_{rad\ C-S} + hc_{c-a}) * A_{co} * M * (T_{c2}^{*} - T_a) \quad (5.66)$$

Where:

T_t^{**} : New guessed value of absorber tube temperature [°K].

T_{c2}^{*}: New guessed value of outer surface of glass cover [°K].

T_{c1}^{*}: New guessed value of inner surface of glass cover [°K].

Then the overall loss coefficient is calculated by the following equation and compared to the assumed value until convergence criteria met, which is difference between calculated value (U_L^{*}) and assumed value(U_L) less than 0.001[64].

$$U_L{}^* = \left(\frac{D_{to}}{(\mathrm{h_{rad\ C-S}} + hc_{c-a}) * D_{co}} + \frac{1}{2 * \mathrm{K_c}} * \ln\left(\frac{D_{co}}{D_{ci}}\right) + \frac{1}{\mathrm{h_{rad\ t-c}}}\right)^{-1} \quad (5.67)$$

Where:

$U_L{}^*$: Calculated value of overall loss coefficient [W/m^2.°K].

Once U_L met the convergence criteria, then last iteration loop will run to calculate new value of outlet temperature from solar field ($T_{fo}{}^*$) by the following Equation (5.68) and compare it with the assumed value of T_{fo} until convergence criteria met, which is difference between T_{fo} and $T_{fo}{}^*$ less than 0.001.

$$T_{fo}{}^* = T_{fi} + \frac{Q_u}{CP_f * \dot{m_{SF}}} \quad (5.68)$$

Where:

$T_{fo}{}^*$: Calculated value of outlet temperature from solar field [°K].

Finally, collected energy and solar field efficiency could be calculated by the following Equations (69 - 70):

$$Q_{collected} = Q_u * N \quad (5.69)$$

$$\eta_{SF} = \frac{Q_{collected}}{DNI * \cos(\theta) * IAM * \mathrm{A_{SF}}} \quad (5.70)$$

Where:

$\mathrm{A_{SF}}$: Total area of solar field [m^2].

$Q_{collected}$: Total collected energy from solar field [W].

η_{SF}: Solar field efficiency.

5.3 STEAM TURBINE WITH HEAT RECOVERY STEAM GENERATOR

5.3.1 Steam Turbine Cycle

The steam cycle is based on Rankin vapor cycle. It works by combustion of coal or fuel oil, etc. To compress and convert liquid to vapor and then expand the vapor through a turbine in order to convert heat to mechanical energy, there are:

Four processes are employed by the ideal Rankin cycle:

1- Compression the fluid using a pump.

2- Heat addition through boiler to convert water to steam.

3- Expansion of the vapor through turbine.

4- Heat rejection in condenser to condensate steam to water.

5.3.2 Heat Recovery Steam Generator (HRSG)

Heat recovery steam generation system (HRSG) uses the exhaust of the GT to generate and superheat some steam which is driven to be expanded in the steam turbine. As a result, more electricity is generated and the overall efficiency of the combined cycle (CC) is improved. Heat recovery steam generator and steam turbines can be connected with gas turbine and solar collector to achieve hybrid solar combined cycle as shown in Fig. 5.10a.

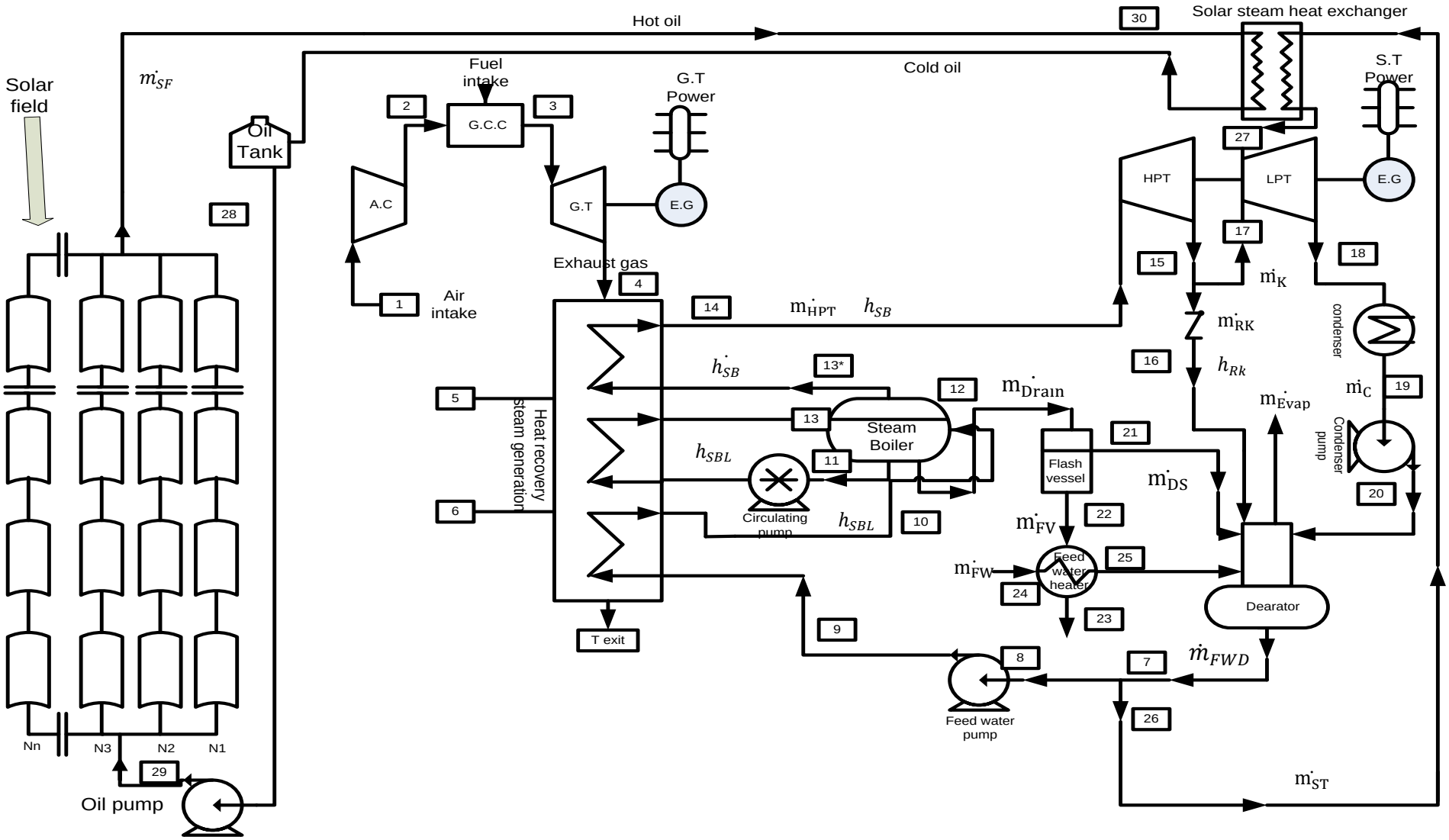

Figure 5.10a Schematic diagram of hybrid solar combined cycle

5.4 OVERVIEW OF HYBRID SOLAR COMBINED CYCLE (HYCS) ANALYSIS

As shown in Fig. 5.10a, HYCS contains three major components. The first component is solar collector field; it is working as indirect steam generator. The second is gas turbine unit (GTU). The last component is steam turbine unit with HRSG. This configuration of hybridization solar with CC which is re-generative cycle, where HRSG can be utilized to make use of hot exhaust gasses from GTU, can be utilized to generate portion of steams before entering low pressure steam turbine (LPT). Fig. 5.10b shows TS diagram of steam turbines in HYCS cycle, which presents pressures and temperatures at different states. Moreover, this configuration can be switched easily from HYCS to conventional combined CC after sun set. Analysis of this configuration will be discussed in details in the rest of this chapter. First of all, solar system will be in service during the sunny hours. On the other hand, gas turbine unit GTU will be in service during the whole day; it will give a constant output of electrical power and hot exhaust gasses. The hot exhaust gasses can be utilized by sending them through HRSG instead of sending them to the stack. Now, steam generation in HYCS has two ways. The first way is during day time and the second way is during night time. During day time, steam will be generated by two different heat sources which are HRSG and solar collector. On the other hand, steam will be generated by HRSG only in night time. Steam generation in HYCS during day time will follow this procedure; the first portion of steam will be generated via available solar energy before entering Low pressure steam turbine (LPT) at state (27) and the second portion of it will be generated by HRSG before entering high pressure steam turbine (HPT) at state (14). Steam generation by HRSG will pass through three stages.

The first stage is pre-heating process; saturated waters flow in this stage started from state (9) to be heated before entering steam boiler at state (10). The second stage is evaporating process, where hot waters flow in this stage started from state (11) and do heat exchanging with hot exhaust gasses until evaporation at state (13). The last stage is super heating process, where steam flows in this stage started from state (13*) to be super-heated before entering HPT at state (14). After sun set, steam can be generated by HRSG only.

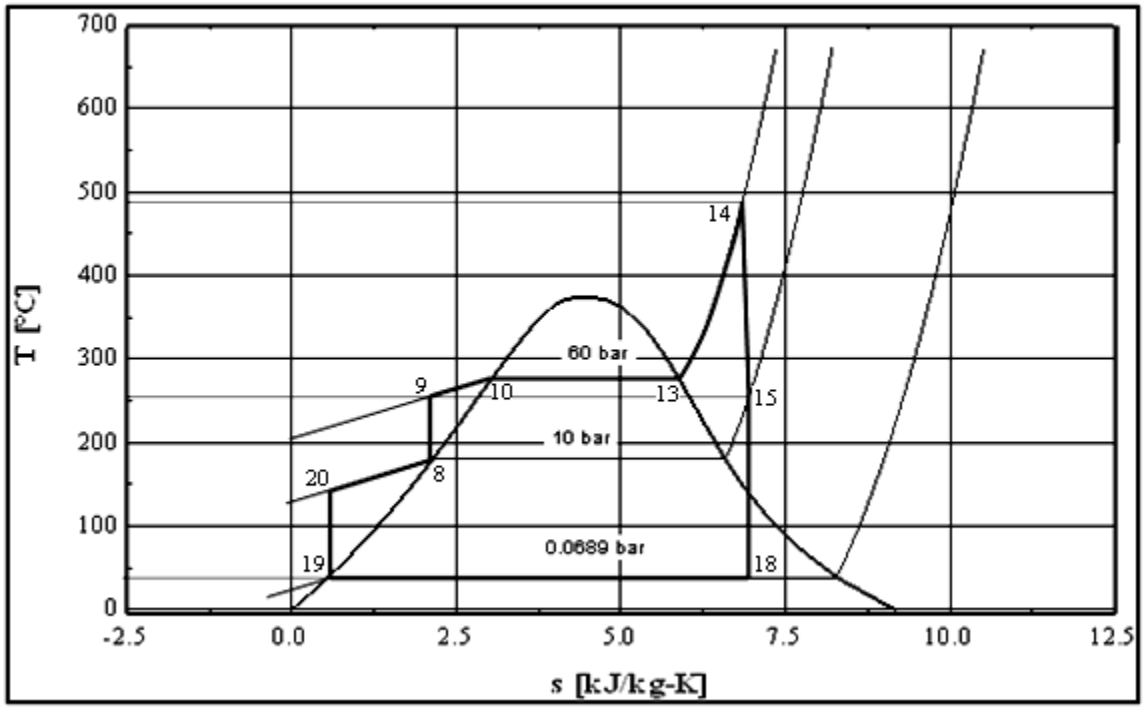

Figure 5.10b T.S diagram of steam turbines in hybrid solar combined cycle

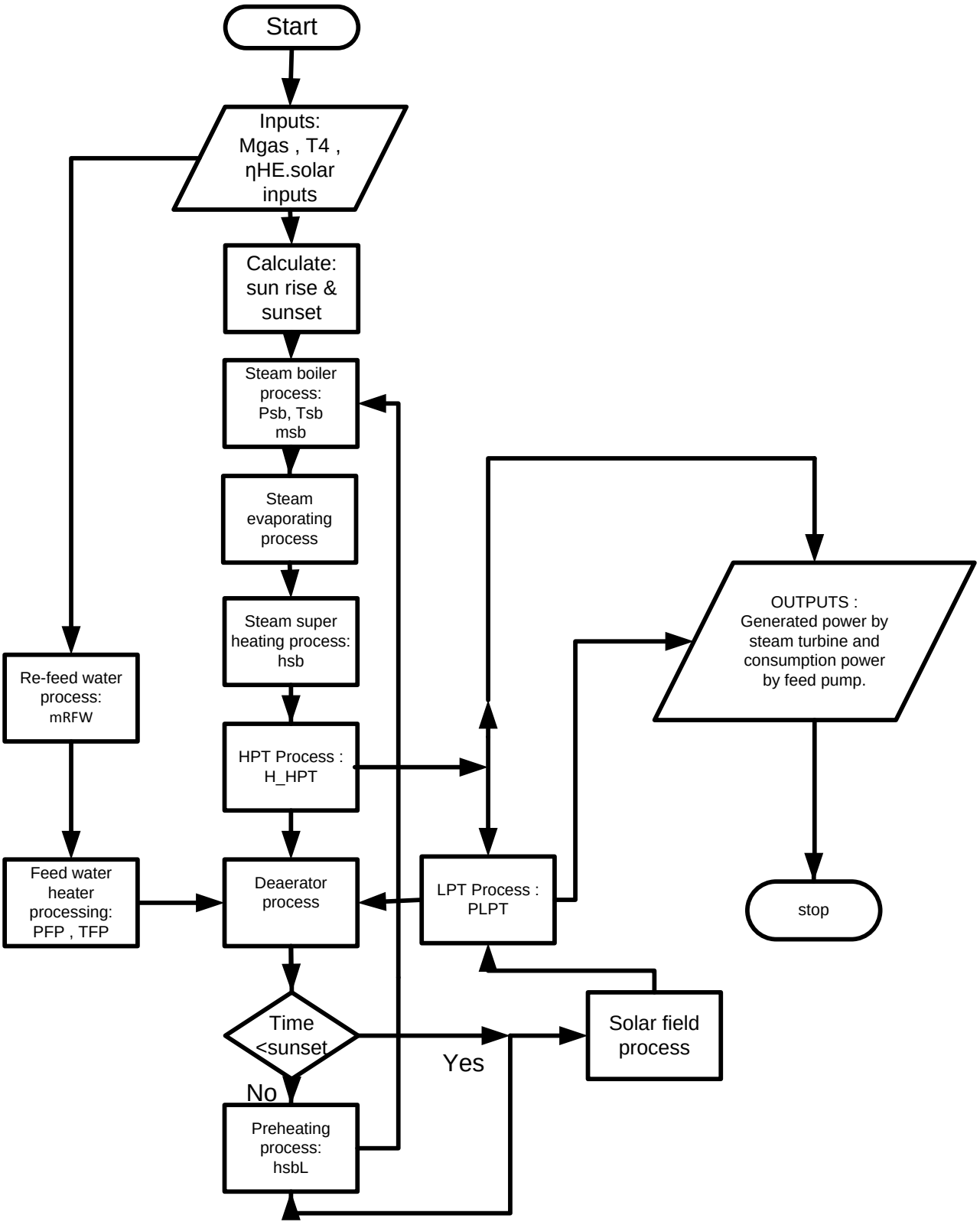

Figure 5.11 Flow chart of HYCS cycle

5.4.1 Thermal analysis of hybrid solar combined cycle configuration Which is Shown in Fig. 5.10a

1- Mass balance of main branching point in hybrid solar combined cycle (HYCS):

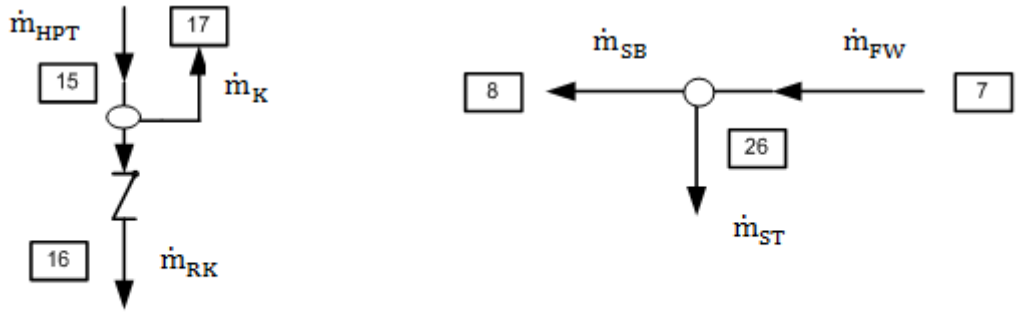

$$\dot{m}_{HPT} = \dot{m}_K + \dot{m}_{RK}$$

$$\dot{m}_{FW} = \dot{m}_{SB} + \dot{m}_{ST}$$

Figure 5.12 Schematic diagram of mass balance of main branching point

2- Steam boiler:

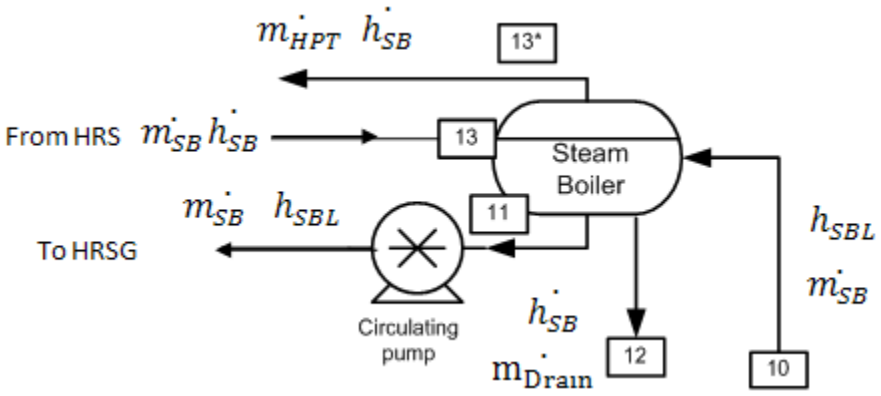

Figure 5.13 Schematic diagram of steam boiler

Mass balance of steam boiler

mass flow rate in = mass flow rate out

$$\dot{m_{SB}} = \dot{m_{Drain}} + \dot{m_{HPT}} \quad (5.71)$$

Energy balance of steam boiler

$$\dot{m_{SB}} * h_{SBL} + Heat = \dot{m_{Drain}} * \dot{h_{SB}} + \dot{m_{HPT}} * \dot{h_{SB}} \quad (5.72)$$

Where:

$Heat$: Absorbed heat from evaporator in HRSG = $\dot{m_{SB}} * \left(\dot{h_{SB}} - h_{SBL}\right)$.

h_{SBL}: Water specific enthalpy at the inlet of steam boiler.

$\dot{h_{SB}}$: Steam specific enthalpy at the outlet of evaporation section.

$\dot{m}_{SB}$: Mass flow rate of steam at inlet of the steam boiler, state (10).

$\dot{m}_{Drain}$: Mass flow rate of drain steam from drum, state (12).

$\dot{m}_{HPT}$: Mass flow rate of steam at the outlet of steam boiler, state (13*).

Pressure of steam boiler:

$$P_{SB} = (1 + \xi_{SB}) * P_{HPTi} \quad (5.73)$$

Where:

P_{HPTi}: Inlet pressure of HPT.

ξ_{SB}: The pressure loss coefficient (assumed value is 6%).

Temperature of steam boiler:

$$T_{SB} = T_{HPTi} + 5\ ^{0}C \quad (5.74)$$

Where:

T_{HPTi}: Inlet temperature of HPT.

3- Superheating heat exchanger:

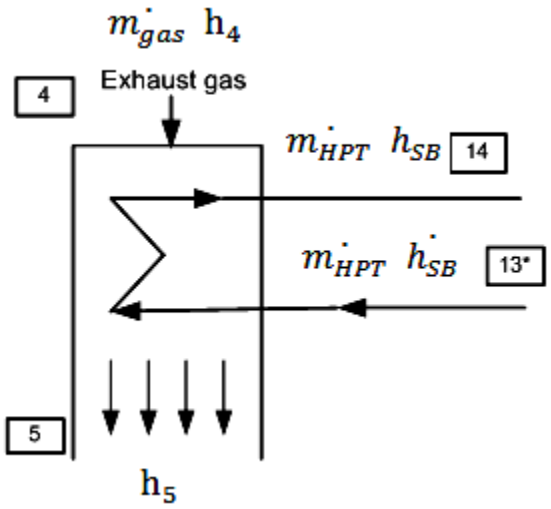

Figure 5.14 HRSG superheating section

Energy balance of super heating section:

$$m_{gas}^{\cdot} * (h_4 - h_5) * \eta_{GH1} = m_{HPT}^{\cdot} * (h_{SB} - h_{SB}^{\cdot}) \quad (5.75)$$

Where:

η_{GH1}: Effectiveness of super heater = 0.98. [18]

h_4: Evaluated specific enthalpy of exhaust gasses.

h_5: Evaluated specific enthalpy of exhaust gasses at the cold end of the superheating heat exchanger.

$m_{gas}^{\cdot}$: GT exhaust gasses' mass flow, state (4).

h_{SB}: Steam specific enthalpy at superheating section exit.

$$T_5 = T_{SB} + T_{min} \quad (5.76)$$

Where:

T_5 : Temperature of exhaust gasses at the end of the super heating stage; it is given assuming that it is above the water temperature inlet by the minimum allowed temperature difference at the heat exchanger (T_{min}).

4- Circulating process between boiler and HRSG:

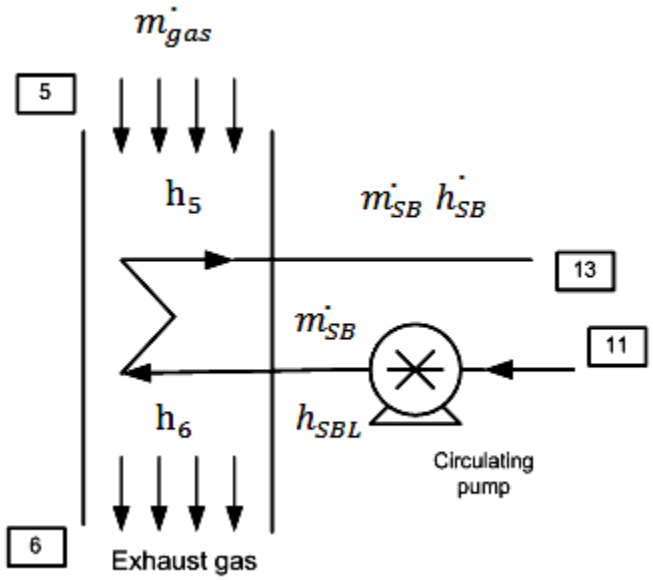

Figure 5.15 HRSG evaporating section

Energy balance of evaporating section:

$$m_{gas}^{\cdot} * (h_5 - h_6) * \eta_{GH2} = m_{SB}^{\cdot} * (h_{SB}^{\cdot} - h_{SBL}) \quad (5.77)$$

Where:

h_6: Evaluated specific enthalpy of exhaust gasses at the outlet of evaporating stage.

η_{GH2}: Effectiveness of the evaporator = 0.98. [18]

5- Feed water pump:

At state (9):

$$P_{FP} = (1 + \xi_P) * P_{HPTi} \quad (5.78)$$

Where:

P_{FP}: Pressure at the exit of feed water pump (bar).

ξ_P: Hydraulic losses coefficient for HRSG (assumed 0.12).

Gained heat due to water pressurizing by feed water pump:

$$\beta_{FP} = \frac{(P_{FP} - P_D) * Vf * 10^2}{{\eta_H}^P} \quad (5.79)$$

Where:

β_{FP}: Gained heat from pressurizing process of feed water pump, between state (8&9). (KJ/Kg)

P_D: Dearator pressure (bar).

${\eta_H}^P$: The hydraulic efficiency of water feed pump = 0.95. [65]

Vf: Specific volume of feed water (m^3/Kg).

Specific enthalpy of saturated water after the pressurizing process is given by Equation (5.80).

$$h_{FP} = \beta_{FP} + \dot{h_D} \quad (5.80)$$

Where:

$\dot{h_D}$: Specific enthalpy of saturated water provided by deaerator, state (7).

h_{FP}: Specific enthalpy of saturated water after the pressurizing process, state (9).

6- Preheating section:

Energy balance of pre-heating section:

$$m_{gas}^{\cdot} * (h_6 - h_{Exit}) * \eta_{GH3} = \dot{m}_{SB} * (h_{SBL} - h_{FP}) \quad (5.81)$$

Where:

h_{Exit}: Specific enthalpy of exhaust gasses at the end of HRSG.

η_{GH3}: Effectiveness of preheater = 0.98 [18].

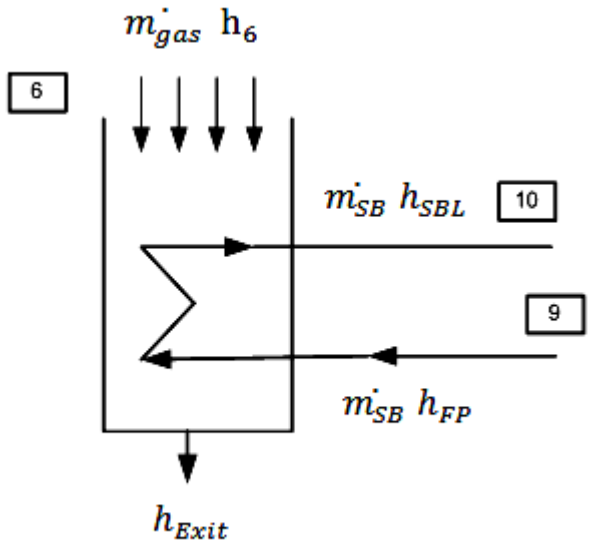

Figure 5.16 HRSG preheating section

7- Make up water system analysis:

This component contains two main parts. The first one is flash vessel (FV) and the second part is feed water heater (FWH).

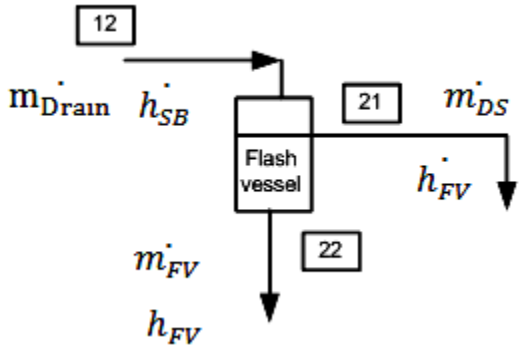

Figure 5.17 Flash vessel which is included in makeup water system

1- Equation of mass balance, (5.82), and energy balance,(5.83), for the flash vessel of make up water system as the following:

Mass flow rate in = Mass flow rate out

$$\dot{m_{drain}} = \dot{m_{FV}} + \dot{m_{DS}} \quad (5.82)$$

Where:

$\dot{m}_{Drain}$: Mass flow rate of drain steam from drum, state (12).

$\dot{m_{FV}}$: Mass flow rate of saturated liquid through flash vessel, state (22).

$\dot{m_{DS}}$: Mass flow rate of outlet saturated vapor from flash vessel, state (21).

$$\dot{m_{FV}} * h_{FV} + \dot{m_{DS}} * \dot{h_{FV}} = \dot{m_{drain}} * \dot{h_{SB}} * \eta_{FV} \quad (5.83)$$

Where:

h_{FV}: Specific enthalpy of saturated liquid at FV pressure, state (22).

$h_{FV}^{\cdot}$: Specific enthalpy of saturated vapor at FV pressure, State (21).

η_{FV}: Flash vessel efficiency = 0.98.

$$P_{FV} = 1.06 * P_D \quad [18] \tag{5.84}$$

Where:

P_{FV}: Flash vessel pressure.

2- Feed water heater of make up water system (FWH):

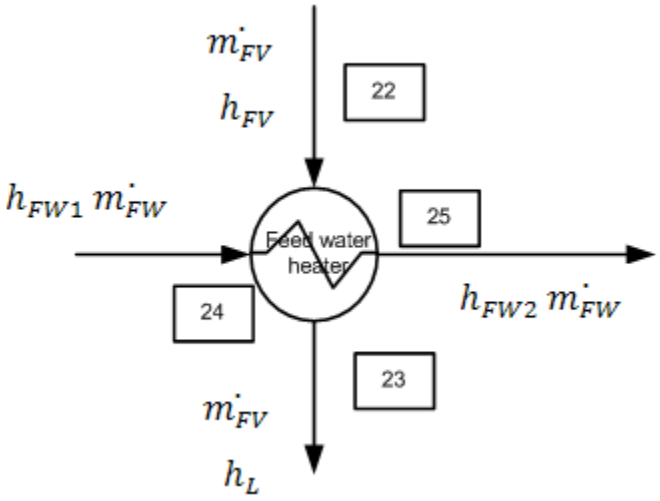

Figure 5.18 Schematic diagram of feed water heater

At state (24), temperature of makeup water = 30 °C

At state (23), temperature of rejected water = 60 °C

Energy balance

$$\dot{m_{FW}} * (h_{FW2} - h_{FW1)} = \dot{m_{FV}} * (h_{FV} - h_L) * \eta_{FWH} \quad (5.86)$$

Where:

$$\dot{m_{FW}} = \dot{m_{FV}} + \dot{m_{evap}} \quad (5.85)$$

$\dot{m_{FW}}$: Mass flow rate of makeup water, state (24 & 25).

$\dot{m_{Evap}}$: Mass flow rate of evaporated steam from deaerator.

h_{FW1}: Specific enthalpy of make up water, state (24).

h_{FW2}: Specific enthalpy of make up water, state (25).

h_L: Specific enthalpy of saturated water at outlet of FWH, state (23).

η_{FWH}: Efficiency of feed water heater =0.98.

8- The deaerator energy and mass balance:

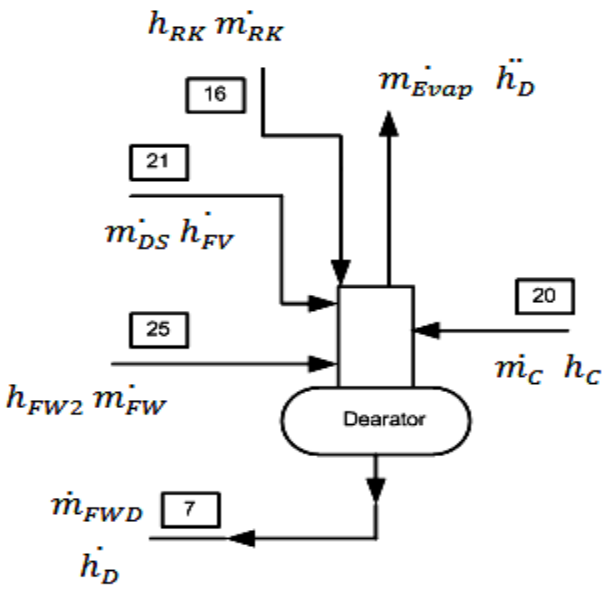

Figure 5.19 Deaerator thermal analysis

Mass balance

mass flow rate in = mass flow rate out

$$\dot{m}_{RK} + \dot{m}_C + \dot{m}_{DS} + \dot{m}_{FW} = \dot{m}_{FWD} + \dot{m}_{Evap} \quad (5.87)$$

Where:

$\dot{m}_{RK}$: Mass flow rate of steam extracted from HPT to operate deaerator, state (16).

$\dot{m}_C$: Condenser mass flow rate, state (20).

$\dot{m}_{FWD}$: Mass flow rate from deaerator, state (7).

$\dot{m}_{FW}$: Mass flow rate of makeup water, state (25).

$\dot{m}_{DS}$: Mass flow rate of outlet steam from flash vessel, state (21).

$\dot{m}_{Evap}$: Mass flow rate of evaporated steam from deaerator.

Energy balance

$$[\dot{m}_{RK} * h_{RK} + \dot{m}_C * h_C + \dot{m}_{DS} * \ddot{h}_{FV} + \dot{m}_{FW} * h_{FW2}] * \eta_D = \dot{m}_{FWD} * \dot{h}_D + \dot{m}_{Evap}\ddot{h}_D \quad (5.88)$$

Where:

h_{RK}: Specific enthalpy of extracted steam from HPT, state (16).

h_C: Specific enthalpy of condenced water by condencer, state (20).

$\ddot{h}_D$: Specific enthalpy of evaporated steam within the deaerator.

$\dot{h}_D$: Specific enthalpy of saturated liquid at deaerator's outlet.

η_D: Deaerator efficiency = 0.98. [18]

9- High pressure turbine (HPT) analysis:

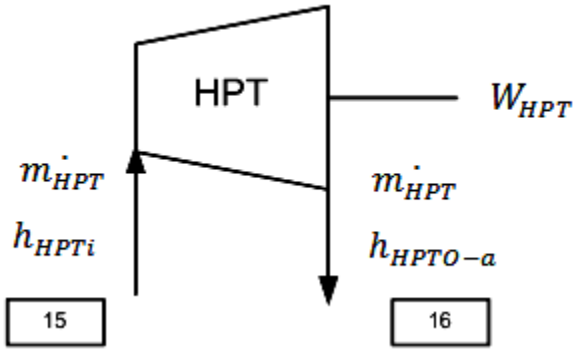

Figure 5.20 Schematic diagram of HPT

Design parameters give the steam conditions at the HPT exit.

$$S_i = f(P_{HPTi}, T_{HPTi}) \tag{5.89}$$

Where:

S_i: Specific entropy at the HPT inlet.

Due to isentropic expansion, entropy at terminals of the turbine will be the same.

S_o=S_i

$$h_{HPTo}{}^{S} = f(P_{HPTo}, S_o) \tag{5.90}$$

$$h_{HPTO-a} = h_{HPTi} - \eta^{HPT} * (h_{HPTi} - h_{HPTo}{}^{S}) \tag{5.91}$$

Where:

$h_{HPTo}{}^{S}$: Specific enthalpy at the end of the isentropic expansion of the steam in HPT.

h_{HPTO-a}: Actual Specific enthalpy of the steam at the outlet of high pressure turbine.

h_{HPTi}: Specific enthalpy of the steam at the inlet of high pressure turbine.

η^{HPT}: Isentropic efficiency of High pressure turbine which can be calculated by Equation (5.13). [18]

Energy balance of HPT

$$\dot{m_{HPT}} * (h_{HPTi} - h_{HPTO-a}) = W_{HPT} \tag{5.92}$$

Where:

W_{HPT}: Actual work of HPT (KW).

10- Low pressure turbine (LPT) analysis:

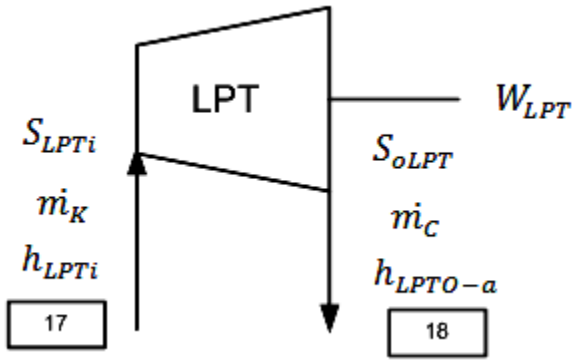

Figure 5.21 Schematic diagram of LPT in conventional combined cycle (CC)

Where:

$$\dot{m}_C = \dot{m}_K$$

Design parameters give the steam conditions at the LPT exit.

$$S_{iLPT} = f(P_{LPTi}, T_{LPTi}) \quad (5.93)$$

$$S_{iLPT} = S_o \quad (5.94)$$

Similar to HPT, $S_{iLPT} = S_{oLPT}$ (5.95)

$$h_{LPTo}{}^{S} = f(P_{LPTo}, S_{oLPT}) \quad (5.96)$$

$$h_{LPTO-a} = h_{LPTi} - \eta^{LPT} * (h_{LPTi} - h_{LPTo}{}^{S}) \quad (5.97)$$

$$h_{LPTi} = h_{HPTO-a} \quad (5.98)$$

Where:

S_{iLPT}: Specific entropy of steam at the inlet of LPT, state (17).

S_{oLPT}: Specific entropy of steam at the outlet of LPT, state (18).

h_{LPTi}: Specific enthalpy of steam at the inlet of low pressure turbine, state (17).

$h_{LPTo}{}^{S}$: Specific enthalpy at the end of the isentropic expansion of the steam in LPT.

h_{LPTO-a}: Actual Specific enthalpy of steam at the outlet of low pressure turbine, state (18).

η^{LPT}: Isentropic efficiency of low pressure turbine which can be calculated by Equation (5.13). [18]

Energy balance of LPT as a component of a combined cycle (CC) only

$$\dot{m}_C * (h_{LPTi} - h_{LPTO-a}) = W_{LPT} \quad (5.99)$$

Where:

W_{LPT}: Actual work of LPT in CC mode. (KW)

Effect of solar integration

The affected part in hybrid solar combined cycle (HYCS) by solar energy is LPT.

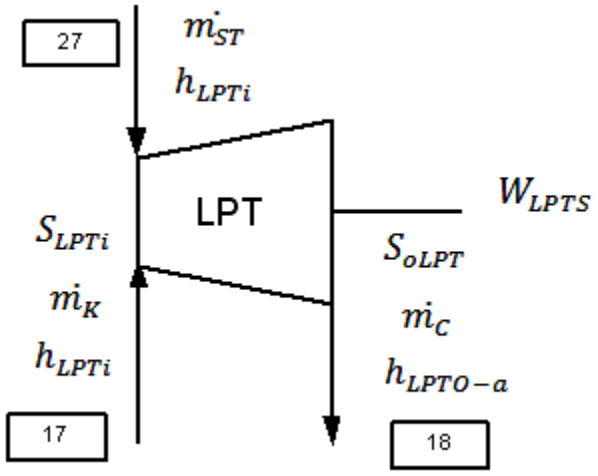

Figure 5.22 Schematic diagram of LPT in HYCS mode.

$$\dot{m}_{ST} = \dot{m}_{SF} * \left(h_{HTF,O} - h_{HTF,I}\right) * \eta_{SH}/(h_{Sto} - \dot{h}_D) \quad (5.100)$$

Where:

$\dot{m}_{ST}$: Steam generated in steam generator due to gained heat by solar field, state (27).

$\dot{m}_{SF}$: Mass flow rate of solar collectors' field.

$h_{HTF,O}$: Specific enthalpy of heat transfer fluid (HTF) at outlet of solar field.

$h_{HTF,I}$: Specific enthalpy of HTF at inlet of solar field.

$h_{ST,O}$: Specific enthalpy of steam generated in steam generator.

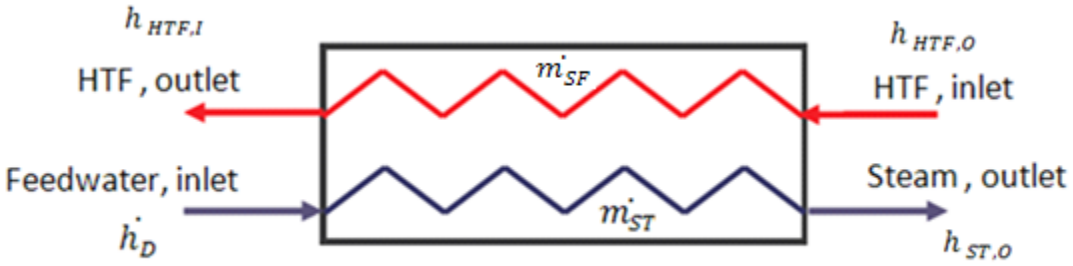

Figure 5.23 Solar steam generator

$$h_{ST,O} = h_{LPTi} \quad (5.101)$$

Mass balance of LPT in hybrid solar combined cycle (HYCS)

mass flow rate out = mass flow rate in

$$\dot{m}_C = \dot{m}_{ST} + \dot{m}_K \quad (5.102)$$

Where:

$\dot{m}_K$: Mass flow rate of steam which expanded in LPT in HYCS mode, state (17).

Energy balance of LPT as a component of hybrid solar combined cycle (HYCS):

$$\dot{m}_C * (h_{LPTi} - h_{LPTO-a}) = W_{LPTS} \quad (5.103)$$

Where:

W_{LPTS}: Actual work of LPT in HYCS mode (KW).

Output of electrical power in CC &HYCS mode:

1- The generated electricity from HPT and LPT in CC mode in (W):

$$NE_{ST} = (W_{HPT} + W_{LPT}) * 10^3 \quad (5.104)$$

2- The generated electricity from HPT and LPT in HYCS mode in (W):

$$NE_{STS} = (W_{HPT} + W_{LPTS}) * 10^3 \quad (5.105)$$

3- The energy consumption by water feed pump in (W):

$$N_{FP} = \frac{1000 * m_{FW} * \tau_{FP}}{\eta_{mp} * \eta_{ep}} \quad (5.106)$$

Where:

η_{mp}: Mechanical efficiency of feed pump.

η_{ep}: Electrical efficiency of feed pump.

CHAPTER 6

CODE VALIDATION

Validation of EES code with Thermo-flex software code has been done. This validation has been carried out for four components as follows.

1- Simple gas turbine unit.

2- Combined cycle unit.

3- Parabolic trough solar collector.

4- Hybrid solar combined cycle.

The first part is comparison between results of EES code and Thermo-flex code for the same gas turbine unit, as shown in Fig. 6.1. Table 6.1 shows inputs and outputs of each code, where any parameter is adjusted as input that means it is given or it is taken from the other code. In conclusion, two codes are matching very well with highest percentage of error 1% between two codes.

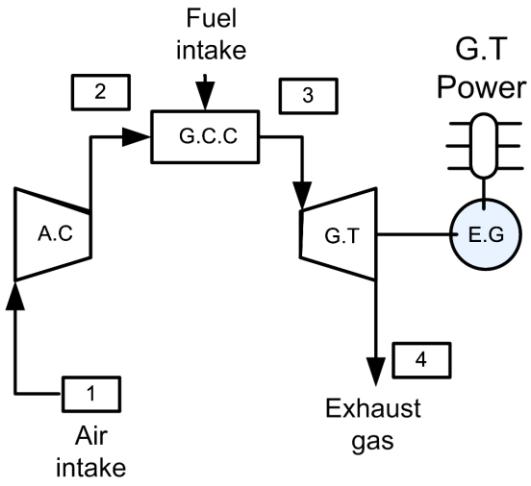

Figure 6.1 Schematic diagram of gas turbine

Table 6.1 Comparison between EES code and Thermo-flex code for gas turbine unit

property	Unit	Status (EES)	Status (THX)	EES value	THX value	Difference (%)
T_1	°K	Input	Input	288.1	288.1	0.00
P_1	Bar	Input	Input	1.01325	1.01325	0.00
$CP_{Air,C}$	KJ/Kg. °K	Input	Input	1.039	1.039	0.00
$\dot{m_{air}}$	Kg/sec	Output	Input	202.1	203.5	0.70
T_2	°K	Output	Output	676.2	676.2	0.00
P_2	Bar	Output	Output	15.91	15.91	0.00
$\dot{m_{fuel}}$	Kg/sec	Output	Output	3.57	3.564	0.10
T_3	°K	Input	Input	1373	1373	0.00
P_3	Bar	Output	Output	15.3	15.3	0.00
$CP_{Air,T}$	KJ/Kg. °K	Input	Input	1.209	1.209	0.00
T_4	°K	Input	Input	759.3	759.3	0.00

P_4	Bar	Input	Input	1.01325	1.01325	0.00
η_c	%	Input	Output	86.05	86.05	0.00
η_T	%	Input	Output	92.75	92.75	0.00
P_C	KW	Output	Output	81515	82069.4	0.60
P_T	KW	Output	Output	155356	153727.8	1.00
P_{Net}	KW	Output	Output	69795	69795	0.00
η_{GTU}	%	Output	Output	39.06	39.13	0.01
η_{mech}	%	Input	Input	99.8	99.8	0.00
η_{elec}	%	Input	Input	98.3	98.3	0.00

There is one difference between two codes as the following:

1- Compressor and turbine power of EES code have small differences compared with results of Thermo-flex code due to slightly difference of air mass flow rate.

The second part of code validation is dealing with combined cycle as shown in Fig. 6.2. Table 6.2 shows good agreement between results of two codes. This combined cycle generates steam without burning extra fuel. The main source of heat in this combined cycle is exhaust gases. The difference between specific enthalpies in gas side for each heat exchanger will be different due to different composition of exhaust gas in two codes. This difference directly will affect the amount of steam generated, and then it will affect the output work of steam turbines.

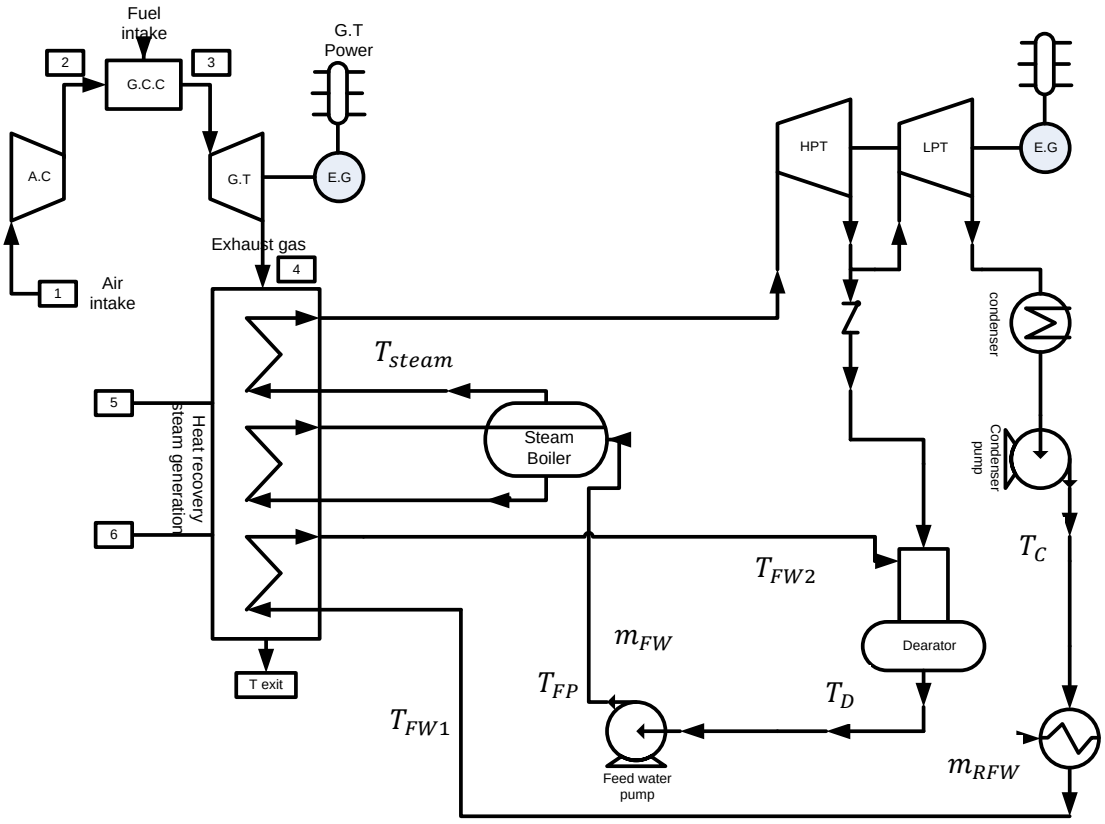

Figure 6.2 Schematic diagram of gas turbine combined cycle

Table 6.2 Comparison between EES code and Thermo-flex code for HRSG and steam turbines

property	Unit	Status (EES)	Status (THX)	EES value	THX value	Difference (%)
$T_{5\ air}$	ºK	Input	Output	645.5	645.5	0.00
T_{HPTi}	ºK	Input	Output	758.3	758.3	0.00
H_{HPTi}	Kj/Kg	Output	Output	3378	3378	0.00
T_{steam}	ºK	Output	Output	550	550	0.00
H_{steam}	Kj/Kg	Output	Output	2783	2783	0.00
T_{FP}	ºK	Output	Output	454	454.3	0.00

H_{FP}	Kj/Kg	Output	Output	769.7	771.28	0.08
T_D	ºK	Output	Output	453	453	0.00
H_D	Kj/Kg	Output	Output	762.8	762.8	0.00
T_C	ºK	Output	Output	311.9	311.9	0.00
H_C	Kj/Kg	Output	Output	162.1	162.1	0.00
T_{RFW}	ºK	Input	Input	288.1	288.1	0.00
H_{RFW}	Kj/Kg	Output	Output	62.71	63	0.46
T_{FW1}	ºK	Output	Output	310.3	311.8	0.48
H_{FW1}	Kj/Kg	Output	Output	161.1	162.71	1.00
T_{FW2}	ºK	Output	Output	453	453	0.00
H_{FW2}	Kj/Kg	Output	Output	762.8	762.76	0.01
T_{HPTo}	ºK	Output	Output	529.6	530.8	0.15
H_{HPTo}	Kj/Kg	Output	Output	2956	2959.7	0.13
η_{HPT}	%	Output	Output	87.78	87.24	0.62
P_{HPTi}	Bar	Input	Input	60	60	0.00
P_{HPTo}	Bar	Input	Input	10	10	0.00
T_{LPTi}	ºK	Output	Output	529.6	530.8	0.15
H_{LPTi}	Kj/Kg	Output	Output	2956	2959.74	0.13
η_{LPT}	%	Output	Output	83.31	84.22	1.00
P_{LPTi}	Bar	Input	Input	10	10	0.00
P_{LPTo}	Bar	Input	Input	0.0689	0.0689	0.00
P_D	Bar	Input	Input	10	10	0.00
P_C	Bar	Input	Input	0.0689	0.0689	0.00
m_{HPTi}	Kg/sec	Output	Output	19.59	19.27	1.60

m_{LPTi}	Kg/sec	Output	Output	19.59	19.27	1.60
m_{FW}	Kg/sec	Output	Output	19.69	19.37	1.60
W_{HPT}	KW	Output	Output	8359	8215	1.75
W_{LPT}	KW	Output	Output	13509	12972	4.13
W_{pumps}	KW	Output	Output	210	206.3	1.80
W_{Net}	KW	Output	Output	21437.4	20978.7	2.18

There are some negligible differences between two codes as the following:

1- Outlet conditions (temperature and specific enthalpy) of HPT are different due to negligible difference between turbines efficiencies.

2- Inlet conditions (temperature and specific enthalpy) of LPT are different due to negligible difference between turbines efficiencies.

3- Steam flow rates in HPT and LPT are slightly different due to difference between exhaust gas and air compositions.

4- Power of steam turbines is different due to negligible difference between turbines efficiencies and difference of steam mass flow rate.

The third part of validation is carried out for parabolic trough solar collector. This part is divided into two divisions. The first division is estimating solar radiation for a specific location (site). The second division is evaluating the solar collector performance. Table 6.3 shows site specifications and Table 6.4 shows comparison of estimated solar radiation which is generated by two codes, EES and Thermo-flex. Table 6.5 shows collector

specifications which are common between two codes. Table 6.6 shows comparison between results of two codes.

Table 6.3 Site specifications to estimate solar radiation

Property	Unit	Value
Latitude	º	26.5
Altitude	m	91
Location		Dhahran/K.S.A

Table 6.4 Comparison between EES code and Thermo-flex code for estimated solar radiation

property	Unit	Status (EES)	Status (THX)	EES value	THX value	Difference (%)
Day of the year	Day	Input	Input	23 March(82)	23 March(82)	----------
Hour of the day (solar time)	Hour	Input	Input	12	12	----------
Estimated site direct irradiance	W/m^2	Output	Output	759.6	758.2	0.18

Table 6.5 Specifications of parabolic trough solar collector

Parameter	Unit	Value
D_{co}	m	0.136
D_{ci}	m	0.133
D_{to}	m	0.07
D_{ti}	m	0.067
W_a	m	5.6
ε_t	-------	0.31
ε_c	-------	0.9
f_n	m	1.66

Table 6.6 Comparison between EES code and Thermo-flex code for solar collector performance

Parameter	Unit	Status (EES)	Status (THX)	EES value	THX value	Difference (%)
T_{fi}	°K	Input	Input	454.3	454.3	0.00
P_i	bar	Input	Input	67.38	67.38	0.00
$\dot{m_{collec}}$	Kg/sec	Output	Output	4.8415	4.8415	0.00
L_{collec}	m	Input	Output	726.4	726.4	0.00
Number of rows connected in parallel	----	Input	Output	2	2	0.00
T_{fo}	°K	Output	Output	555.5	550	1.00
η_{collec}	%	Output	Output	65.5	65.31	0.30

Code validation shows good agreement between two codes with small variation in specific components such as gas turbine unit. Difference (%) values calculated by the following equation, where Thermo-flex value is taken as reference value.

$$Difference(\%) = \frac{Abs(EES_{value} - THX_{value})}{THX_{value}} * 100\% \quad (6.1)$$

Finally, all previous components have been connected together as shown in Fig. 6.3 where solar collector connected parallel with steam evaporator and each one evaporates half of the steam required to be expanded in high pressure turbine. This is called direct steam generation which is reported in this section. The purpose of this validation is to make sure that mathematical model which is used in Thermo-Flex software agrees with the mathematical model of published works. Based on the light of this validation, indirect steam generation has been used with little modifications on the HYCS cycle in the next section.

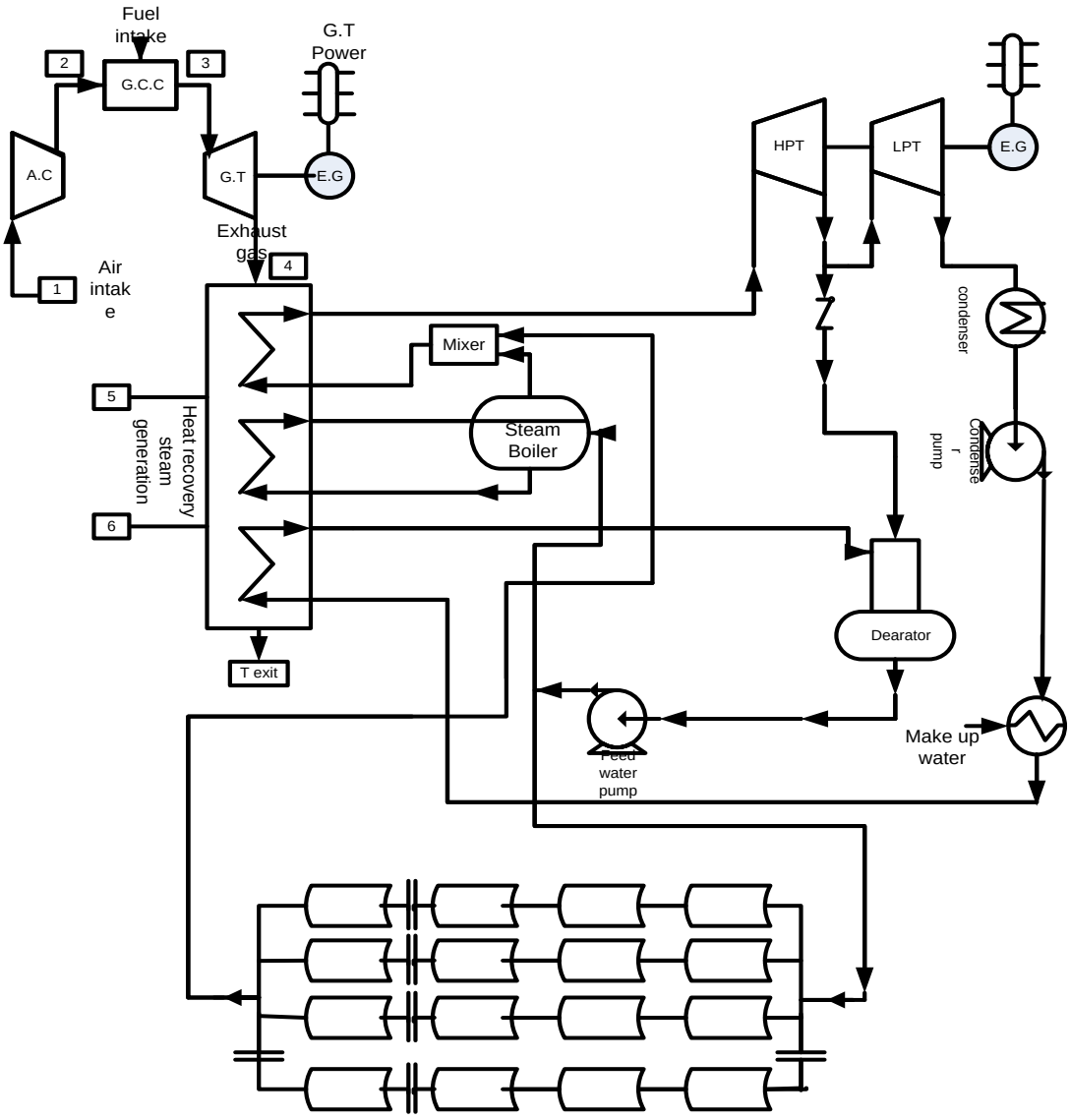

Figure 6.3 Schematic diagram of hybrid solar combined cycle

Table 6.7 Comparison between EES code and Thermo-flex code for performance of hybrid solar combined cycle

Parameter	Status (EES)	Status (THX)	EES value	THX value	Difference (%)
Total power (KW)	Output	Output	91453	90773.7	0.74
Electric efficiency (%)	Output	Output	51.18	50.89	0.57

As shown from previous validation, there are negligible differences and reasons of each one are mentioned under each table. Also, for hybrid system comparison there is negligible differences due to dependency of the hybrid system on these components.

CHAPTER 7

RESULTS AND DISCUSSIONS

7.1 ELECTRICAL LOAD IN SAUDI ARABIA

Electrical load of Saudi Arabia from 1994 - 2007 has been plotted in Fig. 7.1. Electrical load of the most recent year which is 2007 has been selected to be utilized in this analysis as shown in Fig. 7.2. Assumed electrical load has been suggested, as shown in Fig. 7.3 based on simple calculations as given in Table 7.2.

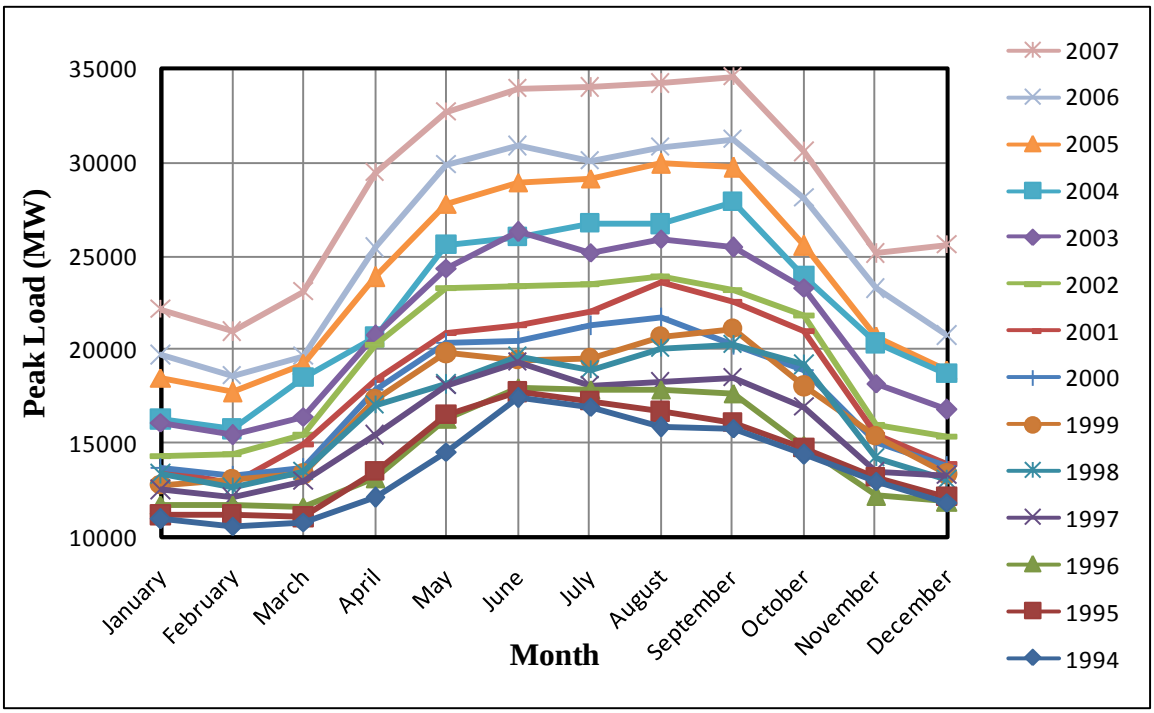

Figure 7.1 Electrical load of Saudi Arabia from 1994 – 2007

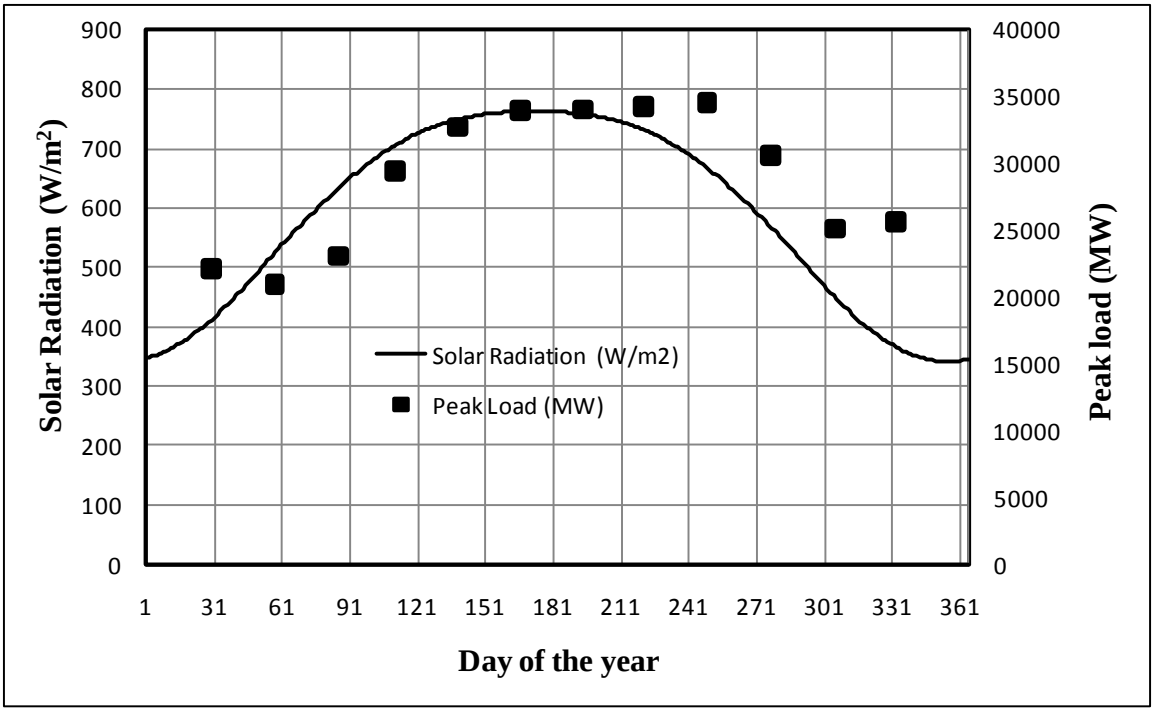

Figure 7.2 Synchronization solar radiation and electrical load of Saudi Arabia (2007)

Table 7.1 Electrical load of Saudi Arabia (2007)

Month	Load (MW)
January	22165
February	20929
March	23059
April	29453
May	32661
June	33923
July	33988
August	34192
September	34527
October	30551
November	25098
December	25579

Table 7.2 Calculations based on electrical load of Saudi Arabia (2007)

Average (MW)	29450.91
Peak (MW)	34527
Difference between the peak and the average load	17.23577

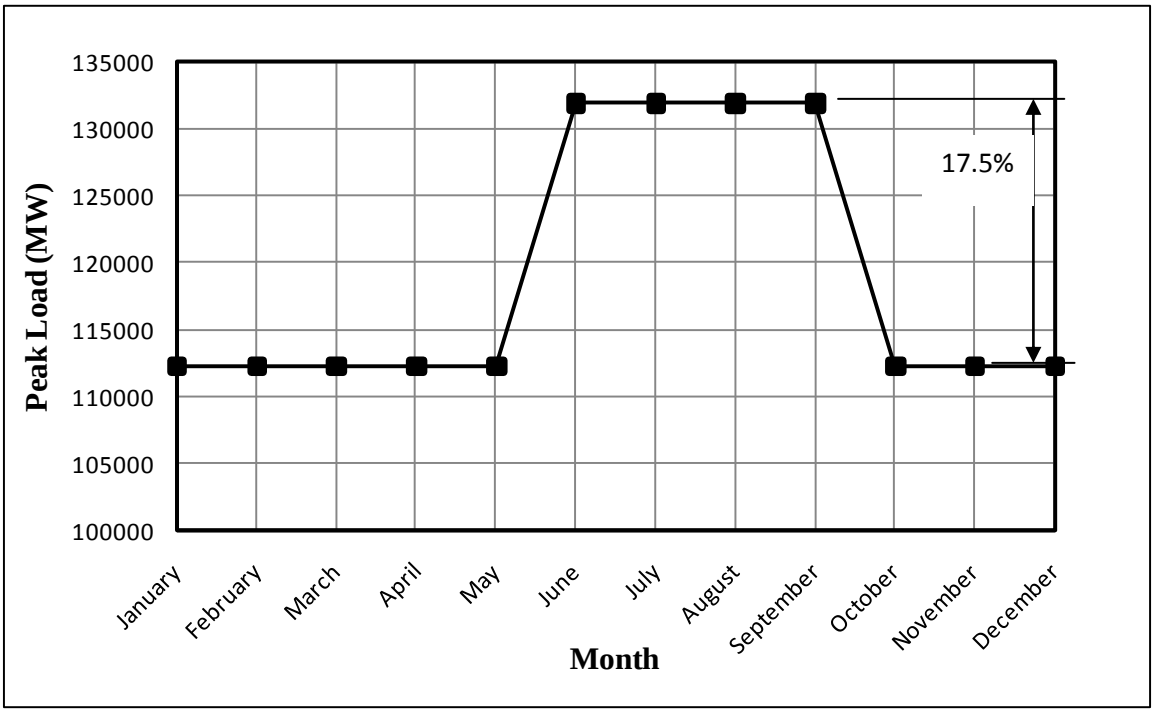

Figure 7.3 Simplified electrical load of small scale plant as representative for K.S.A load data provided in Table (7.2)

How to simulate this hybrid solar combined cycle for the whole year?

As known, every day has solar time and none solar time. This hybrid solar combined cycle can be switched from hybrid solar combined cycle into conventional combined cycle to be operated in none solar time where duct burner will burn proper amount of fuel to cover specific load. During solar time, daily average of solar radiation has been taken because processing time for each hour of the year takes around 1 minute. So, each run for different solar share will take around three days. Calculations for two different days based on hourly radiation and based on daily average solar radiation have been calculated as shown in Table 7.3 and Table 7.4. The first day is 21st June which is summer day and the second day is 1st January which is winter day. In conclusion, the difference doesn't exceed 0.91% for both days. So, using daily average solar radiation will not affect

performance of the hybrid solar combined cycle if and only if we use proper averaging method. Three averaged values for every day have been calculated. The first averaged value is based on 9 hours and the second averaged value is based on 11 hours. The third averaged value is based on 13 hours. Those averaged values have been applied to the same solar field size and same operation conditions. Results reveal averaging based on 11 or 13 hours is better than averaging based on 9 hours especially for summer's months (June, July, August, and September) as shown in Fig. 7.4. Averaging based on 13 hours gives the same values of averaging based on 11 hours as shown in Fig. 7.4. This is due to sun rise and sun set times. In other words, after 11 hours there is no solar radiation can be used.

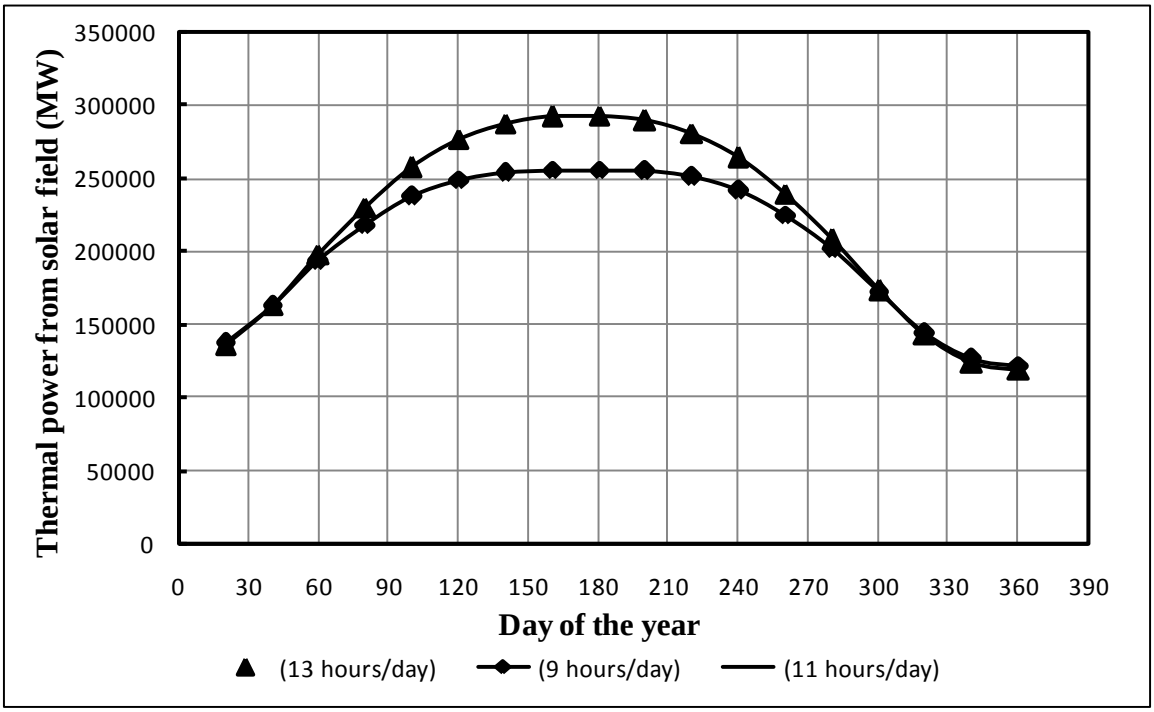

Figure 7.4 Thermal power of solar field based on different averaged value

Time estimation of three scenarios solarization steam and solarization gas turbine in combined cycle as the following:

Each scenario of solarization steam has thirteen different cases to be simulated. In this case, 1072 hrs are needed to complete one scenario. In order to complete all three scenarios, 3081 hrs are needed for simulations as computer real time operation without the required time of analysis. Moreover, there are ten cases need to be simulated as solarization gas turbine which need around 790 hrs. In summary, 167 days of continuous computer operation time are needed for these simulations using the best computer specifications (I7 CPU and 4 GIGA RAM).

Table 7.3 Thermal power gained from solar field based on hourly solar radiation and average daily solar radiation for 21st June

Hour	7	8	9	10	11	12	13	14	15	16	17
Solar radiation (W/m^2)	548.9	706.7	795.6	844	867.6	874.5	867.6	844	795.6	706.7	548.9
Solar thermal Power (KW)	18531	24459	27817	29654	30521	30580	30521	29654	27817	24459	18531
Total solar energy/day (KWh/day): based on hourly radiation						292544					
Total solar energy /day (KWh/day): based on daily average solar radiation multiplied by 11hours						293106					
Difference (%)						0.19					

Table 7.4 Thermal power gained from solar field based on hourly solar radiation and average daily solar radiation for 1st January

Hour	7	8	9	10	11	12	13	14	15	16	17
Solar radiation (W/m^2)	18	230.7	448	484.9	487.6	485.4	487.6	484.9	448	230.7	18
Solar thermal Power (KW)	0	6580	14650	15984	16060	15966	16060	15984	14650	6580	0
Total solar energy /day (KWh/day): based on hourly radiation						122514					
Total solar energy /day (KWh/day): based on daily average solar radiation multiplied by 11 hours						121396					
Difference (%)						0.91					

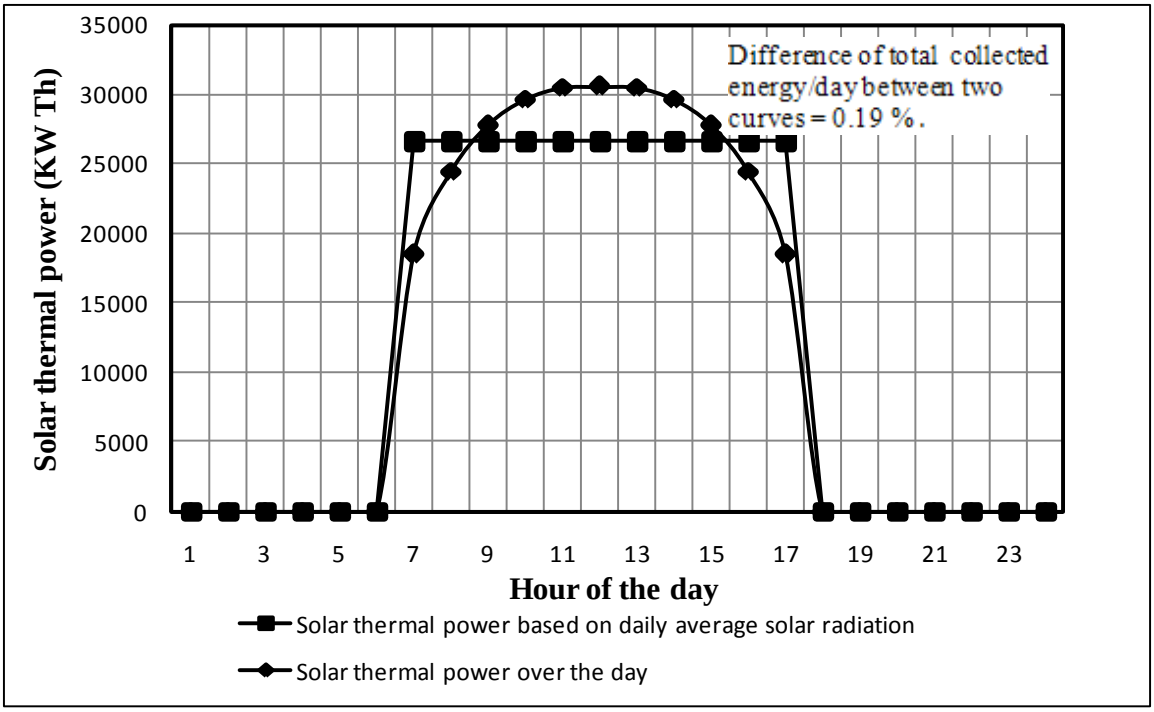

Figure 7.5 Solar thermal power over the day (21st June)

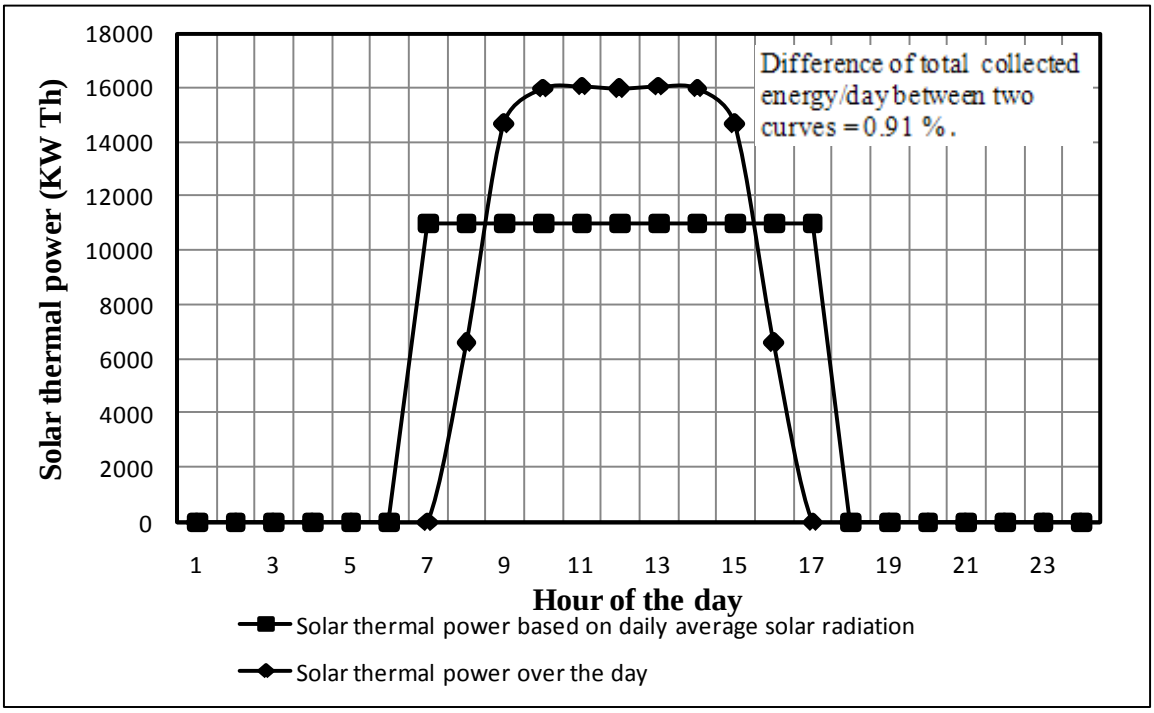

Figure 7.6 Solar thermal power over the day (1st January)

7.2 PROCEDURE TO SIMULATE HYBRID SOLAR COMBINED CYCLE

1- Follow the load of small scale plant as shown in Fig. 7.3.

2- Select and fix solar field size which is designed based on solar radiation at noon time for 21st June to be integrated with the optimized combined cycle, where the peak load happened frequently many times in this month from 1994 – 2007 as shown in Fig. 7.1.

3- Oil mass flow rate in the solar field is fixed.

4- Thermal power from solar field is varying according to the solar radiation intensity for every day in the year. As a result, the outlet temperature of the steam is changing but duct burner is operated to substitute the rest of the required energy for steam turbine.Any time solar field will not be able to cover specific load, duct burner will be operated.

6- Any time solar filed has more than enough energy which is needed to cover specific load, one of the following might take place:

1- Extra power is generated.

2- Solar field collectors are operated partially which means some loops are out of service.

3- Gas turbine is operated partially.

7- Evaluate performance of hybrid solar combined cycle for the three options which are mentioned above based on figures of merit such as annual solar share, avoidance of CO_2 emission, levelized electricity cost, and solar levelized electricity cost.

8- Go back to step (2) to increase or decrease solar field size which is known as solar multiple and do all steps until reach step (8). The purpose of changing solar multiple is to achieve the best solar share based on figures of merit.

Notes:

1- Solar multiple is representing ratio of thermal power produced by solar field to the input thermal power of turbine at design hour [66].

$$SM = \frac{P_{th,solar}}{P_{th,turbine}} \tag{7.1}$$

2- Increasing or decreasing of solar multiple (solar field size) can be carried out by increasing or decreasing the mass follow rate of oil (heat transfer fluid) with fixing inlet and outlet temperatures of the solar field (in design mode). In other words, design of different solar field sizes have been done at the same design hour but for different mass flow rates.

3- $$solar\ \ thermal\ \ \ power = \dot{m}_{oil} * (h_{outlet,SF} - h_{inlet,SF}) \tag{7.2}$$

7.2.1 Optimization of Conventional Combined Cycle

The first step in the whole system optimization is optimization of conventional combined cycle which contains gas turbine, heat recovery steam generator, and single-reheat steam turbine under optimal operation conditions (565 °C/125 bar) as mentioned in [17] and [67]. Furthermore, integrates different solar field sizes with the optimized conventional combined cycle. The difference from cycle to cycle depends on the sizes of gas turbine and steam turbine (ST/GT). In order to achieve the optimal ratio of (ST/GT), different ratios of (ST/GT) are simulated using Thermo-Flex with ambient temperature 25.6 °C as shown in Fig. 7.8. This configuration either CC or HYCS is regenerative reheat cycle with proper values of pressure and temperature which lead to long life of steam turbine. Fig. 7.9 shows TS diagram of steam turbines in CC and HYCS.

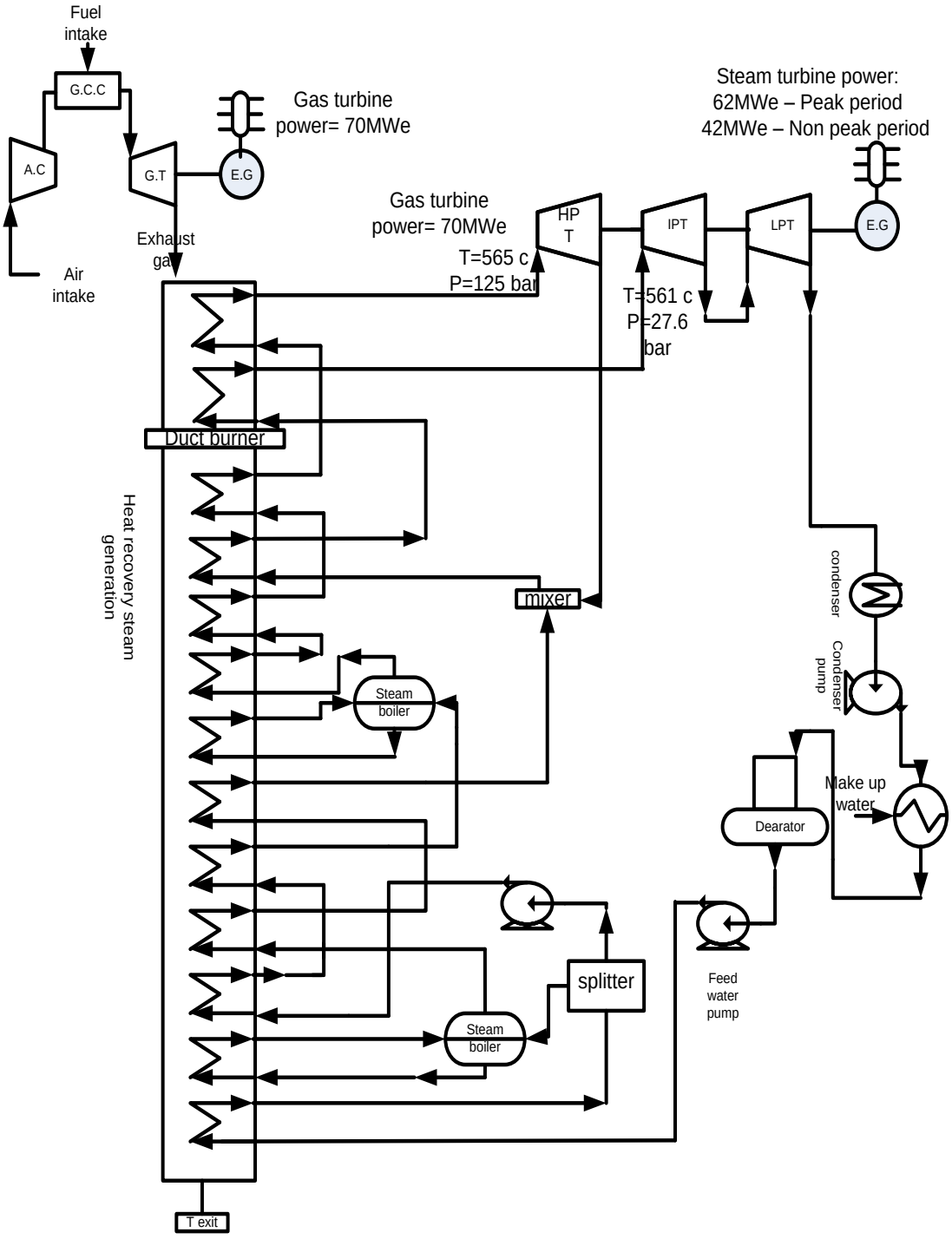

Figure 7.7 Schematic diagram of reference combined cycle which is shown in

Fig.7.8

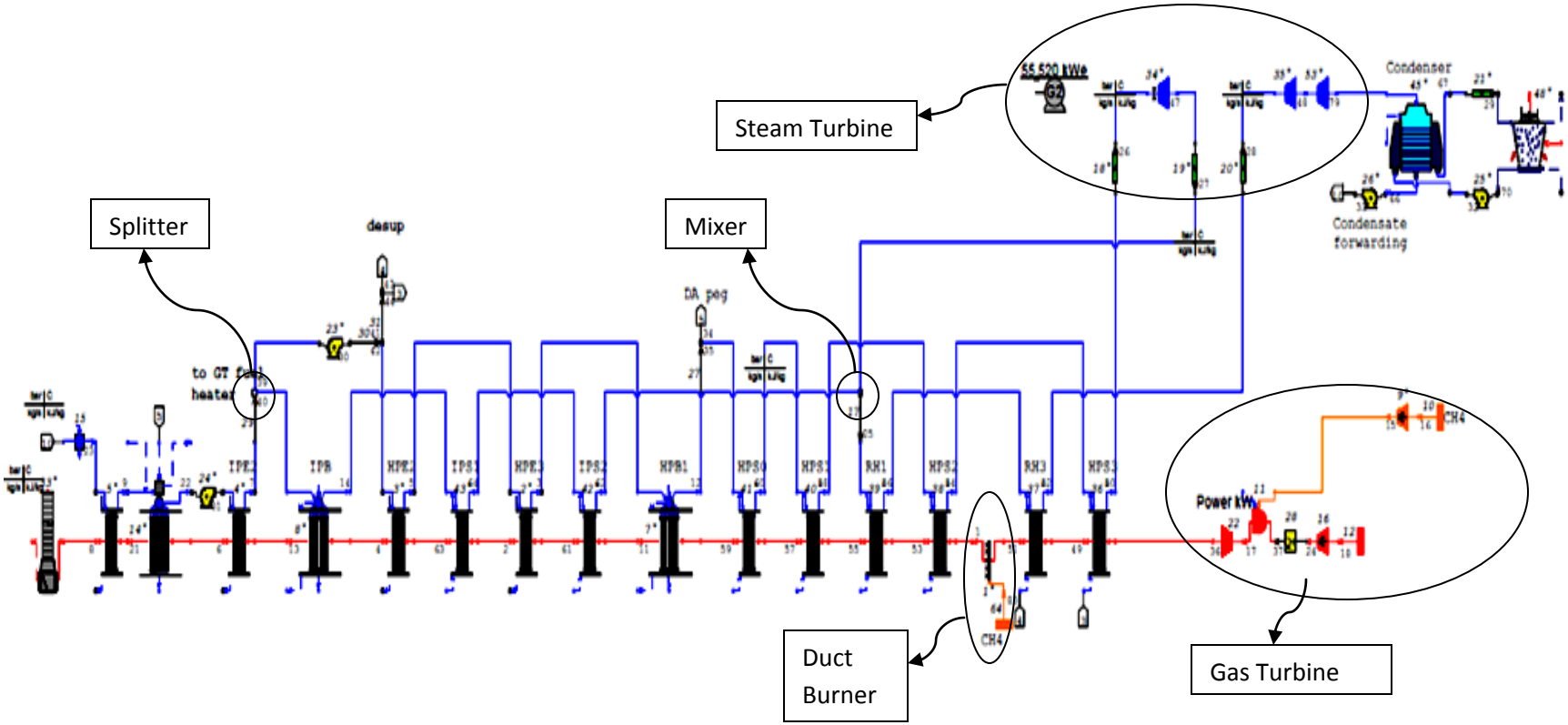

Figure 7.8 Schematic diagram of conventional combined cycle which has been simulated by Thermo-Flex

Table (7.5) shows the different ratios of ST/GT with LEC and evaporation energy required. As shown from tabulated results in Table (7.5) and specifically from Fig. 7.10, LEC which is the most important parameter is increasing with increasing ratio of ST/GT further 1 and increasing with decreasing ST/GT less than 1.

Table 7.5 Thermo-economic performance of different combined cycles

Power plant	Steam turbine	Combined cycle							Gas turbine
ST power (KW)	140623	94854	87207	71935	68065	40108	31089	18256	0.0
Actual GT power (KW)	0.0	44009	50981	65419	68862	96838	104822	116719	133736
Net Power of combined cycle (MW)	132	132	132	132	132	132	132	132	132
Ratio= ST/GT	---	2.155332	1.710578	1.099604	0.988426	0.414176	0.296589	0.15641	---
LEC(USD$/MWh)	71.9	62.8	61.6	58.9	57	57.9	62.4	65.2	71.6
Efficiency (%)	34.75	43.09	44.84	50.69	49.41	49.42	41.33	38.21	32.13
Mass flow rate of fuel in CC (Kg/s)	0.0	6.118	5.881	5.203	5.338	5.337	6.38	6.901	8.233
Mass flow rate of fuel in Duct burner (Kg/s)	7.59	3.936	3.28	1.346	1.304	0.864	0.0	0.0	0.0
Mass flow rate of water (Kg/s)	102.5	71.45	62.77	48.69	47.63	31.16	41.24	13.96	0.0
$h_{sat,vapor}$ **vapor(KJ/Kg)**	2802	2802	2802	2802	2802	2802	2802	2802	0.0
$h_{sat,liquid}$ **liquid(KJ/Kg)**	168.89	168.89	168.89	168.89	168.89	168.89	168.89	168.89	0.0
Evaporation energy (KW)	269893.775	188135.7	165280.3	128206.1	125415	82047.71	108589.5	36758.22	0.0

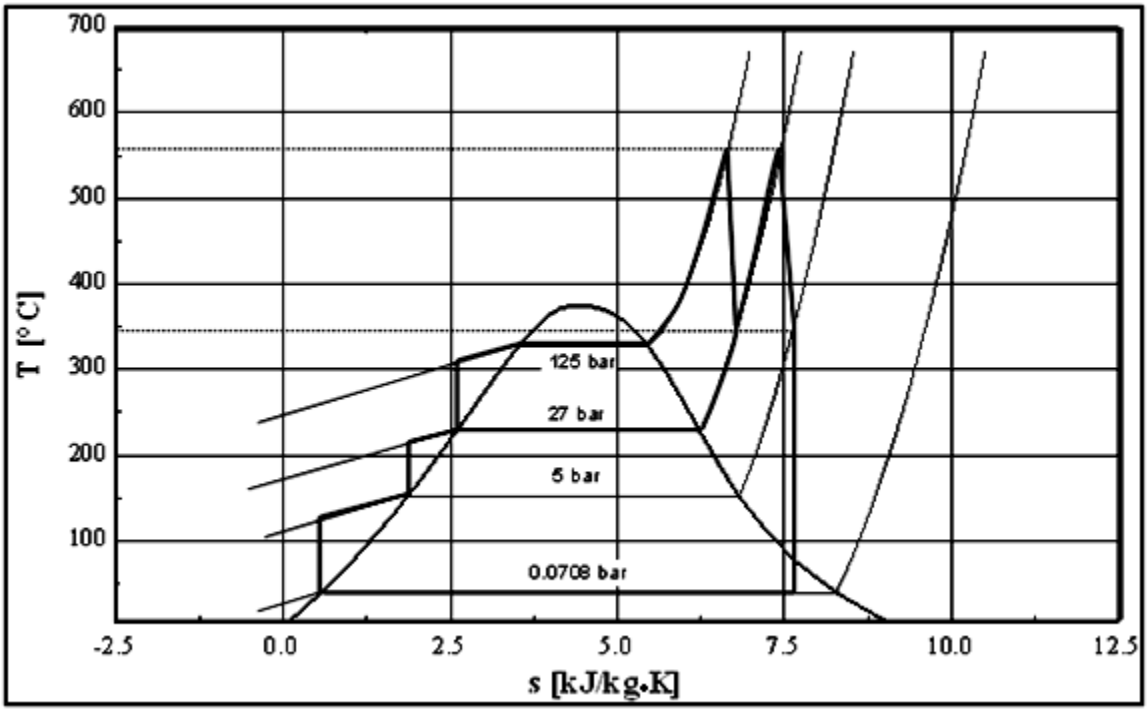

Figure 7.9 T.S diagram of steam turbines in CC and HYCS

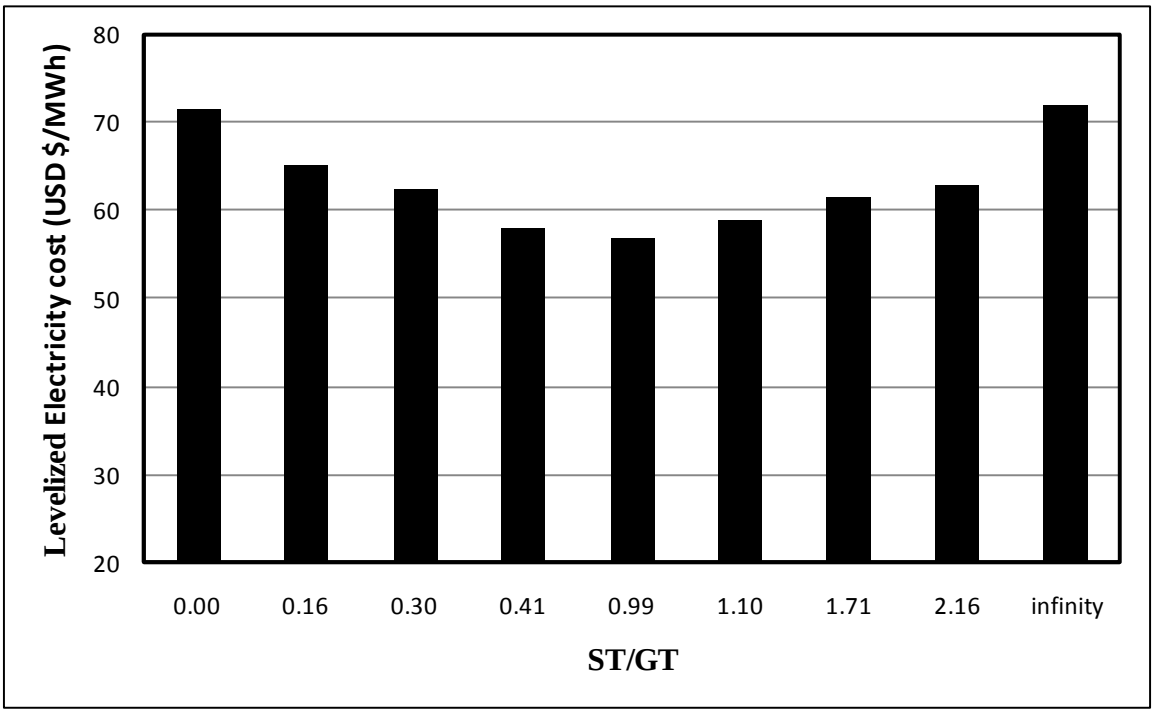

Figure 7.10 Levelized Electricity cost of different conventional combined cycles

7.2.2 Results and Analysis of Hybrid Solar Combined Cycle:

This section is about integration of solar with the optimized conventional combined cycle which has ratio of ST/GT around 1 for different configurations under Dhahran weather conditions as follows:

A. Integrating solar with steam side in combined cycle.

B. Integrating solar with gas turbine in combined cycle.

C. Integrating the optimum case of the first option with the optimum case of the second option.

After achieving the optimal integration configuration, different weather cities will be applied for the same optimal integration configuration to compare the results among different locations in Saudi Arabia.

A. Integrating solar with steam side in combined cycle under Dhahran weather conditions

In such configuration, solar field is integrated with steam side in conventional combined cycle for boiling process. In this regard, different solar thermal powers have been added into gas combined cycle to simulate hybrid solar combined cycle as shown in Fig. 7.11, by increasing area of solar field which is parabolic trough solar collector, solar collector properties and dimensions are given in Table 7.6. As mentioned before, there are three operating options (scenarios) need to be studied in order to evaluate performance of HYCS which are generation of extra power, following the load by operating solar field partially, and following the load by operating gas turbine partially.

Solar multiple has been increased due to increasing of solar field area as shown in Fig. 7.13 for all operating options. Solar thermal power will be the heat source to generate fraction of steam as much as possible under Dhahran weather conditions to operate steam turbine unit which is triple-pressure, single-reheat steam turbine under optimal operation conditions (565 °C/125 bar) as mentioned in [17] and [67]. Performance of hybrid solar combined cycle has been studied for those different solar shares in order to cover specific load. This specific load has non-peak demand of electricity for all months of the year except 4 months which are June, July, August, and September as shown in Fig.7.3. Those four months considered as peak demand period which equals 17.5% more than non-peak electrical demand of small scale plant.

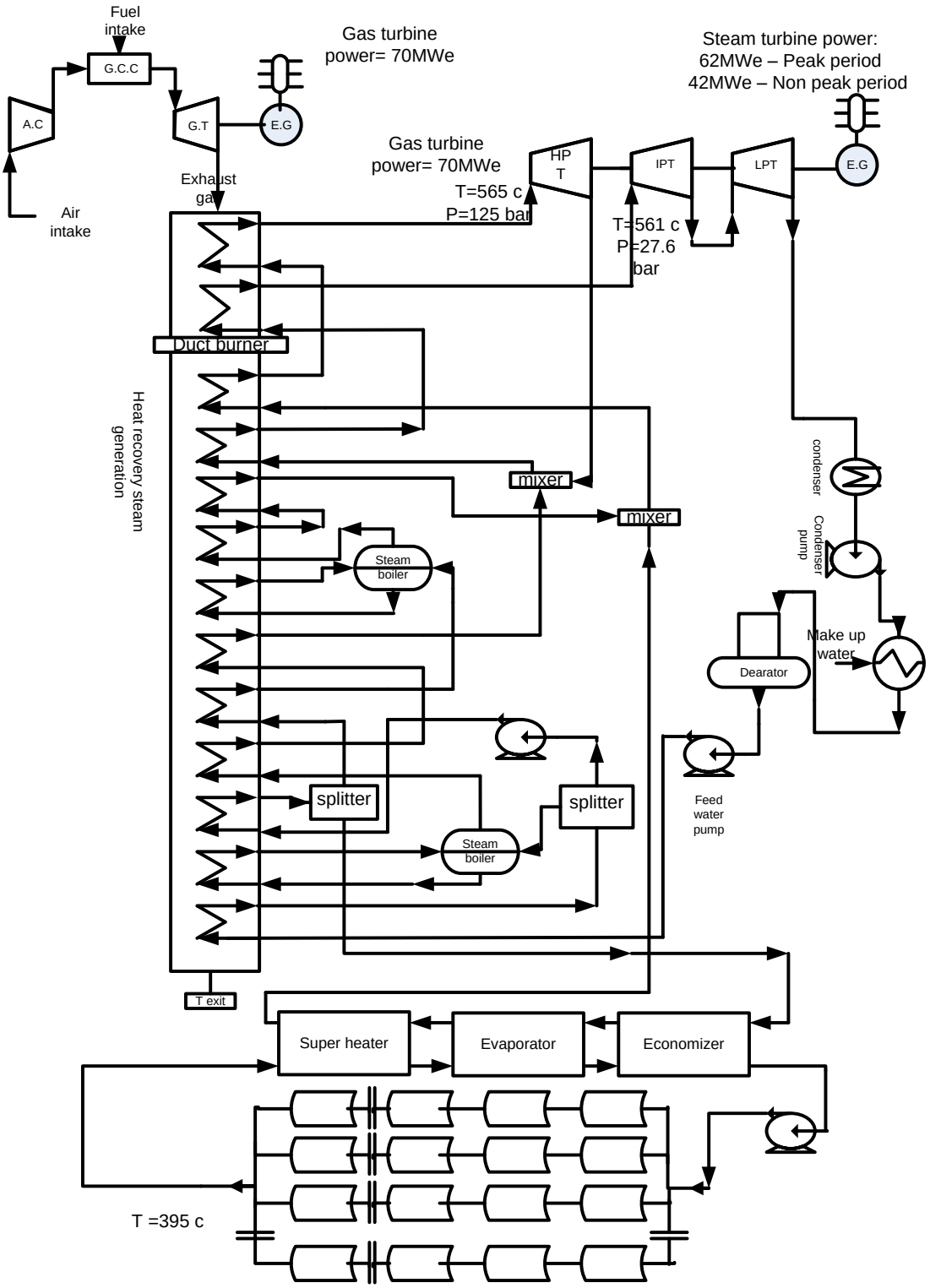

Figure 7.11 Schematic diagram of hybrid solar combined cycle (Solarization Steam side)

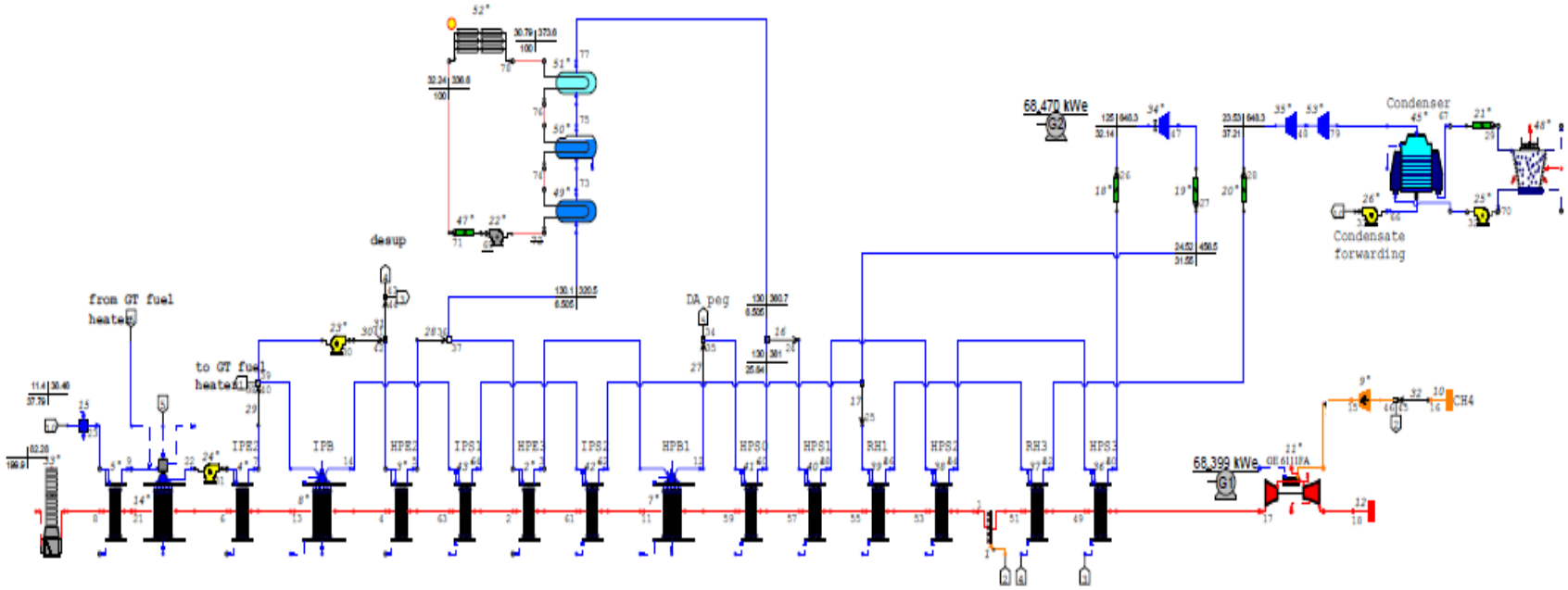

Figure 7.12 Schematic diagram of HYCS which has been simulated by Thermo Flex (Solarization Steam side)

Table 7.6 Dimensions and properties of solar collector [4]

Type	Luz (LS-3)
Aperture width [m]	5.76
Receiver tube outside diameter [m]	0.07
Receiver tube inside diameter [m]	0.067
Concentration ratio	82
Optical efficiency [%]	0.8
Receiver absorptivity	0.96
Mirror reflectivity	0.94
Receiver remittance	0.19
Focal length [m]	1.71

As mentioned previously, solar multiple is representing ratio of thermal power produced by solar field to the input thermal power of steam turbine at design hour. In this configuration, solar collector is integrated with high pressure steam turbine only. So, solar multiple represents the thermal power produced by solar field to the input thermal power of high pressure steam turbine at design hour as shown in Equation (7.3).

$$SM_{Steam} = \frac{P_{th,solar}}{P_{th,HPT}} \tag{7.3}$$

$$\boldsymbol{P_{th,HPT} = \dot{m}_{steam,HPT} * H_{in,HPT}}$$

$\boldsymbol{P_{th,HPT}}$=3416.4 KJ/Kg * 44.43 Kg/s = 151,791 KW

At the beginning, fluctuation of ambient temperature from hour to hour is affecting the performance of gas turbine as well as combined cycle. So, air temperature at the inlet of gas turbine has been fixed to study the effect of integrating solar with optimized CC for different configurations which are mentioned in the beginning of this section. As known,

air with low temperatures has higher density than air with high temperatures which leads to improve the efficiency of gas turbine. Two different temperatures have been simulated 39 ºC which is summer temperature and 25.6 ºC, which can be achieved by using evaporative cooler as example in summer, in order to compare the performance of solarization steam configuration in CC at different ambient temperatures for ‘’generation of extra power’’ operation scenario. Results reveal that thermo-economic performance of HYCS simulation with 25.6ºC is better than thermo-economic performance of HYCS simulation with 39ºC when 29 hectares of parabolic solar collectors are integrated with optimized CC. As shown in Table 7.7, LEC of HYCS simulation with 25.6 ºC is less than LEC of HYCS simulation with 39 ºC because the annual energy produced is higher. On the other hand, annual and instantaneous solar shares for case 39 ºC are higher than solar shares of case 25.6 ºC due to big room for solar collector to give more power since gas turbine performance is degraded. In this study, inlet temperature of gas turbine has been fixed as 25.6 ºC because it gives the best overall performance of HYCS which presented by LEC.

Table 7.7 Comparison of thermo-economic performance of HYCS for two different ambient temperatures

Assessment parameter	Solarization steam side (ambient temperature=25.6°C)	Solarization steam side (ambient temperature=39°C)
LEC ($/MWh)	63.17	65.16
Solar levelized electricity cost (LEC,solar) ($/MWh)	262	231
Annual CO_2 emission (K tonne)	385.2	385.56
CO_2 Avoidance (%)	6.83	7.54
Instantaneous net electrical solar share (%)	22.36	24.33
Annual solar share (%)	7.05	8.591

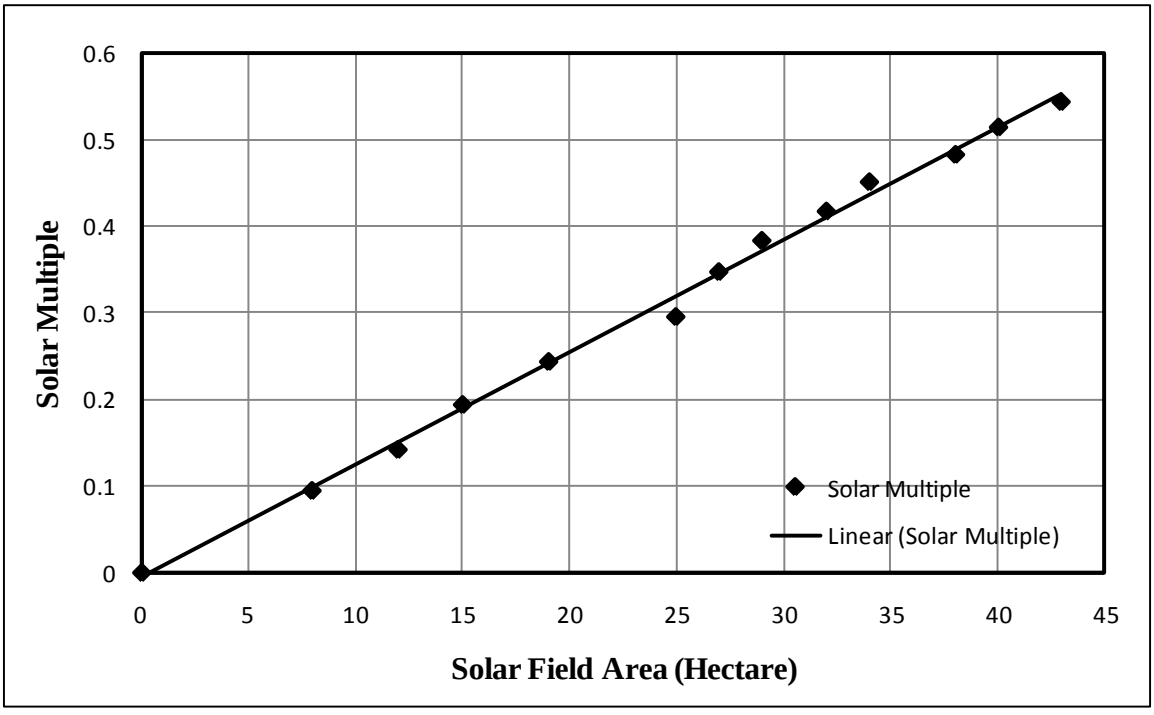

Figure 7.13 Solar multiple for different solar filed sizes

As shown from Fig. 7.13, solar multiple has increasing behaviour with increasing solar field size. This increasing of solar multiple save more amount of fuel as well as prevent more amount of CO_2 emissions.

Different parameters have been used to evaluate performance of integrating different solar field sizes with the optimized conventional combined cycle such as instantaneous net electrical solar share at design hour and annual solar share. Those parameters can be calculated by the following formulas where annual solar share gives an indication of how much power is produced annually by solar.

Instantaneous net electrical solar share:

$$X_{net,electrical,solar} = \frac{\eta_{net-incremental\ solar} * P_{th,solar}}{P_{el,net}} \tag{7.4}$$

$$\eta_{net-incremental\ solar} = \frac{P_{el,net} - \eta_{ref} * \dot{m}_{fuel} * LHV}{P_{th,solar}} \tag{7.5}$$

Where $X_{net,electrical,solar}$ is instantaneous net electrical solar share; $P_{th,solar}$ is thermal power produced by solar; $P_{el,net}$ is net electrical power from hybrid system; η_{ref} is efficiency of reference combined cycle.

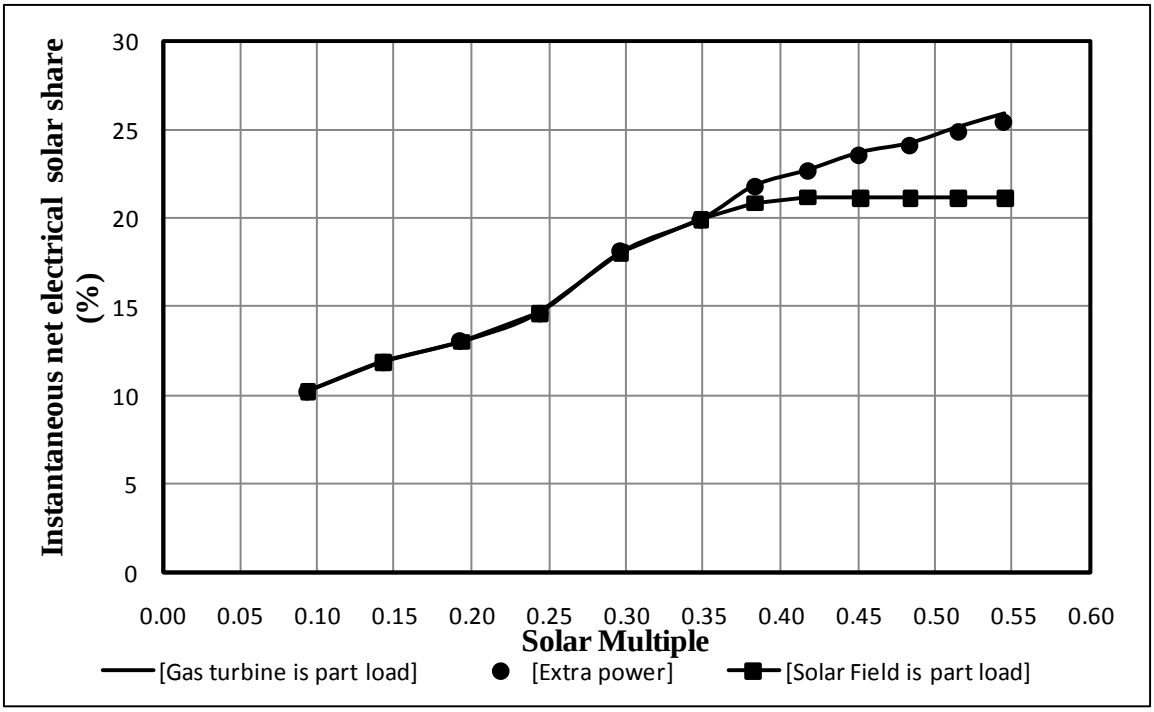

Figure 7.14 Instantaneous net electrical solar share for different solar multiples

As shown in Fig. 7.14, all three scenarios have the same instantaneous solar share from beginning up to 0.35 solar multiple. This is because solar thermal energy is less than thermal energy which is required for the hybrid system. Beyond 0.35 solar multiple, the three scenarios have different instantaneous solar shares. In fact, scenario of following the electrical load by operating solar field partially has fixed instantaneous solar shares due to limited thermal energy that is absorbed by solar collector. The remaining scenarios have different behaviours due to full absorption of collected solar energy. This full absorption of solar energy translates to another word which is saving fuel either scenario of following the load by operating gas turbine partially or generation of extra power is applied. So, they don't have fixed instantaneous solar shares.

Regarding Annual solar share, there are two definitions can be used to calculate annual solar share. The first one is based on input and output data (fuel consumption/KWh) as shown in the following equation.

$$Annual\ Solar\ Shar(SS) = 1 - \frac{(Annual\ Fuel\ consumption/\ KWh)_{HYCS}}{(Annual\ Fuel\ consumption/\ KWh)_{Reference\ CC}} \qquad (7.6)$$

And the second definition is based on output data (annual energy produced by solar) as shown in the following equation:

$$Annual\ Solar\ Share(X, o) = \frac{E_{Hybrid,annual} - \dot{m}_{fuel,Hybrid} * LHV * \eta_{Reference}}{E_{Hybrid,annual}} \qquad (7.7)$$

According to the first derivation in appendix C, the two expressions of annual solar share lead to the same results of annual solar share either its calculated based on fuel consumption/KWh or based on energy produced by solar.

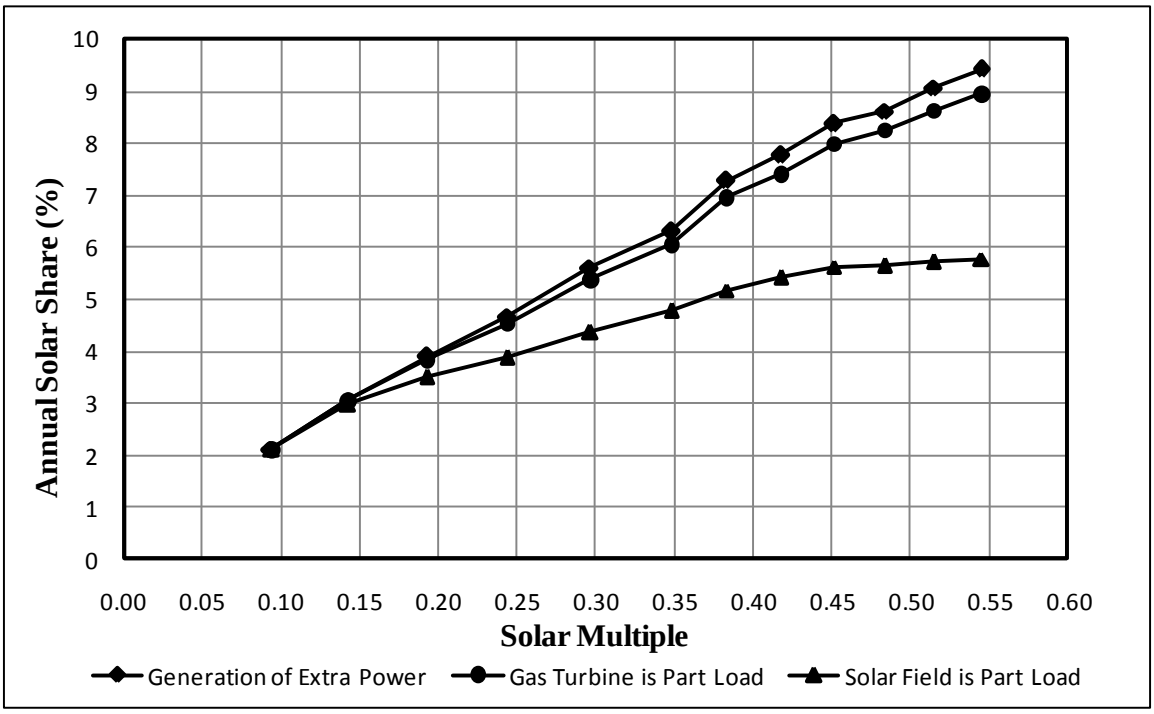

Figure 7.15 Annual solar share for different scenarios

In general, Fig. 7.15 shows annual solar share of different operation scenarios for different sizes of solar field. As shown from Fig. 7.15, scenario of following the electrical load by operating solar field partially has the lowest annual solar share. The reason behind this is some of solar loops are out of service when the absorbed thermal energy of solar field gives more than the specific electrical load. On the other hand, the remaining scenarios have used the whole absorbed thermal energy by solar field. So, they have increasing profile of annual solar share when solar multiple is increasing. This configuration has an environmental effect since increasing of solar share result in reduction of total fuel mass which is required for conventional combined cycle to cover specific load, and then CO_2 emissions have reduced as shown in Fig. 7.16. Also, CO_2 avoidance has been calculated based on the following formula.

$$\Delta co_2(\%) = \frac{co_{2_{HYCS}} - co_{2_{Ref}}}{co_{2_{Ref}}} * 100\% \tag{7.8}$$

Tabulated results in Table 7.8 show the highest CO_2 avoidance for the highest solar multiple for each operating option (scenario) which is much friendly to environment. Furthermore, using such hybridization systems reduce the penalty of CO_2 emission when it exceeds the allowable limit. As known, penalty of CO_2 emission equals 25 $/ tonne [68].

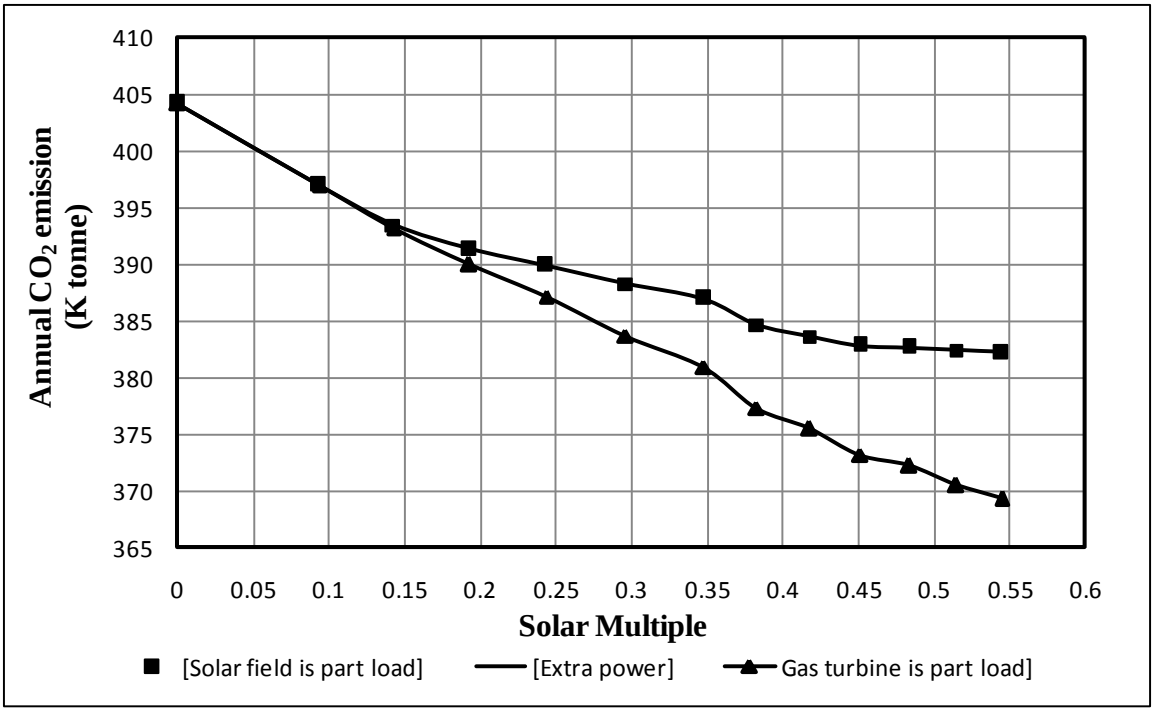

Figure 7.16 Annual CO_2 emissions for different solar multiples

Table 7.8 CO_2 avoidance for different solar multiples

Solar Multiple	CO_2Avoidance (Δco_2%) [Extra power]	CO_2Avoidance (Δco_2%) [Gas turbine is part load]	CO_2Avoidance (Δco_2%) [Solar field is part load]
0.00	0	0	0
0.09	1.80	1.80	1.80
0.14	2.75	2.74	2.67
0.19	3.60	3.53	3.20
0.24	4.36	4.23	3.56
0.30	5.32	5.09	3.95
0.35	6.12	5.77	4.28
0.38	6.96	6.66	4.85
0.42	7.47	7.13	5.11
0.45	8.08	7.70	5.30
0.48	8.32	7.93	5.34
0.51	8.77	8.35	5.40
0.54	9.13	8.67	5.48

After sunset, HYCS runs by burning fossil fuels only. So, fuel consumption is the same for different solar shares. It is obvious from Fig. 7.16 and Table 7.8 any increasing of solar multiple result in increasing of CO_2 avoidance. In conclusion, all different solar shares covered the specific load for all operating options (solar field is part load; gas turbine is part load, and generation of extra power).

Economic Analysis:

Economic analysis has been done in terms of levelized electricity cost (LEC) and solar levelized electricity cost (SLEC). Both terms can be calculated from the following equations. LEC can be calculated by the following formula. Table 7.9 provides parameters for performance and economical evaluation.

$$LEC = \frac{\left(f_{cr} * C_{investment} + C_{operation\,\&\,maintenace}\right)}{E_{Net}} \tag{7.9}$$

$$f_{cr} = \frac{K_d * (1 + K_d)^n}{(1 + K_d)^n - 1} + K_{insurance} \tag{7.10}$$

Where f_{cr} is annuity factor; K_d is the real debt interest ; $K_{insurance}$ is annual insurance rate; n is depreciation period in years; $C_{investment}$ is total investment of the plant; $C_{operation\&maintenace}$ is annual operation, and maintenance costs including fuel cost; and E_{Net} is annual net electricity [66].

Table 7.9 Parameters for performance and LEC evaluation

Fuel Heat rate (LHV) (KJ/Kg)	Debt interest rate (%)	Annual insurance rate (%)	Depreciation period (Year)	Fuel cost (USD/GJ)
50046.7	9	1	20	4.5

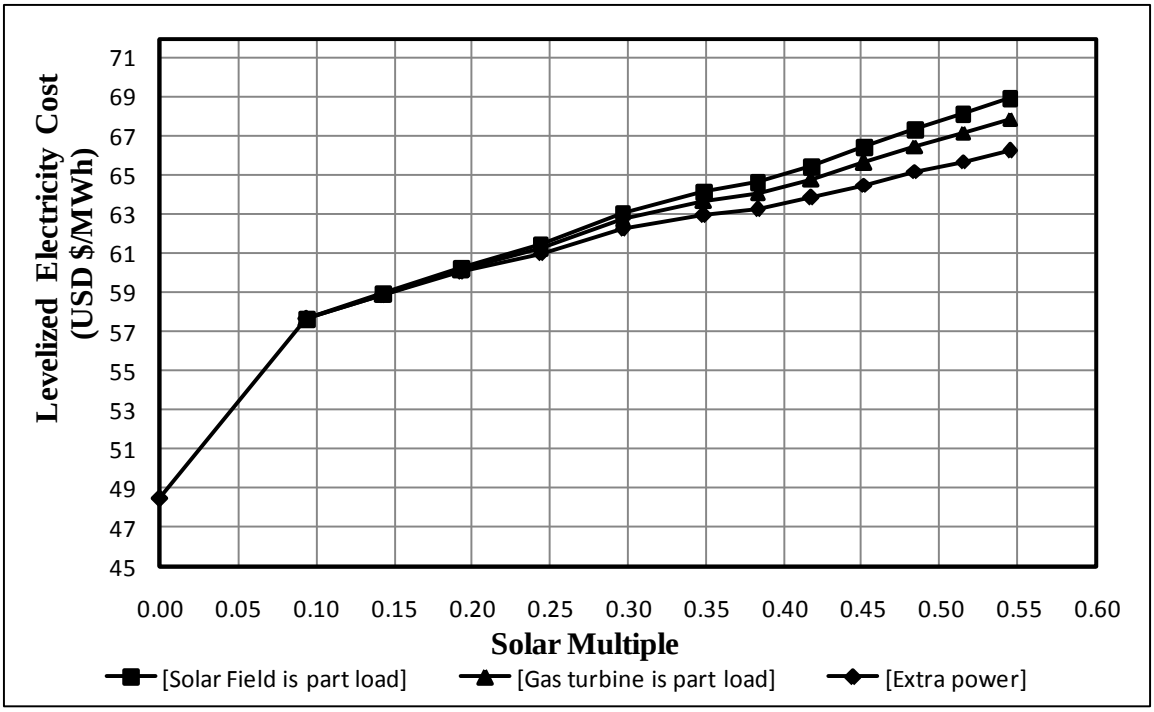

Figure 7.17 Levelized electricity cost of HYCS for different solar multiples

Fig. 7.17 shows the lowest levelized electricity cost of operating HYCS when extra power has been generated. This extra power can be sold for neighboured countries. Now, the best operating option (scenario) has been determined but still optimum solar multiple need to be determined.

The second parameter of economic analysis is SLEC which has been expressed in different forms in literature but with the same physical meanings as follows:

1- Calculate solar levelized electricity cost by considering solar field cost over annual energy produced by solar as shown in the following formula:

$$Solar, LEC = \frac{Cost_{solar\ field}}{W_s} \tag{7.11}$$

2- Calculate solar levelized electricity cost when annual solar share is based on output data (annual energy produced by solar) as shown in the following formula.

$$Solar, LEC = \frac{LEC_{HYSC} - \left[(1 - X_s) * LEC_{Ref.CC}\right]}{X_s} \quad (7.12)$$

Based on this option, there are 2 ways to calculate SLEC as follows:

a) Calculate SLEC when reference cycle is producing the same annual energy of HYCS.
b) Calculate SLEC when reference cycle is consuming the same amount of HYCS's fuel.

3- Calculate solar levelized electricity cost when annual solar share is based on input and output data (fuel consumption/KWh) as shown in the following formula.

$$Solar, LEC = \frac{LEC_{HYSC} - \left[(1 - SS) * LEC_{Ref.CC}\right]}{SS} \quad (7.13)$$

As mentioned previously, all forms for calculation $Solar, LEC$ have the same physical meanings which lead to the same results as shown in the second derivation in appendix C.

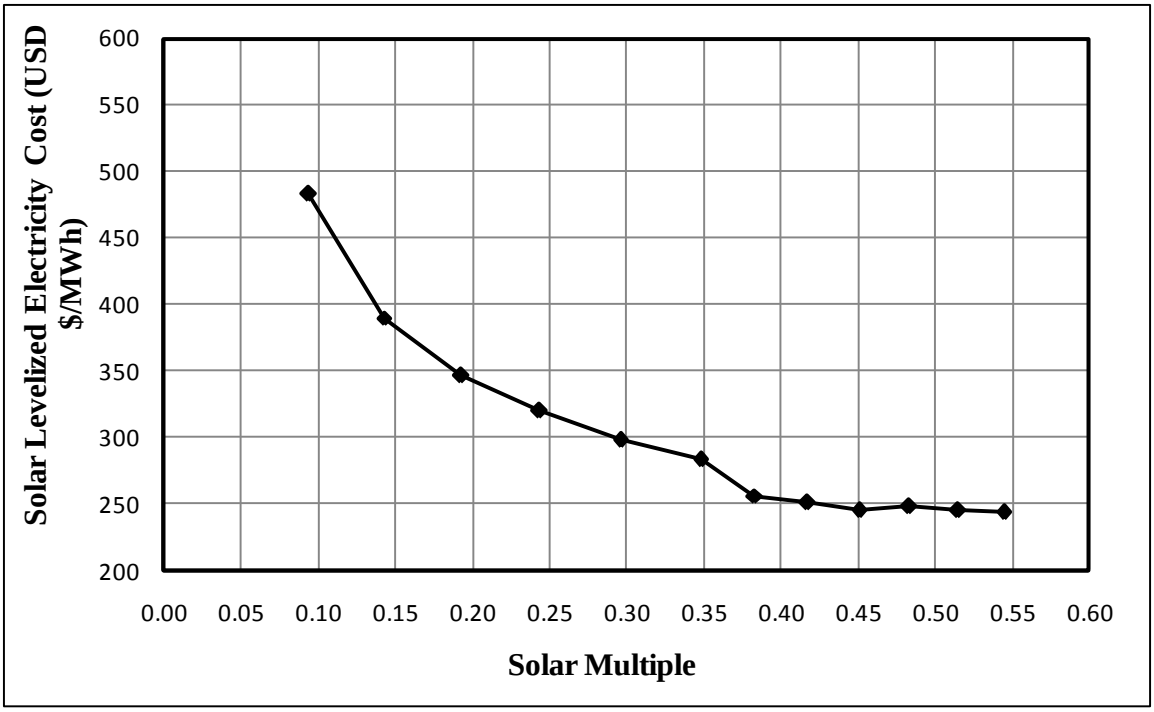

Figure 7.18 Solar levelized electricity cost of HYCS for different solar multiples (Generation of extra power)

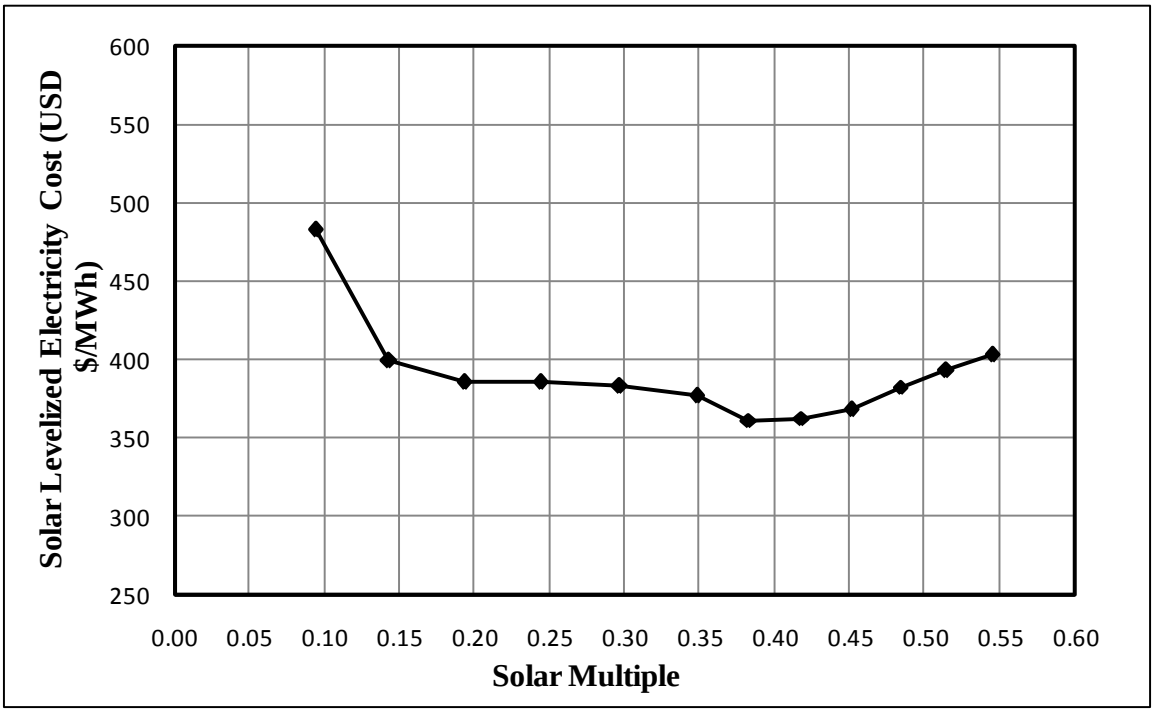

Figure 7.19 Solar levelized electricity cost of HYCS for different solar multiples (Solar field is part load)

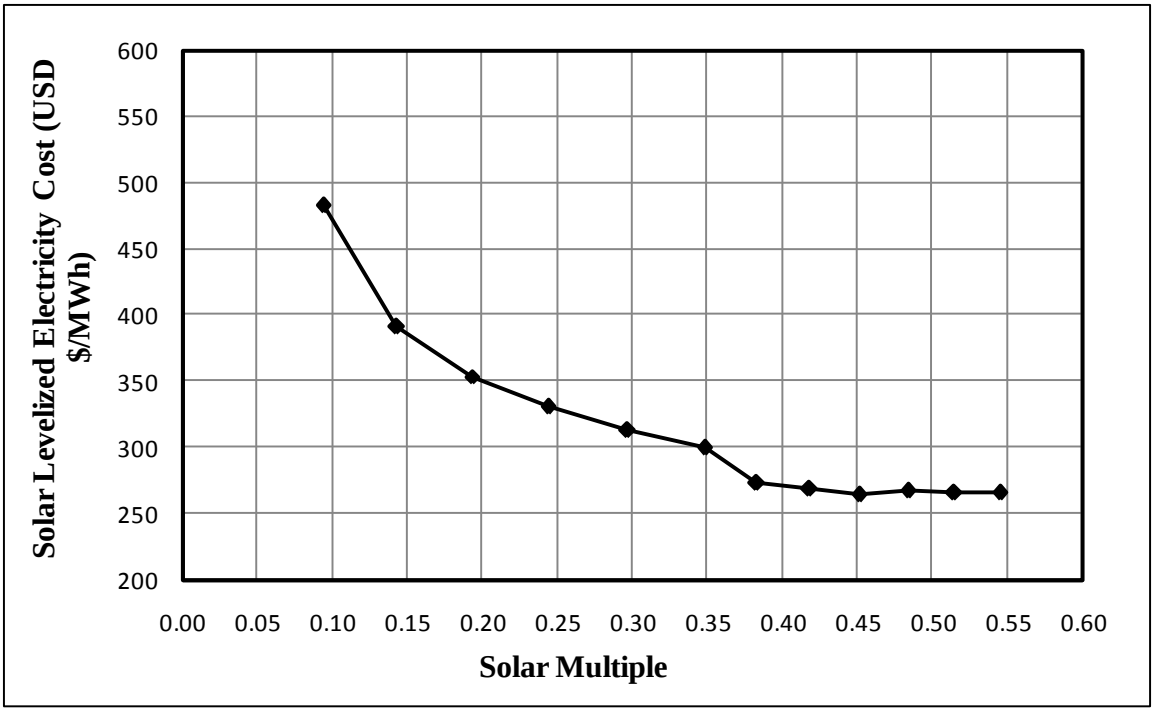

Figure 7.20 Solar levelized electricity cost of HYCS for different solar multiples (Gas turbine is part load)

As shown from Figs. (7.18 and 7.20), solar levelized electricity cost is reducing when solar multiple is increasing. On the other hand, Fig. 7.19 shows decreasing behaviour ended up by increasing behaviour due to partial operation of solar field loops which makes the optimum point is 0.38 solar multiple. For such configuration of hybridization solar combined cycle, SM_{Steam} never reaches one because that means gas turbine is out of service and the total power comes from steam turbine. In other words, the configuration switched from hybrid solar combined cycle into hybrid steam power plant. Moreover, simulation results satisfied the second derivation which says SLEC has the same values when SLEC has been calculated based on reference cycle which is using the same amount of HYCS's fuel, based on output energy of reference cycle which produces the same amount of HYCS's energy, or based on solar field cost over annual electrical energy which is produced by solar field.

B. Integrating solar with gas turbine in combined cycle under Dhahran weather conditions as shown in Fig. 7.21

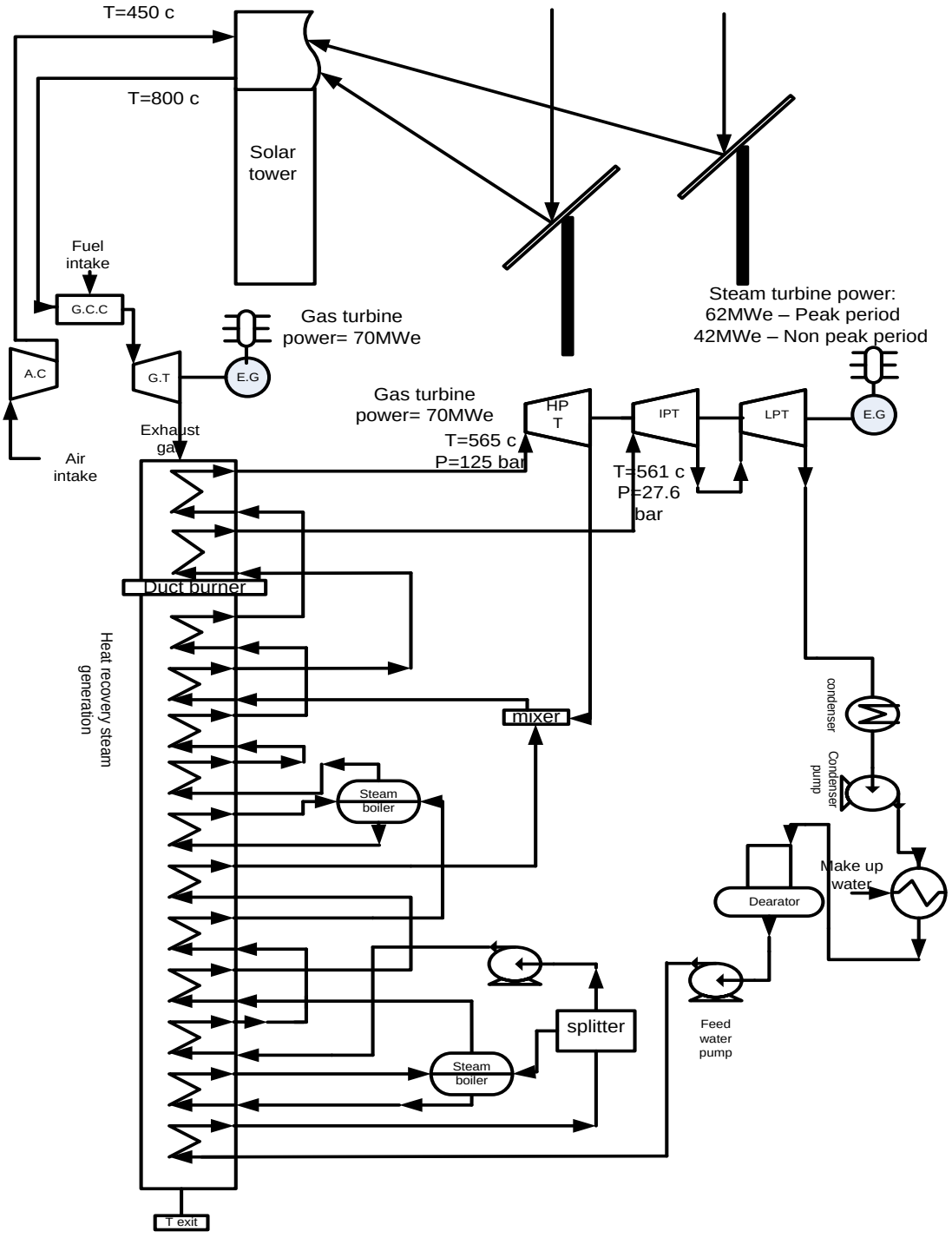

Figure 7.21 Schematic diagram of integrating solar with gas turbine in combined cycle

In this configuration, solar tower collector has been used to preheat air before entering combustion chamber. This solar tower has been selected from [12] since it is the optimum size of solar tower to be integrated with gas turbines as mentioned in the literature review. In this study, several solar field sizes have been used based on the optimum size of solar field, which is 3.7615 Hectare with optical efficiency 43.65%, in order to determine the optimum solar field size that will be integrated with gas turbine in gas combined cycle for three different pressure ratios which are 15.5 and 17.7 as shown in Fig. 7.21. Definition of solar multiple in this configuration is a ratio between produced thermal power by solar tower to the required thermal power for combined cycle as shown in Equation (7.14). The reason behind this way of defining solar multiple in this configuration, solar thermal energy has been utilized in two ways. The first way is direct usage which is preheating air before entering combustion chamber and the second way is indirect usage where exhaust gases have been used to super heat steam in HRSG.

$$SM_{Gas} = \frac{P_{th,solar}}{P_{th,steam\ turbine} + P_{th,gas\ turbine}} \tag{7.14}$$

$P_{th,steam\ turbine}$ and $P_{th,gas\ turbine}$ can be calculated using the following formulas:

$$P_{th,steam\ turbine} = \dot{m}_{Steam,HPT} * H_{in,HPT} + \dot{m}_{Steam,IPT} * H_{in,IPT} + \dot{m}_{Steam,LPT} * H_{in,LPT}$$

$$P_{th,gas\ turbine} = \dot{m}_{gas} * H_{in,GT}$$

Table 7.10 Required thermal power of gas and steam turbines for different pressure ratios (Pr)

Gas Turbine Model	GE 6111 FA	Ansaldo AE 64.3 A
Pressure ratio of gas turbine	Pr =15.5	Pr = 17.7
$\dot{m}_{Steam,HPT}$ **(Kg/s)**	27.73	25.27
$h_{in,HPT}$ **(KJ/Kg)**	3483.42	3495.43
$\dot{m}_{Steam,IPT}$ **(Kg/s)**	32.93	30.98
$h_{in,IPT}$ **(KJ/Kg)**	3589.51	3591.23
$\dot{m}_{Steam,LPT}$ **(Kg/s)**	33.1	31
$h_{in,LPT}$ **(KJ/Kg)**	3150.41	3151.72
$P_{th,steam\ turbine}$ **(KW)**	319076	297290
$\dot{m}_{gas}$ **(Kg/s)**	200	187.3
$h_{in,GT}$ **(KJ/Kg)**	1566.77	1696.6
$P_{th,gas\ turbine}$ **(KW)**	313354	317773
Total Power (KW)	632430	615062

As shown from Table 7.10, steam enthalpy at the inlet of each turbine's stage is almost the same for those different pressure ratios but mass flow rate of steam in different stages of steam turbine is related to the required power which should be generated by steam turbine beside the generated power by gas turbine in order to cover the electrical load. So, when generated power by gas turbine is decreasing; the generated power from steam turbine is increasing by increasing steam mass flow rate, and visa versa.

As known, solar multiple is a rational number. So, based on the thermal required powers which are given in Table (7.10) solar multiple for each case will be produced as shown in the complement of this chapter.

Results of pressure ratio (Pr =15.5) as hereunder:

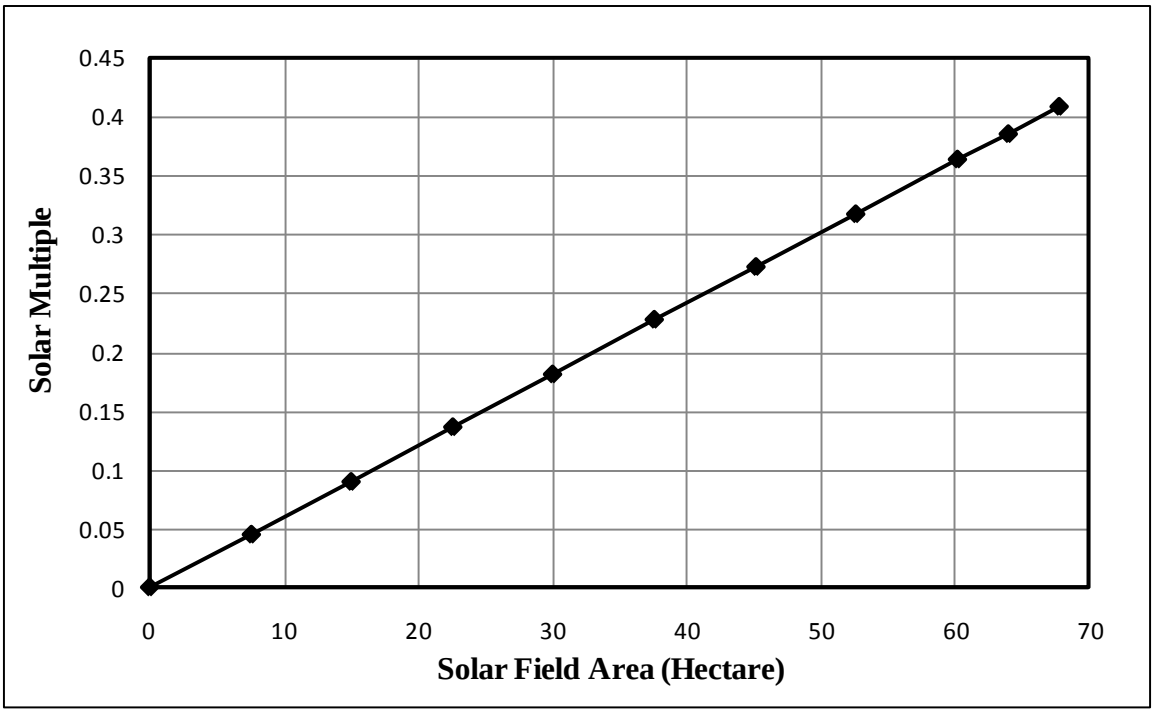

Figure 7.22 Solar multiples for different solar field sizes of Pr=15.5

As shown in Fig. 7.22, solar multiple has a proportional relation with solar field size which is multiple of the optimal field size (3.7615 Hectare) as given by [12].

Also, figures of merit such as instantaneous solar share, annual solar share, CO_2 avoidance, LEC, and solar LEC have been calculated for each solar multiple in order to assess the performance of hybrid solar combined cycle, and then determining the optimum solar multiple. First of all, instantaneous solar share and annual solar share can

be calculated for this configuration as the previous configuration using these Equations (7.4 and 7.6).

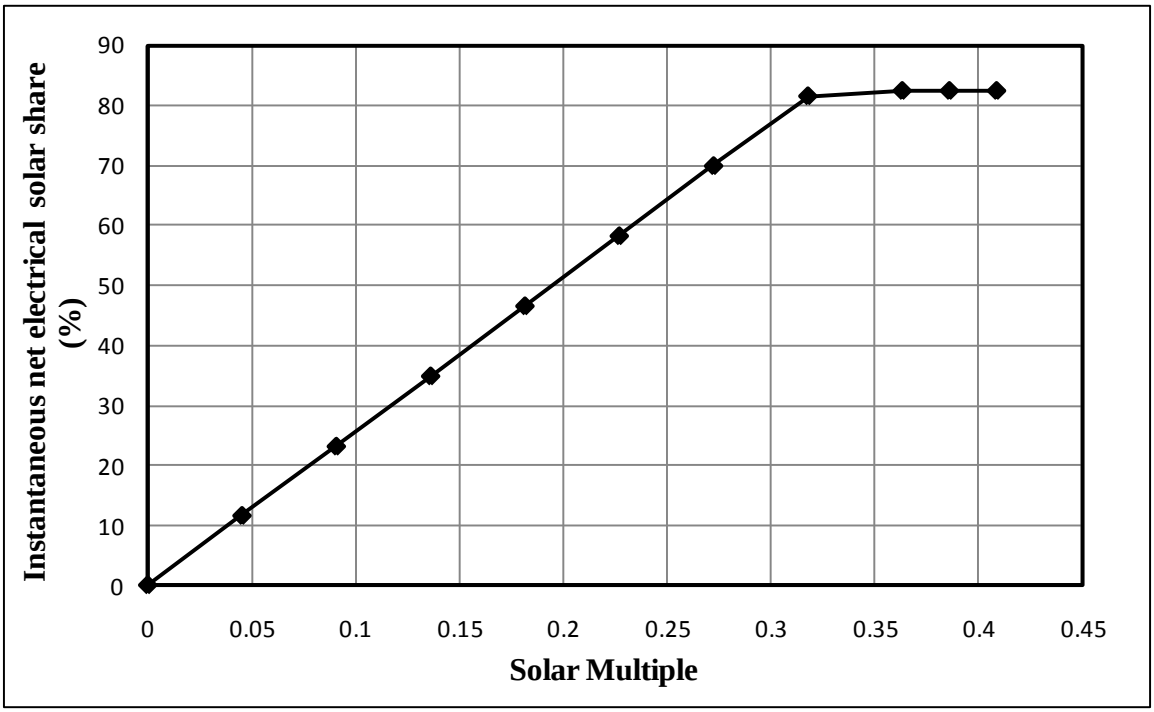

Figure 7.23 Instantaneous net electrical solar share for different solar multiples of Pr=15.5

As shown in Fig. 7.23, instantaneous net electrical solar share is increasing while solar multiple is increasing up to 0.32 solar multiple. After solar multiple 0.32, instantaneous net electrical solar share doesn't increase because all of them provide the total required heat of gas turbine at design hour. On the other hand, solar share over the entire year is not being constant as shown in Fig. 7.24 because extra size of solar field is utilized when solar radiation has low intensity.

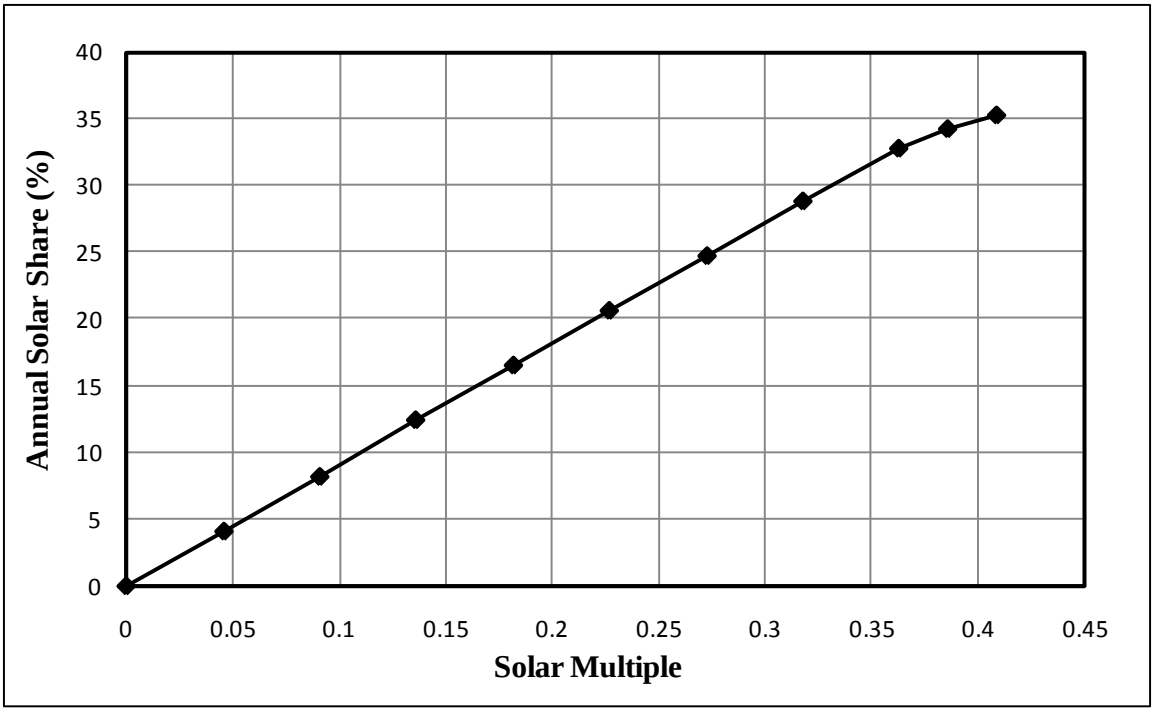

Figure 7.24 Annual solar share for different solar multiples of Pr=15.5

As a result of increasing annual solar share, CO_2 emissions have been reduced to reach 240 K tonne of CO_2 annually, when the biggest solar tower size has been used, instead of 362 K tonne for conventional combined cycle as shown in Fig. 7.25.

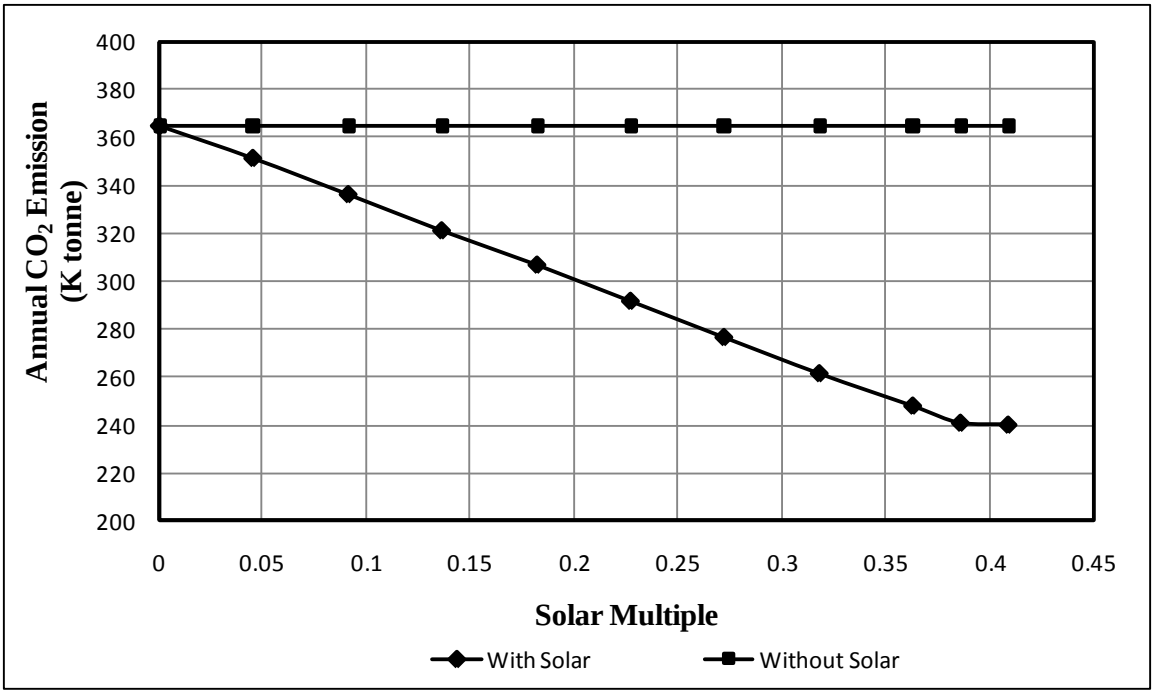

Figure 7.25 Annual CO_2 emissions for different solar multiples of Pr=15.5

As shown from Fig. 7.25, this reduction of CO_2 emissions is very attractive but there are other considerations beside reduction of CO_2 emissions such as levelized electricity cost and solar levelized electricity cost. Economic and performance parameters which are given in Table 7.9 have been used in order to evaluate economic performance of each solar multiple.

Regarding LEC and SLEC, they are calculated for this configuration as the previous configuration using these Equations (7.9 and 7.11).

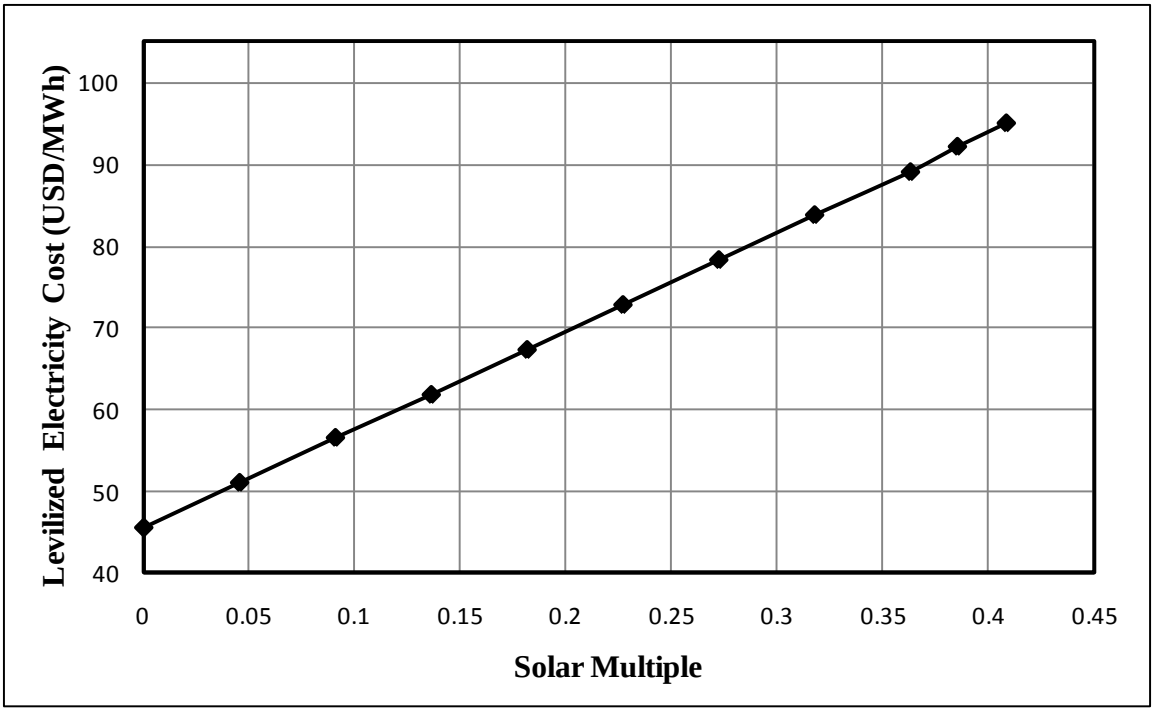

Figure 7.26 Levelized electricity cost of HYCS for different solar multiples of Pr=15.5

There is a negligible difference between LEC of conventional combined cycle when solar is integrated with steam side or gas side. This is because the way of building gas turbine in each configuration. In solarization steam side one closed block of gas turbine has been used as provided by Thermo-Flex software which has some losses as industrial unit. On the other hand, this closed block can't be used in solarization gas turbine because there is no way to add heat after compressor. So, gas turbine has been built component by component to allow adding heat after compressor. As a result of this difference, operation cost has changed slightly.

Fig. 7.26 shows increasing behaviour of levelized electricity cost which make the optimum solar multiple is unclear but if solar levelized electricity cost has been

considered, the optimum solar multiple can be determined which is 0.32 as shown in Fig. 7.27.

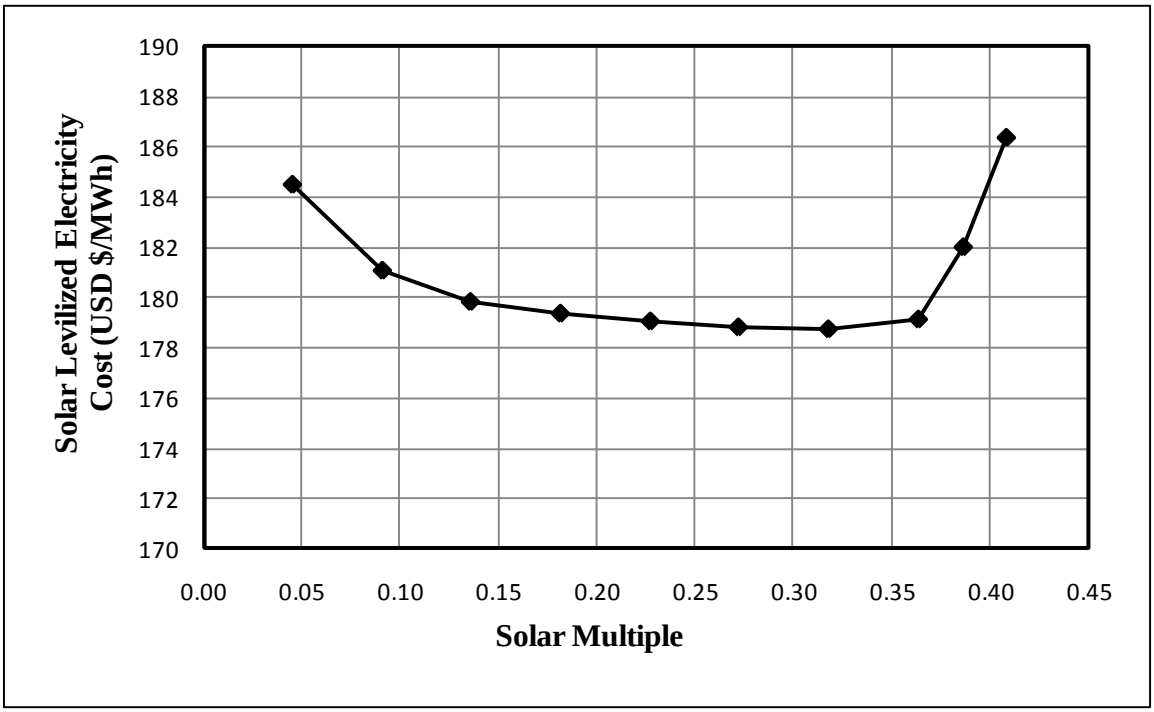

Figure 7.27 Solar levelized electricity cost of HYCS for different solar multiples of Pr=15.5

As shown from Fig. 7.27, solar levelized electricity cost is decreasing when solar multiple is increasing up to 0.32 solar multiple. Beyond 0.32 solar multiple, solar levelized electricity cost is increasing. The reason behind this behaviour, there is over sizing of solar tower size which is not useable after solar multiple 0.32.

Results of pressure ratio (Pr=17.7) as hereunder:

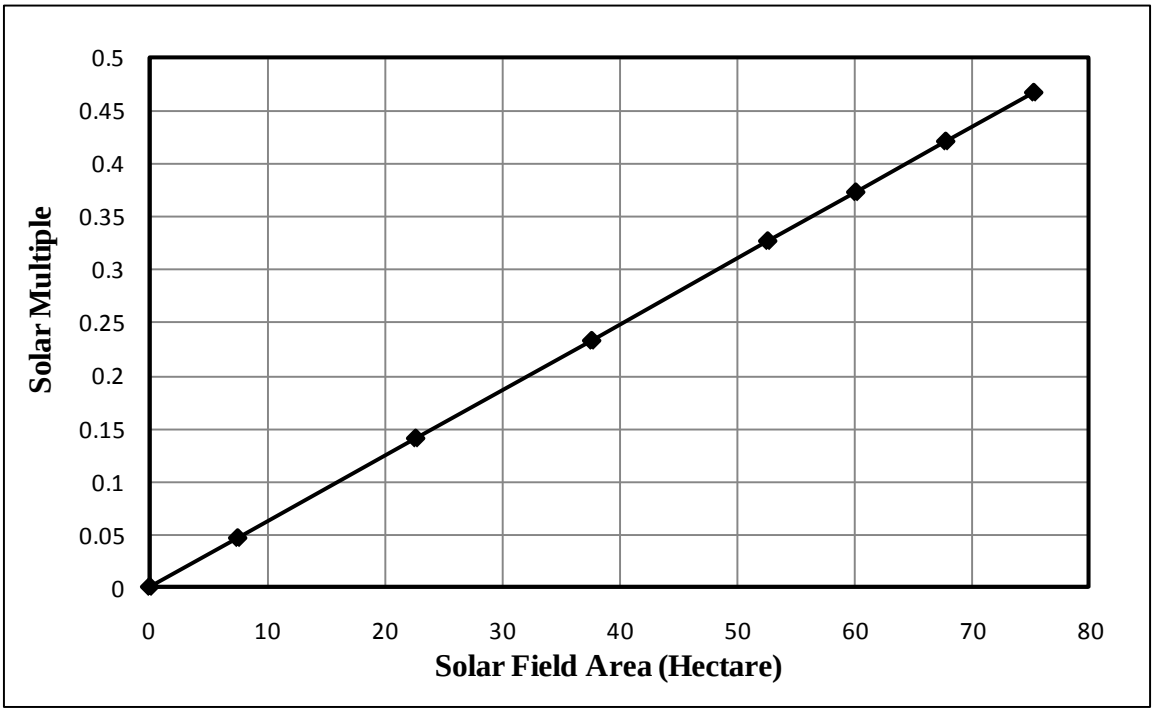

Figure 7.28 Solar multiples for different solar field sizes of Pr=17.7

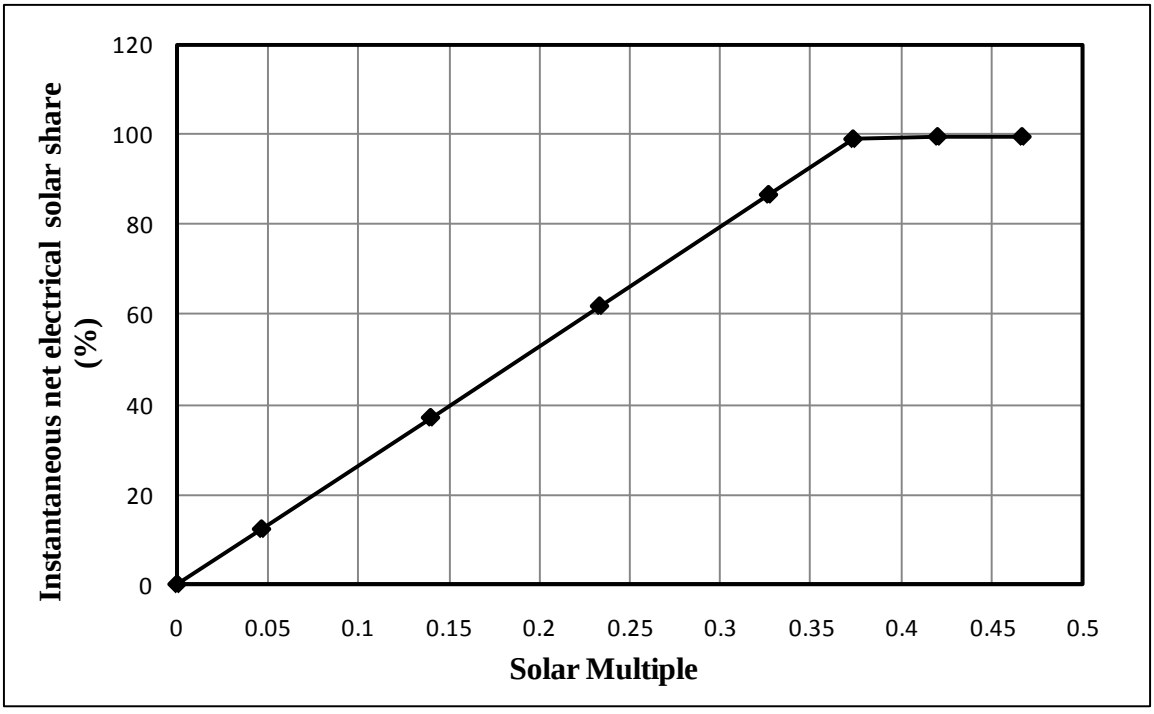

Figure 7.29 Instantaneous net electrical solar share for different solar multiples of Pr=17.7

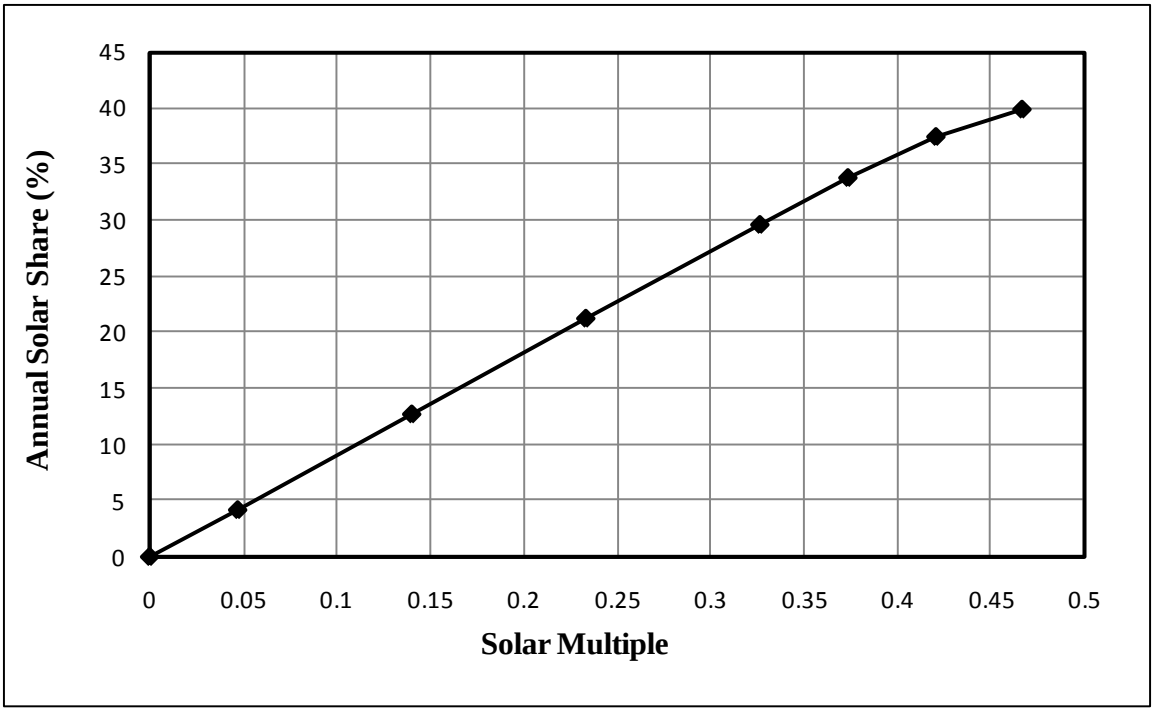

Figure 7.30 Annual solar share for different solar multiples of Pr=17.7

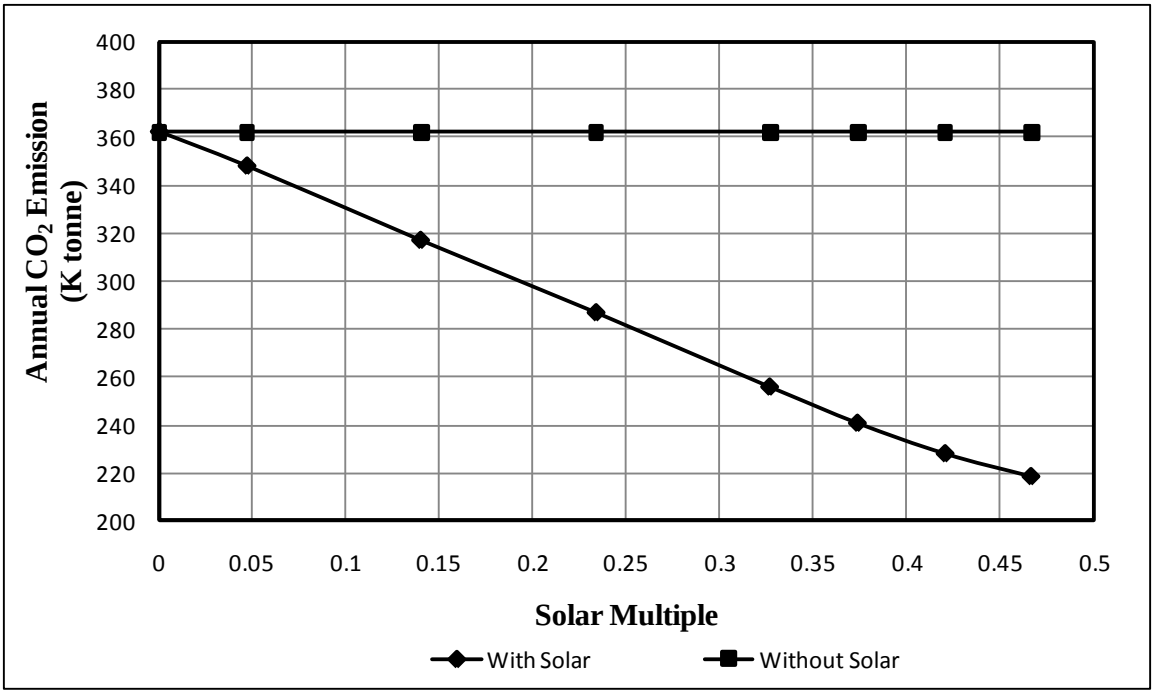

Figure 7.31 Annual CO_2 emissions for different solar multiples of Pr=17.7

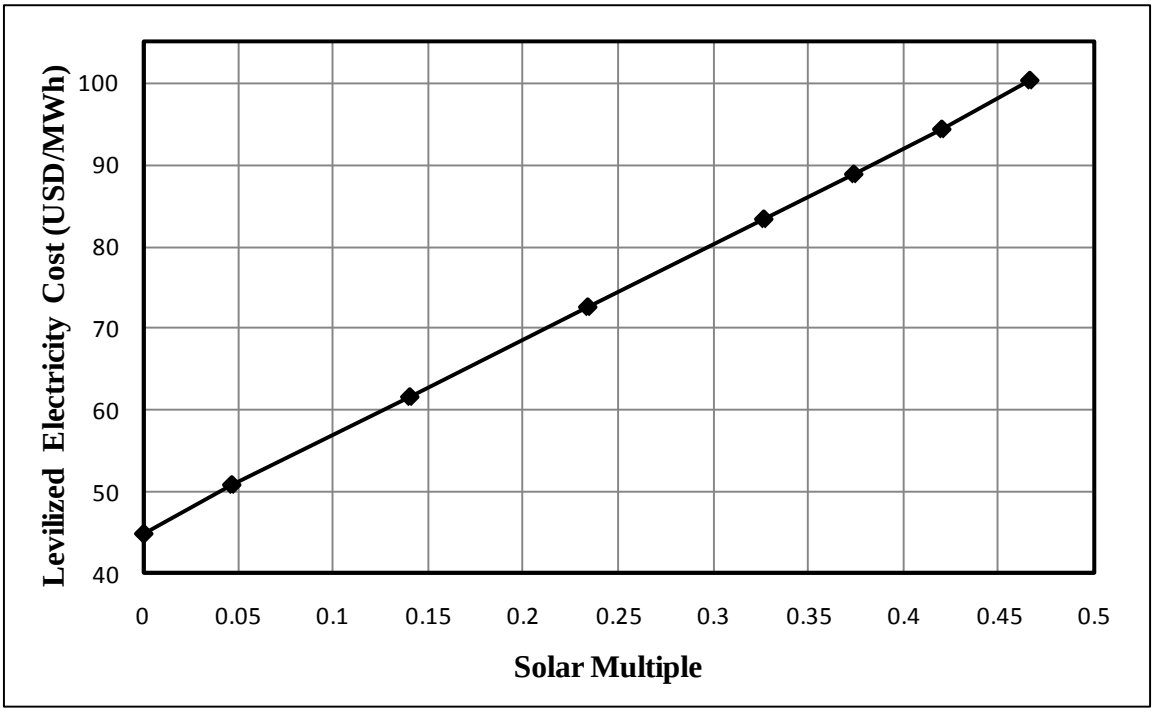

Figure 7.32 Levelized electricity cost of HYCS for different solar multiples of Pr=17.7

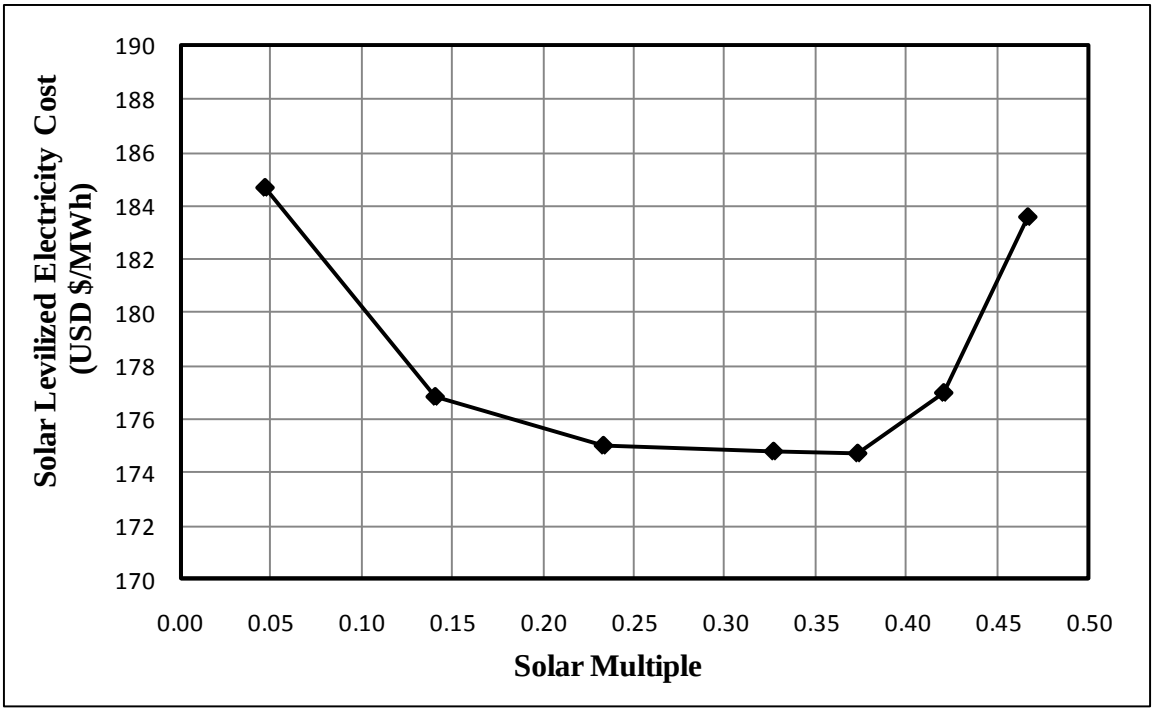

Figure 7.33 Solar levelized electricity cost of HYCS for different solar multiples of Pr=17.7

As shown in the previous results of different pressure ratios, changing pressure ratios has an effect on the thermo-economic performance of HYCS. In fact, changing of pressure ratio changes other parameters in gas turbine such as investment cost of gas turbine, outlet temperature of combustion chamber, and air mass flow rate through the turbine. All these parameters are changing as per data bank of gas turbines in Thermo-Flex software. As a result of the previous simulations of different pressure ratios, the most parameter affects the amount of energy that will be utilized by gas turbine from solar tower collector is outlet temperature of combustion chamber which is 1327 °C when Pr =15.5 and 1421 °C when Pr =17.7 . Based on this point, the optimization parameter (SLEC) which shows the effect of LEC and annual solar share has different values among different pressure ratios as shown in Figs. (7.27 and 7.33). The optimal solar multiple of (Pr =15.5) is 0.32 which has LEC 83.71 USD$/MWh, SLEC 178.71 USD$/MWh, and annual CO_2 emission 261.56 K tonne; the optimal solar multiple of (Pr =17.7) is 0.37 which has LEC 88.77 USD$/MWh, SLEC 174.69 USD$/MWh, and annual CO_2 emission 241 K tonne.

C. Solarization of steam side and gas side in combined cycle

In this section, solar energy has been integrated with the gas turbine and steam turbine as shown in Fig. 7.34. This configuration designed in order to investigate the combination of the optimum CSP technologies which are given as results from the previous two configurations under Dhahran weather conditions and generation of extra power as operating scenario will be used. Solar multiples of CSP technologies that have been used are 0.38 for parabolic trough and 0.32 for solar tower. All figures of merit have been used to assess the thermo-economic performance of this configuration as hereunder in Table 7.11.

Table 7.11 Parameters for performance and LEC evaluation

Figure of merit	Value	Unit
LEC	96.44	$/MWh
Solar levelized electricity cost (LEC,solar)	192.35	$/MWh
Annual CO_2 emission	248.77	K tonne
CO_2 Avoidance	31.78	%
Instantaneous net electrical solar share	88	%
Annual solar share	34.77	%

As shown in Table 7.11, this configuration has the highest instantaneous and annual solar share among the previous three configurations which lead to high reduction of CO_2 emissions reaches up to 31.78 %. This means one third of annual CO_2 emissions of conventional combined cycle has been eliminated which is much friendly to environment. On the other hand, economic indicators have risen due to increment of total investment cost because there are 2 CSP costly technologies have been included in the total investment cost.

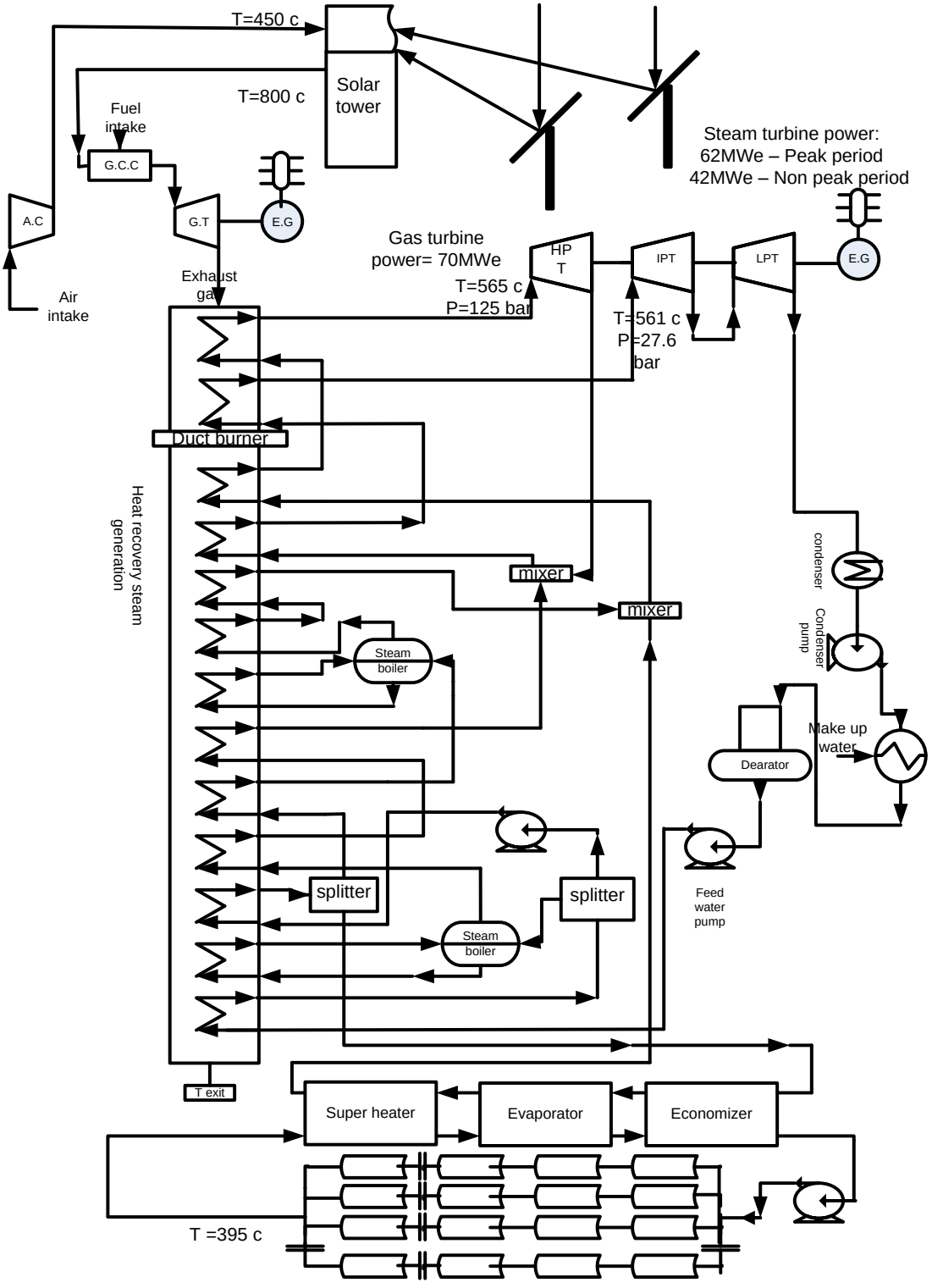

Figure 7.34 Schematic diagram of integrating solar with steam side and gas turbine side in combined cycle

The following Table 7.12 summarizes the performance of the optimum cases of the two major configurations which are solarization steam and solarization gas side beside solarization of steam and gas sides together.

Table 7.12 Comparison among three different configurations of HYCS

Assessment parameter	Solarization steam side	Solarization gas side	Solarization both steam and gas side
LEC ($/MWh)	63.17	83.71	96.44
Solar levelized electricity cost (LEC,solar) ($/MWh)	262	178.71	192.35
Annual CO_2 emission (K tonne)	385.2	261.56	248.77
CO_2 Avoidance (%)	6.83	28.28	31.78
Instantaneous net electrical solar share (%)	22.36	81.61	88
Annual solar share (%)	7.05	28.77	34.77

Table 7.13 shows LEC of different solar technologies beside average LEC of combined cycle. From previous analysis, LEC of combined cycle is 48 $/MWh and SLEC of the optimum configuration is 262 $/MWh as given in Table 7.12. This value of SLEC of hybrid solar combined cycle is very close to the lowest LEC of solar PV plant as given in Table 7.13.

Table 7.13 LEC of different technologies

LEC of PV plants [69]	LEC of Parabolic troughs plants[69]	Average LEC of combined cycles [70]	Cost of 1 million BTU or 1,000 cubic feet
200-800 $ /MWh	120-180 $/MWh	66 $/MWh	4.5$

Applying the optimal integration configuration for different locations in Saudi Arabia

After achieving the optimal integration configuration under Dhahran weather conditions, the optimal configuration which is solarisation steam side with generation extra power scenario will be applied for different cities in Saudi Arabia. Those different cities are Jeddah, Jizan, Riyadh, and Tabuk.

After studying the performance of HYCS under different locations, instantaneous solar share for the same plant in different locations has the same value which is 21.7. That is due to negligible difference of solar radiation at design hour for those different locations. On the other hand, annual solar share has different profile trend among different locations as shown in Fig. 7.35.

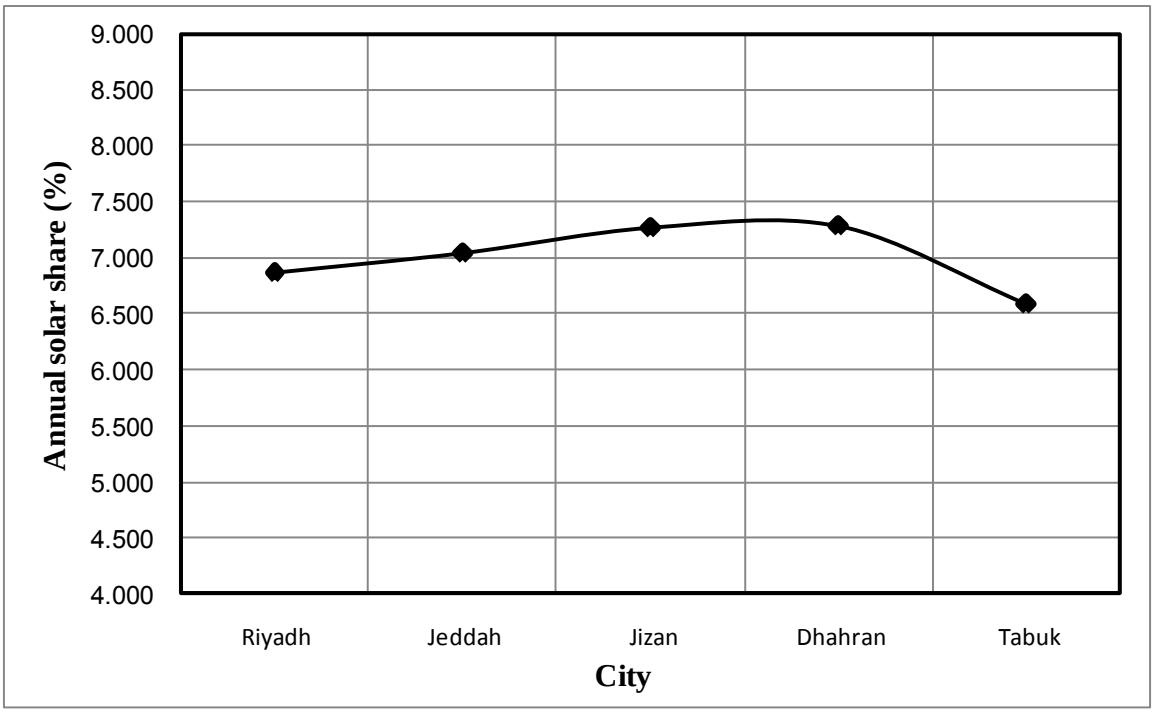

Figure 7.35 Annual solar share for different cities in Saudi Arabia

Due to accumulation way of HYCS performance over the entire year, annual solar share has a room to give variation among different locations which will affect the economic performance parameters (LEC and SLEC) as shown in Figs. (7.37 and 7.38). This has been done by kept annual fuel consumption almost the same which gives similar annual CO_2 emission for different used locations as shown in Fig. 7.36. That means operation cost is almost similar but variation of LEC and SLEC is due to annual exported energy from the HYCS which varies according to the solar intensity, where annual energy is one important parameter of LEC and SLEC.

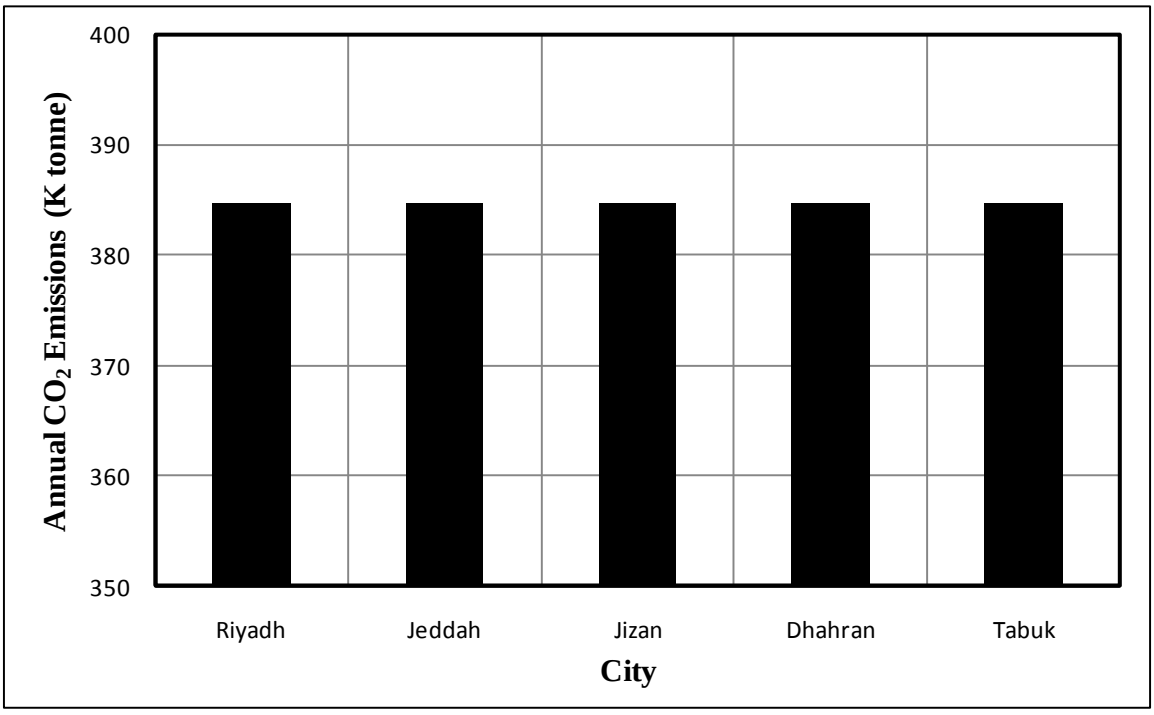

Figure 7.36 Annual CO_2 emission for different cities in Saudi Arabia

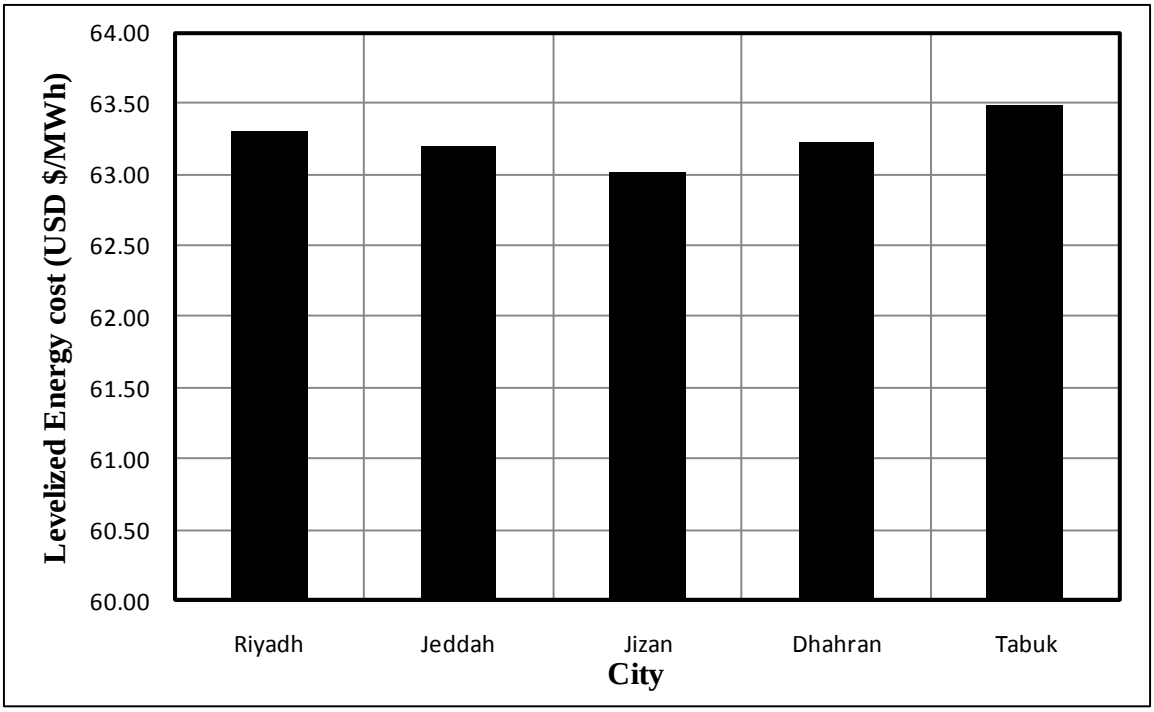

Figure 7.37 Levelized electricity cost for different cities in Saudi Arabia

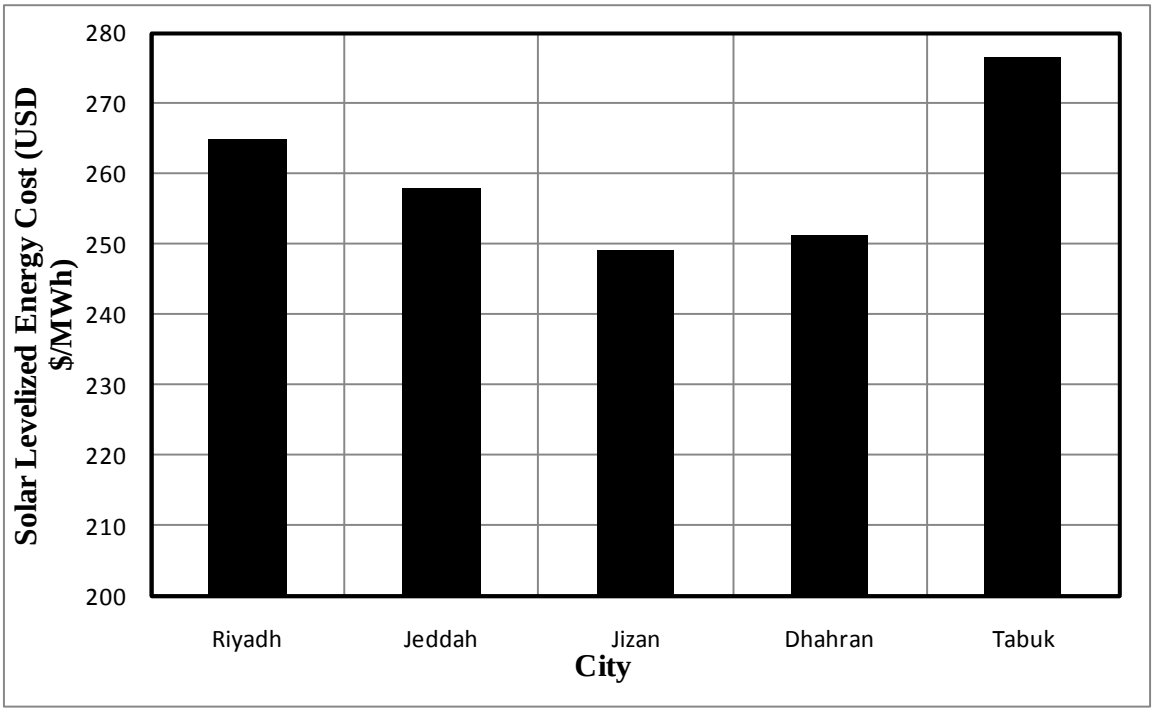

Figure 7.38 Solar levelized electricity cost for different cities in Saudi Arabia

From previous economic figures, Jizan city has the lowest LEC which is 63 USD $/MWh and SLEC which is 249 USD $/MWh. That means the proper location to apply this integration configuration which is solarisation steam side with generation extra power scenario among used locations is Jizan city. This conclusion makes sense where Jizan has known high temperature level over the year.

7.2.3 Comparison between Different CO_2 Avoiding Technologies

In real life, there is a technology for CO_2 avoiding which is called CO_2 capture technology. Also in this work, one of the important reasons of this hybridization solar with conventional combined cycle is global warming which is related to CO_2 emissions. So, comparison between these two different technologies is very important to assess whether this hybridization is economical feasible or not. Table (7.14 and 7.15) presents comparison between different CO_2 avoiding technologies.

Table 7.14 Comparison between different CO_2 avoiding technologies for solarisation steam side in HYCS

Cycle	Reference cycle 1	Solarization steam side	With CO_2 capture
Annual CO_2 emissions (K tonne/year)	404.3	385.2	
LEC ($/MWh)	48.45	63.17	71.25

Table 7.15 Comparison between different CO_2 avoiding technologies for solarisation gas side and both sides steam and gas in HYCS

Cycle	Reference cycle 2	Solarization gas side	With CO_2 capture	Solarization both steam and gas side	With CO_2 capture
Annual CO_2 emissions (Ktonne/year)	364.7	261.56		248.77	
LEC ($/MWh)	45.53	83.71	85.08	96.44	91.38

Calculation of CO_2 capture was based on the following assumptions: [71]

Thermal Efficiency decreases from 8-12%.

Capturing 1 tonne of CO_2 requires 160 $.

As shown from Table (7.14 and 7.15), hybridization solar with conventional combined cycle has proved the economical feasibility more than CO_2 capture technology for solarization gas side and for the optimal case which is solarisation steam side. Unfortunately, hybridization solar with both gas and steam side doesn't give the same behaviour due to high value of LEC.

CHAPTER 8

CONCLUSIONS AND RECOMMENDATIONS

In this work, modeling and optimization of hybrid solar combined cycle (HYCS) have been done. In HYCS modeling, mathematical modeling for each component of HYCS has been programmed by E.E.S software. E.E.S code has been validated with Thermo-Flex code as component level as well as integrated system level. In conclusion, the two codes (E.E.S and Thermo-Flex) are matching very well with these percentages of errors 0.74% of total generated power and 0.57% of thermodynamics efficiency.

In optimization stage,

1- Thermo-economic code has been used to optimize the HYCS under Dhahran weather conditions. Furthermore, different configurations of HYCS have been studied beside conventional combined cycle as follows:
   a- Optimization of conventional combined cycle.
   b- The first configuration of HYCS is integration of solar with steam side in conventional combined cycle.
   c- The second configuration of HYCS is integration of solar with gas turbine in conventional combined cycle.
   d- The third configuration of HYCS is integration of solar with steam side and gas turbine in conventional combined cycle.

2- Simulation the optimal configuration from the previous configurations under different locations weather in Saudi Arabia.
3- Comparison between different CO2 avoiding technologies.

In the first branch of point 1 which is optimization of conventional combined cycle, different steam and gas turbine sizes have been integrated together to be simulated as conventional combined cycle. All these conventional combined cycles satisfied the control parameter which is net electrical output of conventional combined cycle (132 MW). Results reveal that ST/GT =1 is the optimal size of steam and gas turbine since it has the lowest LEC which equals 57 USD$/MWh.

In the first configuration of HYCS which is integration solar with steam side, performances of integration different solar field sizes of parabolic trough collector with the optimized combined cycle have been assessed based on different parameters. One of the important parameters is annual solar share. In this study annual solar share is varying from 2.1- 9.43 when generation of extra power, 2.1 - 5.77 when solar field is part load, and 2.1 – 8.95 when gas turbine is part load option has been used. This increasing of annual solar share leads to considerable reduction of CO_2 emissions. This output is very attractive but there is limitation to increase solar share which is cost perspective as shown in Fig. 7.19. As a result of this configuration, the optimum scenario of HYCS operation is ‘Generation of Extra Power’ because it has the lowest levelized electricity cost 63.17 $/MWh which is corresponding to the optimum solar multiple 0.38 since it has the lowest SLEC which is 262 $/MWh. This solar multiple requires 29 hectare ($29 * 10^4 m^2$) of total solar field area included distance between each two parallel rows which equals 14.5 m to reduce shading effect.

In the second configuration of HYCS which is integration solar with gas turbine, performances of integration different solar field sizes of solar tower collector with optimized combined cycle have been assessed based on different parameters. One of the important parameters is annual solar share. In this study annual solar share is varying from 4 – 35.3. In this simulation, annual solar share is high due to direct and indirect usage of solar energy. Direct usage of solar energy is representing by heating the air before entering combustion chamber. In this regard, fuel consumption of gas turbine has been reduced. Regarding indirect usage of solar energy, the exhaust gases from gas turbine goes to heat recovery steam generator to produce steam without burning any amount of fuel if there is no need. This increasing of annual solar share leads to considerable reduction of CO_2 emissions. Also, this output is very attractive but there is limitation to increase solar share which is cost perspective as shown in Fig. 7.27. As a result of this configuration, the optimal solar multiple is 0.32 based on solar levelized electricity cost which is 178.71 $/MWh as shown in Fig. 7.27. The LEC of this solar multiple is 83.71 $/MWh. This solar multiple requires 52 hectare ($52 * 10^4\ m^2$) of total solar field area.

In the third configuration of HYCS which is integration solar with steam side and gas turbine side, figures of merits have been used to assess the thermo-economic performance. As a result of this investigation, the highest instantaneous and annual solar shares have been achieved with comparison to the previous two configurations 88 and 34.77, respectively. Moreover, high reduction percentage of CO_2 emissions reaches up to 31.78 %. On the other hand, economic indicators (LEC and SLEC) have risen to reach 96.44 and 192.35, respectively.

In the second point which is simulation the optimal configuration under different locations' weather, four cities (Jeddah, Riyadh, Jizan, and Tabuk) have been simulated in addition to Dhahran city. As a result of these simulations, the most proper location to construct this HYCS system is Jizan city because it has the lowest cost of LEC and SLEC which are 63 USD$/MWh and 249 USD$/MWh, respectively. Moreover, it is too much friendly to the environment where it emits 385.2 K tonne of CO_2 insted of 404.3 K tonne of CO_2 for conventional combined cycle.

In the third point which is comparison between different CO_2 avoiding technologies, economic comparison is carried out between this hybridization solar with conventional combined cycle and CO_2 capture technology. In conclusion, this hybridization solar with conventional combined cycle has proved the economical feasibility more than CO_2 capture technology specifically for the optimal case which is solarisation steam side; since the LEC of the optimal configuration of HYCS and CO_2 capture technology which emit the same amount of annual CO_2 (385.2 K tonne) are 63.17 USD$/MWh and 71.25 USD$/MWh, respectively.

Finally, such integrations of solar with conventional combined cycles are better than using CO_2 capturing technology with the same conventional combined cycle because:

1. Durability of solar and decay of fuel.
2. CO_2 capturing technology reduces the cycle efficiency which requires more fuel.
3. Emission more amount of CO_2 as a sequential result of increased amount of fuel consumption.

RECOMMENDATIONS FOR

FURTHER WORK:

- Providing the drinking water is a very important issue for majorities of world's countries, especially Saudi Arabia, so an investigation about the solar cogeneration power plants in Saudi Arabia is highly recommended.
- An investigation about hybrid solar – combined cycle power plants with different types of thermal storages is very important.

APPENDICES

APPENDIX A: WEATHER DATA OF DIFFERENT CITIES IN SAUDI ARABIA

Table A.1 Location data of different locations in Saudi Arabia

City	Dhahran	Jizan	Jeddah	Riyadh	Tabuk	Unit
Latitude	26.5	16.9	21.67	24.72	28.37	°N
Longitude	50.25	42.58	39.15	46.72	36.63	°E
Elevation	91	3	12	612	770	m

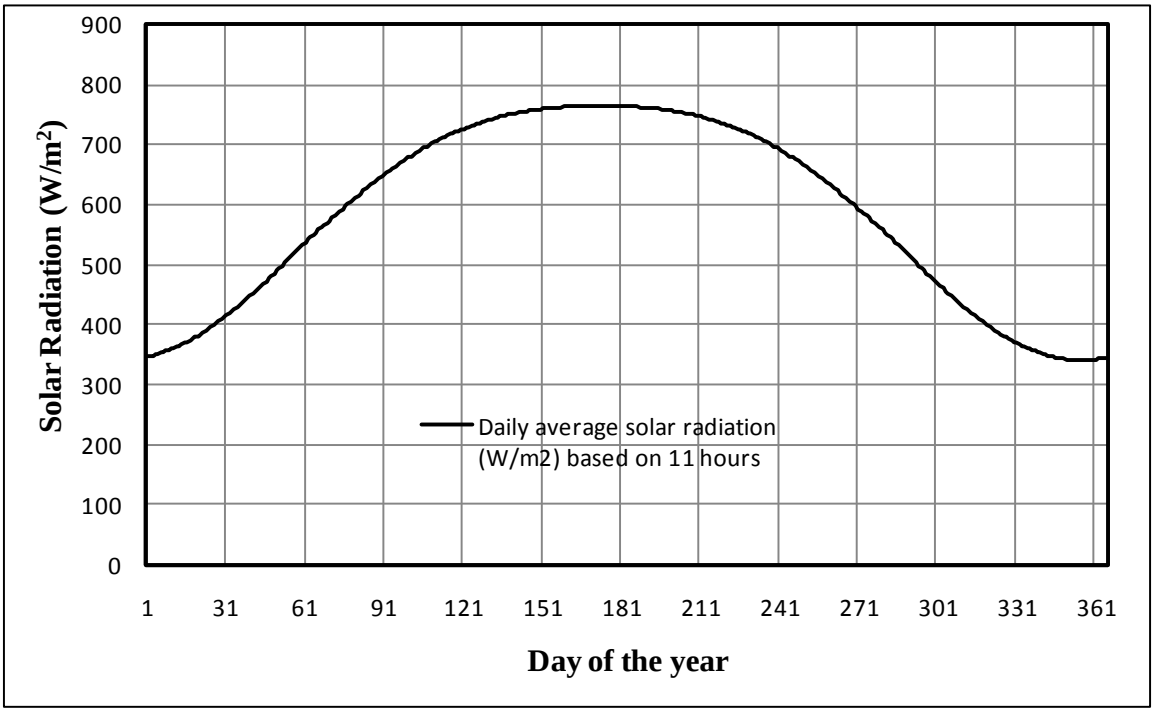

Figure A.1 Daily average solar radiation of Dhahran city

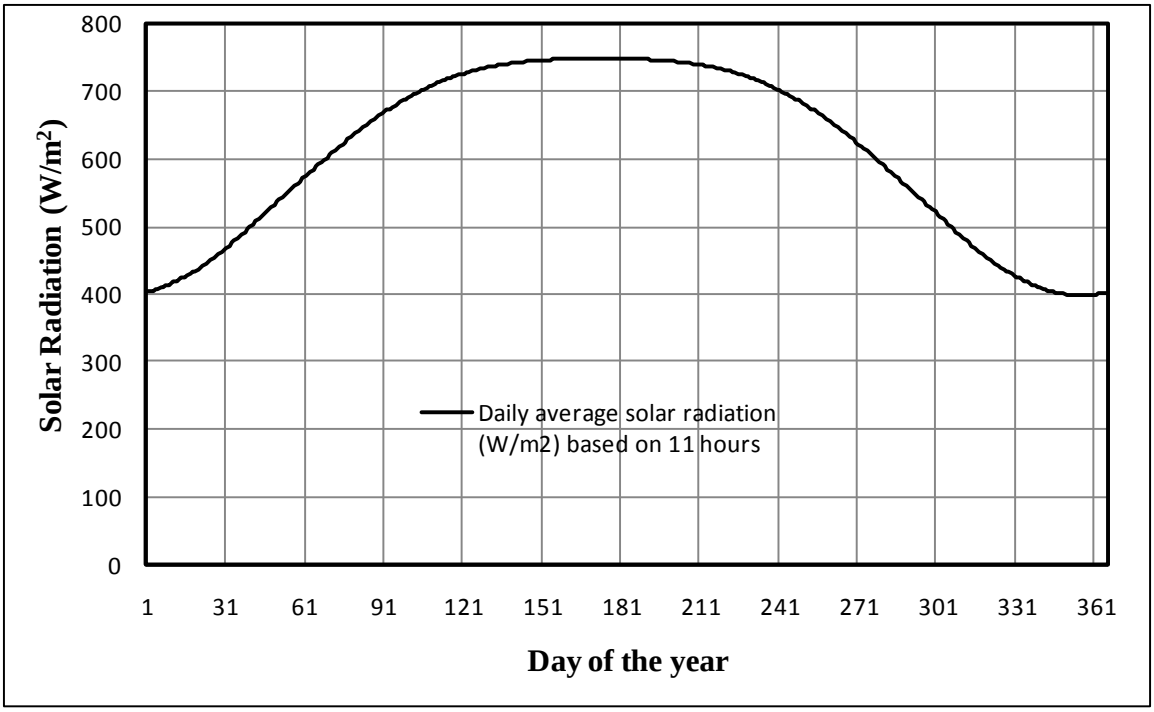

Figure A.2 Daily average solar radiation of Jeddah city

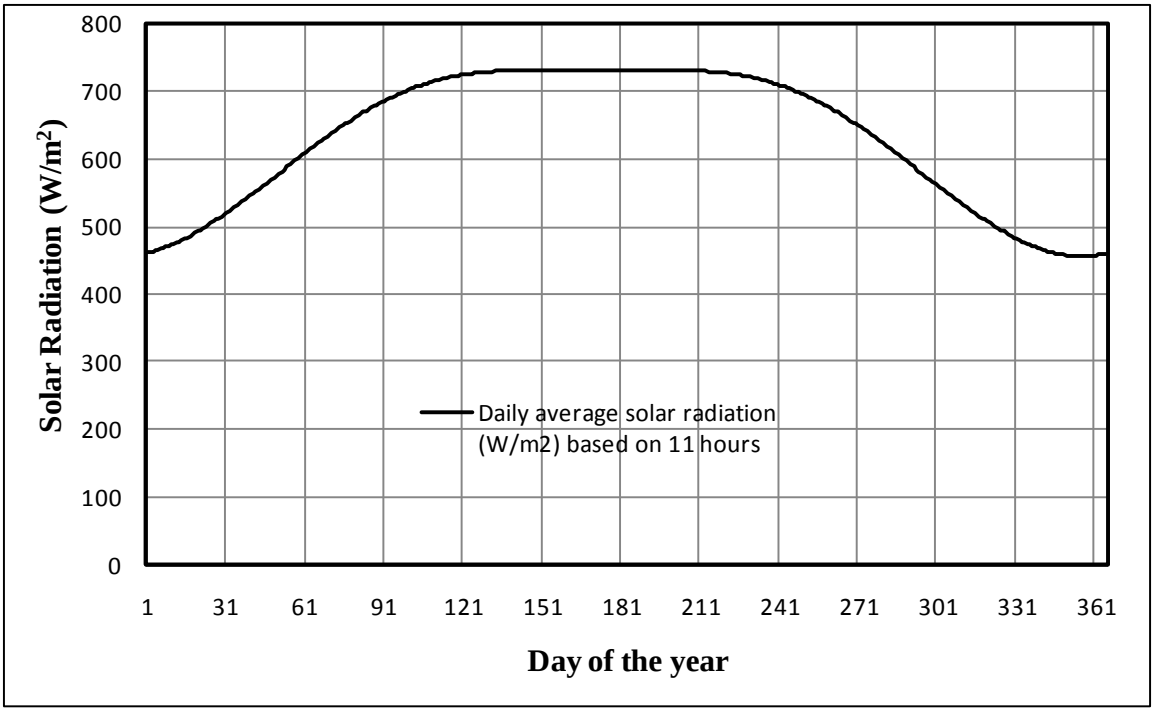

Figure A.3 Daily average solar radiation of Jizan city

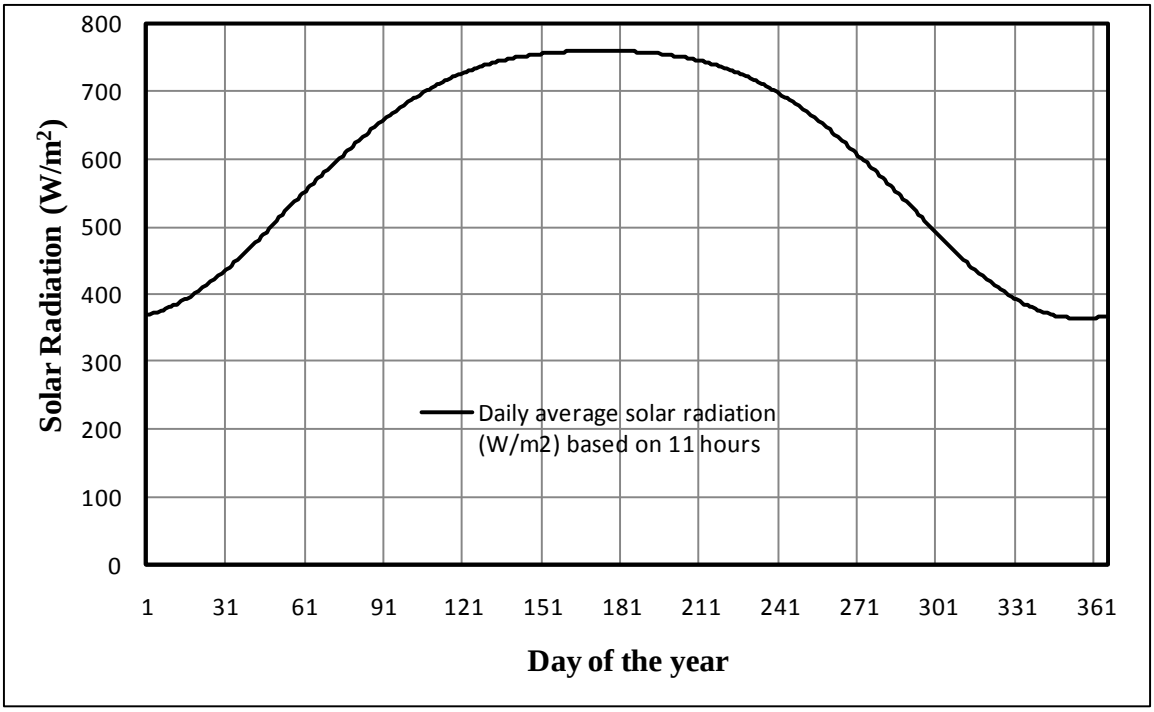

Figure A.4 Daily average solar radiation of Riyadh city

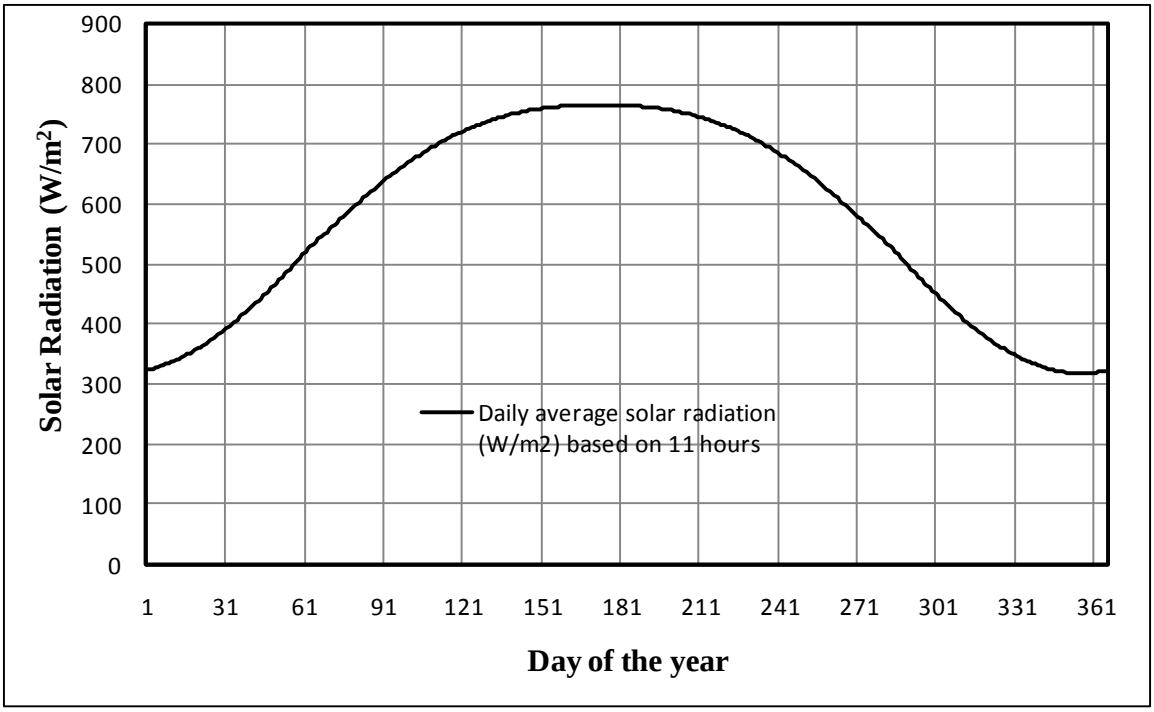

Figure A.5 Daily average solar radiation of Tabuk city

APPENDIX B: OPERATION AND CONTROL PARAMETERS OF HYCS

Abstract:

Simulation of hybrid solar combined cycle has different parameters which are need to be adjusted. This appendix presents the major parameters of HYCS. In addition, which parameters should be changed if scenario of simulation is changed? As known, there are three scenarios to simulate HYCS when integration of solar is with steam side in combined cycle. These three scenarios as follows:

1- Generation of extra power.

2- Following the load by operating solar field partially.

3- Following the load by operating gas turbine partially.

Also, there is solarization of gas turbine.

Procedure:

1- Solarization steam side in combined cycle

First of all, HYCS that is shown in Fig. B.1 has been simulated under Dhahran weather conditions. Also, reference combined cycle that is shown in Fig. B.2 has been simulated. In this regard, there are general parameters which are common between the three scenarios such as inlet temperature of gas turbine and steam turbine, solar irradiation for each day. Solar radiation can be inserted as input data for any simulation, and then output will be the net output power, fuel consumption, and CO2 emission. By

the way, all these scenarios are governed by the same control loop which is net output power of the system. This net output power of the system should be similar to the load in order to prevent any failure of covering the load but if the available thermal energy from solar is more than the load, here one of the scenarios will be executed. In order to execute scenario of generation extra power, this control loop will be off some times. On the other hand, any time there is no enough energy from the solar, duct burner will be operated to substitute thermal energy. So, the parameter of control loop will be the fuel amount in duct burner and this is applicable for other scenarios. In order to follow the load, as mentioned previously, there are two ways. For these 2 scenarios, control loop will be the same which is net output power but parameter of the control loop will be different. For instance, load of gas turbine will be the parameter of the control loop in order to give net output power equals to the load. As a result of this execution, fuel amount which is required for gas turbine will be reduced as well as CO_2 emission. Parameter of the last operation scenario which is following the load by operating solar field partially will be the number of operation flow paths for solar collector. Now for any scenario, if the solar multiple has been changed, similar procedure will be followed. For different solar multiples, oil mass flow rate is increasing while solar multiple is increasing but oil mass flow rate will be fixed for each solar multiple. As a result, outlet temperature will decrease with decreasing of solar radiation, and then steam temperature will decrease but duct burner will be operated if there is any need.

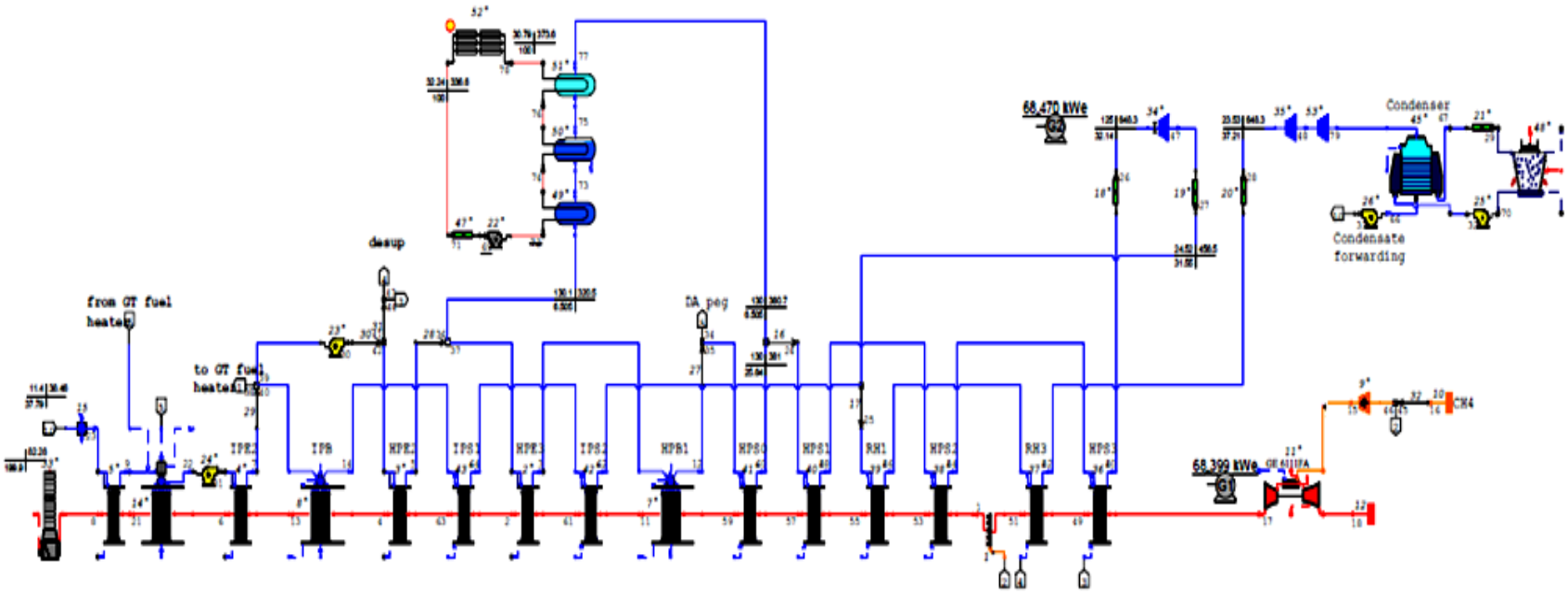

Figure B.1 Schematic diagram of HYCS which has been simulated by Thermo Flex

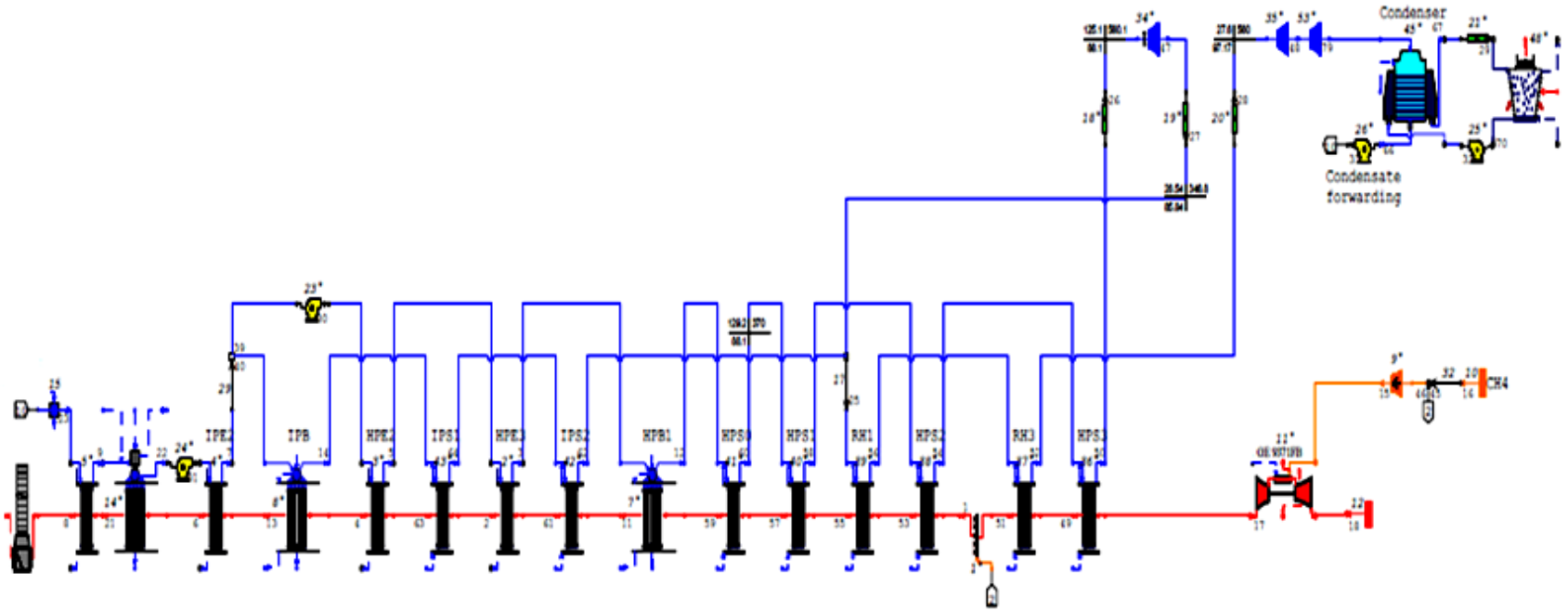

Figure B.2 Schematic diagram of reference combined cycle which has been simulated by Thermo Flex

2- Solarization gas side in combined cycle

First of all, HYCS that is shown in Fig. B.3 has been simulated under Dhahran weather conditions. Also, reference combined cycle that is shown in Fig. B.4 has been simulated. In this regard, there are general parameters which are common between this scenario of solarization and steam solarization such as inlet temperature of gas turbine and steam turbine, solar irradiation for each day, etc. Solar radiation can be inserted as input data, and then output will be the net output power, fuel consumption, and CO_2 emission. Also, this scenario is governed by the same control loop of solarization steam turbine which is net output power of the system. This net output power of the system should be similar to the load in order to prevent any failure of covering the load but if the available thermal energy from solar is more than the demand of gas turbine, here gas turbine will be fully operated by solar and extra solar energy will be useless. On the other hand, any time there is no enough energy from the solar, combustion chamber will burn more fuel to satisfy the outlet conditions of the combustion chamber which is 1327 °C as example. So, the parameter of control loop will be the fuel amount which is burned in combustion chamber, air flow rate in gas turbine, and outlet temperature of gases from the combustion chamber. Now, if the solar multiple has been changed, similar procedure will be followed.

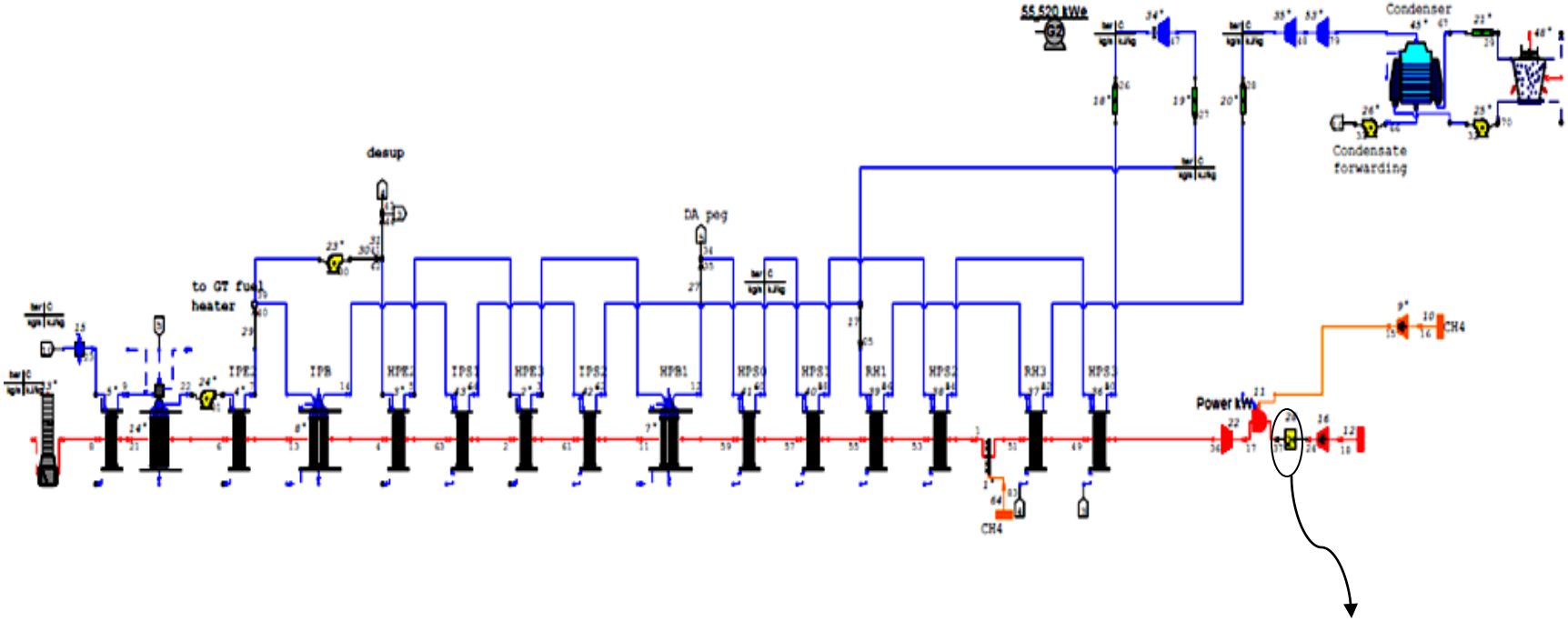

Heat Adder which presents solar tower

Figure B.3 Schematic diagram of HYCS which has been simulated by Thermo Flex

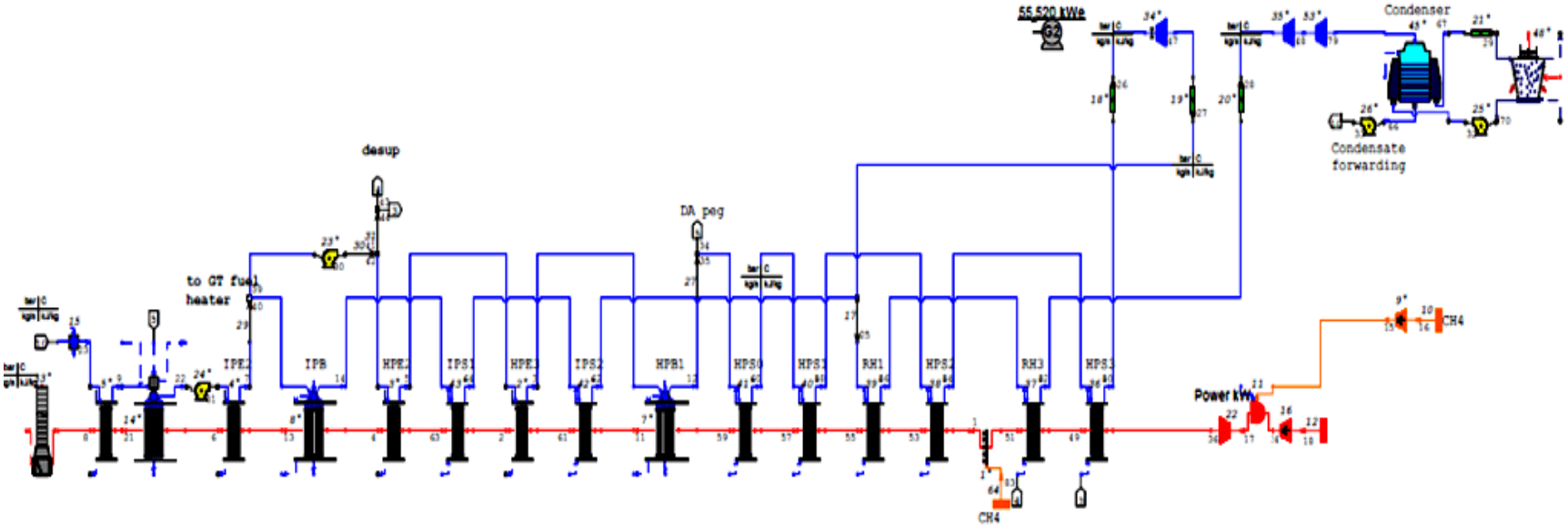

Figure B. 4 Schematic diagram of reference combined cycle which has been simulated by Thermo Flex

Summary:

Table B.1 Operation and control parameters of 3 scenarios of solarization steam turbine

Scenario	Operation parameters	Control parameters
Generation of extra power	1-Different solar radiation based on day number. 2-Inlet temperature of gas turbine will be fixed equals 25.6 °C. 3-Inlet temperature of steam turbine will be fixed 561°C. 4-Pressure of high pressure turbine will be 125 bar. 5-Fxed oil mass flow rate for each simulation of solar multiples.	Fuel mass in duct burner if solar thermal energy is not enough to cover the load otherwise there is no control parameters.
Solar field is part load		Fuel mass in duct burner if solar thermal energy is not enough to cover the load otherwise solar field will be operated at part load.
Gas turbine is part load		Fuel mass in duct burner if solar thermal energy is not enough to cover the load otherwise gas turbine will be operated at part load.

Table B.2 Operation and control parameters of solarization gas turbine

Scenario	Operation parameters	Control parameters
Solarization of gas turbine	1-Different solar radiation based on day number. 2-Inlet temperature of gas turbine will be fixed equals 25.6 °C. 3-Inlet temperature of steam turbine will be fixed 561°C.	Air flow rate in gas turbine, outlet temperature of combustion chamber, and fuel flow rate in duct burner.

APPENDIX C: DERIVATIOS OF ANNUAL SOLAR SHARE AND SOLAR LEVELIZED ELECTRICITY COST

1- Derivation of the relation between the annual solar share based on the annual fuel consumption and annual solar produced electric energy as given in the literature.

In its simplest form the annual solar share is nothing but the ratio of the annual electric energy produced by the solar energy to the total electric energy by the hybrid cycle

$$Annual\ solar\ Share\ (X_s) = \frac{E_s}{E_{hyb}}$$

Where: Es = annual electric energy produced from solar energy in the hybrid cycle:

$$Annual\ Energy\ \ produced\ \ from\ solar\ Energy\ (E_s) = E_{hyb} - \eta_{ref} \times m_{f,hyb} \times LHV$$

$$Annual\ solar\ Share\ (X_s) = \frac{E_{hyb} - \eta_{ref} \times m_{f,hyb} \times LHV}{E_{hyb}} \quad \text{(I)}$$

This expression is to be compared with the expressions found in the literature

$$SS = \left(1 - \frac{(m_f / kWh)_{hyb}}{(m_f / kWh)_{ref}}\right) \quad \text{(II)}$$

The objective now is to show whether the expressions (II) is equivalent to the first physically straight expression (I).

To show this we have to go back to the definition of the reference cycle.

1. Reference cycle is the conventional combined cycle that uses the same fuel as that of the hybrid cycle (and consequently will produce a different power (or annual energy))
2. Reference cycle is the conventional combined cycle that produces the same power as that of the hybrid cycle (and consequently it will consume a different annual amount of fuel)

First Definition (same fuel: $m_{f,\,ref} = m_{f,\,hyb}$)

$$SS = \left(1 - \frac{(m_f / kWh)_{hyb}}{(m_f / kWh)_{ref}}\right), \; cancel \; m_f$$

$$SS = \left(1 - \frac{(1/kWh)_{hyb}}{(1/kWh)_{ref}}\right) = \left(1 - \frac{(kWh)_{ref}}{(kWh)_{hyb}}\right)$$

$$SS = \left(\frac{(kWh)_{hyb} - (kWh)_{ref}}{(kWh)_{hyb}}\right) = \frac{E_{hyb} - \eta_{ref} \times m_{f,hyb} \times LHV}{E_{hyb}} = X_s$$ as given by eq. (I)

Second Definition (same energy: $E_{ref} = E_{hyb}$)

$$SS = \left(1 - \frac{(m_f / kWh)_{hyb}}{(m_f / kWh)_{ref}}\right) = \left(1 - \frac{(m_f / E)_{hyb}}{(m_f / E)_{ref}}\right) = \left(1 - \frac{m_{f,hyb} / E_{hyb}}{m_{f,ref} / E_{ref}}\right), \; cancel \; E$$

$$SS = \left(1 - \frac{m_{f,hyb}}{m_{f,ref}}\right) = \left(\frac{m_{f,ref} - m_{f,hyb}}{m_{f,ref}}\right)$$

Now : $m_{f,hyb}$ should equal to the electric energy produced by the conventional part of the hybrid cycle (in other word the total hybrid energy – solar energy electric part) divided by the efficiency of the conventional cycle multiplied by the LHV. Thus

$$SS = \left(1-\frac{m_{f,hyb}}{m_{f,ref}}\right)=\left(\frac{m_{f,ref}-m_{f,hyb}}{m_{f,ref}}\right)=\left(\frac{m_{f,ref}-\frac{E_{hyb}-E_s}{\eta_{ref}\times LHV}}{m_{f,ref}}\right)$$

$$SS = \frac{m_{f,ref}-\frac{E_{hyb}-E_s}{\eta_{ref}\times LHV}}{m_{f,ref}}=\frac{\frac{\eta_{ref}\times m_{f,ref}\times LHV-E_{hyb}+E_s}{\eta_{ref}\times LHV}}{m_{f,ref}}=\frac{\eta_{ref}\times m_{f,ref}\times LHV-E_{hyb}+E_s}{\eta_{ref}\times m_{f,ref}\times LHV}$$

But for this case the $E_{hyb} = E_{ref}$:

$$\eta_{ref}\times m_{f,ref}\times LHV = E_{ref} = E_{hyb}$$

Then:

$$SS = \frac{m_{f,ref}-\frac{E_{hyb}-E_s}{\eta_{ref}\times LHV}}{m_{f,ref}}=\frac{\frac{\eta_{ref}\times m_{f,ref}\times LHV-E_{hyb}+E_s}{\eta_{ref}\times LHV}}{m_{f,ref}}=\frac{\eta_{ref}\times m_{f,ref}\times LHV-E_{hyb}+E_s}{\eta_{ref}\times m_{f,ref}\times LHV}$$

$$SS = \frac{\eta_{ref}\times m_{f,ref}\times LHV-E_{hyb}+E_s}{\eta_{ref}\times m_{f,ref}\times LHV}=\frac{E_{hyb}-E_{hyb}+E_s}{E_{hyb}}$$

$$SS = \frac{E_s}{E_{hyb}}$$

Thus;

SS = the original definition of Xs

2- Derivation of the relation between the SLEC physical meaning and the equation based on the annual solar share based on the output as given in the literature.

In its simplest form the cost of converting solar energy into electric energy should be calculated as the annualized cost of the infra-structure, maintenance and operation (mainly labor and electric circulation pumps) of the solar field integrated with the conventional system divided by the annual electric energy produce by the solar field.

$$SLEC = \frac{Annual\ cost\ of\ solar\ \ field\ and\ solar\ accessories}{Annual\ \ Energy\ produced\ by\ solar} = \frac{S_{field\ cost}}{W_s}$$

This expression is to be compared with the expressions found in the literature

$$SLEC = \frac{LEC_{hyb} - (1 - X_s)\ LEC_{ref}}{X_s}$$

X_S: is the solar annual solar share based on the output definition.

$$SLEC = \frac{LEC_{hyb} - \left(1 - \frac{W_{hyb} - W_{ref}}{W_{hyb}}\right) * LEC_{ref}}{X_s}$$

Where: $LEC_{hyb} = \frac{S_{field\ cost} + C.C_{cost}}{W_{hyb}}$, $LEC_{ref} = \frac{C.C_{cost}}{W_{ref}}$

Where, W_{ref} is the annual energy produced by the reference cycle consuming the same fuel of the pertinent hybrid cycle.

$$SLEC = \frac{\frac{S_{field\ cost} + C.C_{cost}}{W_{hyb}} - \left(\frac{W_{hyb} - W_{hyb} + W_{ref}}{W_{hyb}}\right) \times \frac{C.C_{cost}}{W_{ref}}}{\frac{Ws}{W_{hyb}}}$$

$$SLEC = \frac{\frac{S_{field\ cost} + C.C_{cost}}{W_{hyb}} - \left(\frac{W_{ref}}{W_{hyb}}\right) \times \frac{C.C_{cost}}{W_{ref}}}{\frac{Ws}{W_{hyb}}} = \frac{\frac{S_{field\ cost} + C.C_{cost}}{W_{hyb}} - \frac{C.C_{cost}}{W_{hyb}}}{\frac{Ws}{W_{hyb}}}$$

Where:

C. C_{cost}: is the annual cost of the conventional cycle (capital cost + maintenance and labor cost + fuel consumption cost)

$S_{field\ cost}$: is the annual cost of the solar field and its pertinent accessories (capital cost + maintenance and labor cost + fuel consumption cost)

$$SLEC = \frac{S_{field\ cost} + C.C_{cost} - C.C_{cost}}{W_s}$$

$$SLEC = \frac{S_{field\ cost}}{W_s} = \frac{Annual\ cost\ of\ solar\ \ field\ and\ solar\ accessories}{Annual\ \ Energy\ \ produced\ by\ solar}$$

In the following derivation we will consider the LEC_{ref} for either case of considering:

1) the reference cycle is that of the same fuel consumption with less power output than that of the hybrid cycle

2) the reference cycle is that of the same output power but consumes more fuel than that of the hybrid

$$LEC_{ref} = \frac{Capital\ Installation\ Cost + Ma\,\text{int}\,enance\ \&\ Operation\,Cost + Fuel\ Cost}{Total\ Annual\ Energy\ produced}$$

let :

$$CM_{\cos t} = Capital\ Installation\ Cost + Ma\,\text{int}\,enance\ \&\ Operation\,Cost$$

$$W = Total\ Annual\ Energy\ produced$$

$$C_f = Fuel\ \cos t / unit\ mass\ of\ \ fuel$$

$$m_f = Annual\ Fuel\ consumption$$

$$LEC_{ref} = \frac{CM_{\cos t} + m_f \times C_f}{W} = \frac{CM_{\cos t}}{W} + \frac{m_f \times C_f}{W}$$

$$W_{ref} = \eta_{ref} \times m_f \times LHV$$

So:

$$LEC_{ref} = \frac{CM_{\cos t}}{W} + \frac{m_f \times C_f}{\eta_{ref} \times m_f \times LHV} = \frac{CM_{\cos t}}{W} + \frac{C_f}{\eta_{ref} \times LHV} \qquad \text{(III)}$$

It is known that the capital installation cost and the maintenance and operation (labor) as well as the fuel cost are proportional to the size (output power of the plant). This will lead to the fact that LEC_{ref} will be constant for either of the

above two definitions of the referenced cycle. Expression (III) is the same for both definitions.

NOMENCLATURE

A_a	Aperture area [m^2].
A_i	Inside cross sectional area of the absorber tube [m^2].
A_{SF}	Total area of solar field [m^2].
A_{ti}	Inner surface area of absorber tube for one collector [m^2].
A_{to}	Outer surface area of absorber tube [m^2].
Ab_{HCE}	Absorbability of the HCE selective coating. [%]
be	Specific fuel consumption of the gas turbine unit (tonne/MWh).
B^{GT}	Gas turbine fuel consumption [tonne/hour].
$CP_{Air,C}$	Heat capacity of air within compression process.[KJ/Kg.°K]
$CP_{Air,T}$	Heat capacity of air within expansion process.[KJ/Kg.°K]
CP_f	Heat capacity of HTF [KJ/Kg.°K]
CC	Combined cycle
D_{ci}	Inner diameter of glass cover [m].
D_{co}	Outer diameter of glass cover [m].
D_{ti}	Inner diameter of absorber tube. [m]
D_{to}	Outer diameter of absorber tube [m].
DNI	Direct normal insolation [W/m^2].
E	Time [min].
$E_{el,hybrid}$	The net electric power of the hybrid solar combined cycle (KW)
$E_{fuel,hybrid}$	Thermal energy for consumed fuel of hybrid system (KJ/Kg)
E_{gen}^{ann}	The annual generated power of the system (KWh)
End loss	Performance factor that accounts for losses from ends of HCE.

f	Focal length of the collectors [m].
f_2	Friction factor for the inner surface of the absorber pipe
fcr	Annuity factor
F_{tc}	View factor between tube and cover, for two long concentric cylinders, view factor equals one.
F_{PV}^{ann}	Present value of annual fixed cost ($)
$G_{accuracy}$	Geometric accuracy of the collector mirrors. [%]
h_C	Specific enthalpy of condenced water by condencer, state (20). [KJ/Kg]
hc_{c-a}	Convection heat transfer coefficient from glass cover to ambient air [W/m^2.ºK].
$\dot{h_D}$	Specific enthalpy of saturated water provided by deaerator, state(7). [KJ/Kg]
$\ddot{h_D}$	Specific enthalpy of evaporated steam within the deaerator. [KJ/Kg]
h_{Exit}	Specific enthalpy of exhaust gasses at the end of HRSG. [KJ/Kg]
h_{FP}	Specific enthalpy of saturated water after the pressurizing process, state (9). [KJ/Kg]
$\dot{h_{FV}}$	Specific enthalpy of saturated water at FV pressure, state (22). [KJ/Kg]
$\ddot{h_{FV}}$	Specific enthalpy of saturated steam at FV pressure, State (21). [KJ/Kg]
H_{FW1}	Specific enthalpy of saturated water at outlet of feed water heater [KJ/Kg]
H_{FW2}	Specific enthalpy of saturated water at outlet of economizer [KJ/Kg]
h_{HPTi}	Specific enthalpy of steam at the inlet of high pressure turbine. [KJ/Kg]
$h_{HPTo}{}^{S}$	Specific enthalpy at the end of the isentropic expansion of the steam in the HPT. [KJ/Kg]

h_{HPTO-a} Actual Specific enthalpy of steam at the outlet of high pressure turbine. [KJ/Kg]

$h_{HTF,I}$ Specific enthalpy of HTF at inlet of solar field. [KJ/Kg]

$h_{HTF,O}$ Specific enthalpy of heat transfer fluid (HTF) at outlet of solar field. [KJ/Kg]

h_L Specific enthalpy of saturated water at outlet of RFWH, state (23). [KJ/Kg]

h_{LPTi} Specific enthalpy of steam at the inlet of low pressure turbine, state (17). [KJ/Kg]

$h_{LPTo}{}^{S}$ Specific enthalpy at the end of the isentropic expansion of the steam in LPT. [KJ/Kg]

h_{LPTO-a} Actual Specific enthalpy of steam at the outlet of low pressure turbine, state (18). [KJ/Kg]

$h_{\text{rad C-S}}$ Radiation heat transfer coefficient between glass cover and sky [W/m^2.°K].

$h_{\text{rad t-c}}$ Radiation heat transfer coefficient between tube and cover [W/m^2.°K]

h_{RFW1} Specific enthalpy of makeup water, state (24). [KJ/Kg]

h_{RFW2} Specific enthalpy of makeup water, state (25). [KJ/Kg]

h_{RK} Specific enthalpy of extracted steam from HPT, state (16). [KJ/Kg]

h_{SB} Steam specific enthalpy at superheating section exit. [KJ/Kg]

$\dot{h_{SB}}$ Water specific enthalpy at evaporating section inlet. [KJ/Kg]

h_{SBL} Specific enthalpy of saturated water at steam boiler pressure. [KJ/Kg]

$h_{ST,O}$ Specific enthalpy of steam generated in steam generator. [KJ/Kg]

h_1	Specific enthalpy at the inlet of compressor [KJ/Kg].
h_2	Actual specific enthalpy at the outlet of compressor [KJ/Kg].
${h_2}^s$	Isentropic specific enthalpy at the exit of compressor [KJ/Kg].
h_3	Specific enthalpy of gasses before entering gas turbine [KJ/Kg].
h_4	Actual specific enthalpy of gasses at the outlet of gas turbine [KJ/Kg].
${h_4}^s$	Isentropic specific enthalpy of gasses at the outlet of gas turbine [KJ/Kg].
h_4	Evaluated specific enthalpy of exhaust gasses. [KJ/Kg]
h_5	Evaluated specific enthalpy of exhaust gasses at the cold end of the superheating heat exchanger. [KJ/Kg]
h_6	Evaluated specific enthalpy of exhaust gasses at the outlet of evaporating stage. [KJ/Kg]
HCE	Heat collector element.
HCE_{dust}	Losses due to covering of HCE by dust on the glass envelope. [%]
HCE_{misc}	Miscellaneous factor to adjust for other HCE losses. [%]
IAM	Incidence angle modifier.
I_{PV}^{tot}	Present value of total investment cost ($)
$ISCCS$	Integrated solar combined cycle
K_a	Evaluated value of thermal conductivity at temperature of ambient air [W/m.°K].
K_t	Thermal conductivity of absorber tube [W/m.°K].
L	Collector length. [m]
L_{Local}	The local meridian of the collector site [deg].
L_{space}	Distance between two parallel collectors [m].

$L_{standard}$	Standard meridian for the local time zone [deg].
LEC	Levelized Electricity Cost ($/MWh)
lHV	Lower heating value of fuel [KJ/Kg]
$LSCA$	Length of a single solar collector [m].
M	Number of collectors connected in series.
m_a	Air mass flow rate [Kg/sec].
$\dot{m}_C$	Condenser mass flow rate, state (18). [Kg/sec]
$\dot{m}_{Drain}$	Mass flow rate of drain steam from drum, state (12). [Kg/sec]
$\dot{m}_{DS}$	Mass flow rate of steam extracted by flash vessel, state (21). [Kg/sec]
$\dot{m}_{Evap}$	Mass flow rate of evaporated steam from deaerator. [Kg/sec]
m_f	Fuel mass flow rate [kg fuel/kg air].
$\dot{m}_{FV}$	Mass flow rate of saturated water through flash vessel, state (22). [Kg/sec]
$\dot{m}_{fuel}$	Mass flow rate of fuel [Kg/sec]
$\dot{m}_{FWD}$	Mass flow rate from deaerator, state (7). [Kg/sec]
$\dot{m}_{gas}$	GT exhaust gasses mass flow, state (4). [Kg/sec]
$\dot{m}_{HPT}$	Mass flow rate of steam at the inlet of HPT, state (13*). [Kg/sec]
$\dot{m}_K$	Mass flow rate of steam which expanded in LPT in HYCS mode, state (17). [Kg/sec]
m_{loss}	Relative air losses mass flow, its typical value 0.005 [kg air/kg air].
$\dot{m}_{RK}$	Mass flow rate of steam extracted from HPT to operate deaerator, state (16). [Kg/sec]
$\dot{m}_{FW}$	Mass flow rate of makeup water, state (24 & 25). [Kg/sec]
$\dot{m}_{SB}$	Mass flow rate of steam at inlet of the steam boiler, state (10). [Kg/sec]

$\dot{m}_{SF}$	Mass flow rate of solar collectors' field. [Kg/sec]
$\dot{m}_{ST}$	Steam generated in steam generator due to gained heat by solar field, state (27). [Kg/sec]
Mir_{clean}	Mirror cleanliness. [%]
Mir_{ref}	Mirror reflectivity. [%]
N	Number of parallel rows.
n	The day number of the year.
NE^{GT}	The gas turbine unit output (MWe).
Nu_a	Nusselt number of ambient air.
OM_{PV}^{ann}	Present value of operating and maintenance cost ($/annual)
P_a	Atmospheric pressure =1.01325 [bar].
$P_{el,net}$	The net power of the integrated solar combined cycle [KWe]
$P_{el,ref}$	The net power of the reference cycle [KWe]
Pr	Pressure ratio of gas turbine
$P_{th,solar}$	Thermal power collected by solar field [KWt]
P_D	Dearator pressure. [Bar]
Pr_a	Evaluated value of Prandtl number at temperature of ambient air.
Pr_c	Evaluated value of Prandtl number at temperature of outer surface of glass cover (T_{C2}).
P_{FP}	Pressure at the exit of feed water pump. [Bar]
P_{FV}	Flash vessel pressure. [Bar]
P_{HPTi}	Inlet pressure of HPT. [Bar]
Pr_1	Prandtl number evaluated at the HTF temperature, (T_{fi}).

Pr_2	Prandtl number evaluated at the absorber inner surface temperature (T_t).
P_3	Pressure of air at outlet of combustion chamber [Bar].
P_4	Pressure of air at outlet of gas turbine [Bar].
P_T	Specific output power of gas turbine. [KJ/Kg]
P_{Net}	Net output power of gas turbine. [KW]
$Q_{absorbed}$	Solar radiation absorbed by the receiver tubes [W/m2].
$Q_{collected}$	Total collected energy from solar field [W].
Q_{cv}	Fuel calorific value [MJ/Kg].
Q_L	Loss energy [W].
Q_{SF}	Nominal solar field of absorbed energy. [KJ/Kg]
Q_u	Useful energy [W].
r_p	Compressor ratio.
Re_a	Reynolds number of ambient air.
Row shadow	Performance factor that accounts for mutual shading of parallel collector rows during early morning and late evening.
S_i	Specific entropy at the HPT inlet. [KJ/Kg]
S_{iLPT}	Specific entropy of steam at the inlet of LPT, state (17). [KJ/Kg]
S_{oLPT}	Specific entropy of steam at the outlet of LPT, state (18). [KJ/Kg]
$SEGS$	Solar electric generation system
SS	Solar share
SH_{Loss}	Losses from covering ends of HCE due to bellows.
$standard\ time$	Based on a standard meridian for the local time zone [h].
T_a	Ambient temperature [°K].

T_{Cm}	Mean cover temperature. [°K]
T_{C1}	Inner temperature of glass surface. [°K]
T_{C2}	Outer temperature of glass surface. [°K]
T_{c1}^{*}	New guessed value of inner surface of glass cover [°K].
T_{c2}^{*}	New guessed value of outer surface of glass cover [°K].
T_{fi}	Inlet temperature of solar field. [°K]
T_{fo}	Outlet temperature of solar field. [°K]
T_{fo}^{*}	Calculated value of outlet temperature from solar field [°K].
T_{HPTi}	Inlet temperature of HPT.[°K]
T_S	Sky temperature. [°K]
T_t	New guessed value of absorber tube temperature. [°K]
T_t^{**}	New guessed value of absorber tube temperature [°K].
T_2^{S}	Isentropic temperature at the compressor exit [°K].
T_2	Air temperature at outlet of compression process in gas turbine [°K].
T_3	Air temperature at outlet of combustion chamber in gas turbine [°K].
T_4	Gas temperature at the end of the expansion process [°K].
T_5	Temperature of exhaust gasses at the end of the super heating stage. [°K]
TRR	Total annual revenue
Tr_{glass}	Transmissivity of the glass envelope.
TT_{error}	Tracking and twisting error associated with the collector type. [%]
T_{steam}	Steam temperature [°K].

T_{FP} Temperature of water at outlet of feed pump [°K].

T_D Temperature of water at outlet of darateor [°K].

T_C Temperature of water at outlet of condenser [°K].

T_{RFW} Temperature of reefed water [°K].

T_{FW1} Temperature of water at outlet of reefed water heater [°K].

T_{FW2} Temperature of water at outlet of economizer [°K].

T_{HPTo} Temperature of water at outlet of high pressure turbine [°K].

T_{LPTi} Temperature of water at inlet of low pressure turbine [°K].

U_a Ambient air velocity [m/sec].

U_f Velocity of HTF inside the tube. [m/sec]

U_L^* Calculated value of overall loss coefficient [W/m^2.°K].

Vf Specific volume of feed water. [m^3/Kg]

W_a Aperture width [m].

W_C Compressor specific work. [KJ/Kg]

W_{HPT} Actual work of HPT. (KW)

W_{LPT} Actual work of LPT in CC mode. (KW)

W_{LPTS} Actual work of LPT in HYCS mode. (KW)

W_{Net} Net relative output of gas turbine [KJ/Kg].

W_T Total relative work of the gas turbine. [KJ/Kg]

$X_{net,elec,solar}$ Instantaneous solar share [%]

τ_{FP} Heat gain from pressurizing process of feed water pump, between state (8&9).

ξ_P Hydraulic losses coefficient for HRSG (assumed 0.12)

ξ_{SB}	The pressure loss coefficient (assumed value is 6%)
$\Delta_{E,el}$	Instantaneous net electrical solar share (%)
Δ_{co_2}	CO_2 avoidance

Greek Symbols

$\emptyset$	Latitude location of the solar field
v_a	Kinematic viscosity at ambient temperature [m^2/sec]
η	Efficiency [%]
σ	Stefan Boltzmann constant = 5.67×10^{-8}[W/m^2.°K^{-4}]
ε	Emissivity
ɣa	specific heat ratio or isentropic expansion factor.
η_c	Compressor isentropic efficiency [%]
${\eta_n}^k$	Compressor polytropic efficiency [%]
η_T	Turbine isentropic efficiency [%]
${\eta_n}^T$	The turbine polytropic efficiency [%]
$б$	Expansion ratio
ɣ	Heat Capacity Ratio
θ	Angle of incidence [deg].

Subscripts

c	Glass cover
$c.c$	Combustion Chamber
D	Deaerator
ep	Electrical of feed pump
$field$	Solar Field

FV	Flash Vessel
G	Electrical of Gas Turbine
GH	Gas heat exchanger of HRSG
GTU	Gas Turbine Unit
H	Hydraulic
h_{in}	Specific enthalpy at the inlet of turbine.
HCE	Heat Collector Element
m	Mechanical of Gas Turbine
mp	Mechanical of feed pump
net_incr_solar	The net incremental solar
ref	Reference cycle
$RFWH$	Reefed Water Heater
SF	Solar Field
t	Receiver tube
T	Gag Turbine
HPT	High Pressure Turbine
IPT	Intermediate Pressure Turbine
LPT	Low Pressure Turbine

Superscripts

P	Water Feed Pump
LPT	Low Pressure Turbine
G	Gasses' Products

REFERENCES

[1] "International Energy Outlook ", U. S. E. I. Administration, Ed., ed, 2009.

[2] S. Al-Ajlan, A. Al-Ibrahim, M. Abdulkhaleq, and F. Alghamdi, "Developing sustainable energy policies for electrical energy conservation in Saudi Arabia," Energy Policy, vol. 34, pp. 1556-1565, 2006.

[3] IPCC. (2001, Third assessment report—climate change 2001. Available: /http://www.ipcc.chS.

[4] R. Quadrelli and S. Peterson, "The energy-climate challenge: Recent trends in CO_2 emissions from fuel combustion," Energy Policy, vol. 35, pp. 5938-5952, 2007.

[5] http://en.wikipedia.org/wiki/Renewable_energy [Online].

[6] S. Rehman and A. Ahmad, "Assessment of wind energy potential for coastal locations of the Kingdom of Saudi Arabia," Energy, vol. 29, pp. 1105-1115, 2004.

[7] http://en.wikipedia.org/wiki/Solar_energy [Online].

[8] W. Alnaser and N. Alnaser, "Solar and wind energy potential in GCC countries and some related projects," Journal of Renewable and Sustainable Energy, vol. 1, p. 022301, 2009.

[9] P. Woditsch, "Kostenreduktionspotenziale bei der Herstellung von PV-Modulen," Proceedings of FVS Themen, pp. 72–86, 2000.

[10] H. Price and S. Carpenter, "The potential for low-cost concentrating solar power systems," 1999, pp. 1-5.

[11] V. Quaschning, "Technical and economical system comparison of photovoltaic and concentrating solar thermal power systems depending on annual global irradiation," Solar Energy, vol. 77, pp. 171-178, 2004.

[12] P. Schwarzbözl, R. Buck, C. Sugarmen, A. Ring, M. Marcos Crespo, P. Altwegg, and J. Enrile, "Solar gas turbine systems: Design, cost and perspectives," Solar Energy, vol. 80, pp. 1231-1240, 2006.

[13] P. Heller, M. Pfänder, T. Denk, F. Tellez, A. Valverde, J. Fernandez, and A. Ring, "Test and evaluation of a solar powered gas turbine system," Solar Energy, vol. 80, pp. 1225-1230, 2006.

[14] H. Alrobaei, "Novel integrated gas turbine solar cogeneration power plant," Desalination, vol. 220, pp. 574-587, 2008.

[15] S. Odeh, M. Behnia, and G. Morrison, "Performance evaluation of solar thermal electric generation systems," Energy Conversion and Management, vol. 44, pp. 2425-2443, 2003.

[16] Y. Yang, Y. Cui, H. Hou, X. Guo, Z. Yang, and N. Wang, "Research on solar aided coal-fired power generation system and performance analysis," Science in China Series E: Technological Sciences, vol. 51, pp. 1211-1221, 2008.

[17] J. Dersch, M. Geyer, U. Herrmann, S. Jones, B. Kelly, R. Kistner, W. Ortmanns, R. Pitz-Paal, and H. Price, "Trough integration into power plants--a study on the performance and economy of integrated solar combined cycle systems," Energy, vol. 29, pp. 947-959, 2004.

[18] G. Elsaket, "'Simulating The Integrated Solar Combined Cycle for Power Plants Application in Libia' " MSc Thesis, M.E, Libia, 2007.

[19] R. Charles, K. Davis, and J. Smith, "Assesment of concentrating solar power technology cost and performance forecasts," Presented at Electric Power, vol. 2005, 2005.

[20] D. Mills, "Advances in solar thermal electricity technology," Solar Energy, vol. 76, pp. 19-31, 2004.

[21] D. Mills, G. Morrison, P. Le Lièvre, E. Square, and B. St, "Project proposal for a compact Linear Fresnel reflector solar thermal plant in the Hunter Valley," ed, 2002.

[22] D. Mills, G. Morrison, and P. Le Lievre, "Design of a 240 MWe solar thermal power Plant," in Eurosun Conference., 2004.

[23] M. Feidt, "Optimization of a Brayton cycle engine in contact with fluid thermal capacities," Revue Generale de Thermique, vol. 35, pp. 662-666, 1996.

[24] J. Roco, S. Velasco, A. Medina, and A. Hernández, "Optimum performance of a regenerative Brayton thermal cycle," Journal of Applied Physics, vol. 82, p. 2735, 1997.

[25] C. Cheng and C. Chen, "Efficiency optimizations of an irreversible Brayton heat engine," Journal of Energy Resources Technology, vol. 120, p. 143, 1998.

[26] L. Chen, Y. Li, F. Sun, and C. Wu, "Power optimization of open-cycle regenerator gas-turbine power-plants," Applied Energy, vol. 78, pp. 199-218, 2004.

[27] A. Polyzakis, C. Koroneos, and G. Xydis, "Optimum gas turbine cycle for combined cycle power plant," Energy Conversion and Management, vol. 49, pp. 551-563, 2008.

[28] Y. El Sayed and M. Tribus, "A Theoretical comparison of Rankine and Kalina cycles," 1985, p. 97.

[29] C. Wu, "Power optimization of a finite-time Rankine heat engine," International Journal of Heat and Fluid Flow, vol. 10, pp. 134-138, 1989.

[30] D. Wei, X. Lu, Z. Lu, and J. Gu, "Performance analysis and optimization of organic Rankine cycle (ORC) for waste heat recovery," Energy Conversion and Management, vol. 48, pp. 1113-1119, 2007.

[31] C. Fielden, "Industrial GT for Combined Power Generation–Optimisation Issues," MSc Thesis, Cranfield University, UK, 1995.

[32] M. Valdés and J. Rapún, "Optimization of heat recovery steam generators for combined cycle gas turbine power plants," Applied Thermal Engineering, vol. 21, pp. 1149-1159, 2001.

[33] L. Attala, B. Facchini, and G. Ferrara, "Thermoeconomic optimization method as design tool in gas-steam combined plant realization," Energy Conversion and Management, vol. 42, pp. 2163-2172, 2001.

[34] A. Franco and A. Russo, "Combined cycle plant efficiency increase based on the optimization of the heat recovery steam generator operating parameters," International Journal of Thermal Sciences, vol. 41, pp. 843-859, 2002.

[35] M. Valdés, M. Durán, and A. Rovira, "Thermoeconomic optimization of combined cycle gas turbine power plants using genetic algorithms," Applied Thermal Engineering, vol. 23, pp. 2169-2182, 2003.

[36] C. Casarosa, F. Donatini, and A. Franco, "Thermoeconomic optimization of heat recovery steam generators operating parameters for combined plants," Energy, vol. 29, pp. 389-414, 2004.

[37] K. Lovegrove, A. Luzzi, I. Soldiani, and H. Kreetz, "Developing ammonia based thermochemical energy storage for dish power plants," Solar Energy, vol. 76, pp. 331-337, 2004.

[38] M. Kane, D. Favrat, K. Ziegler, and Y. Allani, "Thermoeconomic analysis of advanced solar-fossil combined power plants," International Journal of Thermodynamics, vol. 3, pp. 191-198, 2010.

[39] J. Blanco, D. Alarcón, W. Gernjak, and E. Guillén, "Polygeneration of power and desalination with solar energy," 1st European Conference on Polygeneration, 2007.

[40] A. Lewandowski and D. Simms, "An assessment of linear Fresnel lens concentrators for thermal applications," Energy, vol. 12, pp. 333-338, 1987.

[41] M. Eck and E. Zarza, "Saturated steam process with direct steam generating parabolic troughs," Solar Energy, vol. 80, pp. 1424-1433, 2006.

[42] "European research on concentrated thermal energy," ed.

[43] E. Zarza, M. Rojas, L. González, J. Caballero, and F. Rueda, "INDITEP: The first pre-commercial DSG solar power plant," Solar Energy, vol. 80, pp. 1270-1276, 2006.

[44] G. Morrison, D. Mills, and S. Corporation, "Solar thermal power systems-Stanwell power station project," 1999.

[45] M. Montes, A. Abánades, and J. Martinez-Val, "Performance of a direct steam generation solar thermal power plant for electricity production as a function of the solar multiple," Solar Energy, vol. 83, pp. 679-689, 2009.

[46] H. Hong, H. Jin, J. Ji, Z. Wang, and R. Cai, "Solar thermal power cycle with integration of methanol decomposition and middle-temperature solar thermal energy," Solar Energy, vol. 78, pp. 49-58, 2005.

[47] A. Segal and M. Epstein, "Optimized working temperatures of a solar central receiver," Solar Energy, vol. 75, pp. 503-510, 2003.

[48] A. Imenes, D. Buie, D. Mills, P. Schramek, and S. Bosi, "A new strategy for improved spectral performance in solar power plants," Solar Energy, vol. 80, pp. 1263-1269, 2006.

[49] I. Martínez and R. Almanza, "Experimental and theoretical analysis of annular two-phase flow regimen in direct steam generation for a low-power system," Solar Energy, vol. 81, pp. 216-226, 2007.

[50] W. Stine and R. Harrigan, "Solar energy fundamentals and design," ed: John Wiley and Sons, Inc., New York, NY, 1985.

[51] Options for hybrid solar and conventional fossil plants, [Online].

[52] P. Hank, L. Eckhard, K. David, Z. Eduardo, C. Gilbert, G. Randy, and M. Rod, "Advances in parabolic trough solar power technology," Journal of Solar Energy Engineering, vol. 124, pp. 109-125, 2002.

[53] "Survey of thermal storage for parabolic trough power plants," NREL/SR-550-27925, September 2000

[54] H. Alrobaei, "Thermodynamic parametric study for combined cogeneration power plants," Engineering, vol. 38, pp. 80-91, 1998.

[55] T. a. M. Eastop, A., Applied thermodynamics for engineering technologists: 5th ed, Longman, London., 1993.

[56] J. A. Duffie, and Beckman, William A., Solar Engineering of Thermal Processes, 3rd edition ed. New York: John Wiley and Sons, Inc, 2005.

[57] V. E. Dudley, G. Kolb, A. Mahoney, T. Mancini, C. Matthews, M. Sloan, and D. Kearney, "Test results: SEGS LS-2 solar collector," Sandia National Labs., Albuquerque, NM (United States)1994.

[58] T. A. Stuetzle, "Automatic control of the 30MWe SEGS VI Parabolic Trough plant," Master, Department of Mechanical Engineering, University of Wisconsin –Madison, 2002.

[59] A. M. Patnodea, "Simulation and Performance Evaluation of Parabolic Trough Solar Power Plants," Master Thesis, Mechanical Engineering, University of Wisconsin-Madison, 2006.

[60] F. Lippke, "Simulation of the part-load behavior of a 30 MWe SEGS plant," Sandia National Labs., Albuquerque, NM (United States)1995.

[61] R. Forristall and N. R. E. Laboratory, Heat transfer analysis and modeling of a parabolic trough solar receiver implemented in engineering equation solver: Citeseer, 2003.

[62] F. D. Incropera, D, Fundamentals of Heat and Mass Transfer, Third Edition ed. New York,NY: John Wiley and Sons, 1990.

[63] V. Gnielinski, "New equations for heat and mass transfer in turbulent pipe and channel flow," International Chemical Engineering, vol. (16:2), pp. 359–363., 1976.

[64] E. Jacobsona, N. Ketjoya, S. Nathakaranakulea, and W. Rakwichiana, "Solar parabolic trough simulation and application for a hybrid power plant in Thailand," vol, vol. 32, pp. 187-199, 2006.

[65] T. M. Hunt, T. Hunt, N. Vaughan, N. Vaughan, and R. H. Warring, The hydraulic handbook: Elsevier science, 1996.

[66] M. Montes, A. Abánades, and J. Martínez-Val, "Performance of a direct steam generation solar thermal power plant for electricity production as a function of the solar multiple," Solar Energy, vol. 83, pp. 679-689, 2009.

[67] X. G. Casals, "Modeling and optimizing the use of parabolic trough technology with Rankine cycles for electricity production," January 2000.

[68] Available: http://en.wikipedia.org/wiki/Carbon_tax

[69] S. Price, "2008 Solar Technologies Market Report," 2010.

[70] Available: http://en.wikipedia.org/wiki/Cost_of_electricity_by_source

[71] IEA Energy Technology Essentials, Report, December 2006

VITA

Name: AHMAD ETER

Place of Birth: Riyadh, Saudi Arabia.

Nationality: Jordanian

Permanent Address: Jenin,

Palestine.

Telephone: +970599292974, +966595960712

Email Address: eng.eter@yahoo.com

Educational Qualification:

M.S (Mechanical Engineering)

October 2011

King Fahd University of Petroleum and Minerals

Dhahran, Saudi Arabia.

B. Tech. (Mechanical Engineering)

January 2009

An-Najah National University,

Nablus, Palestine.